

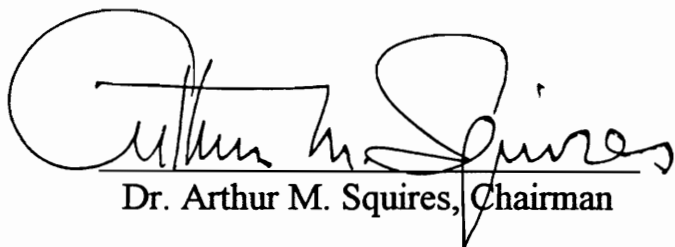
**SENSITIVITY OF METHANOL-TO-OLEFIN
REACTION TO AXIAL GAS DISPERSION :
DETERMINATION IN A VIBRATED-BED
MICROREACTOR**

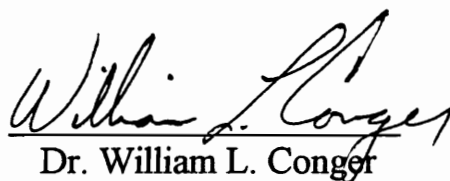
by

Samuel Nhlanganiso Tshabalala

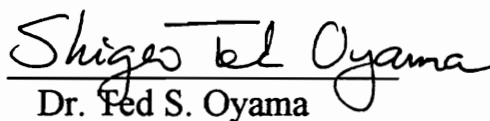
Dissertation submitted to the Faculty of the
Virginia Polytechnic Institute and State University
in partial fulfillment of the requirements for the degree of
DOCTOR OF PHILOSOPHY
in
Chemical Engineering

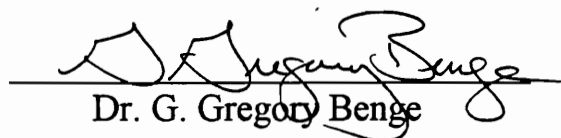
APPROVED:

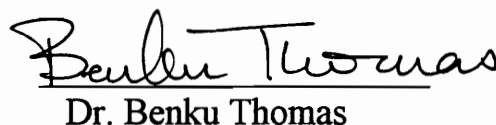

Dr. Arthur M. Squires, Chairman


Dr. William L. Conger


Dr. Harold M. McNair


Dr. Fed S. Oyama


Dr. G. Gregory Bengt


Dr. Benku Thomas

August, 1995
Blacksburg, Virginia

SENSITIVITY OF METHANOL-TO-OLEFIN REACTION TO AXIAL
GAS DISPERSION : DETERMINATION IN A VIBRATED-BED
MICROREACTOR

by

Samuel Nhlanganiso Tshabalala

Arthur M. Squires, Chairman

Chemical Engineering

(ABSTRACT)

A microreactor has been developed to study the sensitivity of Methanol-To-Olefin (MTO) reaction to axial gas dispersion. It comprises a rectangular horizontal duct, 12.7 mm in height, 25.4 mm in width, variable in length, charged with a 1-mm-deep layer of HZSM-5 catalyst. The microreactor is constructed of aluminum alloy and heated with cartridge heaters. A glass reference duct with the same catalyst loading is mounted directly above the microreactor to provide visual check of the coherent-expanded vibration state achieved by vibrating the setup at 24 hertz and 4.3-mm vertical displacement. In this state, catalyst powder expands to full duct height during a portion of each vibration cycle, with intense vertical mixing of powder and little horizontal.

Axial gas dispersion coefficient varies linearly with superficial gas velocity, and axial Peclet Number (Pe_{ax}) can be studied over a wide range of values

simply by varying duct length while holding weight hourly space velocity constant.

Conducting the MTO reaction in microreactors of 7.62-, 15.24-, and 22.86-cm length ($Pe_{ax} = \text{ca. } 2, 9, \text{ and } 19$ respectively) revealed the reaction to be sensitive to axial gas mixing. Trend in light olefin yield versus Pe_{ax} agrees with earlier turbulent fluid-bed data. Loss in olefins with increase in axial gas dispersion (decrease in Pe_{ax}) suggests that a circulating fluid bed may be the preferred reactor for this reaction.

Researchers can use the microreactor to determine, quickly and inexpensively, how reaction outcomes vary with axial gas dispersion. The microreactor could help R&D managers to avoid expense of a fluid bed R&D effort where an economically significant outcome of a reaction is acutely sensitive to axial gas dispersion, and where a fixed bed is an acceptable alternative.

ACKNOWLEDGEMENTS

The research presented in this study was supported in part by National Science Foundation joint industry-university research grant CBT-8620244. Partial support for my graduate studies was provided by; (i) Penn South Africa Fellowship, ASA Educational Trust, South Africa; (ii) United Nations Educational and Training Programme for Southern Africa; (iii) Foundation for Research Development, University Bursary Programme, South Africa.

I express my gratitude to Dr A.M. Squires (my advisor) for his assistance, guidance and insightful discussions regarding the meaning and significance of our research results. I am indebted to him for placing me at Virginia Polytechnic Institute and State University (VPI & SU). I thank Okson Yi and Benku Thomas who initiated the contact with Dr A.M. Squires.

I express my gratitude to Dr H.M. McNair for his friendship and generous support of this research work. He helped in planning and interpreting gas chromatographic analysis of Methanol-To-Olefin reaction products. I thank him for use of his; (i) Perkin Elmer Autosystem GC; (ii) graduate student, Yuwen Wang; (iii) standard samples of high molecular weight hydrocarbons, and (iv) HP 3390A Integrator.

I have consulted with Dr B. Thomas on a number of occasions concerning various aspects of the vibration system and thank him, for his helpful advice and comments.

I thank Dr W.L. Conger for his encouragement and support particularly during this summer in order to complete the work. I also thank him for placing me in Unit Operations Laboratory during the past five summer sessions.

In addition, I thank the other members of my committee, Drs T.S. Oyama and G. G. Bengé for their timely assistance.

Billy Williams and Wendal Brown deserve special thanks for their prompt and thorough attention to the shop work needed for the design and development of the vibrated bed microreactor system.

Special thanks are due to Riley Chan for his help and useful advice regarding the experiments. I thank both Drs D. Cox and R. Rony for the use of their HP 3390A Integrator and ISCO Model 314 Syringe Pump, respectively.

I acknowledge the professional help of Diane Patty, Judy Coleman, Carol Stables, Chris Moore and Diane Cannaday. I thank Sukhtej Dhingra and

Qinchun Charles Hu for sharing use of their equipment and also for their help with Microsoft Word in typing the document.

I express my appreciation to the faculty and students at VPI & SU who I have worked with during my term as President of the African Students Association.

It is impossible to thank all who have in many ways made Blacksburg, an enjoyable living experience for me and my family. I gratefully acknowledge the support and special friendship of; (i) Dr Richard Zody and his family; and (ii) Dr Josiah Tlou and his family. Additionally, I thank all those not mentioned here for lack of space, for their valued friendship.

I remain forever thankful to my late parents, Amos Cornelius and Nomashinini Roselina, who without their guidance and dedication, it would have been impossible to reach this stage of my educational career from my modest upbringing.

Finally, I thank Ntombizandile, my wife, for her undying love, support and patience during our stay in Blacksburg. I also thank my wonderful kids, Mpumelelo and Siphesihle, for their love. I hope to have more time to watch cartoons and read library storybooks with them.

TABLE OF CONTENTS

1. INTRODUCTION	1
1.1 TURBULENT FLUID BED SCALE-UP PROBLEM	2
1.2 PROPOSED NEW APPROACH TO SCALE-UP	5
1.3 VIBRATED BED MICROREACTOR (VBMR) CONCEPT	6
1.4 SENSITIVITY OF GAS-SOLID CATALYTIC REACTION TO AXIAL GAS DISPERSION IN THE MICROREACTOR	9
1.5 OVERVIEW OF THE DISSERTATION	12
 2. SCOPE OF THE STUDY	 14
2.1 RESEARCH GOALS	14
2.2 RESEARCH OBJECTIVES	15
2.3 METHODOLOGY	16
2.3.1 OVERALL PLAN OF STUDY	16
2.3.2 COMPARING MICROREACTOR DATA WITH FLUID BED DATA	18
2.4 SIGNIFICANCE OF THIS WORK	19
2.4.1 FLUID BED REACTOR DESIGN AND SCALE-UP	20
2.4.2 CATALYST SCREENING STUDIES	21
 3. SCALE-UP OF TURBULENT FLUID BED	 24
3.1 GAS SOLID CONTACTING	25

3.1.1 EFFECT OF SOLID PROPERTIES	26
3.1.2 FLUIDIZATION BEHAVIOR	26
3.2 THE CONVENTIONAL SCALE-UP PROCESS	34
3.2.1 GAS VELOCITY	34
3.2.2 BED INTERNALS	36
3.2.3 CONCLUDING REMARK	36
3.3 AXIAL DISPERSION MODEL IN FLUID BED SCALE-UP	37
3.3.1 USE OF AXIAL DISPERSION MODEL IN HOMOGENEOUS SYSTEMS	41
3.3.2 OPERATIONAL STRATEGY TO OBTAIN A HOMOGENEOUS BEHAVIOR IN A TURBULENT FLUID BED	42
4. VIBRATED BED MICROREACTOR (VBMR) CONCEPT	44
4.1 THEORY OF VIBRATION	45
4.2 VIBRATED BED DYNAMICS	46
4.3 COHERENT-EXPANDED (C-E) VIBRATION STATE	47
4.4 FEASIBILITY STUDY OF THE VBMR CONCEPT	52
4.4.1 AXIAL DISPERSION MODEL IN VBMR	52
4.4.2 MAXIMUM GAS VELOCITY	53
4.4.3 TRACER GAS STUDY	54
4.4.4 PLANNING EXPERIMENTS IN VBMR	57
4.4.5 THE PRESENT STUDY	59

5. METHANOL-TO-OLEFINS (MTO) REACTION	61
5.1 A BRIEF REVIEW ON ZSM-5 CATALYST	65
5.1.1 BACKGROUND	66
5.1.2 CRYSTAL STRUCTURE	66
5.1.3 PROPERTIES OF ZSM-5 CATALYST	70
5.1.4 COMMERCIAL APPLICATIONS	71
5.1.5 PREPARATION OF ZSM-5 CATALYST	75
5.2 A BRIEF REVIEW ON MTO REACTION	77
5.2.1 OPERATIONAL CONDITIONS	79
5.2.2 FLUID BED SCALE-UP OF MTO REACTION	80
5.2.2.1 MICROFLUID BED REACTOR	80
5.2.2.2 PILOT PLANT	83
5.2.2.3 DEMONSTRATION PLANT	83
5.2.2.4 SUMMARY OF OBSERVATIONS ON THE SCALE-UP	90
5.2.3 MTO REACTION MECHANISMS	95
5.2.4 MTO PRODUCT ANALYTICAL METHOD	95
6. APPARATUS, MATERIALS AND PROCEDURE	98
6.1 METHANOL FEEDING SYSTEM	100
6.2 VIBRATION SYSTEM	102
6.2.1 VIBRATION SUPPORT STRUCTURE	102
6.2.2 GENERATION AND MEASUREMENT OF VERTICAL	

VIBRATION	107
6.2.3 CONCLUDING REMARKS	108
6.3 EQUIPMENT DEVELOPMENT	109
6.3.1 BASIC DESIGN DIMENSIONS OF THE MICROREACTOR	110
6.3.2 MATERIAL SELECTION	122
6.3.2.1 MATERIAL OF CONSTRUCTION	130
6.3.2.2 DISTRIBUTOR MATERIAL	131
6.3.2.3 GASKET MATERIAL	134
6.3.2.4 INSULATION MATERIAL	135
6.3.3 METHOD OF HEATING	136
6.3.4 GLASS REFERENCE DUCT	137
6.3.5 VIBRATED BED MICROREACTOR SETUP	141
6.4 PRODUCT ANALYTICAL SCHEME	144
6.4.1 SAMPLING VALVE	144
6.4.2 GAS CHROMATOGRAPH	147
6.4.3 PACKED COLUMN	147
6.4.4 CARRIER GAS	150
6.5 OTHER MATERIALS AND SYSTEMS	150
6.5.1 CATALYST USED	152
6.5.2 MISCELLANEOUS	152
6.5.3 LAYOUT OF THE LABORATORY	153

6.5.4 SAFETY PRECAUTIONS AND EQUIPMENT	155
6.6 EXPERIMENTAL PROCEDURE	157
6.6.1 QUALITATIVE ANALYSIS OF MTO PRODUCTS	158
6.6.1.1 IDENTIFICATION OF PEAKS	159
6.6.1.2 REPRODUCIBILITY OF RETENTION TIMES	169
6.6.2 QUANTITATIVE ANALYSIS OF MTO PRODUCTS	174
6.6.3 OVERALL PROCEDURE FOR DATA ANALYSIS	183
7. RESULTS AND DISCUSSION	187
7.1 SENSITIVITY OF MTO REACTION TO AXIAL GAS DISPERSION IN THE MICROREACTOR	204
7.1.1 YIELD OF LIGHT OLEFINS	206
7.1.1.1 SAMPLE TIME	206
7.1.1.2 REACTION INDEX	213
7.1.1.3 PECLET NUMBER	224
7.1.1.4 SUMMARY OF OBSERVATIONS ON RESULTS	229
7.1.2 COMPOSITION OF MTO HYDROCARBON PRODUCT	231
7.2 ACCURACY OF MTO REACTION RESULTS	239
7.2.1 ANALYSIS OF USED HZSM-5 CATALYST	241
7.2.2 BLANK RUN	243
8. CONCLUSIONS	246
8.1 VIBRATED BED MICROREACTOR (VBMR) DESIGN	247

8.2 SENSITIVITY OF MTO REACTION TO GAS DISPERSION IN THE MICROREACTOR	247
8.2.1 YIELD OF LIGHT OLEFINS	250
8.2.2 SUITABILITY OF TURBULENT FLUID BED FOR MTO REACTION	253
8.2.3 COMPOSITION OF MTO HYDROCARBON PRODUCT	254
8.2.4 SIGNIFICANCE OF THE RESULTS	258
9. RECOMMENDATIONS FOR FURTHER STUDY	260
BIBLIOGRAPHY	264
APPENDIX A : DETAILED DRAWINGS OF VIBRATION SUPPORT STRUCTURE	271
APPENDIX B : DESIGNS OF VIBRATED BED MICROREACTOR	289
APPENDIX C : ANALYSIS OF REACTION INDEX	323

LIST OF ILLUSTRATIONS

Figure 1.1: A simplified sketch of a commercial-scale turbulent fluid bed reactor	3
Figure 1.2: A simplified sketch of the vibrated bed microreactor	8
Figure 1.3: Methanol-To-Olefins reaction path	10
Figure 2.1: Typical stages in the design and testing of a solid catalyst	23
Figure 3.1: Geldart's classification of solids	27
Figure 3.2: Fluidization map for gas-fluidization of Group A powder	29
Figure 3.3: Effect of superficial gas velocity on gas-solid contacting in small-diameter laboratory-scale fluid beds	32
Figure 3.4: Effect of superficial gas velocity on gas-solid contacting for large-diameter commercial-scale fluid beds	33
Figure 3.5: Effect of Diameter on Reactor Efficiency during scale-up	38
Figure 4.1: A sinusoidal waveform traced by the vessel and the solid mass during a single vibrational cycle	48
Figure 4.2: A picture of the Coherent-Expanded vibration state	51
Figure 4.3: A plot of axial gas dispersion coefficient against superficial gas velocity for the microreactor and a fixed bed	55
Figure 5.1: Comparison of product distribution from MTO and MTG reactions	64

LIST OF ILLUSTRATIONS

Figure 1.1: A simplified sketch of a commercial-scale turbulent fluid bed reactor	3
Figure 1.2: A simplified sketch of the vibrated bed microreactor	8
Figure 1.3: Methanol-To-Olefins reaction path	10
Figure 2.1: Typical stages in the design and testing of a solid catalyst	23
Figure 3.1: Geldart's classification of solids	27
Figure 3.2: Fluidization map for gas-fluidization of Group A powder	29
Figure 3.3: Effect of superficial gas velocity on gas-solid contacting in small-diameter laboratory-scale fluid beds	32
Figure 3.4: Effect of superficial gas velocity on gas-solid contacting for large-diameter commercial-scale fluid beds	33
Figure 3.5: Effect of Diameter on Reactor Efficiency during scale-up	38
Figure 4.1: A sinusoidal waveform traced by the vessel and the solid mass during a single vibrational cycle	48
Figure 4.2: A picture of the Coherent-Expanded vibration state	51
Figure 4.3: A plot of axial gas dispersion coefficient against superficial gas velocity for the microreactor and a fixed bed	55
Figure 5.1: Comparison of product distribution from MTO and MTG reactions	64

Figure 5.2: Skeletal diagram of the ZSM-5 unit cell	68
Figure 5.3: Pore sizes in straight channels and sinusoidal channels of the ZSM-5 catalyst	69
Figure 5.4: ZSM-5 catalyst exhibits (a) reactant selectivity, (b) transition state selectivity and (c) product selectivity	72
Figure 5.5: MTO reaction path and the reaction index	78
Figure 5.6: Effect of $\text{SiO}_2/\text{Al}_2\text{O}_3$ on the olefin yield	81
Figure 5.7: Illustration of the Micro fluid-bed reactor	82
Figure 5.8: Illustration of the 4 BPD fluid-bed Pilot plant	84
Figure 5.9: Illustration of the 100 BPD Demonstration plant	85
Figure 5.10: Plot of relative catalyst activity against total on-stream hours of operation (TOS) during operation of 100 BPD Demonstration plant	87
Figure 5.11: Effect of temperature on methanol conversion in 100 BPD Demonstration plant	88
Figure 5.12: Effect of pressure on methanol conversion in 100 BPD Demonstration plant	89
Figure 5.13: Olefins Yield from Micro Fluid-bed reactor and 4 BPD Pilot plant at 482 C and 103 kPa	91
Figure 5.14: Olefins Yield from 4 BPD Pilot plant and 100 BPD Demonstration plant at 500 C and 250 kPa	93
Figure 6.1: Overall setup of the experimental apparatus	99

Figure 6.2: Vibrated-bed system	103
Figure 6.3: Isometric drawing of the support structure	105
Figure 6.4: Top view of support structure and vibration table	106
Figure 6.5: A simplified sketch of the Vibration Table with hole patterns drilled to accomodate the microreactors	111
Figure 6.6: Assembly drawing of the final workable design of the microreactor	112
Figure 6.7: The microreactor assembled with cap screws	114
Figure 6.8: Various individual pieces which make up the microreactor ...	115
Figure 6.9: Views of the top half of the middle section namely (a) Isometric view, (b) Top view, (c) Side view and (d) Front view	116
Figure 6.10: Views of the bottom half of the middle section namely (a) Isometric view, (b) Top view, (c) Side view and (d) Front view	119
Figure 6.11: Views of the top half of the inlet section namely (a) Isometric view, (b) Top view, (c) Side view and (d) Front view	123
Figure 6.12: Views of the bottom half of the inlet section namely (a) Isometric view, (b) Top view, (c) Side view and (d) Front view	126
Figure 6.13 (a) : A sketch of the assembled Glass Reference Duct	139
Figure 6.13 (b) : Design dimensions of the aluminum plate	140

Figure 6.14: Sketch of apparatus setup in preparation for an experiment	143
Figure 6.15: Product sampling scheme	145
Figure 6.16: Block diagram of operation of the sampling valve	146
Figure 6.17: Layout of the laboratory	154
Figure 6.18: Typical Chromatogram for paraffins standard gas sample	166
Figure 6.19: Typical Chromatogram for a mixture of paraffins and olefins standard gas sample	167
Figure 6.20: Plot of Adjusted Retention Time against Boiling Point for standard gas samples of paraffins and olefins	168
Figure 6.21: Plot of log(Adjusted Retention Time) against Carbon Number for paraffins and olefins standard gas samples	170
Figure 6.22: Plot of Adjusted Retention Time against Boiling Point for data obtained from HP 5730A GC and PEA GC	173
Figure 6.23: Plot of log(Adjusted Retention Time) against Carbon Number for data obtained from HP 5730A GC and PEA GC	175
Figure 6.24: Plot of Peak Area against Amount for the standard gas sample which contained only olefins	177
Figure 6.25: Plot of Peak Area against Amount for a concentrated sample of ethylene	178
Figure 6.26: Plot of Peak Area against Amount for the standard	

gas sample which contained only paraffins	180
Figure 6.27: Plot of Peak Area against Amount for a concentrated sample of ethane	181
Figure 6.28: Block diagram of steps taken in the analysis of each product sample taken during an experiment	186
Figure 7.1: Transition from C-E to C-C state in high and low density glass beads	192
Figure 7.2: Typical Chromatogram (FID) for a product sample from VBMR-3 (horizontal duct length = 7.62 cm)	199
Figure 7.3: Typical Chromatogram (FID) for a product sample from VBMR-6 (horizontal duct length = 15.24 cm)	200
Figure 7.4: Typical Chromatogram (FID) for a product sample from VBMR-9 (horizontal duct length = 22.86 cm)	201
Figure 7.5: Plot of adjusted retention times against boiling point for olefins and paraffins in the product sample	202
Figure 7.6: Plot of log(adjusted retention time) against carbon number for olefins and paraffins in the product sample	203
Figure 7.7: Yield of Light Olefins observed in VBMR-3 (horizontal duct length = 7.62 cm) plotted against Sample Time	208
Figure 7.8: Yield of Light Olefins observed in VBMR-6 (horizontal duct length = 15.24 cm) plotted against Sample Time	209
Figure 7.9: Yield of Light Olefins observed in VBMR-9 (horizontal duct length = 22.86 cm) plotted against Sample Time	210
Figure 7.10: Yield of Light Olefins from 100 BPD Demonstration	

Plant plotted against Sample Time	212
Figure 7.11: Yield of Light Olefins observed in VBMR-3 (horizontal duct length = 7.62 cm) plotted against Reaction Index	215
Figure 7.12: Yield of Light Olefins observed in VBMR-6 (horizontal duct length = 15.24 cm) plotted against Reaction Index	216
Figure 7.13: Yield of Light Olefins observed in VBMR-9 (horizontal duct length = 22.86 cm) plotted against Reaction Index	217
Figure 7.14: Yield of Light Olefins from MRDC Bench-scale unit against Reaction Index	219
Figure 7.15: Yield of Light Olefins from MRDC 4 BPD Pilot plant against Reaction Index	220
Figure 7.16: Yield of Light Olefins from MRDC 4 BPD Pilot plant against Reaction Index	222
Figure 7.17: Yield of Light Olefins from 100 BPD Demonstration plant against Reaction Index	223
Figure 7.18: Yield of Light Olefins (max and min values) obtained from microreactors against Peclet Number	226
Figure 7.19: Yield of Light Olefins (max and min values) reported by MRDC plotted against Peclet Number	228
Figure 7.20 (a): A typical Chromatogram (FID) obtained during a Blank Run	244
Figure 7.20 (b): A typical Chromatogram (TCD) obtained during a Blank Run	245
Figure 8.1: MTO hydrocarbon product from the microreactors	

plotted against Peclet Number	249
Figure 8.2: Yield of Light Olefins from microreactors and from fluid-bed scale-up plotted against Peclet Number	252
Figure A.1: Isometric view of an assembled vibration support structure	272
Figure A.2: Welded H-beam structure for side walls	273
Figure A.3: Side walls for vibration support structure	274
Figure A.4: Side view of H-beam side walls	275
Figure A.5: Top view of H-beam side walls	276
Figure A.6: Front view of H-beam side walls	277
Figure A.7: Front and back walls made from C-beams	278
Figure A.8: Attachment of brackets to walls	279
Figure A.9: Details of bracket assembly	280
Figure A.10: Bottom plate showing hole pattern	281
Figure A.11: Top view of assembled vibration support structure with vibration table shown in center	282
Figure A.12: Vibration table (end plates not shown)	283
Figure A.13: Vibration table (shown with end plates)	284
Figure A.14: Vibration table (top view)	285
Figure A.15: Vibration table (front view)	286

Figure A.16: Vibration table (side view)	287
Figure A.17: Steel drive shaft	288
Figure B.1: Isometric drawing of the microreactor at 7.62-cm horizontal duct length	290
Figure B.2: Individual pieces which make up the microreactor	291
Figure B.3: Views of the top half of the middle section namely (a) Isometric view, (b) Top view, (c) Side view and (d) Front view	293
Figure B.4: Views of the bottom half of the middle section namely (a) Isometric view, (b) Top view, (c) Side view and (d) Front view	296
Figure B.5: Views of the top half of the inlet section namely (a) Isometric view, (b) Top view, (c) Side view and (d) Front view	299
Figure B.6: Views of the bottom half of the inlet section namely (a) Isometric view, (b) Top view, (c) Side view and (d) Front view	302
Figure B.7: Complete assembled microreactor	305
Figure B.8: Isometric drawing of the microreactor at 22.86-cm horizontal duct length	307
Figure B.9: Individual pieces which make up the microreactor	308
Figure B.10: Views of the top half of the middle section namely (a) Isometric view, (b) Top view, (c) Side view and (d) Front view	309

Figure B.11: Views of the bottom half of the middle section namely (a) Isometric view, (b) Top view, (c) Side view and (d) Front view	312
Figure B.12: Views of the top half of the inlet section namely (a) Isometric view, (b) Top view, (c) Side view and (d) Front view	316
Figure B.13: Views of the bottom half of the inlet section namely (a) Isometric view, (b) Top view, (c) Side view and (d) Front view	319
Figure B.14: Complete assembled microreactor	322
Figure C.1: Reaction Index observed in VBMR-3, (horizontal duct length = 7.62 cm) plotted against Sample Time	324
Figure C.2: Reaction Index observed in VBMR-6, (horizontal duct length = 15.24 cm) plotted against Sample Time	326
Figure C.3: Reaction Index observed in VBMR-9, (horizontal duct length = 22.86 cm) plotted against Sample Time	327
Figure C.4: Reaction Index observed in 100 BPD Demonstration Plant plotted against Sample Time	329
Figure C.5: Plot of Reaction Index observed in microreactors against Peclet Number	331
Figure C.6: Plot of Reaction Index, reported by MRDC, against Peclet Number	333

LIST OF TABLES

Table 4.1: List of Duct Lengths, Velocities and Peclet Numbers	58
Table 5.1: Material balance in fluid bed pilot plant for MTG Reaction	63
Table 5.2: Hydrocarbon yields from MicroFluid-Bed and 4 BPD Pilot plant	92
Table 5.3: Olefins yield from 4 BPD Pilot plant and 100 BPD Demonstration Plant	94
Table 6.1: Mechanical Properties of Aluminum, Stainless Steel and Copper	132
Table 6.2: Chemical Composition of the Aluminum Alloy	133
Table 6.3: Characteristics of the HayeSep D packed column.....	149
Table 6.4: Composition of grade 5.0 helium.....	151
Table 6.5: Standard gas sample of olefins.....	160
Table 6.6: Standard gas sample of paraffins.....	161
Table 6.7: Retention times obtained using isothermal temperatures and optimum oven condition which combined isothermal and temperature programmed steps	163
Table 6.8: Optimum oven conditions used.....	164
Table 6.9: Retention times obtained from HP 5730A GC and from PEA GC	172
Table 6.10: Correlations for the olefinic species investigated	179

Table 6.11: Correlations for the paraffinic species investigated	182
Table 7.1: Actual dimensions of the microreactors	189
Table 7.2: Operational conditions for experiments done in VBMR-3	195
Table 7.3: Operational conditions for experiments done in VBMR-6	196
Table 7.4: Operational conditions for experiments done in VBMR-9	197
Table 7.5: MTO hydrocarbon product obtained in VBMR-3	233
Table 7.6: MTO hydrocarbon product obtained in VBMR-6	234
Table 7.7: MTO hydrocarbon product obtained in VBMR-9	235
Table 7.8: Composition of MTO hydrocarbon product obtained in the fluid-bed scale up of the reaction	237
Table 7.9: Carbon and Hydrogen in used HZSM-5 catalyst sample performed by a commercial analytical laboratory	242
Table 8.1: Composition of MTO hydrocarbon product from microreactors	255
Table 8.2: Comparison of MTO hydrocarbon product obtained from microreactors with results from MRDC MicroFluid Bed and 4 BPD Pilot Plant	257

NOMENCLATURE

BPD : Barrels Per Day

MRDC : Mobil Research and Development Corporation

WHSV : Weight Hourly Space Velocity, hr^{-1}

VBMR : Vibrated Bed Microreactor

VBMR-3 : Vibrated Bed Microreactor (horizontal duct length = 7.62 cm)

VBMR-6 : Vibrated Bed Microreactor (horizontal duct length = 15.24 cm)

VBMR-9 : Vibrated Bed Microreactor (horizontal duct length = 22.86 cm)

C-E : Coherent-Expanded vibrated bed state

FCC : Fluid Catalytic Cracking

ZSM-5 : Zeolite-Socony-Mobil-5

MTG : Methanol-To-Gasoline

MTO : Methanol-To-Olefins

TCD : Thermal Conductivity Detector

FID : Flame Ionisation Detector

GC : Gas Chromatograph

PEA GC : Perkin Elmer Autosystem Gas Chromatograph

RI : Reaction Index

C : degree Celsius

Hz : hertz

kPa : kiloPascal

P_0 : atmospheric pressure

mm Hg : millimeter of Mercury

TOS : Total-On-Stream

D_{ax} : axial gas dispersion coefficient, cm^2/s

D_{mol} : molecular diffusivity, cm^2/s

U : superficial gas velocity, cm/s

ρ_{cat} : density of catalyst (compacted)

ρ_{gas} : reaction gas density

Pe_{ax} : axial Peclet Number (based upon length of reaction vessel),
dimensionless

L : maximum reactor length or bed height/depth or compacted bed
depth

z : unit dimension in reactor length, cm

z_0 : maximum vessel displacement

ω : angular frequency

- f : frequency, hertz
- t : time, second
- θ : phase angle of vibration
- a_0 : maximum amplitude of vibration, mm
- a : vessel displacement, a function of time
- g : gravitational acceleration, cm/s^2
- K : vibrational intensity factor
- t_c : instant of bed-vessel collision
- t_s : instant of bed-vessel separation
- c : concentration at time, t
- c_0 : initial concentration at time, $t = 0$
- μ : viscosity
- d_p : particle diameter

1. INTRODUCTION

Gas-solid fluidization, hereafter referred to as fluidization, is a chemical engineering unit operation which brings gas and solid into intimate contact, thereby providing a suitable environment for gas-solid catalytic reactions. Fluidization is achieved by flowing gas upward through a bed of solids with a gas velocity sufficient to overcome the weight of the solid particles, transforming the bed into a fluidlike state. Fluidized beds exhibit several features which make them attractive as chemical reactors. These features are closely related to the quality of intimate contact achieved between the gas and solids and the mixing of solids in the bed.

The intense gas-solid mixing characteristic of a fluid bed leads to uniform temperature within the reactor. This is desirable for reactions with strict demands on temperature control, such as (i) reactions which may be explosive outside a narrow temperature range, or (ii) reactions wherein hot spots, if present may lead to rapid deterioration and deactivation of an otherwise stable catalyst (Kunii and Levenspiel, 1991).

The ability to use fine catalyst particles is attractive since it minimizes mass and heat transfer limitations within the catalyst. Using a fluid-bed reactor permits easy addition and withdrawal of solids, advantageous for catalytic reactions in which the catalyst deactivates quickly and has to be

regenerated, so that fresh catalyst must be added in order to maintain constant catalytic activity in the fluid bed reactor.

1.1 TURBULENT FLUID BED SCALE-UP PROBLEM

Turbulent regime is characterized by an environment that is essentially homogeneous and bubble-free, wherein gas and solid catalyst are brought into intimate contact. Figure 1.1 depicts a turbulent fluid bed reactor.

In chemical and petrochemical industries, a reactor in which a fine catalyst powder is fluidized in the turbulent regime is important for conducting catalytic reactions on a commercial scale. Most commercial applications of fluid bed reactors for catalysis employ turbulent or fast fluidized beds (circulating beds) of fine (Geldart Group A) powders.

Despite significant advances in fluidization technology, the number of fluid bed processes in practice today is astonishingly low in light of their great economic significance for the chemical and petroleum industries, Squires et al. (1985). Much of the problem, which has led to a few fluid bed processes being commercialized, arises from a widely held notion that scale-up of a turbulent fluid bed is complicated and risky.



Figure 1.1: A simplified sketch of a commercial-scale turbulent fluid bed reactor.

Historically, this notion has arisen from two failures in scale-up of catalytic fluid bed reactors, for hydrocarbon synthesis and fluid hydroforming. These failures occurred in the early 1950's before practitioners of fluidization arts had: (i) discovered the transition from the bubbling regime to the turbulent regime, (ii) appreciated the importance of the vastly different behaviors of fluid beds of fine and coarse powders, and (iii) realized the significance of maintaining the turbulent regime in a catalytic fluid bed of a fine powder, (Squires, personal communication).

In general scale-up of a turbulent fluid bed process takes longer, is more expensive and abounds with risks and uncertainties for success, than that of a fixed bed process. It is primarily for this reason that industrialists eager to commercialize a chemical process have often shunned the use of fluid beds opting instead for the design of a fixed bed alternative. It is worth noting that only some 14-odd heterogeneous catalytic reactions have achieved commercial operation in fluid-bed reactors (Squires, personal communication).

Moreover it is difficult to adequately simulate the commercial-scale turbulent fluid bed reaction environment in a bench-scale model in the laboratory. A lot more can be said about the intricacies and problems involved in the scale-up of fluid beds, but will be shelved until chapter 3 where a detailed discussion on this issue will be presented.

1.2 PROPOSED NEW APPROACH TO FLUID-BED SCALE-UP

The reaction environment in a commercial-scale turbulent fluid bed is complex to describe theoretically. It is considered to be determined by a combination of factors, such as gas dispersion, solid dispersion (i.e. top-to-bottom mixing and/or circulation), and the unsteady state nature of the system due to the cyclic exposure of the solid catalyst to different gas atmospheres (e.g. varying concentrations of reactant gas and product gas in the gas phase). These factors can individually or in combination have a very significant impact on the overall performance of the reactor.

Of these factors, gas dispersion is chosen as the feature of interest. This does not mean that the other factors are not important, for they are essential for the true picture. However, for a first approximation, one can expect that the fluid bed system can be represented by a lumped-parameter gas axial dispersion coefficient, which represents the overall average value of the dispersion coefficient and is a mild function of solid mixing.

Gas dispersion will therefore in this study be considered a measure of the overall gas-solid contacting environment in the fluid bed.

The current thinking on the process development in fluid bed reactors suggests that much of the problem in scale-up can be attributed to the effect

of fluid dynamics upon reaction kinetics, (Squires et al, 1985). It is assumed that, the fluid-dynamic effects upon reaction kinetics in a commercial-scale fluid bed, may be analyzed in terms of a single dimension (i.e. position along the fluid bed's vertical axis) and in terms of a single parameter (i.e. axial Peclet Number) expressing the degree of gas dispersion along this axis (with the caveat that reaction kinetics may also depend upon top-to-bottom mixing of solid).

Knowledge of the sensitivity of a gas-solid catalytic reaction to gas dispersion is of utmost importance for successful design and scale up of a turbulent fluid bed reactor, Avidan et al. (1990).

1.3 VIBRATED BED MICROREACTOR (VBMR) CONCEPT

The discovery of the coherent-expanded (C-E) vibrated-bed state led to the design and development of a vibrated bed microreactor, which promises to be useful in determining the effect of gas dispersion on a gas-solid catalytic reaction.

The microreactor comprises a rectangular horizontal duct of variable length, with non-porous floor and walls, 12.7 mm in height and 25.4 mm in width, is charged with a 1 mm layer of catalyst. When the microreactor is subjected to vertical sinusoidal vibration, the 1 mm layer of catalyst powder expands

to a height of 12.7 mm, filling the duct during a portion of each vibration cycle, resulting in an intense mixing of the catalyst powder in the vertical direction and little or none in the horizontal (axial) direction.

Figure 1.2 shows a simplified sketch of the vibrated bed microreactor. It should be noted that (i) fluidization of the solid catalyst is achieved entirely by the mechanical vibration of the microreactor and (ii) reactant gas is flown horizontally through the microreactor in a cross-flow relationship with the solid catalyst. On the other hand fluidization of the solid catalyst in a fluid bed: (i) is achieved by flowing gas vertically upwards through the bed of solids, (ii) depends on the velocity of the incoming gas and (iii) the incoming gas and catalyst powder flow co-currently in the inside of the vessel, and counter-currently against the walls of the vessel.

Earlier research on cold-flow model of the microreactor showed that (i) shifting of catalyst powder from inlet toward the outlet was negligible at horizontal superficial air velocities up to 20 mm/s, (Thomas and Squires, 1989), (ii) the microreactor offers a gas-solid contacting environment in which there is no gas bypassing and (iii) most importantly that axial (horizontal) gas dispersion coefficient varies linearly with horizontal superficial gas velocity through the microreactor, (Benge, 1992). This result suggested that when weight hourly space velocity is fixed, the microreactor offers a capability to vary axial gas dispersion (axial Peclet Number) by simply varying horizontal duct length of the microreactor.

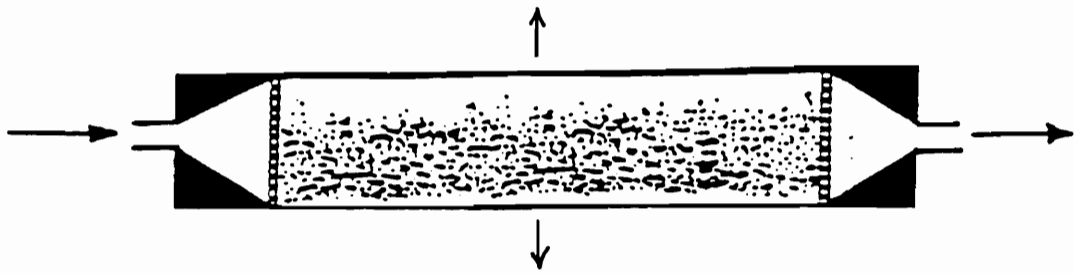


Figure 1.2: A simplified sketch of the vibrated bed microreactor.

A series of experiments in a microreactor of varying horizontal duct lengths, can furnish data on reaction outcomes (conversions, selectivities, etc.) at various axial Peclet Numbers, revealing the sensitivity of the reaction to this variable.

1.4 SENSITIVITY OF GAS-SOLID CATALYTIC REACTION TO AXIAL GAS DISPERSION IN THE MICROREACTOR

An ultimate test of the microreactor is to determine the sensitivity of a typical gas-solid catalytic reaction to axial gas dispersion by conducting it in a microreactor of varying horizontal duct lengths. Our association with Mobil Research and Development Corporation (MRDC) led to the use of Methanol-To-Olefins (MTO) reaction for this study.

Figure 1.3 shows the MTO reaction path. Methanol converts to water and hydrocarbons in the presence of HZSM-5 catalyst at 482 C, in a weight ratio of 56.4 and 43.6 percent, by stoichiometry. Hydrocarbon product consists of Light Olefins, Paraffins, Cycloparaffins and Aromatics. MTO reaction was discovered and scaled-up as a fluid bed process by MRDC in a Bench-scale, 4 BPD Pilot plant and 100 BPD Demonstration plant. Fluid bed scale-up results of the MTO reported by MRDC are presented in chapter 5.

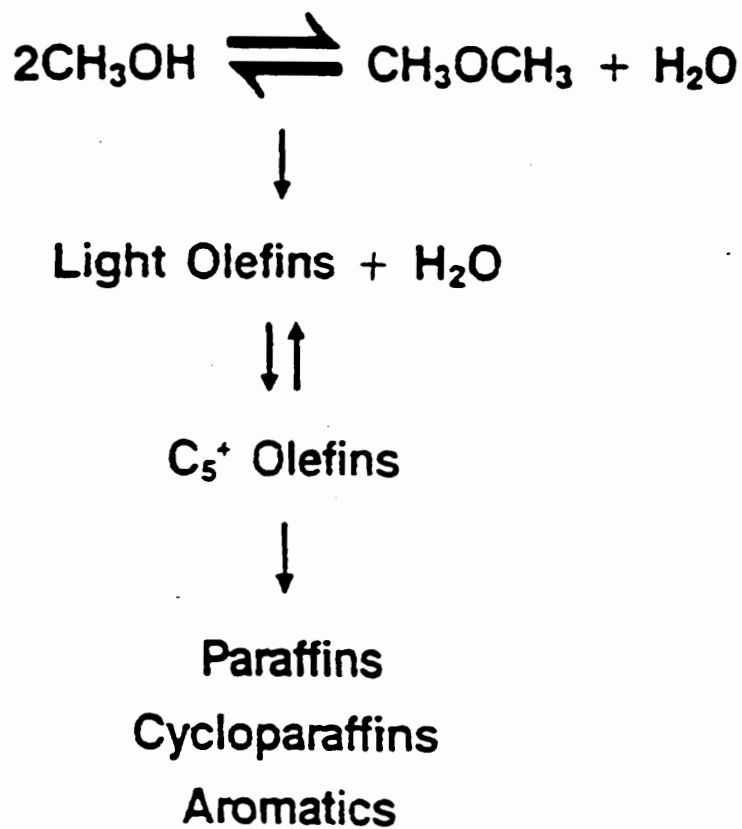


Figure 1.3: Methanol-To-Olefins reaction path.

MRDC provided us with a sample of the HZSM-5 catalyst which they used in 100 BPD Demonstration plant, on condition that the composition and/or fluidization properties of the catalyst would not be investigated or made public.

The cold-flow model of the microreactor used in the early work, is not suitable for high temperature work. The main goals of this research were to (i) design a microreactor capable of operating at 482 C and (ii) conduct the MTO reaction in the microreactor at a range of Peclet Numbers in order to determine its sensitivity to axial gas dispersion.

The work was challenging because: (i) high temperatures such as 482 C been used on vibration equipment for producing the C-E state, and (ii) appropriate product analytical equipment to handle the wide product slate from the MTO reaction was not readily available.

Our hope was that successful completion of this effort would provide proof that the vibrated bed microreactor can be a powerful tool for use in fluid bed reactor design and scale-up, as well as catalyst screening studies. The work was a pioneering effort, the first to use a vibrated bed in the C-E state for conducting a chemical reaction.

1.5 OVERVIEW OF THE DISSERTATION

The remainder of the dissertation is organized as follows. Chapter 2 details the goals and specific objectives of this research. It also discusses the significance of the microreactor in fluid bed research and development as well as in catalyst screening studies.

Chapter 3 discusses problems involved in the scale-up of turbulent fluid beds. This chapter is intended to demonstrate the obvious need for the vibrated bed microreactor.

Chapter 4 covers a complete description of the C-E state, and describes the origin of the vibrated bed microreactor concept with all of the earlier work done in the feasibility study of the concept. This chapter will shed some light on results which led to the present study.

Chapter 5 reviews the MTO reaction and presents results reported by MRDC in their fluid bed scale-up of the process.

Chapter 6 presents the experimental apparatus for conducting the study and describes the procedure by which data will be acquired and how it will be analyzed.

Chapter 7 presents the results of this research study. Results obtained from conducting MTO reaction in microreactors of three different horizontal duct lengths are presented and compared with fluid bed results reported by MRDC.

Chapter 8 gives major conclusions of the work undertaken in this research program, and discusses significance of the results.

Chapter 9 concludes by making recommendations regarding possible future work on the microreactor.

2. SCOPE OF THE STUDY

This chapter presents: (i) the goals and specific objectives of the research program, (ii) basic principles underlying the experimental program and (iii) significance of the microreactor to fluid bed process research and development as well as to heterogeneous catalysis research.

2.1 RESEARCH GOALS

Discovery and elucidation of the C-E vibrated bed state led to a design of a microreactor. Tracer gas studies done earlier in a cold-flow model of the microreactor, revealed that axial gas dispersion coefficient in the microreactor varies linearly with superficial gas velocity, implying that axial gas dispersion (hence Peclet number) varies with horizontal duct length when weight hourly space velocity is kept constant (Benge, 1992). This result suggests that the microreactor may provide the means of testing the sensitivity of a gas-solid catalytic reaction to gas dispersion.

In the proposed research, the sensitivity of Methanol-to-Olefin (MTO) reaction to gas dispersion will be determined. The first goal of the work is to design a microreactor capable of operating at 482 C required for the MTO reaction.

The second and ultimate goal is to determine the sensitivity of MTO reaction to axial gas dispersion using the microreactor. MTO reaction will be conducted in the microreactor at several gas dispersions (or Peclet Number). Results of such tests (e.g. conversions, selectivities) will be plotted versus Peclet Number to provide information on the sensitivity of the process to gas dispersion.

2.2 RESEARCH OBJECTIVES

The design of a microreactor will involve the following objectives listed below.

- select material of construction which can withstand high temperature, without losing its integrity and/or changing its physical properties.
- find reliable means of heating the microreactor uniformly, maintain the desired temperature (482 C) constant, minimize heat loss by convection and radiation.
- find some way of checking (by visual inspection) the state of vibration of the catalyst in the microreactor, so that corrective measures can be taken quickly without interrupting the experiment, if the catalyst is not vibrating in the C-E state.

Determining the sensitivity of MTO reaction to axial gas dispersion in the microreactor will involve the following objectives listed below.

- design three microreactors with horizontal duct lengths of 7.62 cm, 15.24 cm and 22.86 cm.
- establish appropriate MTO reaction product sampling and analytical technique using the basic equipment at our disposal.
- establish a safe way of handling and disposing of toxic reaction products.
- find a reliable way of feeding methanol to the reactor.
- determine ways of handling the data (to be able to do qualitative and quantitative analysis).

2.3 METHODOLOGY

The MTO reaction will be carried out at a temperature of 482 C, atmospheric pressure and at the weight hourly space velocity (WHSV) of one. Reaction product from MTO is water and hydrocarbons. Our main research interest is on the hydrocarbon product which consists of varying amounts of Olefins, Paraffins, Cycloparaffins and Aromatics. We will be monitoring light olefins which include ethylene, propene, 1-butene, 1-pentene and 1-hexene and paraffins which include methane, ethane, propane, n-butane, n-pentane and n-hexane.

2.3.1 OVERALL PLAN OF STUDY

Three microreactors with horizontal duct lengths of 7.62 cm, 15.24 cm and 22.86 cm will be designed. MTO will be conducted in each microreactor in turn.

During the experiment, a product sample will be taken at a particular time and put through a Gas Chromatograph fitted with both Thermal Conductivity Detector for detection of oxygenates and Flame Ionisation Detector for detection of hydrocarbons. All the resulting signals from the detectors will be integrated and displayed by integrators.

Most of the signal peaks displayed by the integrators will be identified by their retention times. The identified signal peaks for light olefins and paraffins will be selected for quantitative analysis. Weight ratio of propane to 1-propene will be computed and referred to as a reaction index (defined by MRDC in their analysis of the data).

Several product samples will be taken and analyzed as indicated above, throughout the experiment. At the end of the experiment the yield of light olefins will be plotted against; (i) sample time and (ii) reaction index. A table will be made that shows amounts of individual olefinic and paraffinic species obtained during the experiment.

MTO reaction will be conducted in each of the three microreactors in turn and data be obtained, analyzed and plotted as indicated above. Once all of

the data from each microreactor is in, a plot of yield of light olefins versus Peclet Number will be made. The plot is significant because it will show the effect of axial Peclet Number (axial gas dispersion) on the yield of light olefins for this reaction.

2.3.2 COMPARING MICROREACTOR DATA WITH FLUID BED DATA

The reaction environment (i.e. gas-solid contacting) in a fluid bed is "complex". It is defined by a combination of gas dispersion, solid dispersion (top-to-bottom mixing and/or circulation) and an unsteady state nature (catalyst is cyclically exposed to different gas atmospheres).

The microreactor offers a "simple" reaction environment characterized only by gas dispersion. There is no back to front solid mixing in the microreactor. It will provide data obtained in an environment characterized by only gas dispersion in a single dimension, horizontally.

Scale-up of the MTO process done by Mobil Research and Development Corporation (MRDC) provides data obtained in a typical fluid bed environment, characterized by a combination of factors mentioned above. A fluid bed scale-up of the MTO reaction was done by MRDC in a Bench-scale, 4 BPD Pilot plant and 100 BPD Demonstration plant wherein the Peclet Number was 14, 10 and 7 respectively.

The data obtained from conducting MTO reaction in a microreactor will be compared with data reported by MRDC from their fluid bed scale-up. This comparison will help to bring out the effect of all factors which define the reaction environment in a fluid bed and point out the validity of the assumption that fluid dynamics effects upon reaction kinetics in a fluid bed can be represented primarily by gas dispersion in a single dimension.

2.4 SIGNIFICANCE OF THIS WORK

A successful completion of this exercise will advance use of the vibrated bed microreactor as a tool to determine the sensitivity of a gas-solid catalytic reaction to gas dispersion. The microreactor will offer opportunity for quick, inexpensive determination of the sensitivity of a gas-solid catalytic reaction to gas dispersion.

Knowledge of the sensitivity of a gas-solid catalytic reaction to gas dispersion has been identified as being the most critical information to have for a successful turbulent fluid bed reactor design and scale-up, Avidan, (1990).

The microreactor which will be designed in the present research will be capable of conducting studies to determine the sensitivity of a gas-solid

catalytic reaction to axial gas dispersion. Other potential uses of the microreactor may include conducting studies to determine the effect of temperature and/or weight hourly space velocity on the conversion of a gas-solid catalytic reaction. These studies are commonly done in scale-up of fluid beds, and also in catalyst screening studies.

The researchers hope that a successful completion of this exercise will provide sufficient proof that the vibrated bed microreactor may be a powerful tool for use in:

- (i) fluid bed reactor design and scale-up, and
- (ii) catalyst screening studies.

2.4.1 FLUID BED REACTOR DESIGN AND SCALE-UP

It is envisaged that this determination (sensitivity of the gas-solid catalytic reaction to axial gas dispersion) will be crucial at an early stage in the development of a fluid bed process. For instance before the actual scale-up of a commercially-attractive gas-solid catalytic reaction can begin, data from gas dispersion sensitivity study will indicate the appropriate reactor type to use, between a fixed bed and a fluid bed.

Certain gas-solid catalytic reactions are better suited for conducting in a fluid bed than in a fixed bed. A gas-solid catalytic reaction that is "very

sensitive" to gas dispersion will be difficult to scale up in a fluid bed because of variations in the degree of gas dispersion in various scales of operation (e.g. bench scale, pilot plant, demonstration plant). This knowledge should help to give greater confidence in scaling up a gas-solid catalytic process.

2.4.2 CATALYST SCREENING STUDIES

Catalyst screening studies considered, may involve testing and studying: (i) a new catalyst formulation for an existing commercial-scale turbulent fluid-bed process, or (ii) the suitability of a known catalyst in a new process or (iii) in some cases an entirely new process which is commercially attractive made possible by a discovery of a new catalyst formulation. Figure 2.1 shows typical stages in the design and testing of solid catalysts (Trimm, 1980).

Often samples of a new formulation of a catalyst are available only in small quantities, since their preparation is typically done in smaller batches. It is quite expensive to test a new catalyst formulation on a large scale, where the test may require hundreds of grams of the sample. To obtain a full appraisal of catalyst activities and selectivities the catalyst sample needs to be tested in an environment comparable if not identical to that of the commercial-scale process.

Catalyst screening studies performed as is commonplace in fixed beds or bubbling beds is risky especially for catalysts destined for use in commercial-scale turbulent fluid bed reactors, because the gas solid contacting patterns are not identical. If the smaller-scale unit cannot simulate the commercial reactor very well, then there is likely to be poor catalyst selection. The microreactor offers a better alternative to the use of fixed beds or bubbling beds for the catalyst screening studies.

If the vibrated bed microreactor concept succeeds, it will be a substantial contribution to fluid bed process development and to heterogeneous catalysis research in general.

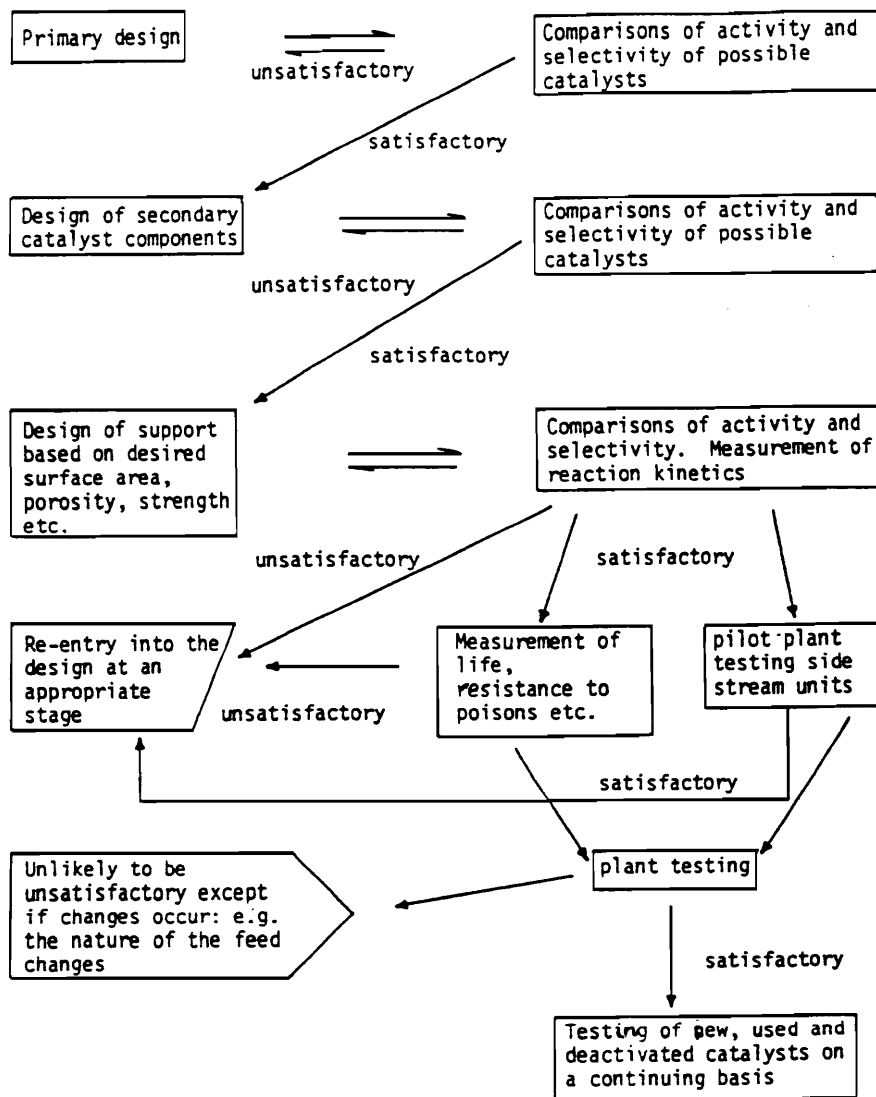


Figure 2.1: Typical stages in the design and testing of solid catalysts (Trimm, 1980).

3. SCALE-UP OF TURBULENT FLUID BED

In the Chemical Process Industry and Petrochemical Industry, a turbulent fluid bed reactor is important for conducting catalytic reactions on a commercial scale. The turbulent fluid bed reactor creates an environment that is essentially homogeneous and bubble-free, wherein gas and solid are brought into intimate contact. Use of the catalytic turbulent fluid bed reactor, however, has been limited, despite its potential, due to a widely held belief that scale-up of a turbulent fluid bed is complicated, risky and expensive.

Scale-up studies are usually done in order to study the feasibility of commercializing a newly discovered catalytic process. These studies involve predicting the conversion in a commercial scale unit from kinetic rate data obtained in a bench scale unit. It is difficult to simulate gas-solid contacting typical of a commercial scale turbulent fluid bed in a laboratory bench-scale because the gas-solid contacting pattern varies with the scale of operation. This tends to complicate scale-up of a fluid bed. Scale up of a fixed bed on the other hand, is simplified by the fact that bench scale tests may be run, employing a single full scale tube from a commercial multitube design. This arrangement offers less risks and gives a design engineer an improved sense of confidence for a successful scale-up.

Industrialists eager to commercialize a chemical process have often avoided the use of fluid beds and chosen instead the fixed bed alternative because the fixed bed process can be scaled up quicker and with less risk than its fluid bed counterpart. Consequently a return on investment in a fixed bed process can be realized sooner.

3.1 GAS-SOLID CONTACTING

It is appropriate at this stage to briefly review fluidization regimes and the corresponding gas-solid contacting in fluid beds. The overall gas-solid contacting environment in a fluid bed is determined by gas-flow patterns (gas mixing or dispersion), solid-flow patterns (solid mixing and/or circulation) and the unsteady-state nature of the system due to solid catalyst being cyclically exposed to different gas atmospheres (i.e. varying concentrations of reactant gas and product gas).

The quality of the gas-solid contacting environment depends on several factors such as gas and solid properties, gas and solid velocities, and hardware (e.g. vessel design, diameter, height, internals). The effect of solid properties on the quality of gas-solid contacting environment in a fluid bed will be discussed in this section whilst the effect of gas velocity and

hardware will be addressed later in a section devoted to scale-up of turbulent fluid bed reactors.

3.1.1 EFFECT OF SOLID PROPERTIES

Geldart (1973) presented a framework whereby solids are classified according to their particle size and density, for a specific fluid density. Figure 3.1 presents Geldart's classification which distinguishes between four groups of powder behavior. Only a brief overview of the characteristics and fluidization behavior of group A solids will be presented since they are of utmost interest in this research work. For a detailed discussion of this classification, the reader is referred to Kunii and Levenspiel (1991).

The present research work is based on HZSM-5 catalysts, whilst the earlier work in the group was done using FCC catalysts. Fluid Catalytic Cracking (FCC) catalysts and HZSM-5 catalysts are typical examples of Group A powders. Typical group A solids have a small mean particle size and/or low particle density. For instance FCC is characterised by broad particle-size distributions (20-130 micron), mean particle diameter sizes around 60-80 micron and densities of 0.8-1.6 g/ml (Avidan, 1982).

3.1.2 FLUIDIZATION BEHAVIOR

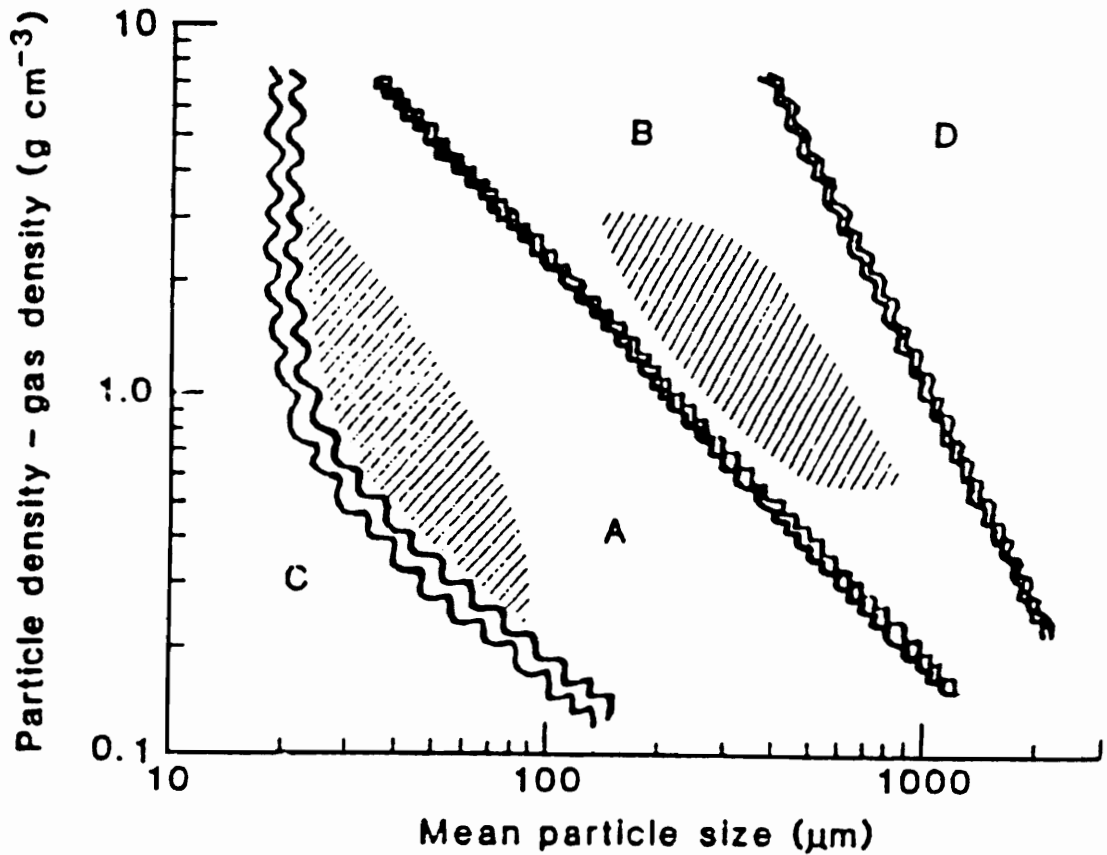


Figure 3.1: Geldart's classification of solids. Shaded regions roughly characterize the Group A aeratable powders and Group B sands. Group C is too cohesive for bubbling fluidization; Group D is spoutable. The boundary between A and B solids shifts to the right with increasing pressure. Squires et al. (1985) after Geldart (1973).

Fluidization map for a Group A solid is depicted in Figure 3.2. This figure illustrates how solid volume fraction, and hence appearance of the fluid bed, changes with varying gas velocity. Squires et al. (1985) discusses this figure and provides illustrative examples of fluid bed designs operating in the various fluidization regimes. The circled letters in the figure are used to identify the existence of varying solid volume fractions in these fluid beds (for meaning of these, see Squires et al., 1985). The fluidization regimes shown give rise to various forms of gas-solid contacting environments in a fluid bed.

At very low velocities, gas flows through void spaces between solid particles in the static (fixed) bed.

At velocities just beyond minimum buoyancy, (i.e. above minimum fluidization velocity) the particles begin to separate slightly, yielding uniform (particulate) expansion of the bed. Group A powder expands smoothly between minimum fluidization velocity and minimum bubbling velocity. Minimum fluidization velocity (or minimum buoyancy) is defined as the velocity at which the particles are just suspended by the upflowing gas.

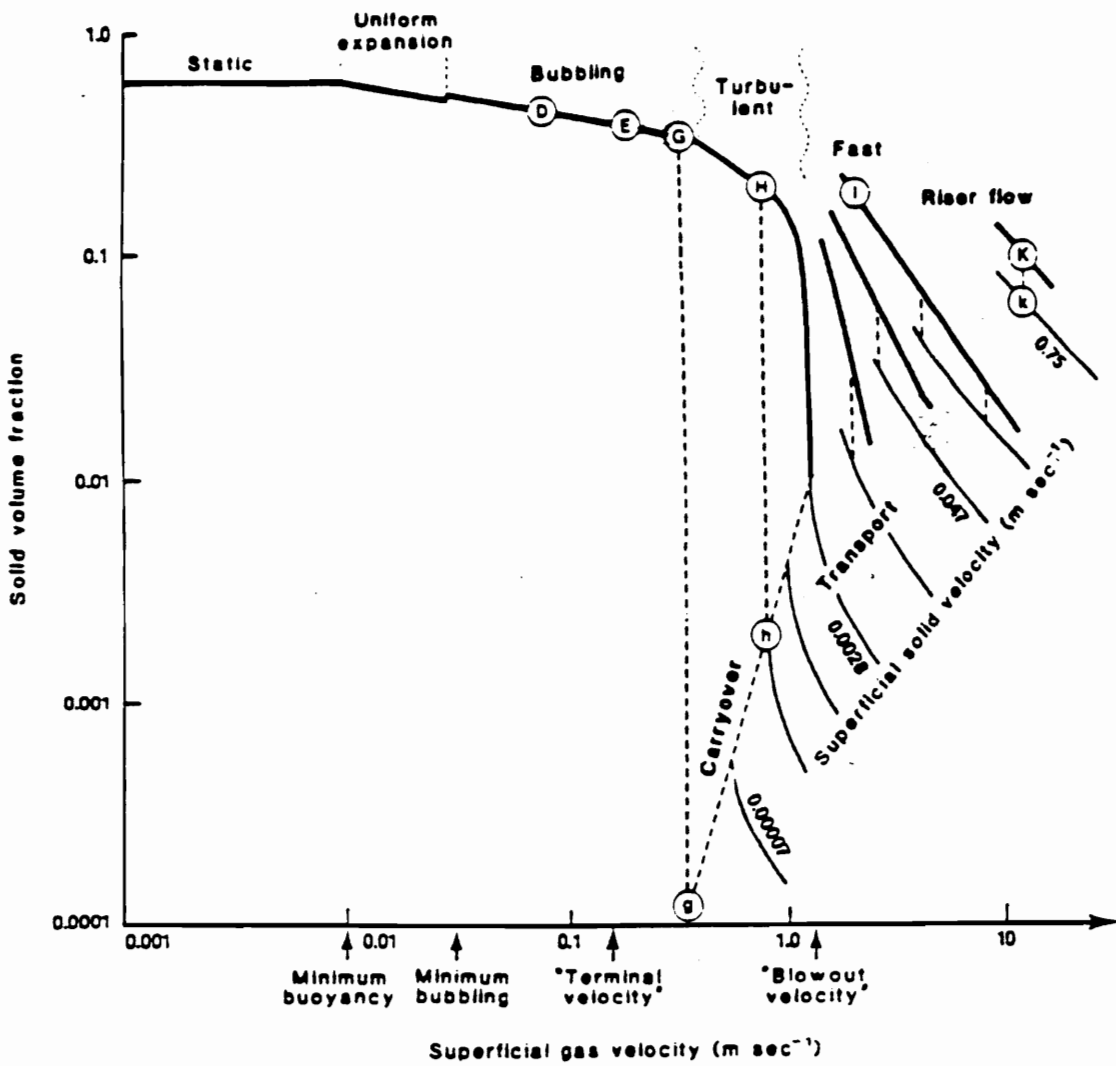


Figure 3.2: Fluidization map for gas-fluidization of Group A powder. The figure demonstrates how the solid volume fraction, and hence the appearance of the bed, changes with varying gas velocity. Adapted from Squires et al. (1985).

As the velocity is increased further, gas bubbles may be observed in the bed. The gas bubbles form, coalesce and grow in size as they rise up the bed. The velocity at which bubbles are first seen is termed the minimum bubbling velocity. This is the bubbling regime.

In conjunction with figure 3.2 one needs to look at Figure 3.3 and Figure 3.4 which illustrate gas-solid contacting in small-diameter laboratory-scale fluid beds and large-diameter commercial-scale fluid beds respectively. In beds of small diameter, the bubbling regime is characterized by bubbles that grow to fill the entire cross-section of the vessel, yielding slug flow, whilst in large-diameter fluid beds, the bubbling bed exhibits a heterogeneous (or two phase) character: a dense phase (or emulsion phase) corresponding to high solid density and a bubble phase (or simply bubbles) corresponding to regions of very low solid density. Large amounts of gas traverse the bed in the form of bubbles and have therefore little, if any, contact with the solid phase (i.e. catalyst).

As gas velocity is increased further, small-diameter beds experience severe elutriation of powder. On the other hand in large-diameter fluid beds the heterogeneous character of the bubbling bed increases through a maximum, then decreases to yield a more uniform homogeneous state. The homogeneous state is the turbulent fluidization regime, which is characterized on the whole by absence of large bubbles or voids.

Avidan (1982) provided a visual description of the turbulent fluid bed behavior as follows, "The main feature of the turbulent fluid bed is its overall homogeneous appearance. Bubbles appear and disappear rapidly, and are virtually in a constant state of breakage and coalescence. Moreover, they assume twisted shapes and a wide range of size distributions.

Occasionally large bubbles appear, but they usually disintegrate before travelling more than a meter or so in the bed. In some cases, the turbulent fluid bed assumes a more heterogeneous nature. The bubbles are usually larger when not enough catalyst fines are present in the bed, as is typical of FCC regenerators. If the fines concentration is large, as in most commercial turbulent fluid beds, the bubbles can be very small, and truly turbulent."

The topic of turbulent fluidization will not be reviewed extensively here as it is not the main emphasis of this work. For an exhaustive review on this topic consult Yerushalmi and Avidan (1985) and Yerushalmi (1986).

A further increase in gas velocity leads to the fast fluidization regime.

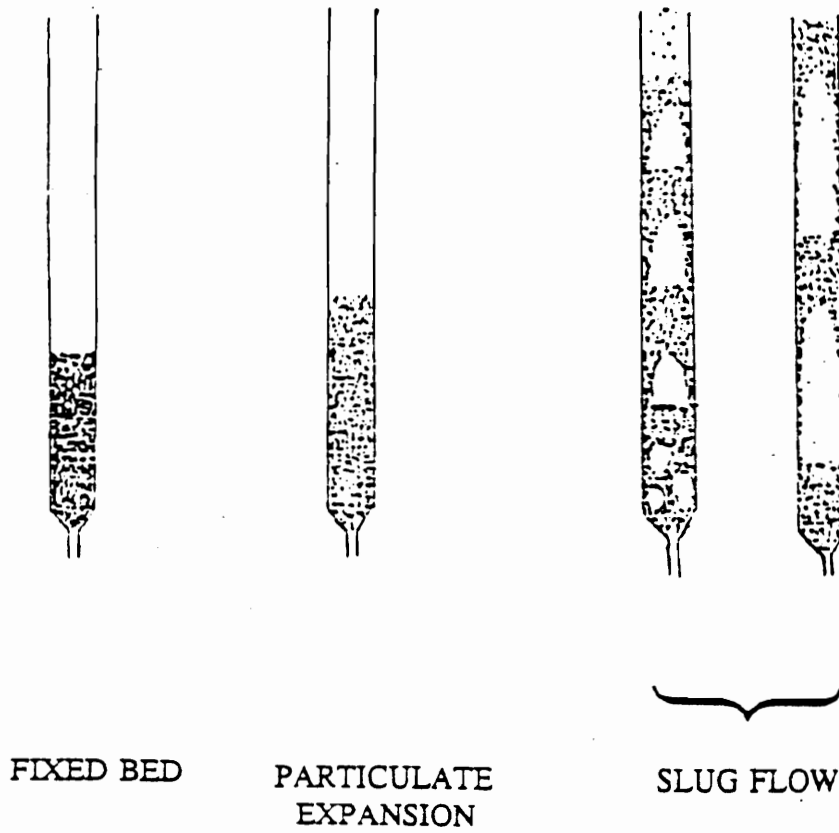


Figure 3.3: Effect of superficial gas velocity on gas-solid contacting in small-diameter laboratory-scale fluid beds. Superficial gas velocity is defined as the gas velocity measured on an empty vessel basis.

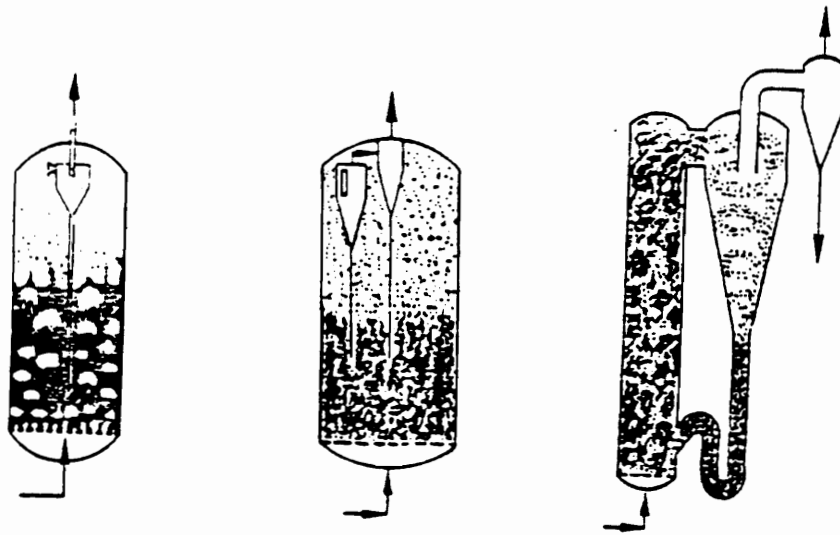


Figure 3.4: Effect of superficial gas velocity on gas-solid contacting for commercial-scale fluid beds.

3.2 THE CONVENTIONAL FLUID BED SCALE-UP PROCESS

The scale-up of a fluid bed process is a long term venture. It often involves operating one or all of the following ; (i) a bench scale microreactor, (ii) a pilot plant reactor, (iii) a demonstration plant reactor, and finally (iv) a commercial-scale reactor.

In order to ensure success in the design and scale up of a fluid bed process, (i) weight hourly space velocity, (ii) gas velocity and (iii) fluidization regime must be held constant during the scale up.

This ensures an identical reaction environment between the different scales of operation and eliminates the uncertainties and risks involved with using reaction kinetics data obtained from the bench scale, to design the larger scales. It is common in the development of a fluid bed process to experience difficulties in holding all of the abovementioned parameters constant between the different scales of operation.

3.2.1 GAS VELOCITY

It requires a very tall bench-scale unit to operate with the same space time and same fluidization regime as the commercial turbulent unit. This is

impractical because a bench scale unit is seldom designed with a great height. A lower height unit is used, with the gas velocity chosen so as to maintain a constant space time.

Elutriation of solids is an inescapable feature of most fluid beds and management of elutriated powder (and its return) is difficult in a bench-scale installation - another difficulty that tends to lead the experimenter toward use of an unrealistically low gas velocity.

The lower height bench-scale unit operating with a lower velocity often leads to a shift from the turbulent regime to bubbling regime, Avidan (1990).

There is a great difference in the gas solid contacting environment in a bubbling fluid bed and a turbulent fluid bed. A bubbling bed exhibit poor gas-solid contacting because of gross gas bypassing coupled with extensive gas backmixing while a turbulent fluid bed offers better gas-solid contacting efficiency. This difference in the gas solid contacting environment between the fluid bed regimes very often leads to different reaction kinetics observed, which when used to design a commercial-scale turbulent fluid bed may result in a poor overall reactor performance.

3.2.2 BED INTERNALS

Fluid bed internals (e.g. horizontal and vertical baffles), are sometimes used in a commercial-scale turbulent fluid bed, to give the bed a more homogeneous character. Catalyst circulation schemes are often employed in commercial scale turbulent fluid beds.

Both these cannot be used in bench scale work because of its small size. Such unavoidable differences between the bench scale and the commercial scale turbulent fluid bed tend to complicate the direct scale-up of these units.

3.2.3 CONCLUDING REMARK

It is difficult to adequately simulate the commercial-scale turbulent fluid bed reaction environment in a bench scale model. Figure 3.5 illustrates changes often encountered in the fluid bed reactor efficiency during scale-up. There are obviously risks involved in scaling up a process to the commercial scale turbulent fluid bed using data obtained in a bench unit.

3.3 THE AXIAL DISPERSION MODEL IN FLUID BED SCALE-UP

Avidan (1990), disagrees with the notion that fluid beds are inherently more difficult to scale-up. He suggests instead that "the difficulty of scale-up depends more on the reaction than on the hardware", maintaining that the problem is not that a fluid bed reactor is more difficult than a fixed bed to scale up rather, it is the sensitivity of the reaction to factors such as gas backmixing or gas dispersion that presents the problem to a successful scale up.

Gas dispersion is considered to be of paramount importance in characterizing the gas-solid contacting environment because it is measurable and can thus be used as a qualitative measure of this environment. Knowledge of the sensitivity of the reaction to gas dispersion is of utmost importance for successful design and scale up of turbulent fluid bed reactors, (Avidan, 1990).

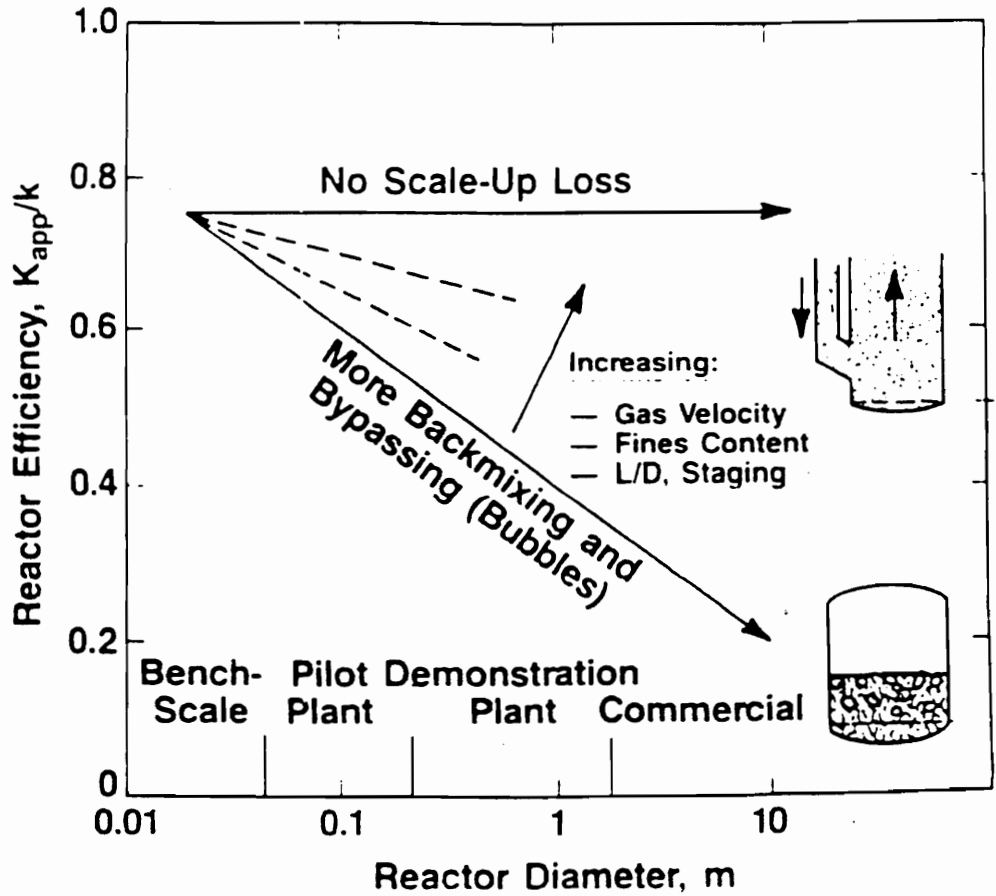


Figure 3.5: Effect of Diameter on Reactor Efficiency during Fluid-Bed Scale-Up.

The axial dispersion model has been widely applied to describe flow systems operated near plug flow where there is a finite amount of mixing that can be attributed to a diffusion or dispersion process superimposed on the plug flow velocity profile. It is known by several names such as the longitudinal-dispersed plug flow model, the axial dispersed plug flow model, the one-dimensional dispersion model, the axial dispersion model, or simply the dispersion model (Benge, 1992). For a complete and detailed review of the axial dispersion model, see Benge (1992).

The axial dispersion model is obtained from the convective diffusion equation for a fluid of constant density (Nauman and Buffham, 1983). We can arrive at the dimensionless axial dispersion model by assuming:

- (i) the reaction term to be negligible,
- (ii) the variation in velocity and concentration profiles in the radial direction to be negligible,
- (iii) bulk flow only in the axial direction,
- (iv) plug flow and
- (v) the axial dispersion coefficient to be constant.

$$\frac{\partial C}{\partial \theta} = \left[\frac{D_{ax}}{UL} \right] \frac{\partial^2 C}{\partial Z^2} - \frac{\partial C}{\partial Z} \quad (3.1)$$

Dimensionless parameters are defined as:

$$Z = z/L \quad (3.2)$$

$$C = c/c_0 \quad (3.3)$$

$$\theta = (tU/L) \quad (3.4)$$

The dimensionless group (D_{ax}/UL) is the vessel dispersion number and is a measure of the extent of axial dispersion (Levenspiel, 1972). Its inverse is the axial Peclet number.

The solution of the axial dispersion model requires an initial condition and two boundary conditions. Proper boundary conditions have been a source of debate (Nauman and Buffham, 1983).

Levenspiel (1972) presented the following solutions to the case of;

(i) small extents of dispersion (i.e. small departure from plug flow, high Peclet numbers). This solution gives a symmetrical C-curve.

$$C = \frac{1}{2\sqrt{\pi(D_{ax}/UL)}} \exp\left[\frac{-(1-\theta)^2}{4(D_{ax}UL)}\right] \quad (3.5)$$

(ii) large amounts of dispersion (i.e. mixed flow)

$$C = \frac{1}{2 \sqrt{\pi \theta (D_{ax} / UL)}} \exp \left[\frac{-(1 - \theta)^2}{4 \theta (D_{ax} UL)} \right] \quad (3.6)$$

3.3.1 USE OF AXIAL DISPERSION MODEL IN HOMOGENEOUS SYSTEMS

The axial dispersion model predicted conversion well in the 100 BPD Demonstration plant developed by MRDC. Conversion was predicted, based on apparent kinetics measured in the bench scale unit. The axial dispersion model was also used to predict effects of catalyst activity, weight hourly space velocity, and other operating conditions (Edwards and Avidan, 1986).

Avidan (1990) states that the model gives accurate prediction of conversion for homogeneous systems, (e.g. turbulent fluid bed) and fails in predicting conversions in strongly heterogeneous systems, (e.g. bubbling fluid bed). He points out that fluid bed systems of industrial importance seldom exhibit strong heterogeneities. This means that scale up of many reactions of practical interest, when conducted in a homogeneous turbulent fluid bed, can be treated essentially as a one dimensional problem requiring only the knowledge of a Peclet number.

Design and scale up of homogeneous turbulent fluid bed reactors requires a knowledge of the axial gas dispersion and reaction kinetics. Gas dispersion is chosen as the measure of gas solid contacting environment in a fluid bed. A fluid bed process may be more difficult to scale up when the reaction is sensitive to gas dispersion because the gas-solid contacting environment does vary with operating conditions of the fluid bed.

3.3.2 OPERATIONAL STRATEGY TO OBTAIN A HOMOGENEOUS BEHAVIOR IN A TURBULENT FLUID BED

Suppression of gas bubbles in the turbulent fluid bed, is important to the success of the homogeneous axial dispersion model and the scale-up itself, because homogeneous reactors are easier to scale up, Edwards and Avidan, (1986).

An operational strategy to use for achieving a homogeneous turbulent fluid bed is recommended by Squires et al. (1985). They indicate that bubbles are suppressed and the turbulent fluid bed takes on a more homogeneous appearance when operated ;

- (i) at high velocities, (i.e. greater than 0.3 m/s),
- (ii) with increased content of fines, (i.e. particles with diameters in the region of 40 micron),
- (iii) with increased length to diameter ratio, and

(iv) with horizontal baffles staging the bed.

Since turbulent fluid beds are typically designed and operated to approach homogeneity, the axial dispersion model has a wide application in these fluid bed systems.

4. VIBRATED BED MICROREACTOR CONCEPT

A bed of solid particles can be transformed into a fluid-like state in the absence of air flow (i.e. without aeration) by simply applying vertical mechanical vibration to the vessel containing the solids. Fluidization begins when vibrational acceleration exceeds gravitational acceleration.

Application of vibration to achieve fluidization is meaningful only in gas-solid beds, Mujumdar (1984). Vibration is a widely used technique in numerous physical processing operations in industry (e.g. Drying, Heating, Cooling, Agglomeration, Coating etc), when the particles handled are difficult-to-fluidize due to stickiness, wide polydispersity, agglomerating tendency, large size and extreme friability.

The term "vibrated bed", is herein used to refer to a bed of solid particles which is fluidized solely through mechanical vibration without the aid of an upward flow of fluidizing gas. Vibrated beds are defined as shallow when the ratio of the solid bed depth to its width is less than unity.

Dr Squires's research group has done extensive work in shallow vibrated beds of Group A powders. The earlier work was done using Fluid catalytic cracking (FCC) catalysts, Glass beads (of soda-lime, barium titanate) and Master beads, which all behave as Geldart's Group A powder. Everything

said about them applies to HZSM-5 catalyst being used in the present study, since it has characteristics consistent with Geldart's Group A powder. This chapter will present a brief review of the work, which led directly to this research program.

4.1 THEORY OF VIBRATION

Consider a vessel which is subjected to a vertical sinusoidal vibration. The vertical displacement of the vessel at any instant is given by:

$$a = a_0 \sin (2 \pi f t) = a_0 \sin (\omega t) = a_0 \sin (\theta) \quad (4.1)$$

Its velocity can be obtained by differentiating the above equation with respect to time, and is given by:

$$\frac{da}{dt} = a_0 \omega \cos (\omega t) \quad (4.2)$$

The vibrational acceleration is obtained by differentiating the velocity equation with respect to time, and is given by:

$$\frac{d^2 a}{d t^2} = -a_0 \omega^2 \sin (\omega t) \quad (4.3)$$

Gravity is a significant factor in vibrated bed systems. Vibrated beds are therefore described in terms of a dimensionless vibrational intensity parameter, which is defined as the ratio of peak acceleration of the vessel to gravitational acceleration. Vibrational intensity parameter is given by:

$$K = \frac{a_0 \omega^2}{g} = \frac{a_0 (2\pi f)^2}{g} \quad (4.4)$$

Vibrational intensity parameter is useful in representing the intensity of vibration to which the vessel is subjected. It is only when the bed of solid particles is vibrated at K-value greater than one, that it becomes mobile and takes on fluid-like properties. Vibrated beds are dynamic systems as can be surmised from the above equations.

4.2 VIBRATED BED DYNAMICS

The following section is intended to give an overview of vibrated-bed dynamics in order to illustrate several important phenomena exhibited by these beds.

There is a particular phase angle in the vibration cycle, where the vessel is accelerated downward faster than the gravitational acceleration of the solid particles. At this point the solid particles separate from the vessel floor and

move in concert, lifting together from the floor. The solid particles experience a period of free flight. The vessel continues downwardly until it reaches its amplitude of vibration and then comes right back up. The vessel finally meets and comes into contact with the bed of solid particles which stays in contact with the vessel floor until it separates again in the next vibrational cycle.

Figure 4.1 indicates a sinusoidal waveform that is traced by the vessel and the solid mass during a single vibrational cycle. The figure illustrates the displacements of the vessel and the bed of solid particles relative to each other, during a single vibration cycle. The bed of solid particles behaves as a single, coherent, plastic body and it does not bounce upon collision with the floor of the vessel (Mason, 1990).

A study of the pressure in the gap created when the bed of solid particles initially separates with the vessel and until they rejoin at the end of a vibration cycle was done and indicated that the pressure varies between a minimum (i.e. vacuum) and a maximum (i.e. compression). See Thomas (1988) for a detailed description of the study and its findings.

4.3 COHERENT-EXPANDED (C-E) VIBRATION STATE

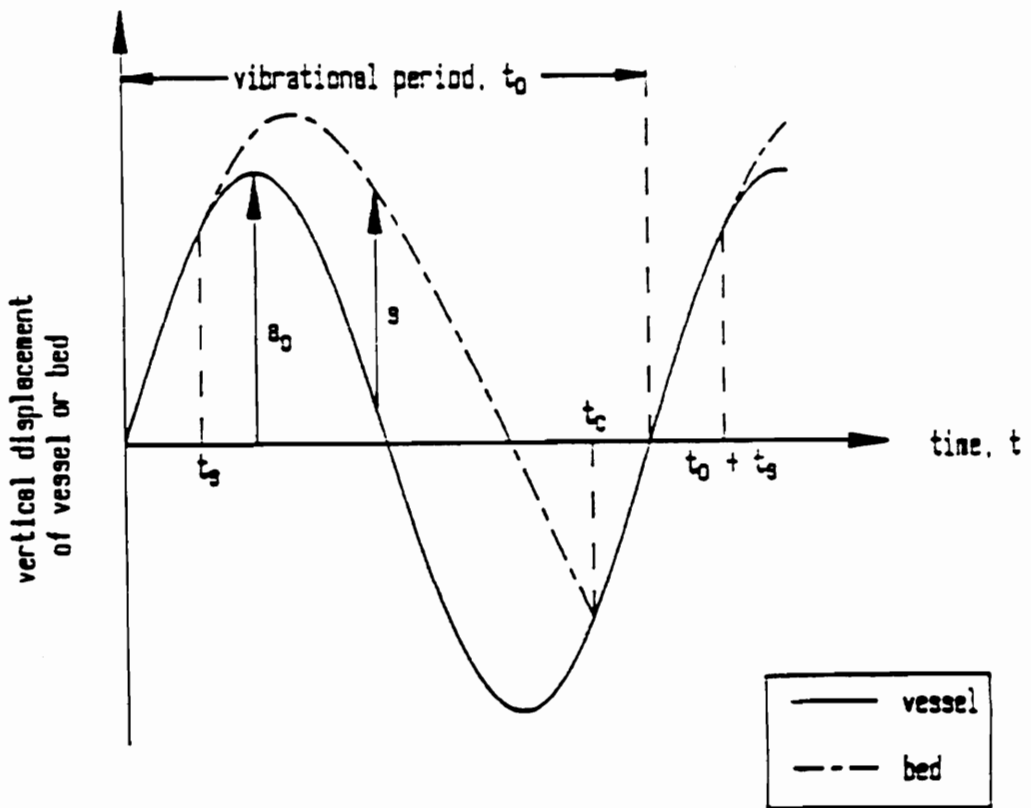
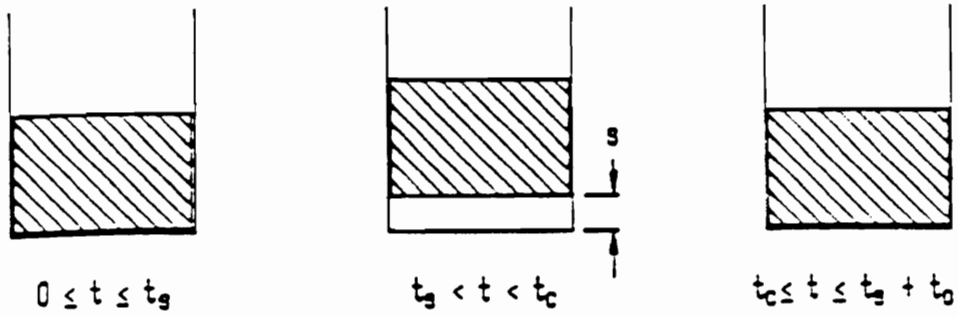


Figure 4.1: A sinusoidal waveform traced by the vessel and the solid mass during a single vibrational cycle. The figure illustrates the displacements of the vessel and the bed of solid particles relative to each other, during a single vibration cycle.

Squires's research team discovered several "states of vibration" (Thomas et al., 1989), one of which is the basis for the present research, whilst studying shallow particulate beds (i.e. bed depth less than 15 millimetres) vibrated at 25 Hz and an amplitude of several millimeters.

Thomas et al. (1989) reported how a shallow bed of particles resting on a horizontal plate that is vibrated sinusoidally in the vertical direction can display one of several "states": (a) A "vibrated bed" comprising a very few particles will present a "Newtonian state," in which particles bounce on the vibrating plate as individuals. There are two such states. (b) At a larger inventory of particles, the "coherent-expanded" state develops, wherein particles move in concert while undergoing vigorous vertical mixing and achieving order-of-magnitude increase in height of travel of particles relative to a compacted bed depth (i.e., before vibration commences). (c) At still larger particle inventory, the "coherent-condensed" state appears. In this state, the bed expands hardly at all (except, for fine particles, in a surface layer). Mixing is sluggish (except in a surface layer), and individual particles tend to remain for some time in a fixed relationship one to another.

Visual inspection of a vibrated bed in the Coherent-Expanded vibrated-bed (C-E) state showed intense gas-solid mixing in the vertical direction, with little or no horizontal solid-mixing. Figure 4.2 presents a picture of the C-E state. This figure indicates the behavior of an ultrashallow layer (960

micron bed depth) of FCC catalyst vibrated at a frequency of 25 Hz and an amplitude of 1.99 millimeters (i.e. vibrational intensity $K = 5$).

Thomas and Squires (1989), indicated that at phase angles between ca. 60 degree and ca. 150 degree the solid layer expands to a height of ca. 4 mm which is about 4 times the original compacted depth of the solid layer. At ca. 150 degree, the layer begins to lift and the gas starts penetrating the layer to form dimples at spacings of a few millimeters and to create a gap between layer and plate. Between ca. 230 degree and ca. 40 degree, the gas in the gap rushes outward through the powder, which expands to as much as 10 mm and reorganizes itself in bands about a millimeter in width, at spacings of a few mm. This repeats 25 times in each second.

The resulting catalyst mixing is intense in the vertical direction. To the eye, no solid mixing is evident in the horizontal direction, although some mixing probably occurs at a micro-scale.

The C-E state provides intense solid mixing patterns and appears likely to provide superb contacting of a solid with a gas. The intimate gas-solid contact in the C-E state is totally independent of the gas flow through the vibrated bed. This allows for the operation of the vibrated bed at a gas flow rate determined from reaction kinetics or heat and mass transfer considerations rather than by fluidization requirements.

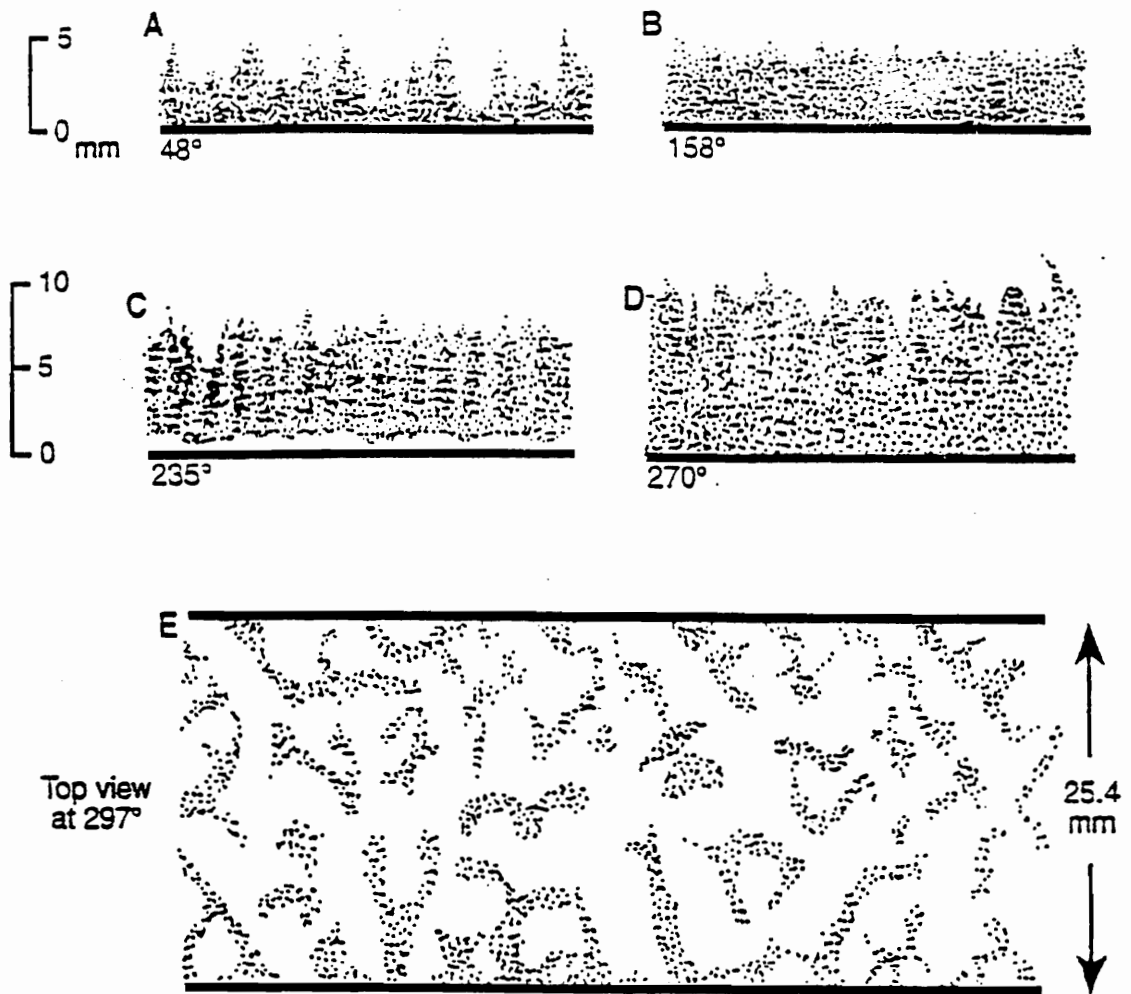


Figure 4.2: Coherent-expanded state in a vibrated bed of Group A powder. The upper four sketches are side views. The lower sketch is a top view. The drawings are tracings from photographs of a vibrated layer of FCC powder (0.96 mm in compacted state) at phase angles noted alongside the drawings (Thomas et al. 1989). Conditions: 25 Hertz; amplitude, 1.99 mm; maximum acceleration, five times gravity. If maximum acceleration is about six to seven times gravity, the layer expands to more than 13 mm at ~ 270 degree.

The discovery of the C-E state lead to the development of a microreactor which utilizes the gas solid contacting patterns inherent in this vibration state.

4.4 FEASIBILITY STUDY OF THE VBMR CONCEPT

Since the discovery and elucidation of the C-E state, the group has put its research effort in the design and development of a vibrated bed microreactor which exploits the gas-solid contacting efficiency characteristic of the C-E state. The microreactor would be vibrated at conditions that yield vibration of the catalyst in the C-E state thus providing an excellent gas-solid contacting environment due to the intense vertical mixing of the catalyst powder. The microreactor is perhaps the first technical use of the C-E state.

The microreactor designed comprises a rectangular horizontal duct of height 12.7 mm and 25.4 mm in width, supplied with a 1-mm-deep layer of a Group A powder, vibrated at an intensity such that the powder enters the C-E state and expands to fill the duct during a portion of each vibrational cycle. Gas flows into the microreactor, horizontally through the duct in a cross-flow relationship with the powder maintained in the C-E state.

4.4.1 AXIAL DISPERSION MODEL IN VBMR

Simple visual observation (best done under strobe lighting at a frequency slightly less than the vibrational frequency) makes it evident that the microreactor duct provides intimate gas-solid contacting and minimal gas bypassing; also, that axial gas dispersion in the duct may be treated appropriately by a simple axial dispersion model (Levenspiel, 1972; Wen et al., 1975), having axial Peclet Number, Pe_{ax} , as parameter:

$$Pe_{ax} = UL / D_{ax} \quad (4.5)$$

The Pe_{ax} of Equation 4.5 is a ratio of two times: time for dispersive relaxation over reactor length L (on the order of L^2 / D_{ax}) divided by fluid residence time (L/U). This Pe_{ax} is sometimes called a “reactor Peclet number” (Fogler, 1986). It should not be confused with the “particle” or “fluid Peclet number” (in which particle diameter replaces L in Equation 4.5), often used in treating gas dispersion in packed beds (Wen et al., 1975; Suzuki et al., 1972).

4.4.2 MAXIMUM GAS VELOCITY

The state of fluidization of the solid catalyst in the microreactor is induced entirely by the mechanical vibration of the vessel. This allows for the operation of the microreactor at a gas flow rate which can be chosen and varied with relative ease.

Thomas and Squires (1989) established the permissible range of gas velocity before the horizontal flow of gas moves catalyst particles toward the outlet of the microreactor's horizontal duct. For FCC powder, there is negligible displacement of solid from duct inlet toward outlet at horizontal superficial air velocities up to approximately 2.0 cm/s. For other gas environments, a maximum prudent velocity in the microreactor can be estimated by multiplying 2.0 cm/s by the ratio, air viscosity divided by viscosity of the other gas.

4.4.3 TRACER GAS STUDY

Pulsed-tracer experiments were done in the microreactor, using nonadsorbing tracers (viz. helium and argon) and an adsorbing tracer (sulfur hexafluoride) in nitrogen carrier. Results indicated that there was no gas bypassing in the microreactor. More importantly results indicated the axial gas dispersion varies linearly with superficial gas velocity. A detailed description of the study and its results are presented by Bengel (1992).

Figure 4.3 indicates the linearity of the axial gas dispersion coefficient with superficial gas velocity for the microreactor data and a fixed bed.

$$D_{ax} - \eta D_{mol} \text{ (cm}^2\text{/sec)}$$

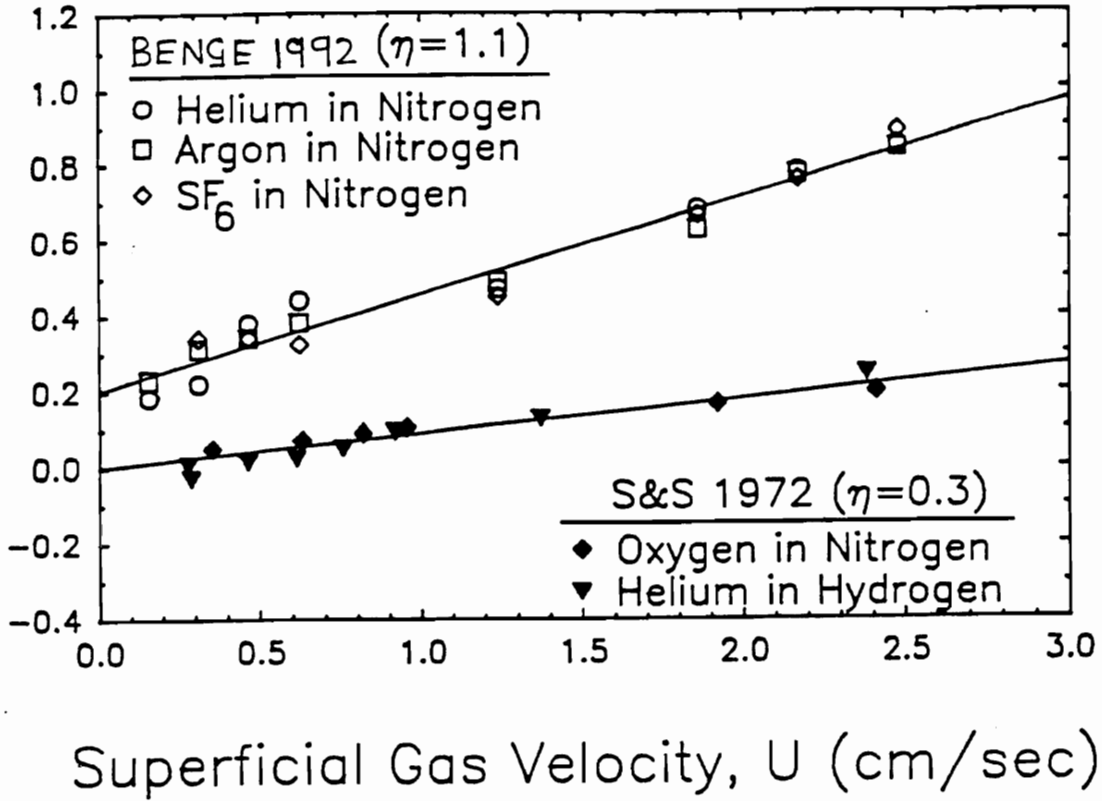


Figure 4.3: Axial gas dispersion coefficient against superficial gas velocity for the microreactor and a fixed bed. The microreactor data was obtained in the group and fixed bed data was reported by Suzuki and Smith (1972), (Benge, 1992).

The microreactor data was obtained in the group, (Benge 1992, Benge and Squires 1995, and Squires and Benge 1995), whilst the fixed bed data is published by Suzuki and Smith (1972). Axial gas dispersion coefficient obtained in the microreactor is larger than that from fixed bed and appears more sensitive to the superficial gas velocity.

An empirical expression for D_{ax} in the microreactor is:

$$D_{ax} = 0.20 + 1.1 D_{mol} + 0.257 U \quad (4.6)$$

At 1-mm compacted catalyst depth and 12.7-mm duct height, and with $S = U/L$, Equations 4.5 and 4.6 combine to give

$$Pe_{ax} = \frac{S L^2}{0.20 + 1.1 D_{mol} + 0.257 S L} \quad (4.7)$$

where $S = 0.1 \rho_{cat} WHSV / (1.27 \times 3600 \rho_{gas})$

It is evident that an experimenter may explore a wide range of Pe_{ax} by conducting a reaction at constant WHSV in several microreactors of various lengths.

4.4.4 PLANNING EXPERIMENTS IN VBMR

To develop an example of Equation 4.7's application for planning a series of microreactor experiments at several lengths of duct, consider the methanol-to-olefin reaction. At 482 C and atmospheric pressure, average D_{mol} of methanol and reaction products is $\sim 0.5 \text{ cm}^2 / \text{s}$. Compacted density of the ZSM-5 catalyst used in the reaction is 0.7534 g/cm^3 . At $\text{WHSV} = 1$, $S = 0.0318 \text{ s}^{-1}$. For several duct lengths, Table 4.1 lists velocities, and axial Peclet numbers (Squires and Bengel 1995).

Using atmospheric air and a typical, equilibrium FCC catalyst, Thomas and Squires (1989) were unable to detect a visible shift in catalyst toward the exit until the superficial air velocity exceeded 2.0 cm/s. The maximum prudent experimental velocity for conducting the MTO reaction at 482 C can be estimated by scaling this velocity for air by the ratio, air viscosity divided by methanol viscosity. The estimated velocity is ca. 1.4 cm/s.

At a ZSM-5 inventory affording a 1-mm-deep compacted layer (in absence of vibration), this maximum prudent velocity would permit an experiment at $\text{WHSV} = 1$ in a 44-cm-long duct. This duct affords a Pe_{ax} value beyond ~ 50 ; i.e. the duct affords something close to plug flow.

Table 4.1: List of Duct Lengths, Velocities and Peclet Numbers (From Squires and Bengtsson 1995)

Length, cm	Velocity, cm/s	Peclet Number
40	1.27	47.2
25	0.79	20.8
15	0.48	8.2
10	0.32	3.8

4.4.5 THE PRESENT STUDY

A microreactor was visualized in which the Peclet Number expressing gas dispersion along reaction path may be systematically varied, simply by varying the length of this path while maintaining a constant WHSV. A series of experiments in a microreactor of varying horizontal duct lengths, can furnish data on reaction outcomes (conversions, selectivities, etc.) at various Peclet Numbers, revealing the sensitivity of the reaction to this variable.

A gas-solid catalytic reaction for which a commercial-scale turbulent fluid bed reactor is appropriate, was sought for the study. Our association with Mobil Research Development and Corporation (MRDC) in earlier work led to our use of their Methanol-To-Olefins (MTO) reaction for the study. MRDC has reported a successful fluid bed scale-up of the MTO process. The process had been scaled-up from Bench-scale, to 4 BPD Pilot plant, and finally a 100 BPD Demonstration plant. As far as we know the process is ready for commercialization. Chapter 5 will present an overview of the MTO reaction and the reported results.

The ultimate goal of the present research program is to determine sensitivity of MTO reaction to axial gas dispersion. Successful completion of the present study will provide sufficient proof that the microreactor is a useful

tool for determining the sensitivity of a gas-solid catalytic reaction to axial gas dispersion.

Knowledge of the sensitivity of a gas-solid catalytic reaction to gas dispersion has been identified as being the most critical information to have for a successful turbulent fluid bed reactor design and scale-up, Avidan, (1990). If the vibrated bed microreactor concept succeeds, it will be a substantial contribution to fluid bed process development and to gas-solid catalysis research in general. It will have opened up an entirely new area of application for the vibrated bed systems. In the past vibrated beds were used primarily in the drying applications.

5. METHANOL-TO-OLEFINS (MTO) REACTION

Olefins, also known as alkenes, are a class of hydrocarbons characterized by existence of a carbon-to-carbon double bond in their structure. This class of hydrocarbons includes ethylene, propenes, butenes, pentenes, etc. They are commonly produced from petroleum and used primarily in the production of materials such as synthetic fibers, plastics, rubber, alkylate, aromatics and petrochemicals.

A process of producing olefins from methanol was discovered by Mobil Research and Development Corporation (MRDC) in the late 1970's. In the presence of HZSM-5 catalyst, at 482 C, methanol converts to water and a hydrocarbon mixture consisting of olefins, paraffins, cycloparaffins and aromatics. The reaction maximizes production of olefins, and does not proceed to form significant amounts of aromatics. It is referred to as **Methanol-To-Olefins (MTO)** reaction.

When the reaction is conducted at 371 C, it produces less olefins and maximum paraffins and aromatics. It is then referred to as **Methanol-To-Gasoline (MTG)** reaction.

Mobil conducts the MTO reaction at weight hourly space velocity (WHSV) of about 1, where conversion of methanol is complete. Incomplete conversion of methanol would be unacceptable in a commercial operation,

since the expense of recovering methanol from a methanol-water mixture, for a recycle of the unconverted methanol, would be prohibitive.

The conversion of methanol to hydrocarbons over HZSM-5 catalyst has a wide product slate which does not contain hydrocarbons with carbon number larger than 10 (Chang and Silvestri, 1987). Table 5.1 indicates typical material balance in fluid bed pilot plant for MTG reaction, conducted at 371 C, atmospheric pressure and weight hourly space velocity of one (Liederman et al, 1978). The product spectrum in MTO reaction and MTG reaction is similar and only varies in amounts (i.e. weight percent). Figure 5.1 shows a comparison of product distribution from MTO and MTG reactions (Socha et al, 1986).

The present research will investigate the sensitivity of MTO reaction to axial gas dispersion in the microreactor. Only the olefin yield will be monitored since it is the major component of the product stream. Olefinic product species beyond hexane are not significant enough to warrant monitoring during this research study.

Table 5.1: Typical material balance in fluid bed pilot plant for MTG reaction, conducted at 371 C, atmospheric pressure and WHSV of one (Liederman et al, 1978).

Material balance no.	26-01	25-10
MeOH charged (lb of MeOH/lb of cat.)	6	203
Product (wt % of charge)		
Methanol	0.32	1.92
Dimethyl ether	0.02	0.43
Hydrocarbons	42.40	43.20
Water	56.77	55.08
CO, CO ₂ , H ₂	0.15	0.23
	<u>99.7</u>	<u>100.8</u>
Hydrocarbons (wt % of hydrocarbons)		
Methane	0.93	0.77
Ethane	0.25	0.14
Ethylene	4.84	6.54
Propane	3.65	2.37
Propene	5.41	7.97
Isobutane	15.71	10.78
<i>n</i> -Butane	1.48	0.92
Butenes	4.64	6.24
Isopentane	12.36	10.07
<i>n</i> -Pentane	0.49	0.33
Pentenes	2.19	3.12
Cyclopentane	0.44	0.07
Methylcyclopentane	0.71	0.53
<i>n</i> -Hexane	4.06	5.42
Methylpentanes	5.46	5.40
Dimethylbutanes	0.99	1.00
Hexenes	0.26	0.47
Cyclohexane	0.03	0.25
C ₇ -PON	3.31	4.29
C ₈ -PON	2.89	3.91
C ₉ -PON	1.64	2.20
C ₁₀ -PON	0.11	0.27
Benzene	0.00	0.00
Toluene	1.38	4.03
Ethylbenzene	0.16	0.17
Xylenes	6.05	5.50
Trimethylbenzenes	8.39	7.20
Methylethylbenzenes	1.34	1.31
Propylbenzenes	0.02	0.03
1,2,4,5-Tetramethylbenzene	1.94	3.93
1,2,3,5,-Tetramethylbenzene	1.52	1.02
1,2,3,4,-Tetramethylbenzene	0.56	0.45
Other C ₁₀ -benzenes	1.36	1.07
C ₁₁ -Benzenes	1.72	0.33
Naphthalenes	1.14	0.01
Other aromatics	2.58	1.86

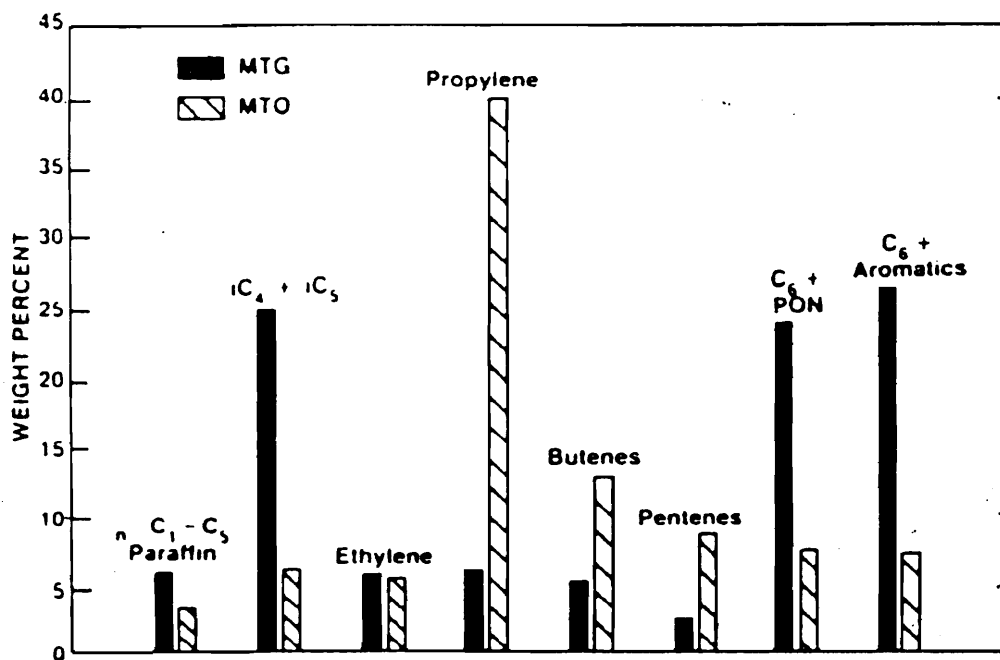


Figure 5.1: Comparison of product distribution from MTO and MTG reactions (Socha et al, 1986).

Conversion of methanol over HZSM-5 catalyst is a complex reaction, which necessitated an extensive search for information that would help provide a complete understanding of:

(i) the ZSM-5 catalyst particularly the preparation, crystal structure and properties (i.e. physical, chemical and catalytic); (ii) the MTO reaction, particularly the effect of temperature, pressure, catalyst (i.e acidity, binder etc.), quality of methanol feed, etc. on the product spectrum.

A major portion of the materials (i.e. publications, patents and reports) from MRDC covered results of the MTG reaction, whilst a small part gave some information on the MTO reaction. The information gathered was not sufficient to gain a complete understanding of the MTO process. A lot seems not to have been disclosed, understandably so because it is proprietary, not to be revealed to the competition. I looked for additional material, published by other researchers working outside of MRDC, that might shed light on any part of the MTO process.

5.1 A BRIEF REVIEW ON ZSM5 CATALYST

This section is intended to give a reader a general description of the ZSM-5 catalyst, in order to gain an appreciation of the material.

MRDC provided us with a sample of their ZSM-5 catalyst, with a condition that its composition and/or characteristics not be investigated and publicized. We declare in this document that we have truthfully adhered to the contract entered into by us with MRDC, when accepting the ZSM-5 catalyst. None of the material presented in this section came from an investigation of the MRDC sample, but was gathered from open literature (i.e. publications made by MRDC itself as well as by other researchers outside of MRDC).

5.1.1 BACKGROUND

Kerr and co-workers at MRDC synthesized a highly siliceous zeolite, the "Zeolite ZSM-5" or simply "ZSM-5". The acronym is derived from Zeolite Socony Mobil (Olson et al., 1980).

ZSM-5 is a silica-rich zeolite that has been synthesized with silica-to-alumina ratio ranging from about 20 to greater than 8000. The silica-to-alumina ratio represents the ratio in the rigid anionic framework of the zeolite crystal, and excludes aluminum in the binder or in cationic or other form within the channels.

5.1.2 CRYSTAL STRUCTURE

Zeolite materials are porous aluminosilicates. The dimensions of their pores can accept for adsorption only molecules of certain dimensions while rejecting those of larger dimensions, hence the name "molecular sieves".

They have a definite crystalline structure within which there are cavities and channels of uniform size. ZSM-5 zeolite is made up of a network of silicon and aluminum tetrahedra crosslinked by the sharing of oxygen atoms. The oxygen atoms are bonded to the silicon or aluminum atoms at the centers of the tetrahedra. The spaces between the tetrahedra are occupied by molecules of water prior to dehydration. The crystal is made up of linked tetrahedra consisting of 5-membered rings which join through edges to form chains. These chains connect to form sheets which lead to the 3-dimensional structure (Kokotailo et al., 1978). Figure 5.2 shows the skeletal diagram of the ZSM-5 unit cell.

The ZSM-5 catalyst has a pore dimension greater than about 5 Angstroms and pore windows of a size provided by 10-membered rings of oxygen atoms. The 10-membered rings of oxygen are formed by the regular disposition of tetrahedra making up the anionic framework of the crystalline aluminosilicate. ZSM-5 has a pore size intermediate of the small pore size, Erionite (3.8 by 5.2 angstroms), and the large pore size, Faujasite (7.4 angstrom), (Chang and Silvestri, 1987). Figure 5.3 shows pore sizes in the straight channels and sinusoidal channels of the ZSM-5 catalyst.

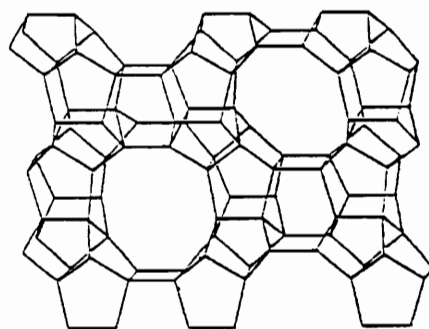
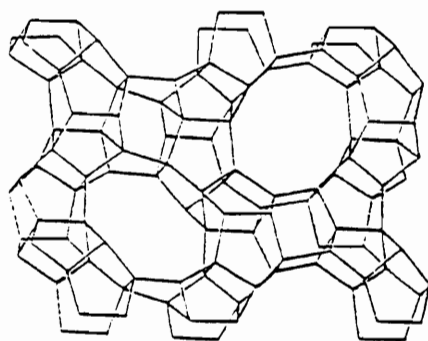


Figure 5.2: Skeletal diagram of the ZSM-5 unit cell (Kokotailo, 1978).

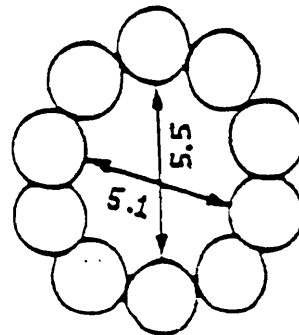
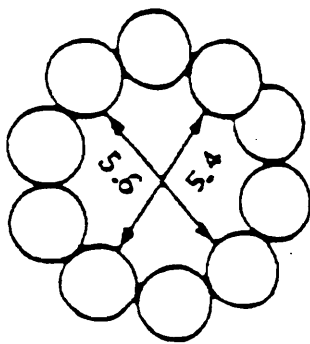
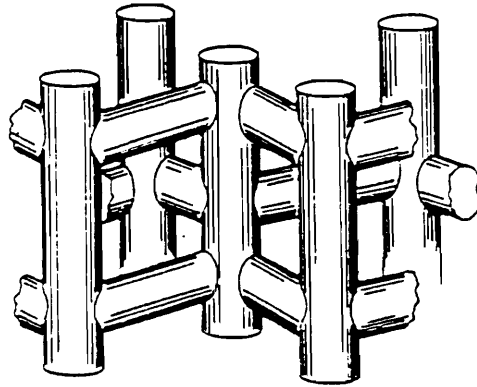


Figure 5.3: Pore sizes in the straight channels and sinusoidal channels of the ZSM-5 catalyst.

5.1.3 PROPERTIES OF ZSM-5 CATALYST

The ZSM-5 catalysts are members of a special class of zeolites exhibiting some unusual properties, which include:

- (i) retention of their crystallinity for long periods in the presence of steam at high temperatures. This environment induces irreversible collapse of the crystal framework of other zeolites such as zeolite X and zeolite A.
- (ii) exhibiting very low coke forming capability. They are thus conducive for use over longer times between regenerations. The regeneration process removes coke (i.e. carbonaceous deposits) by burning at higher temperatures to restore catalytic activity.

Physical, chemical, and catalytic properties of ZSM-5 catalysts are reported and discussed in terms of their structural and compositional dependence (i.e. silica-to-alumina ratio).

Physical properties of the ZSM-5 catalyst are essentially invariant with composition. These include properties such as shape selectivity, X-ray diffraction pattern, pore size and volume, framework density, and refractive index are primarily a result of the structural features. An important characteristic of the crystal structure of the zeolites is that it provides constrained access to, and egress from, the intra-crystalline free space of the catalyst. This makes the ZSM-5 catalyst extremely shape selective. They

exhibit reactant, transition state, and product selectivity as shown in Figure 5.4 (a), (b) and (c) respectively (Meisel, 1988; Davis, 1991).

Chemical properties of ZSM-5 vary with composition. These include properties such as ion exchange capacity, catalytic activity, and hydrophobicity. These properties vary linearly with aluminum content and extrapolate smoothly to an aluminum-free, pure silica ZSM-5, (Olson et al., 1980).

The catalytic activity of zeolites is attributed to framework aluminum atoms and cations associated with these aluminum atoms. ZSM-5 zeolites promote acid-catalyzed reactions. The acid activity originates with protons associated with the negatively charged aluminum (framework) tetrahedra. The acid activity of a series of ZSM-5 showed that the catalytic activity is a linear function of aluminum content. The correlation holds down to alumina levels as low as 100 ppm.

5.1.4 COMMERCIAL APPLICATIONS

Zeolites are utilized in a variety of ways to take advantage of their shape selectivity and many other useful properties. This new class of high silica zeolites is of considerable significance as catalyst material.

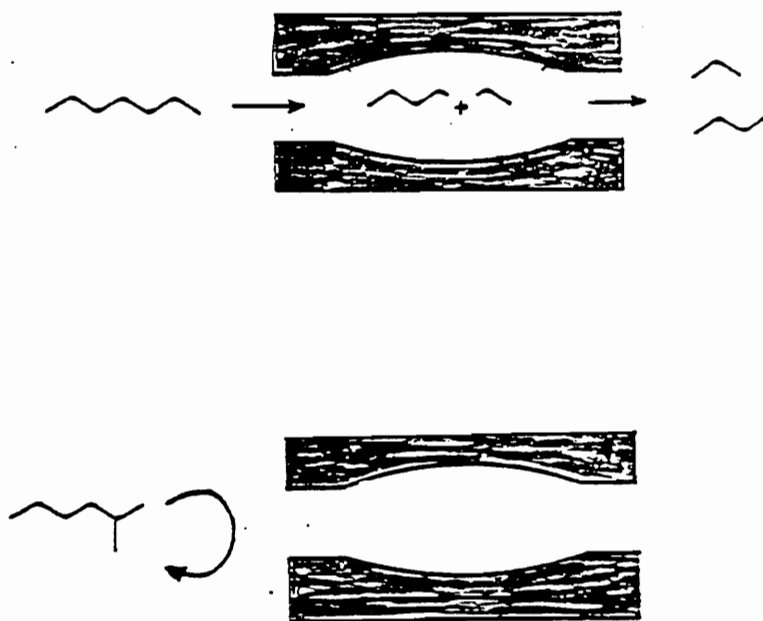


Figure 5.4 (a): ZSM-5 catalyst exhibits reactant selectivity which can be visualized as shown in the sketch (From Davis, 1991).

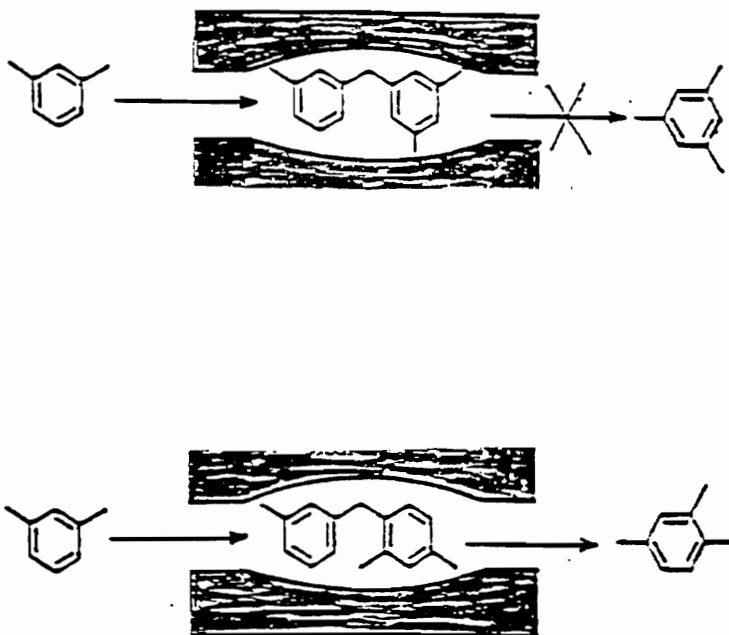


Figure 5.4 (b): ZSM-5 catalyst exhibits transition state selectivity which can be visualized as shown in the sketch (From Meisel, 1988)

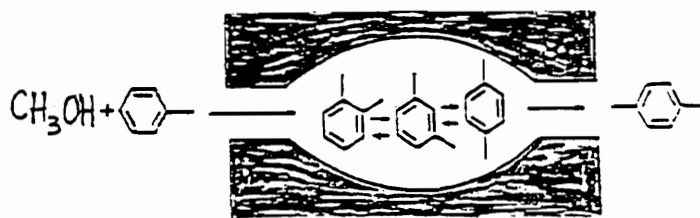


Figure 5.4 (c): ZSM-5 catalyst exhibits product selectivity which can be visualized as shown in the sketch.(From Davis, 1991)

ZSM-5 zeolites have been demonstrated to have catalytic capabilities for various types of hydrocarbon conversion, which includes: (i) conversion of methanol to olefins, gasoline and diesel, (ii) dewaxing of distillates, (iii) reforming, (iv) alkylation, (v) isomerization of n-paraffins and naphthenes, (vi) disproportionation of aromatics, etc. They have also been shown to possess unusual hydrophobicity, leading to potential applications in the separation of hydrocarbons from polar compounds, such as water and alcohols (Argauer and Landolt, 1972; Meisel, 1988).

5.1.5 PREPARATION OF ZSM-5 CATALYST

Zeolites prepared in the presence of organic cations are catalytically inactive. This inactivity is due to intracrystalline free space occupied by organic cations from the forming solution. They are converted to the predominantly hydrogen form (HZSM-5) generally by replacement of the alkali metal or other ion originally present with hydrogen ion precursors, e.g. ammonium ions, which upon calcination yield the hydrogen form.

A solution containing tetrapropyl ammonium hydroxide, aluminum oxide, silica oxide, sodium oxide in water is prepared. This mixture is maintained at 150 C for 5 up to 8 days until crystals of the zeolite are formed. The solid product is cooled to room temperature, filtered and washed with water. The collected solid is dried at 110 C. In order to render the zeolite catalytically

active for hydrocarbon conversion, the zeolite has to be contacted with hydrogen chloride at 80 C where the hydrogen ion will replace the sodium ion. The resulting active catalyst is washed with water and dried. The dried catalyst is calcined in air or other inert gas at temperature of 815 C for up to 48 hours (Argauer and Landolt, 1972).

The activity-enhanced zeolite is incorporated in a matrix comprising material resistant to the harsh temperatures and other severe conditions employed in the process. Such matrix materials include synthetic or naturally occurring substances as well as inorganic materials such as clay, silica and/or metal oxides. Naturally occurring clays which can be composited with the zeolite include those of the montmorillonite and kaolin families. Such clays can be used in the raw state as originally mined or initially subjected to calcination, acid treatment or chemical modification. In addition to the above-mentioned materials, zeolites may be compounded with a porous matrix material, such as silica-alumina. Ternary combinations such as silica-alumina-magnesia can also be used. The matrix may be in the form of a cogel. The relative proportions of zeolite and matrix may vary widely with zeolite content ranging from 5 to 80 percent by weight of the composite.

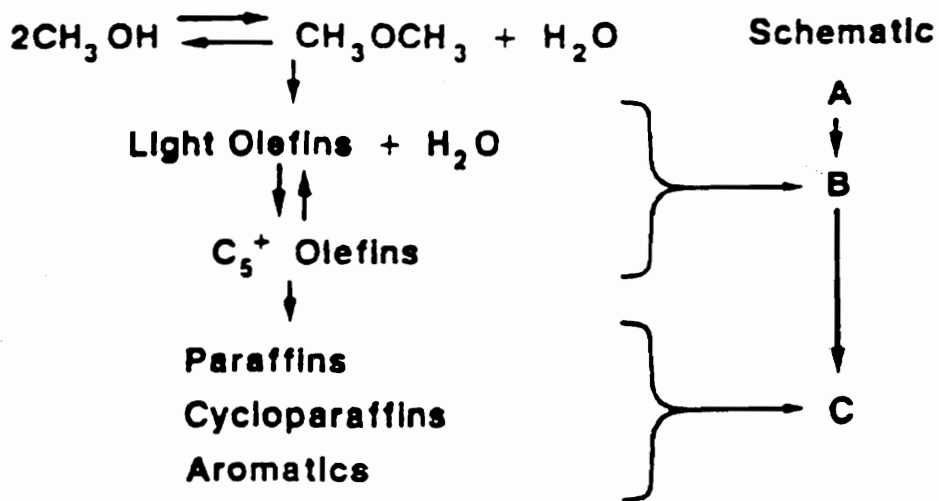
ZSM-5 zeolites can be used either in the alkali metal form, e.g., the sodium form, the ammonium form, the hydrogen form, or another univalent or multivalent cationic form. They can also be used in combination with a

hydrogenating component such as tungsten, vanadium, molybdenum, rhenium, nickel, cobalt, chromium, manganese, platinum, or palladium where a hydrogenation dehydrogenation function is to be performed. Such component can be exchanged into the composition (Argauer and Landolt, 1972). The catalyst may be used in any form such as pellets, beads, extrudate, or a fine powder form.

5.2 A BRIEF REVIEW ON MTO REACTION

Methanol at 482 C, converts to water and a hydrocarbon mixture of Olefins, Paraffins, Cycloparaffins and Aromatics over HZSM-5 catalyst. The reaction maximizes production of Olefins and does not proceed to form significant amounts of Paraffins and Aromatics. It is referred to as **Methanol-To-Olefins (MTO)** reaction.

Figure 5.5 shows MTO reaction path and defines the Reaction Index which is defined by the propane/propene ratio and is a criterion of catalyst activity. Avidan, (1987), “ Since the measurement of on-line catalyst activity is difficult, we found it convenient to follow an on-line ‘reaction index’ (RI), which is a selectivity ratio. The propane/propene RI can be easily monitored by an on-line Gas Chromatograph.”. Reaction Index was found to correlate well with hydrocarbons selectivities and also correlated well with methanol conversion for fixed hydrodynamics (Avidan, 1987).



“Reaction Index”

Propane/Propene Ratio is Proportional to C/B,

In the Schematic Path

Figure 5.5: MTO reaction path and the reaction index, defined as propane/propene ratio (Avidan, 1987).

5.2.1 OPERATIONAL CONDITIONS

The MTO process processes takes methanol feed of any purity. The methanol feed need not be of greater than ordinary technical purity. MRDC conducted the MTO reaction using:

- (i) Raw methanol feed which contained significant amount of water. They reported no loss in the selectivity for light olefins with this feed.
- (ii) A mixture of methanol and a diluent like helium or nitrogen. They reported an increase in olefins when a diluent was used.

The MTO process is carried out at a temperature of 482 C in the reaction zone. It is desirably conducted at atmospheric pressure.

Conversions are based on $-CH_2-$ content of the methanol feed, (i.e. the content of carbon and hydrogen after elimination of oxygen as water). In other words, conversions are expressed as percentage of methanol carbon reporting to carbon in hydrocarbon product.

The MTO reaction is exothermic. The amount of heat generated in the conversion of methanol to hydrocarbon products is estimated to be 1740 kJ per kilogram of methanol consumed. (Squires et al, 1985).

The catalyst acidity is directly related to the amount of aluminum in the framework. A low silica-to-alumina ratio gives the framework high acidity. Figure 5.6 presents the effect of $\text{SiO}_2 / \text{Al}_2\text{O}_3$ on the olefin yield. Olefins are found to be favoured by low acidity. Low acidity is given by a high silica-to-alumina (Chang et al, 1984).

5.2.2 FLUID-BED SCALE UP OF MTO

The scale up of the MTO process (viz. bench scale, pilot plant and demonstration plant) was successfully completed in a series of fluid beds. The process was shown to be economically viable and, as far as we know, it is ready for commercialization.

5.2.2.1 MICRO FLUID-BED REACTOR

Mobil employed a Micro fluid-bed reactor, 28 centimeter high with an internal diameter of 1 centimeter, to study its MTO process at a laboratory bench. The Micro fluid-bed reactor was operated with a catalyst of 1 to 10 grams. Figure 5.7 presents an illustration of the Micro fluid-bed reactor.

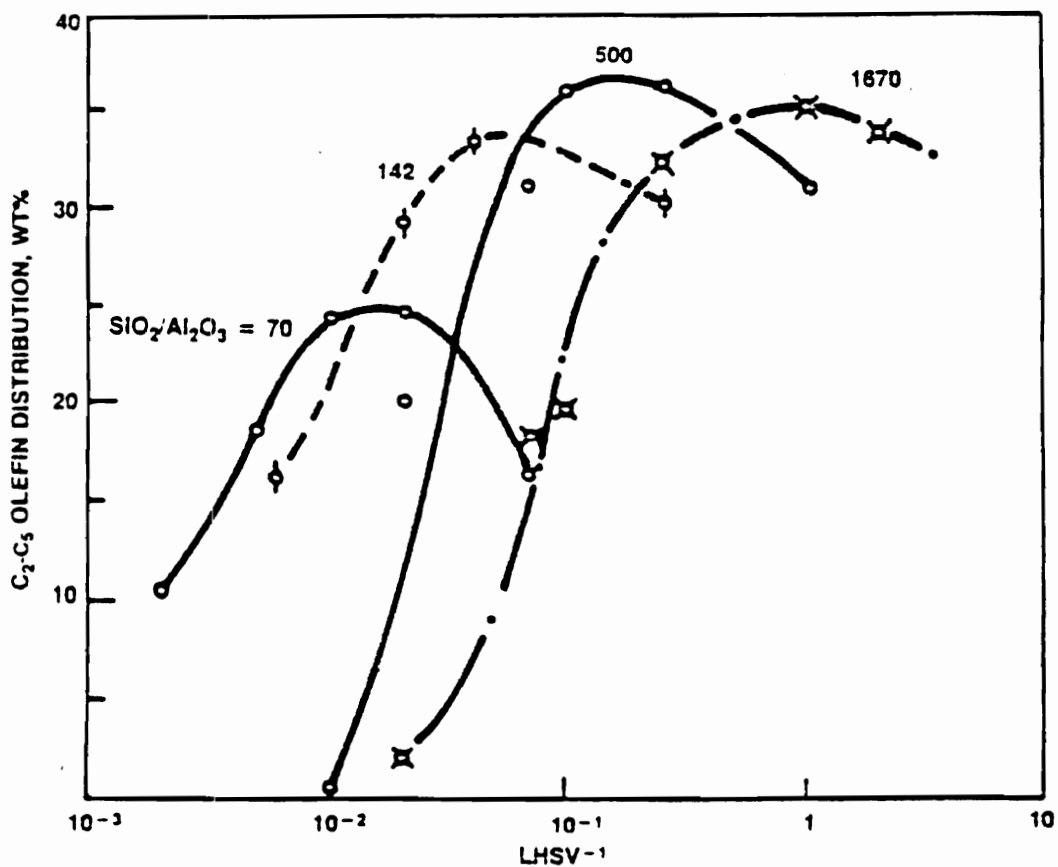
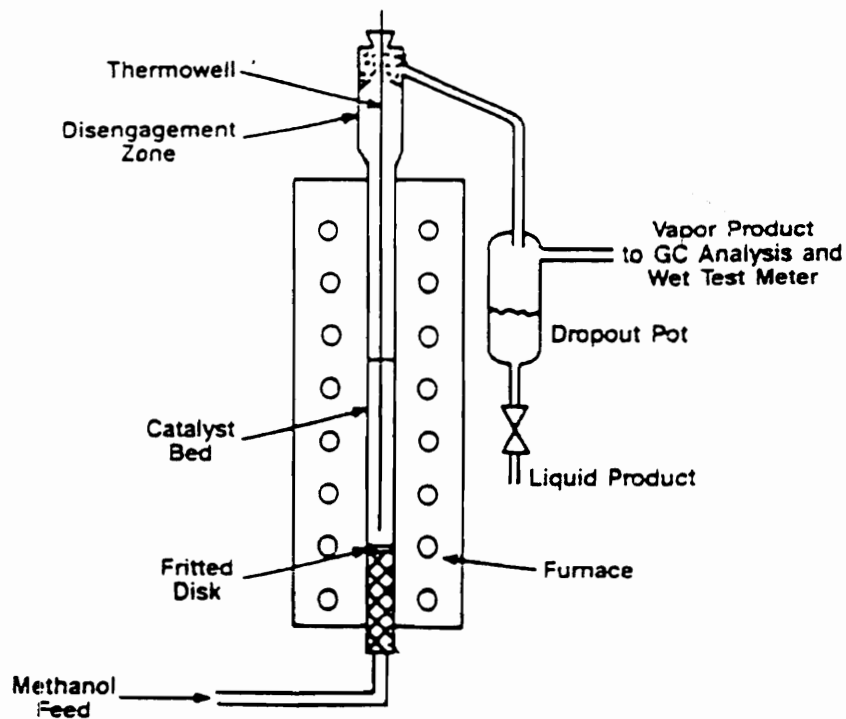


Figure 5.6: Effect of $\text{SiO}_2/\text{Al}_2\text{O}_3$ on the olefin yield. Olefins are favoured by low acidity, which is given by high silica-to-alumina (Chang et al, 1984).



Reactor: 28 cm high x 1.0 cm ID

Figure 5.7: Illustration of the Micro fluid-bed reactor (Gould et al, 1986).

5.2.2.2 PILOT PLANT

The MTO process was scaled-up to a fluid-bed Pilot plant, 7.6 meters high with an internal diameter of 10.2 centimeter. The fluid-bed Pilot plant was operated with 10 up to 25 kilograms ZSM-5 catalyst with a throughput of 4 barrels per day. Figure 5.8 presents an illustration of the fluid-bed Pilot plant.

5.2.2.3 DEMONSTRATION PLANT

Successful scale-up was completed in 1985 in a Demonstration plant at URBK, Wesseling, Federal Republic of Germany. The Demonstration plant was 19 meters high with an internal diameter of 60 centimeters. The plant was loaded with 625 kilograms of ZSM-5 catalyst, with a throughput of 100 barrels per day.

Figure 5.9 presents an illustration of the Demonstration plant. The influence of operating parameters such as temperature, pressure, weight hourly space velocity, catalyst activity, catalyst make-up rates and several options for process improvements were investigated during various test runs done in the 100 BPD Demonstration plant (Gierlich et al, 1985).

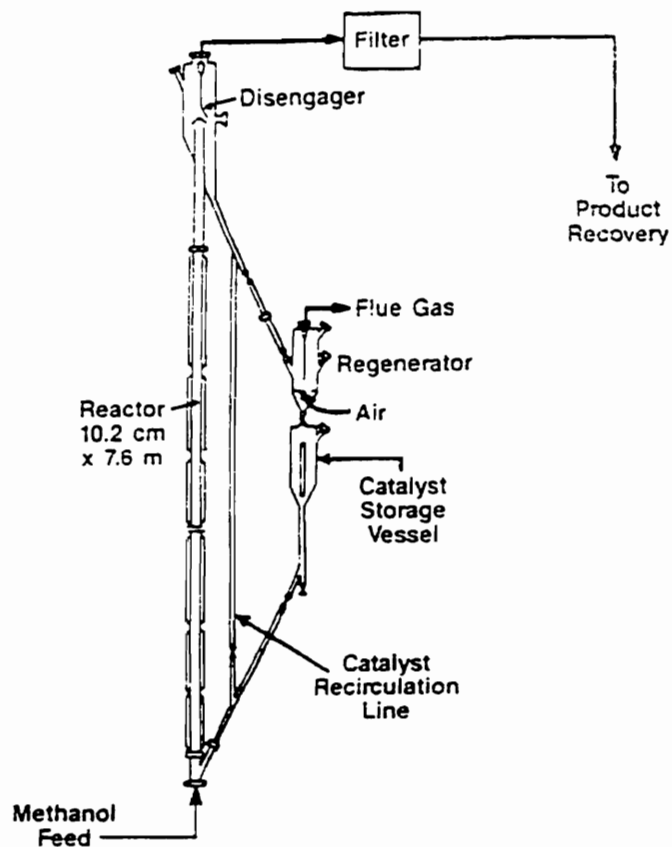


Figure 5.8: Illustration of the fluid-bed Pilot plant (Gould et al, 1986).

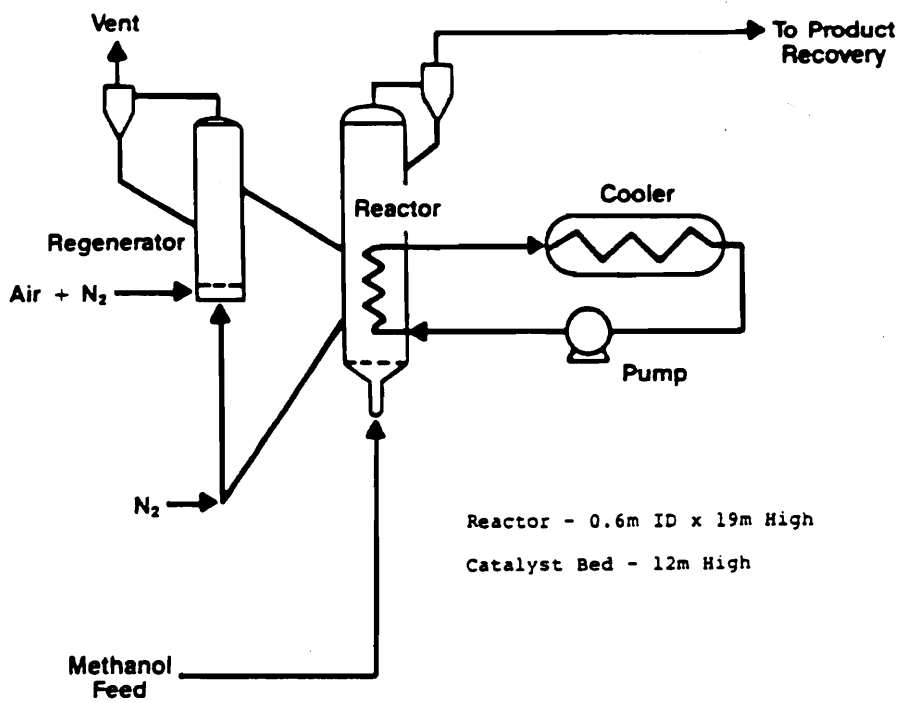


Figure 5.9: Illustration of the Demonstration plant (Gould et al., 1986).

Figure 5.10 shows results of the different periods of operation of the 100 BPD Demonstration plant, by relating the relative catalyst activity to the total on-stream hours of operation (TOS). Plant and Process Verification involved equipment checking, improving control systems and batch regeneration. Sensitivity Test Program included the study of catalyst ageing, high and low activity tests and fines studies. Steady State Run determined catalyst make-up and attrition rates. The important note to make about this figure is the remarkable variation of catalyst activity observed in the unit, during the test runs.

Figure 5.11 shows the effect of temperature on methanol conversion in 100 BPD Demonstration plant. Olefins yield increases with temperature (Soto and Avidan, 1985).

Figure 5.12 indicates the effect of pressure on the methanol conversion in 100 BPD Demonstration plant. Lower pressure was observed to increase olefins yield (Soto and Avidan, 1985).

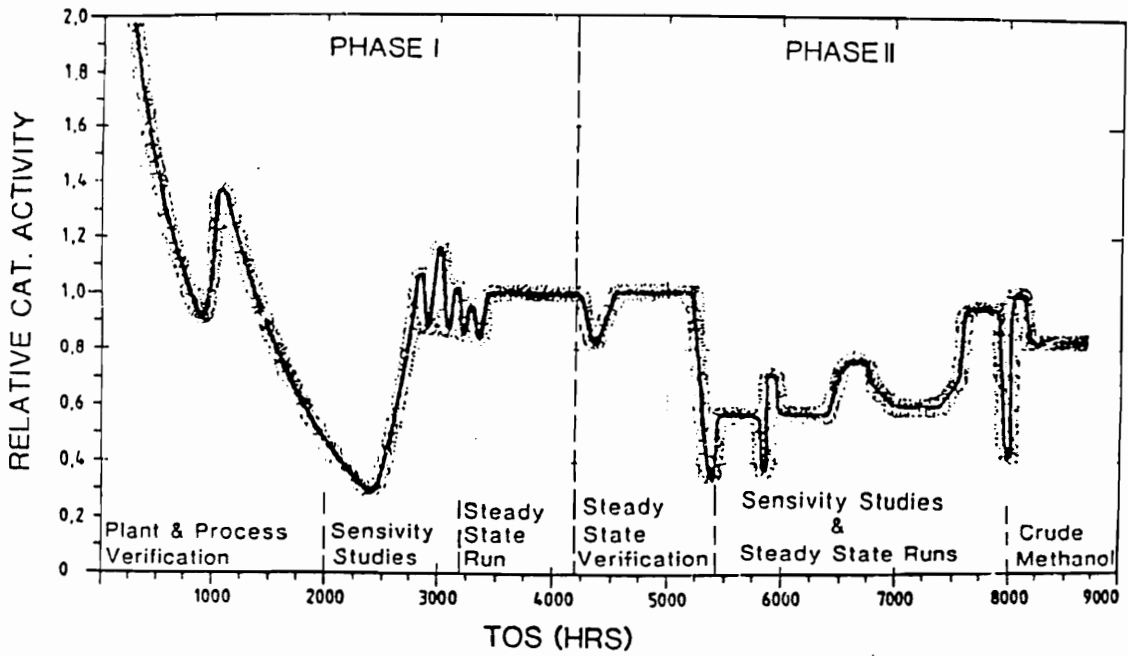


Figure 5.10: Relative catalyst activity against total on-stream hours of operation (TOS) during operation of 100 BPD Demonstration plant (Gierlich et al., 1985).

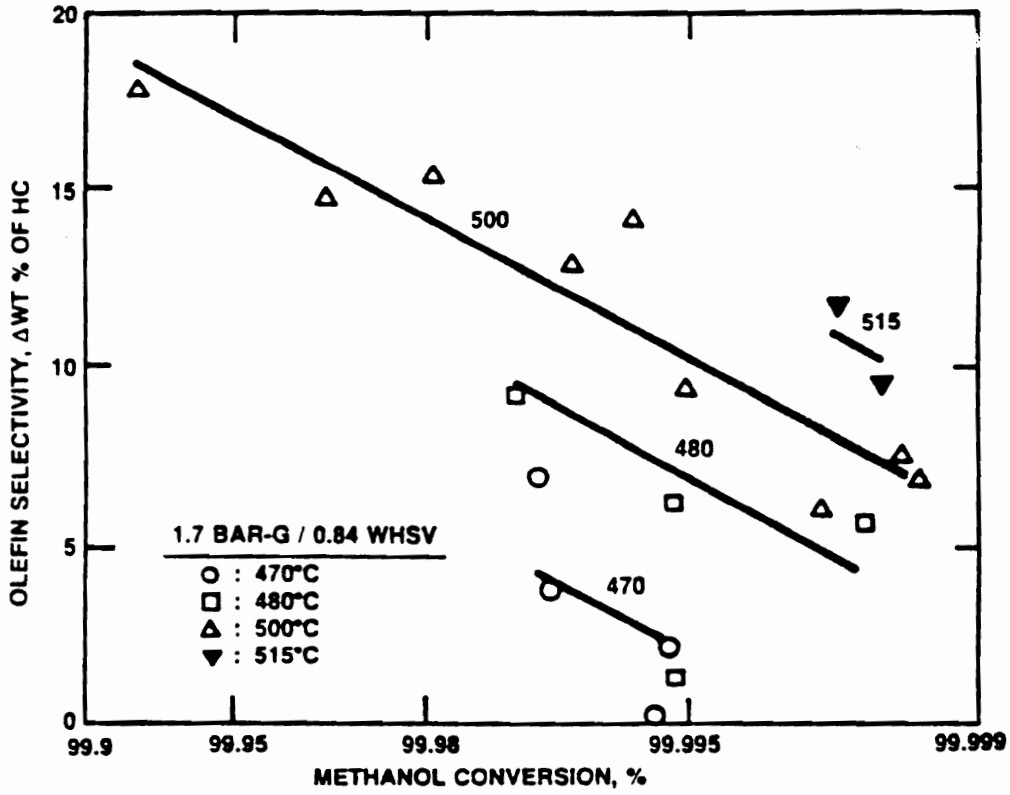


Figure 5.11: Effect of temperature on methanol conversion in 100 BPD Demonstration plant. Olefins yield increases with temperature (Soto and Avidan, 1985).

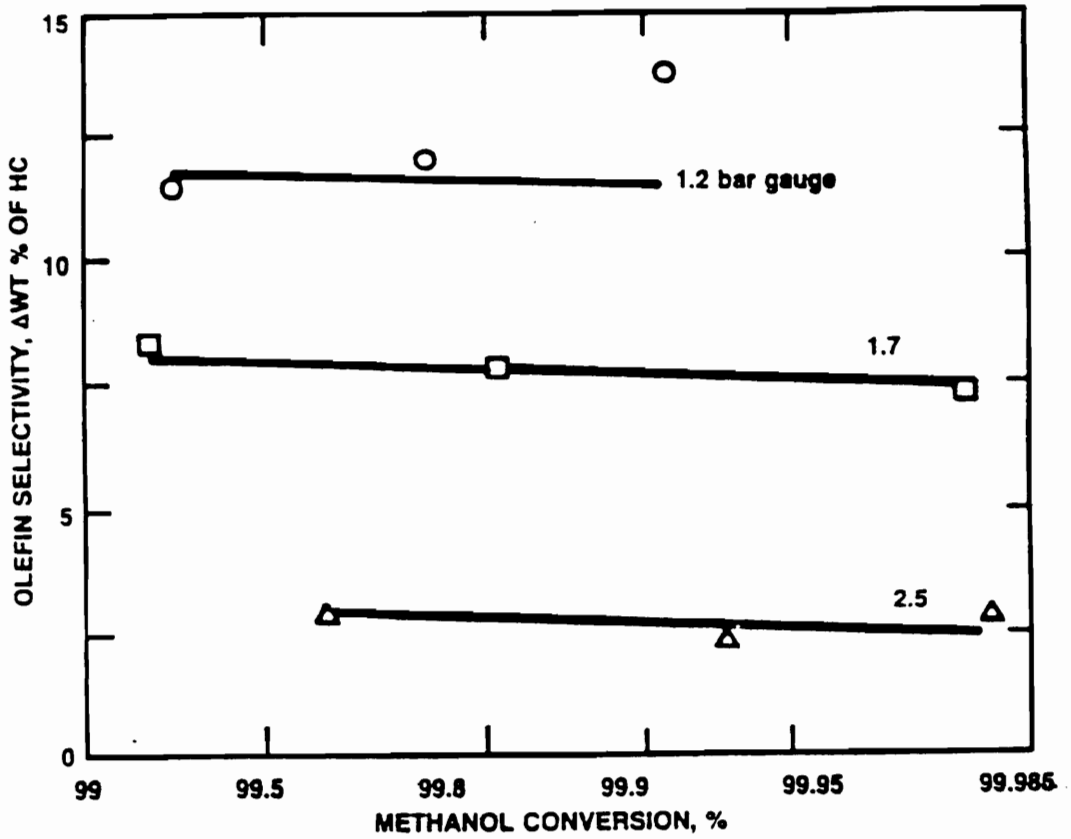


Figure 5.12: Effect of pressure on methanol conversion in 100 BPD Demonstration plant. Lower pressure was observed to increase olefins yield (Soto and Avidan, 1985).

5.2.2.4 SUMMARY OF OBSERVATIONS ON THE SCALE-UP

Figure 5.13 presents Olefins Yield obtained from Micro Fluid-bed reactor and Pilot plant. Results were obtained at 482 C and 103 kPa (Socha et al, 1986). Table 5.2 indicates the hydrocarbon yields (e.g. olefins, paraffins and aromatics) obtained from Micro Fluid-Bed and 4 BPD Pilot plant. The hydrocarbon yields are similar in both scales of operation, which indicates that the MTO process scaled-up successfully.

Figure 5.14 presents Olefins Yield obtained from 4 B/D Pilot plant and 100 B/D Demonstration plant. Results were obtained at 500 degree Celsius and 250 kPa (Soto and Avidan, 1985). Table 5.3 presents olefin yields obtained from 4 BPD Pilot plant and 100 BPD Demonstration plant. The olefin yields are similar in both scales of operation, which indicates a successful scale-up of the process.

MTO was scaled-up successfully as a fluid-bed process. The process is, as far as we know, ready for commercialization.

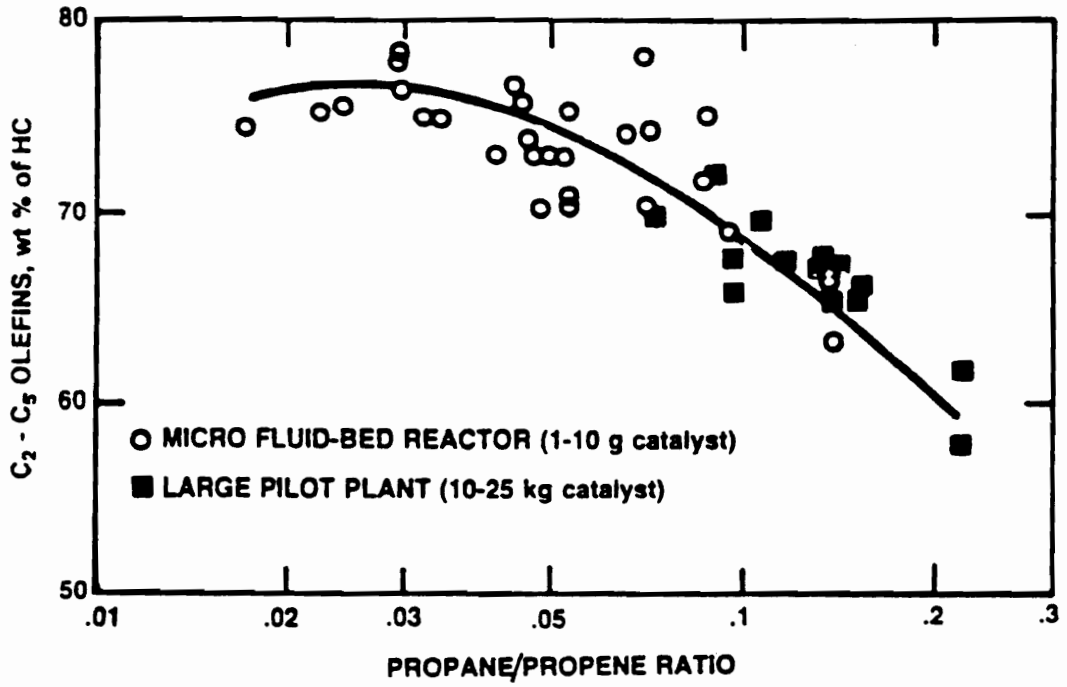


Figure 5.13: Olefins Yield from Micro Fluid-bed reactor and 4 BPD Pilot plant, at 482 degree Celsius and 103 kPa (Gould et al, 1986).

Table 5.2: Hydrocarbon yields (e.g. olefins, paraffins and aromatics) from Micro Fluid-Bed and 4 BPD Pilot plant. The hydrocarbon yields are similar, indicating a successful scale-up (Gould et al., 1986).

	<u>Micro Fluid-Bed</u>	<u>4 BPD Pilot Plant</u>
Conversion, wt %	100	100
Product Yields, wt %		
Ethene	5.8	5.2
Propene	33.7	32.9
Butenes	18.4	19.1
Pentenes	14.8	12.0
C ₆ + Olefins	5.5	7.7
Olefins	78.2	76.9
Paraffins/Naphthenes	15.3	16.6
Aromatics	6.5	6.5
	<u>100.0</u>	<u>100.0</u>

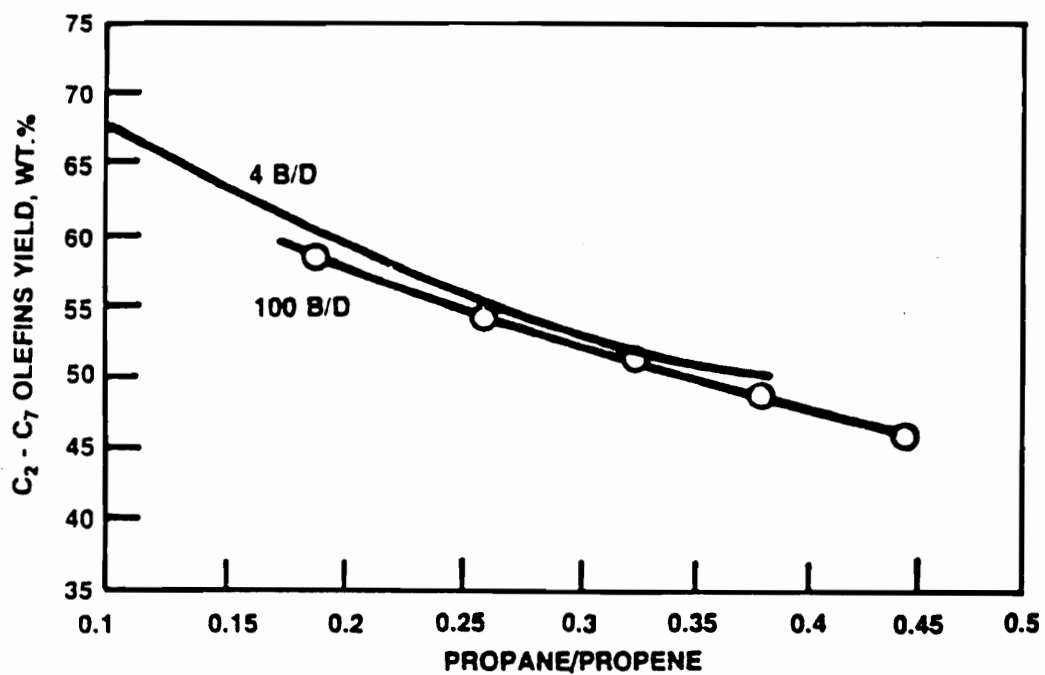


Figure 5.14: Olefins Yield from 4 B/D Pilot plant and 100 B/D Demonstration plant, at 500 degree Celsius and 250 kPa (Soto and Avidan, 1985).

Table 5.3: Olefins yield from 4 BPD Pilot plant and 100 BPD Demonstration plant. The olefin yields are similar, indicating a successful scale-up (Gould et al., 1986).

	4 BPD Pilot Plant	100 BPD Demonstration Plant
Catalyst Bed Height, m	7.9	10.0
Reactor Diameter, m	0.1	0.6
MeOH Conversion, wt %	100	100
C ₂ -C ₅ Olefin Yield, wt %	57	55
Total Olefin Yield, wt %	63	61
C ₃ - Saturates Yield, wt %	7	7

5.2.3 MTO REACTION MECHANISMS

There have been varied opinions as to how the reactions occur inside the catalyst pores. Mechanism of the crucial initial C-C bond formation from methanol-DME is an unsolved problem and the subject of an ongoing controversy (Venuto, 1972; Maiden, 1988; Chang and Chu, 1983; Dessau and LaPierre, 1982).

Our study will neither probe the reaction mechanism nor offer results which might be helpful in settling the controversy surrounding the reaction mechanism of this process.

5.2.4 MTO PRODUCT ANALYTICAL METHOD

This section is included in order to bring out the differences between our analytical techniques of the MTO product stream and the complex arrangement used by MRDC, as we understand this from published accounts of Stockinger (1977), Bloch et al (1977) and Kaufman et al. (1977).

Gas chromatography (GC) is a well established technique that offers potential solutions to many of the inadequate features of the fluorescent indicator adsorption (FIA) procedure ASTM D1319, and conventional mass

spectrometric (MS) methods. FIA results do not provide specific compound identification; and although MS methods give carbon number data for compound type, they also do not give specific compound identification.

MRDC designed an unconventional GC system, which used an aromatic precutter column followed by olefin absorption with mercuric perchlorate-perchloric acid (MP-PA). The aromatics precutter column used was a 150 ft by 0.01 inch i.d. WCOT column coated with OV-275 and the aromatics resolving column used was a 100 ft by 0.02 inch i.d. squalene support-coated open tubular (SCOT) column. The paraffin, naphthene, olefin were resolved using a 200 ft by 0.02 inch i.d. squalene-coated SCOT column. The olefin absorption column used was a 3 ft by 1/8 inch o.d. column.

A high capacity, 8 foot by 1/8 inch, 80/100 mesh, Porapak Q packed column was used in conjunction with a TCD for the detection of low concentrations of permanent gases, water, dimethylether and methanol.

Nitrogen carrier gas was used to get optimum detector sensitivity in detecting hydrogen. It was changed to helium (after detecting hydrogen) to obtain satisfactory sensitivity and detection of nitrogen, carbon monoxide, carbon dioxide, water, methanol and dimethylether.

A minicomputer system (PDP-8 computer/interface system) was utilized for control of sample injections, backflushing, carrier gas changes, venting and

other GC procedures (such as column switching, initializing temperature and pressure flow programming). Peak area detection, peak identification, and final calculations of mole and weight compositions were also performed on the computer system.

6. APPARATUS, MATERIALS AND PROCEDURE

This chapter provides a description of the equipment and techniques that were used to carry out the experiments mentioned in Chapter 2, which detailed the experimental goals and objectives for this work.

Gaining access to new equipment to carry out the research was made impossible because research funds were insufficient. Finding and overhauling old equipment to make it functional and reliable was time consuming. Some equipment has been obtained on loan from other research groups.

The main part of the research was conducted using vibrated bed microreactors. Figure 6.1 shows the overall setup of the experimental apparatus used in the research. The main parts of the experimental apparatus are (i) methanol feeding scheme, (ii) vibrated bed microreactor setup and (iii) gas chromatograph setup.

The experimental apparatus used in this study may be divided into the following categories:

(i) Methanol Feeding System. This will describe the method of feeding methanol into the microreactor in a steady pulse-free flow.

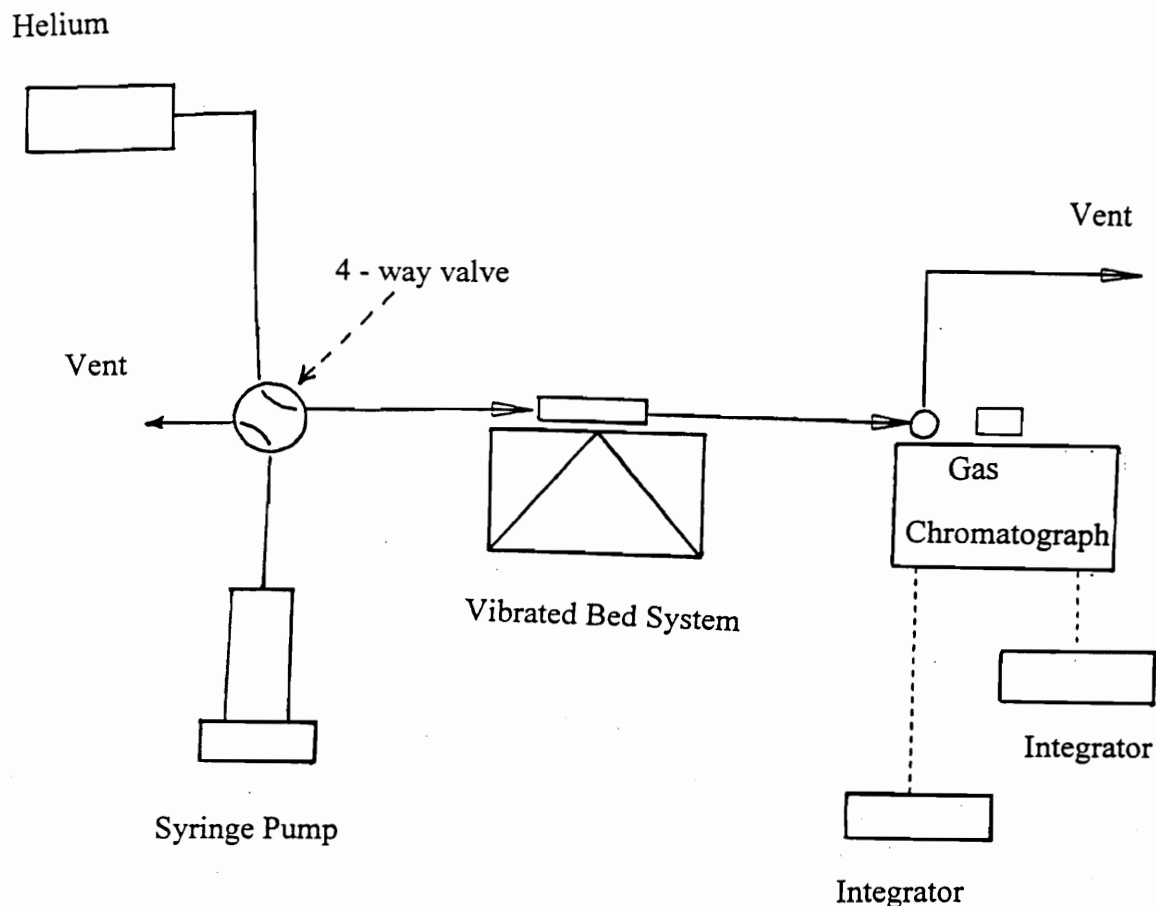


Figure 6.1: Overall setup of the Experimental Apparatus. The sketch shows the methanol feeding scheme, vibration system and the gas chromatograph setup. The 4-way valve is at the highest elevation in the system. After a desired methanol flow rate has been established and the microreactor has reached 482 C and stable C-E state condition, turning the 4-way valve clockwise through 90 degree establishes flow of methanol vapor into the microreactor.

- (ii) Vibration System. This consists of equipment for generating vertical mechanical vibrations, along with the accompanying support structure and the instrumentation for measuring parameters pertaining to the vibration.
- (iii) Equipment Development. This section describes the design of a vibrated bed microreactor, which can be operated at high temperature.
- (iv) Product Analytical Scheme. This will present the system used for taking a product sample and its subsequent analysis.

6.1 METHANOL FEEDING SYSTEM

The MTO reaction was conducted using pure research grade methanol, purchased in 1-litre bottles from the Virginia Tech Chemistry Chemical Stockroom, Room 024, Hahn Hall. Methanol liquid was to be fed into the microreactor in a pulse-free steady flow. We had no suitable equipment of our own to do this. A brainstorming session on this question brought up several ideas on how to accomplish this task.

The first idea was to use a "kettle" in which methanol would be boiled at a calculated rate and fed to the microreactor. After close scrutiny the idea was abandoned because it raised serious safety concerns inherent with such an arrangement.

The second idea was to use a burette whereby liquid methanol would flow steadily into the microreactor by gravity. This idea was tried out. A burette was filled with liquid methanol, positioned vertically at a higher point than the rest of the equipment and was connected to the microreactor. This did not produce a flow of methanol into the microreactor. All of our other attempts with different lengths of burettes and different vertical heights also failed to get methanol to gravitate into the microreactor.

The third idea was to use a Peristaltic Pump, which also failed because it gave a pulsating flow of methanol instead of the desired steady pulse-free flow.

After these failed trials with the burette and a peristaltic pump, we found an unused Syringe Pump which belonged to Dr Rony, who let us use it. We replaced a blown fuse in the Controller and a broken pin on the shaft of the pump, to get it operational. It was tested and found to deliver a suitable range of flowrate. We calibrated it to deliver our chosen flowrates. The syringe pump is an ISCO Model 314 Metering Pump. It can hold 375 ml of liquid methanol and deliver flowrates as low as 0.008 ml/hr up to a maximum of 200 ml/hr. The stem is graduated in divisions of 5 ml. Since all of our flowrates were below 5 ml/hr, the 5 ml graduations on the pump were too large and made it difficult to measure flowrates accurately. The pump is driven electrically and controlled with a Controller.

Methanol liquid from the syringe pump is established at a desired flow via one branch of a 4-way valve. Helium flows to the microreactor via the second branch and a heated line while stable temperature and vibration conditions are being established. The heated line is maintained with calcords at 150 C, higher than the boiling point of 64.5 C for methanol. Thereafter, turning the 4-way valve (clockwise by 90 degree) establishes flow of methanol vapor to the microreactor, commencing a run. The 4-way valve is at the highest elevation in the system in order to prevent liquid methanol ahead of the valve from flowing by gravity into the heated line, creating an uncontrolled initial pulse of methanol vapor into the microreactor.

6.2 VIBRATION SYSTEM

The purpose of the vibration system is to produce mechanical, sinusoidal, vertical vibrations, at specified amplitudes and frequencies, which are imparted to the microreactor to get the catalyst to vibrate in the C-E state. The vibrated-bed system is shown in Figure 6.2. The salient features of the vibration system include: (i) vibration support structure, and (ii) generation and measurement of vertical vibrations.

6.2.1 VIBRATION SUPPORT STRUCTURE

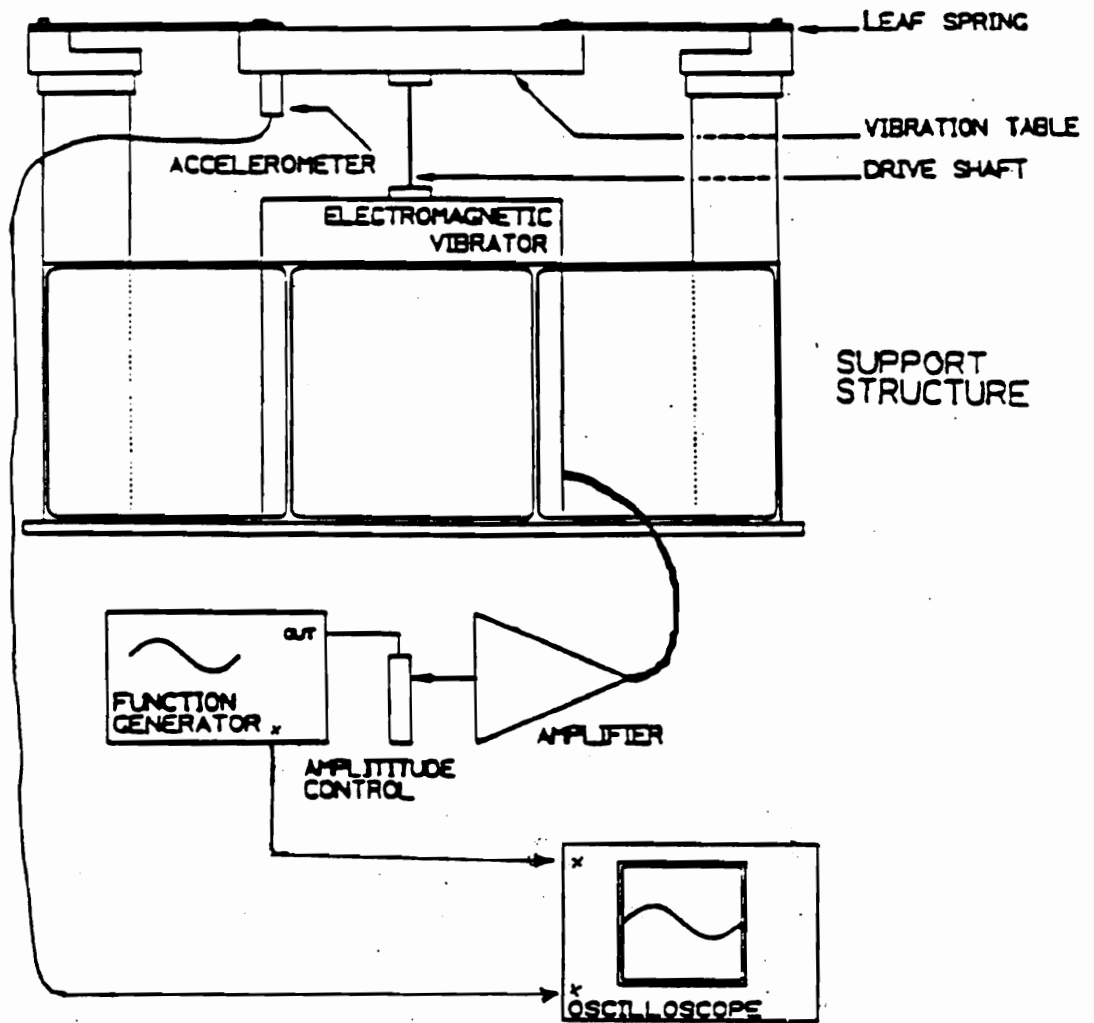


Figure 6.2: Vibrated-bed system.

The purpose of the support structure is to ensure that the vibrations produced are: (i) absolutely vertical and (ii) transferred to the microreactor and none are transferred to the surroundings. It is also to allow operation at near the resonance frequency of the system which is around 25 Hz.

Benku Thomas designed the support structure. Bengt (1992) gave detailed drawings, repeated here in Appendix A. An isometric drawing of the support structure is shown in Figure 6.3. In earlier work done by Thomas (1988), the support structure and vibration table were both circular, and the entire assembly sat on a massive concrete block. In our work, the support structure and the vibration table are both rectangular as can be seen in the top view shown in Figure 6.4. This figure also shows the holes used for attaching leaf springs on: (i) the support structure and (ii) the vibration table, which is in the center. The entire assembly is placed on two 2.5 inch thick pieces of foam rubber padding and mounted in a powerful hood for withdrawing fumes.

Leaf springs are attached on the support structure with mounting brackets. The brackets allow for two dimensional horizontal movements of the leaf springs on the support structure which consequently aids in the positioning of the leaf springs for proper alignment. Precise alignment of the leaf springs is the most important key to reducing non-vertical components of the vibration (Thomas, 1988). Leaf springs are attached to the vibration table with a 1/4 inch bolt and a No. 8 screw.

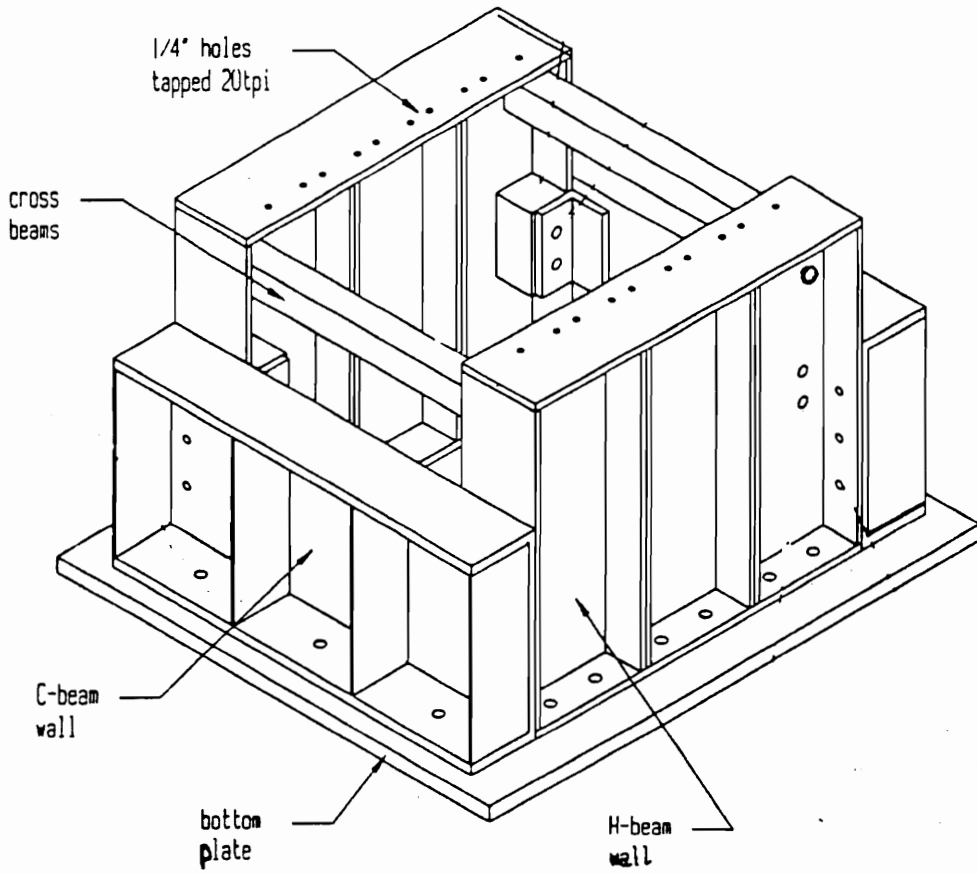


Figure 6.3: Isometric drawing of the support structure.

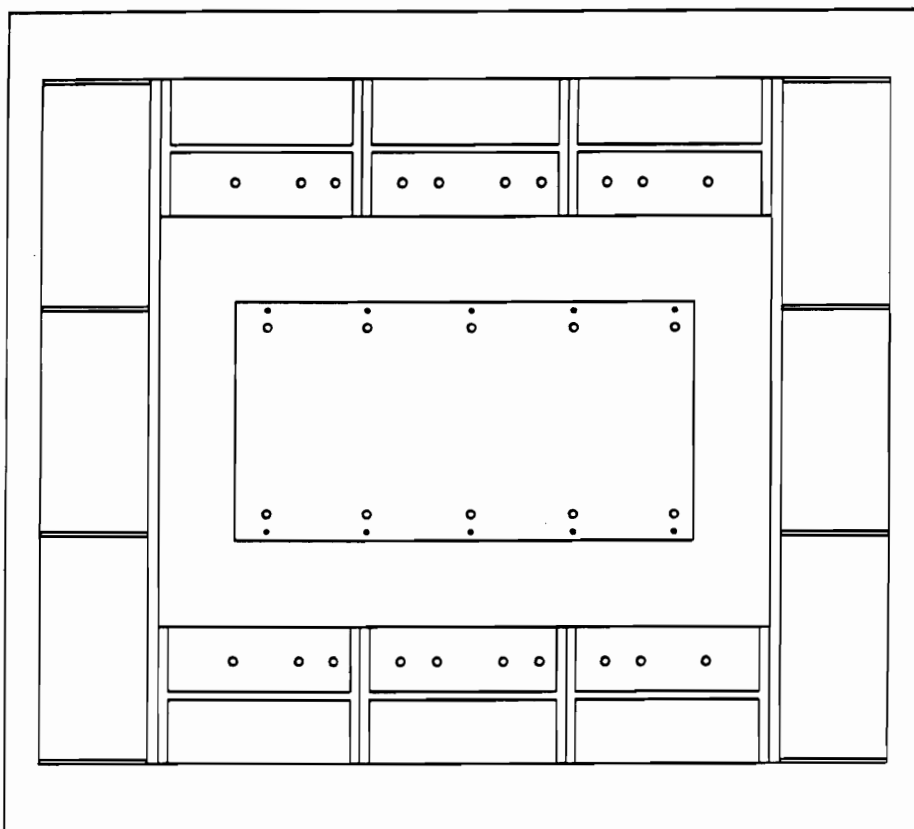


Figure 6.4: Top view of support structure and vibration table.

The vibration table is constructed out of stainless steel, and measures 34.29 cm long, 17.78 cm wide and 4.45 cm thick. It is held in place by suspension with three leaf springs on the front and the back. The 1/4 inch bolts and No. 8 screws are nominally adjusted to finger tight and can be torqued more or less to finely adjust the tension on the leaf spring.

6.2.2 GENERATION AND MEASUREMENT OF VERTICAL VIBRATION

An OK Electronics Model 205 5MHz function generator is used to generate a sinusoidal waveform at a particular frequency. This waveform is fed into a TECHRON Model 5530 power amplifier which is capable of generating up to 155 Watts of output power.

The amplified signal drives a Vibration Test Systems model VG 100-6 electromagnetic vibrator which is attached to the underside of the vibration table via a 3.5 inch long steel rod of 0.094 inch diameter drive shaft.

A Scientific Atlanta DYMATIC Model M99 Series Heavy Duty Industrial Accelerometer, with sensitivity of 100 mV/g and linear frequency response between 3 Hz and 10 KHz, is attached to the underside of the vibration table. It is used to measure the acceleration of the vibration table.

The signal from the accelerometer electronics is monitored on an Elenco Precision Model Mo-1252 35 MHz Dual Trace Oscilloscope. This setup allows for adjustment of the amplifier, i.e. the amplitude of vibration while viewing the output of the attached accelerometer, to set the system at a specified vibrational intensity, K .

A Linear Variable-Differential Transformer (Trans-Tek Model 0243 DC LVDT) displacement transducer was used in the past to measure the vessel displacement. The LVDT transducer is a contact device (i.e. a part of the transducer moves with the vibrating table relative to the rest of the transducer which is stationary). It is not used in this research work, because of lack of space to mount it. The vessel displacement is determined by calculation from the formula for vibrational intensity given in chapter 4.

A strobe light is also available for viewing the microreactor under vibration conditions. In order to view the dynamics of the vibrated bed as a function of time (or more correctly, phase angle) the phase-delayed trigger circuitry should be used (Thomas, 1988).

6.2.3 CONCLUDING REMARKS

Application of strictly vertical vibrations is one of the most difficult (or tricky) aspects of the vibrated-bed system. The weight distribution and

torque on the leaf springs must be matched quite well before strict vertical vibrations are obtained.

The presence of nonvertical components of the vibration are easy to detect by the solid particles shifting in the direction of the stiffest springs or least weight. It is best, when possible, to have a high degree of symmetry in the vibration system and vessels.

6.3 EQUIPMENT DEVELOPMENT

The ultimate goal of the work is to determine the sensitivity of MTO reaction to axial gas dispersion in a vibrated bed microreactor. In order to complete the task a microreactor which is capable of operating at a high temperature has to be designed. The vibrated bed microreactor used for cold-flow work was not suitable for operating at significantly high temperatures (e.g. 482 C) as it was made out of several low temperature materials such as lexan, glass, plexiglass, epoxy and glue. A detailed description of the cold flow model of the microreactor is given by Bengel (1992).

A new design of a microreactor capable of operating at high temperature was called for, in the study of MTO reaction. This study required a microreactor design at three horizontal duct lengths. The microreactors had

to be designed to fit within dimensions of the existing Vibration Table (i.e. 34.3 cm long, 17.8 cm wide and 4.4 cm thick).

Figure 6.5 shows a simplified sketch of the Vibration Table with various hole patterns drilled for the microreactors. The string of holes 4.4 cm (1.75 inch) from the long edge on both sides were drilled to match the hole pattern on each of the three microreactors.

6.3.1 BASIC DESIGN DIMENSIONS OF THE MICROREACTOR

Basic design of the microreactor was arrived at, after many different ideas were considered and discarded.

Figure 6.6 shows an isometric drawing of the microreactor at 15.24-cm horizontal duct length. The figure shows three main sections of the microreactor, Inlet section, Middle section and Outlet section.

The reaction zone is in the form of a rectangular horizontal duct contained in the Middle section. All of the three Vibrated Bed Microreactors were similar, differing only in their horizontal duct lengths. Design dimensions for the microreactor of duct length 7.62 cm and 22.86 cm are presented in Appendix B.

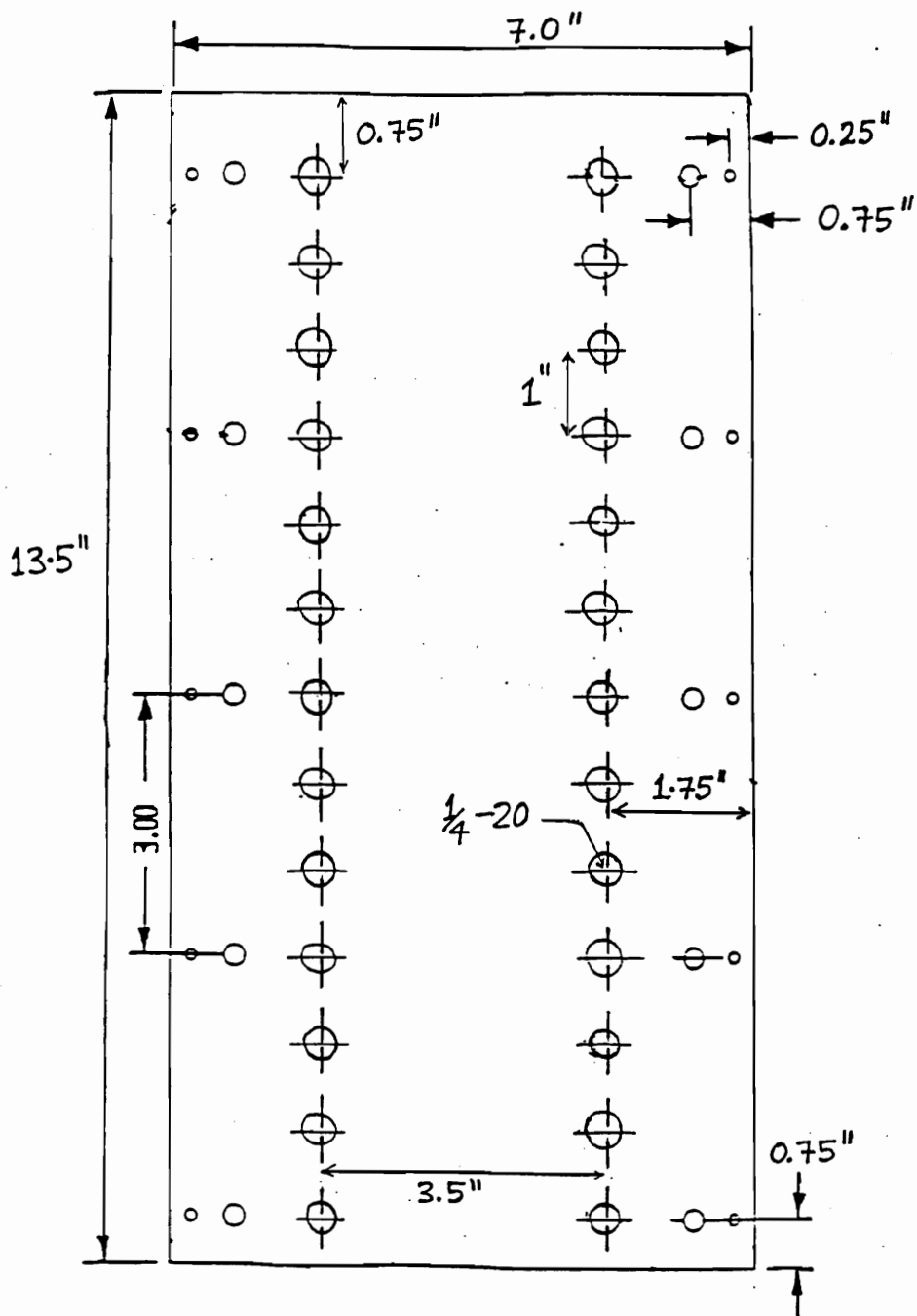


Figure 6.5: A simplified sketch of the Vibration Table made out of stainless steel. The figure shows various hole patterns drilled to accommodate the microreactors.

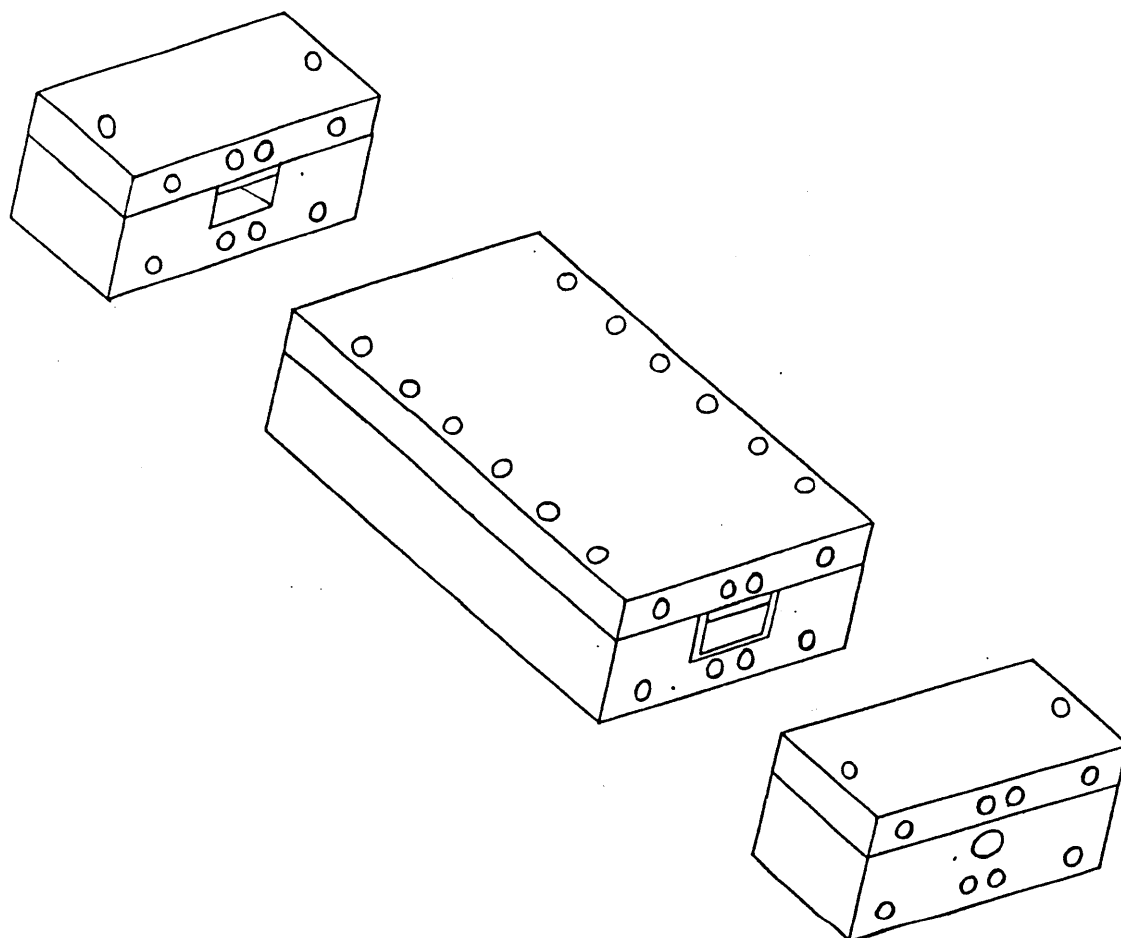


Figure 6.6: Isometric drawing of microreactor at 15.24-cm horizontal duct length. The figure shows three main sections of the microreactor, Inlet section, Middle section and Outlet section.

The microreactor is heated to the desired temperature with a set of 4 cartridge heaters. Two cartridge heater holes are located above and below the reaction zone, and extend along the entire length of the microreactor. Other holes are drilled for cap screws which: (i) hold various pieces of the microreactor together and (ii) mount the microreactor to the vibration table. Figure 6.7 shows the microreactor assembled with the cap screws.

Figure 6.8 shows six individual pieces making up the microreactor. The two middle pieces make up the reaction zone at a horizontal duct length of 15.24 cm. Inlet section and Outlet section are similar.

Each of the main sections of the microreactor (i.e. inlet, middle and outlet) has two parts (i.e. top and bottom). Design dimensions for the middle section (top and bottom parts) and inlet section (top and bottom parts) are presented in the following figures.

Several views of the top half of the middle section (viz. mid-top section) are shown in Figure 6.9 namely (a) Isometric view, (b) Top view, (c) Side view and (d) Front view.

Figure 6.10 shows several views of the bottom half of the middle section (viz. mid-bottom section) namely (a) Isometric view, (b) Top view, (c) Side view and (d) Front view.

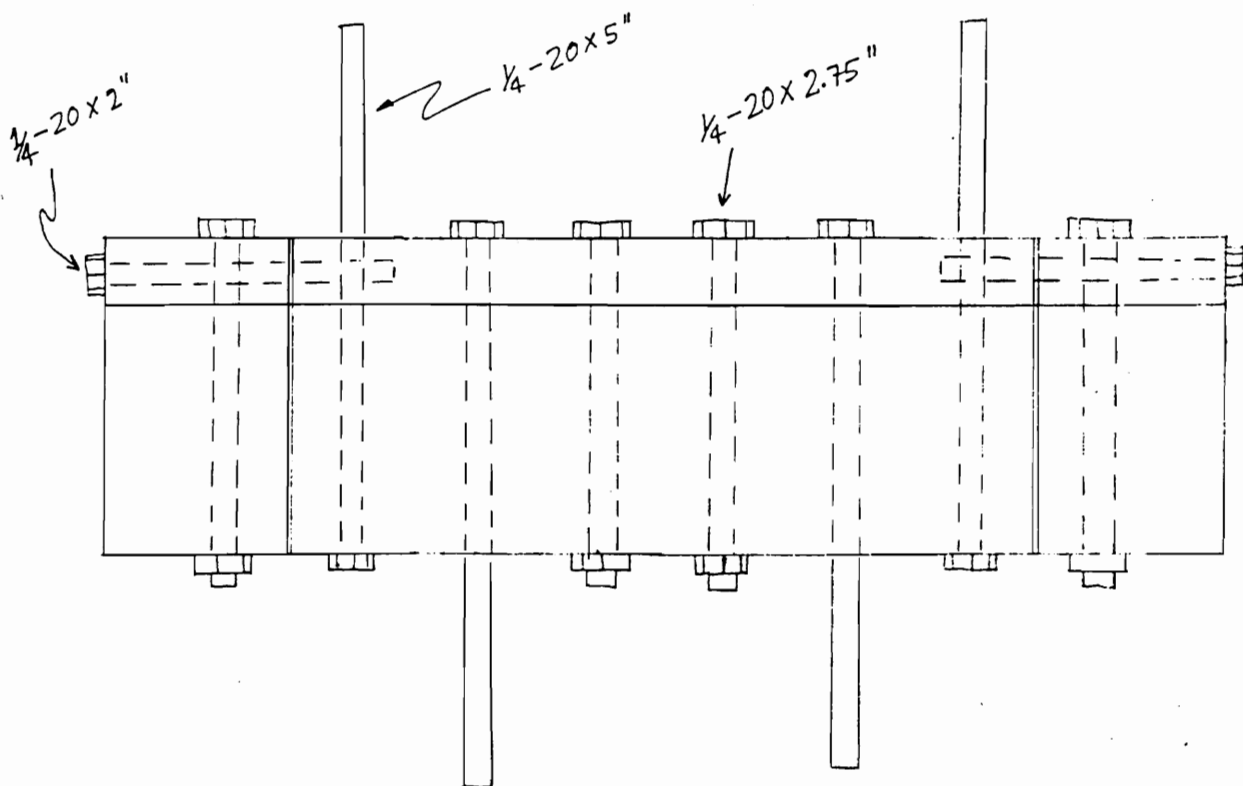


Figure 6.7: The microreactor assembled with the cap screws.

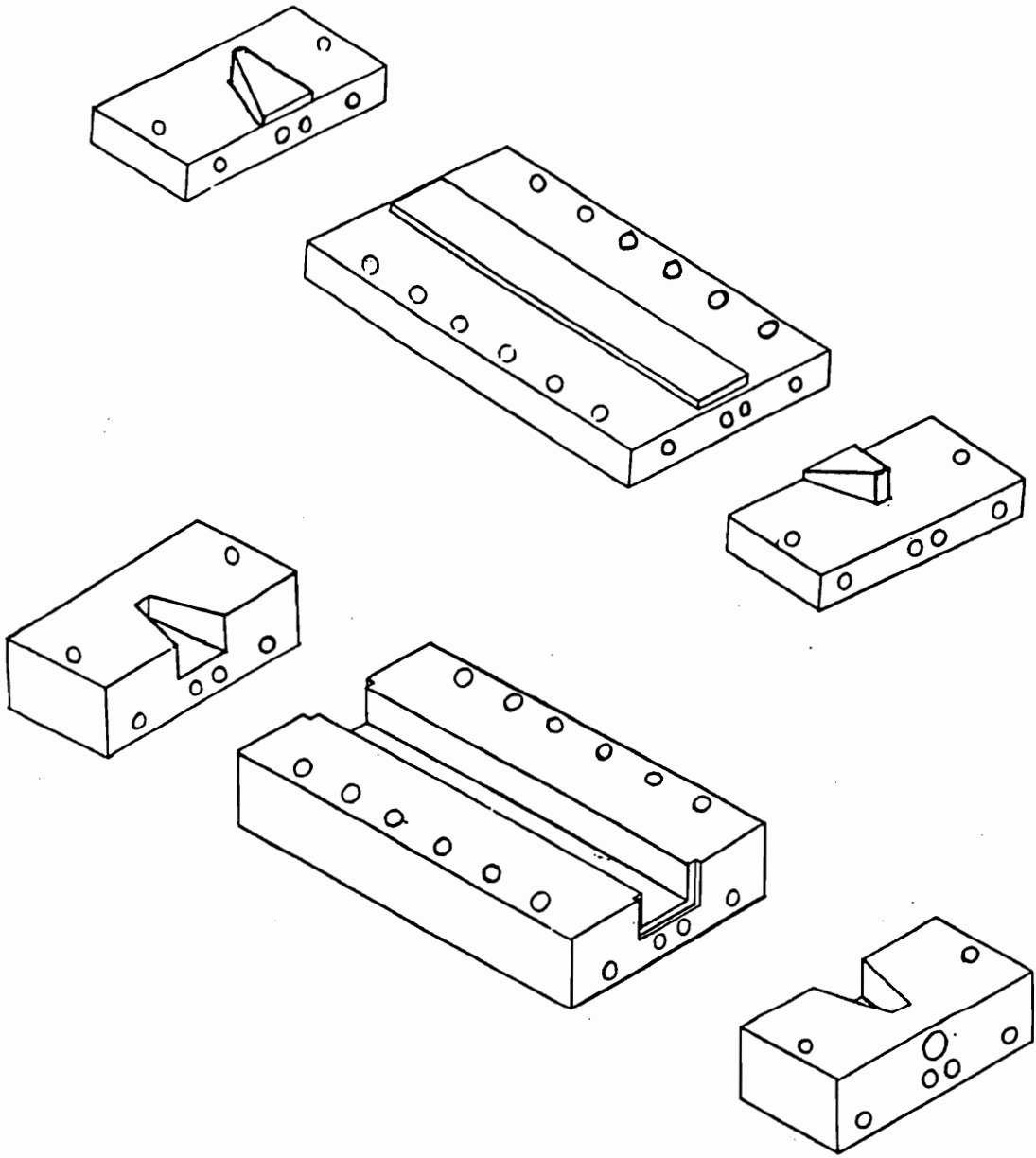


Figure 6.8: Individual pieces making up the microreactor. Center pieces are for horizontal duct at a length of 15.24 cm. Inlet section and outlet sections are similar.

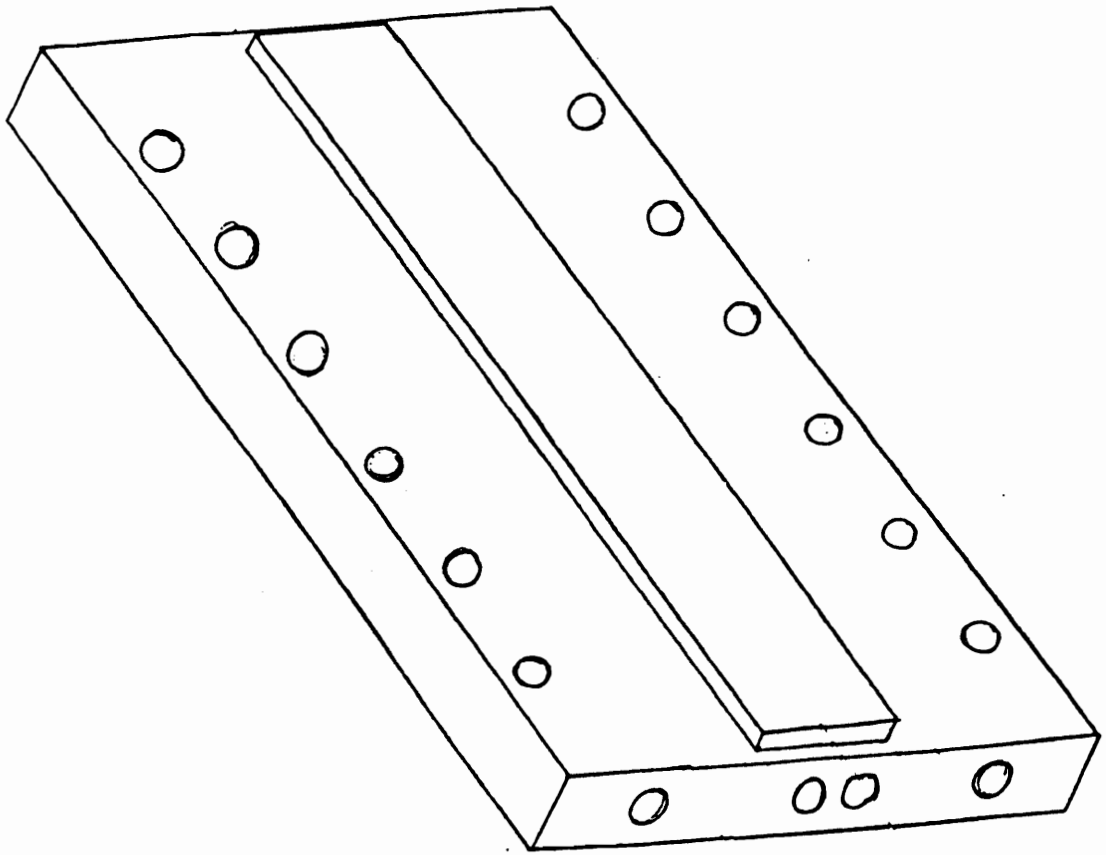


Figure 6.9 (a): Isometric view of the top half of the middle section (viz. mid-top section).

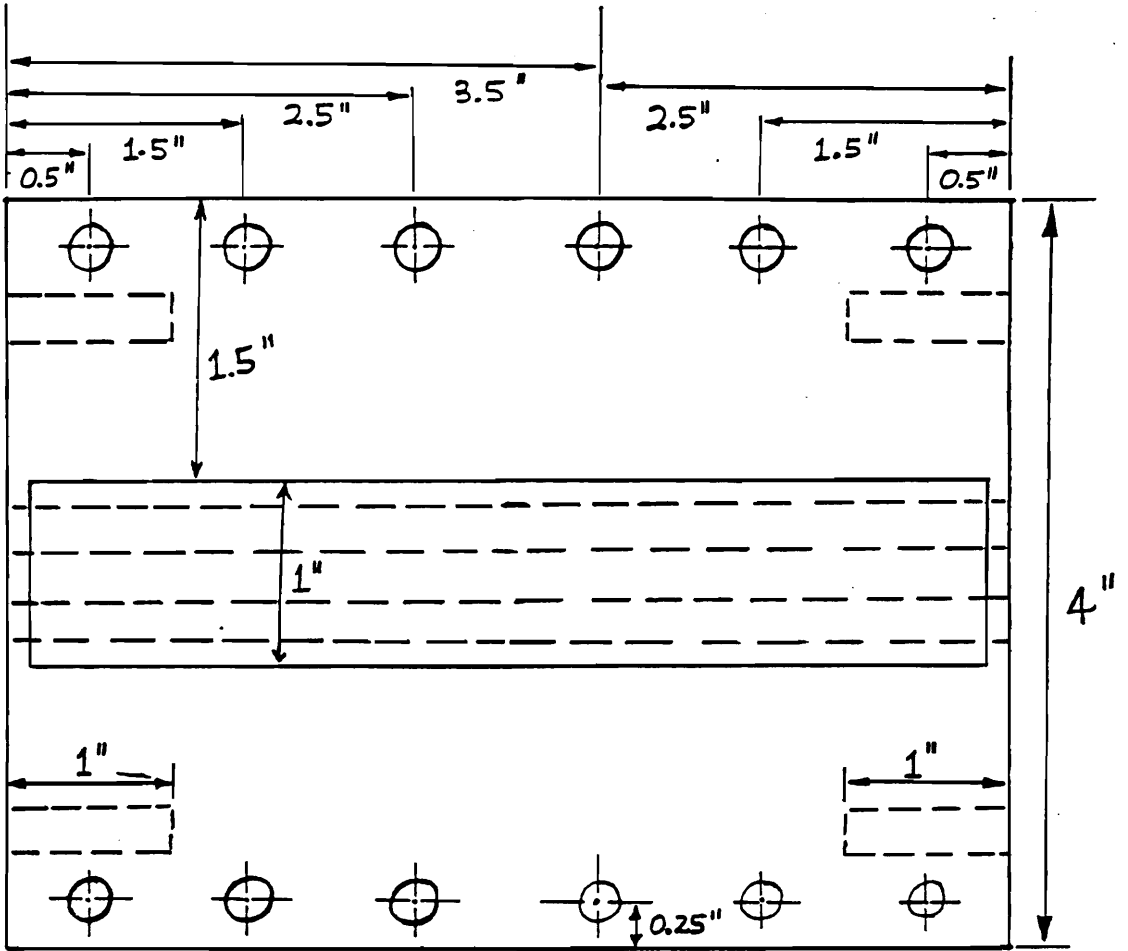


Figure 6.9 (b): Top view of the top half of the middle section (viz. mid-top section).

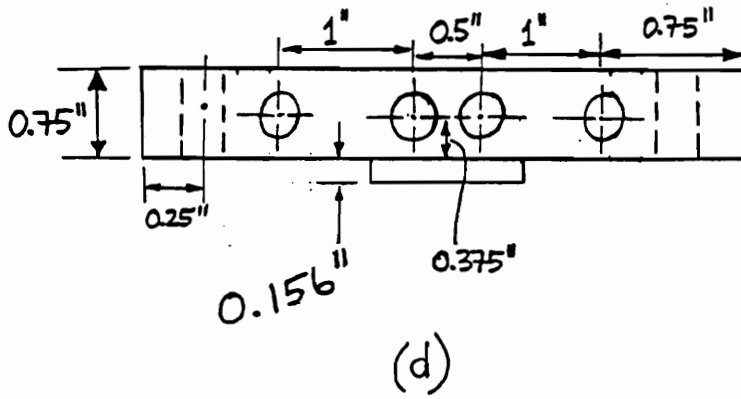
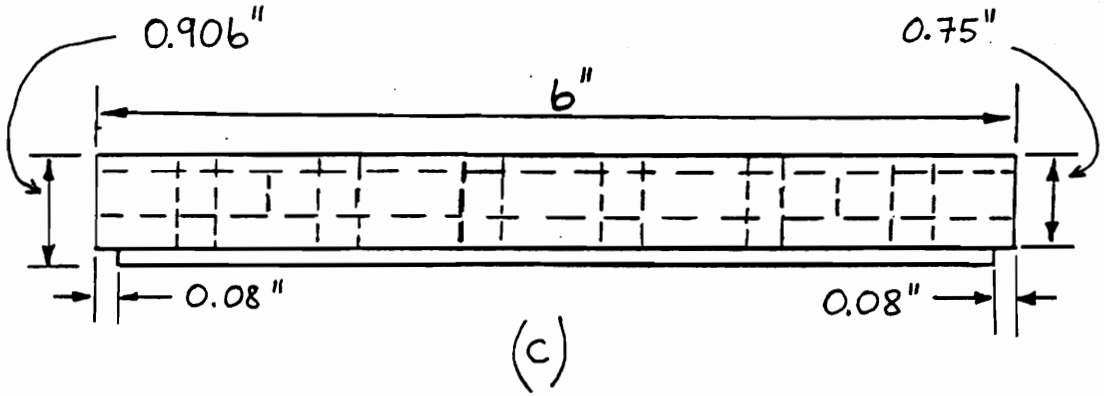


Figure 6.9: Side view (c), and Front view (d), of the top half of the middle section (viz. mid-top section)

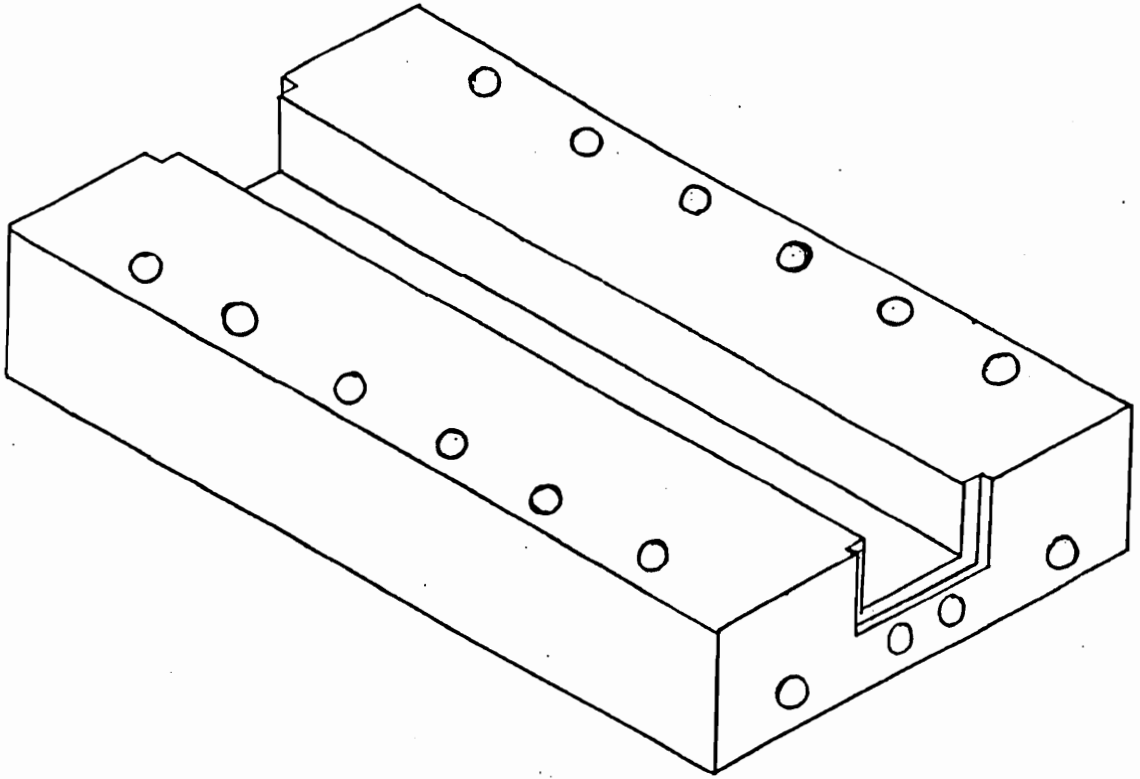


Figure 6.10 (a): Isometric view of the bottom half of the middle section (viz. mid-bottom section).

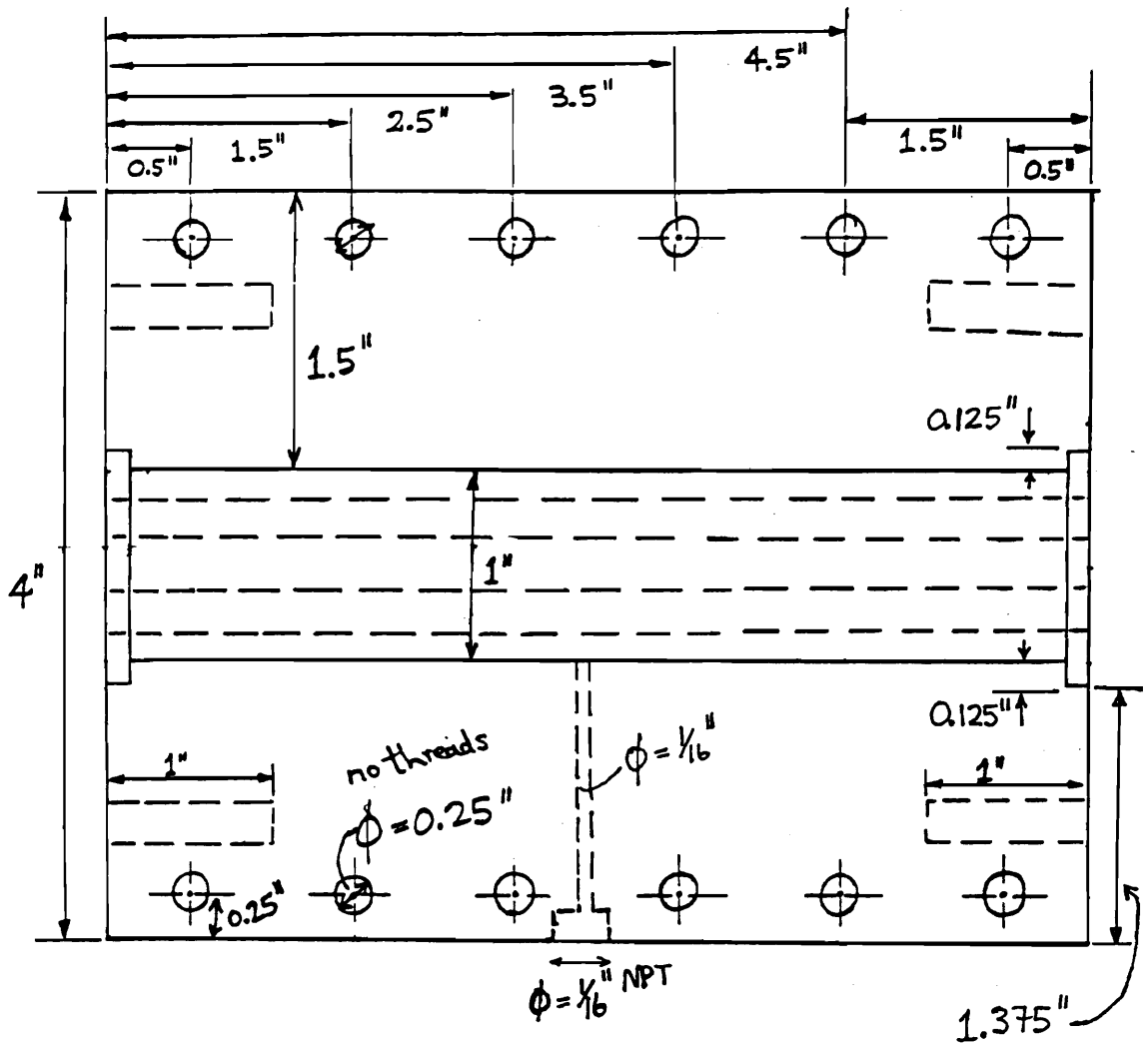


Figure 6.10 (b): Top view of the bottom half of the middle section (viz. mid-bottom section).

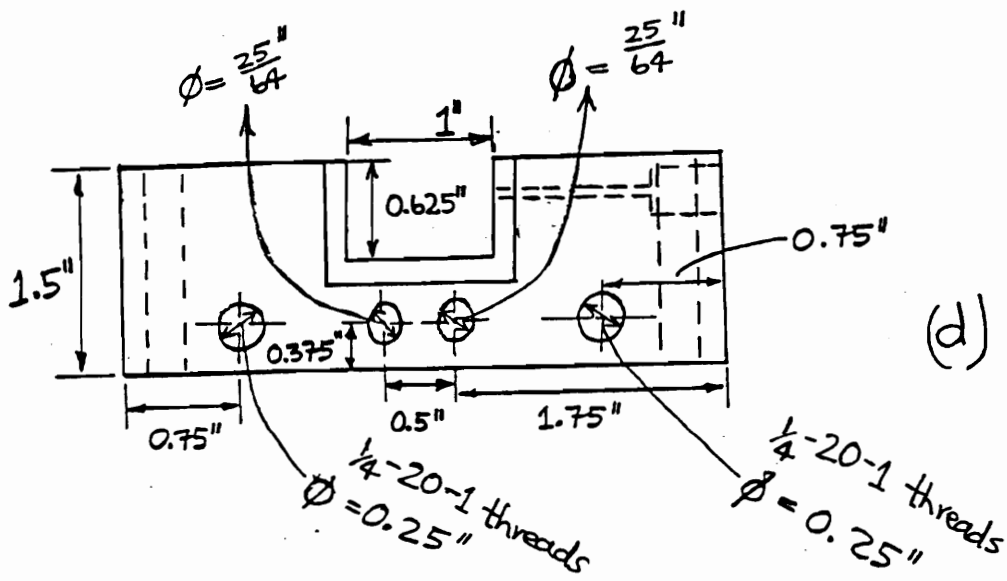
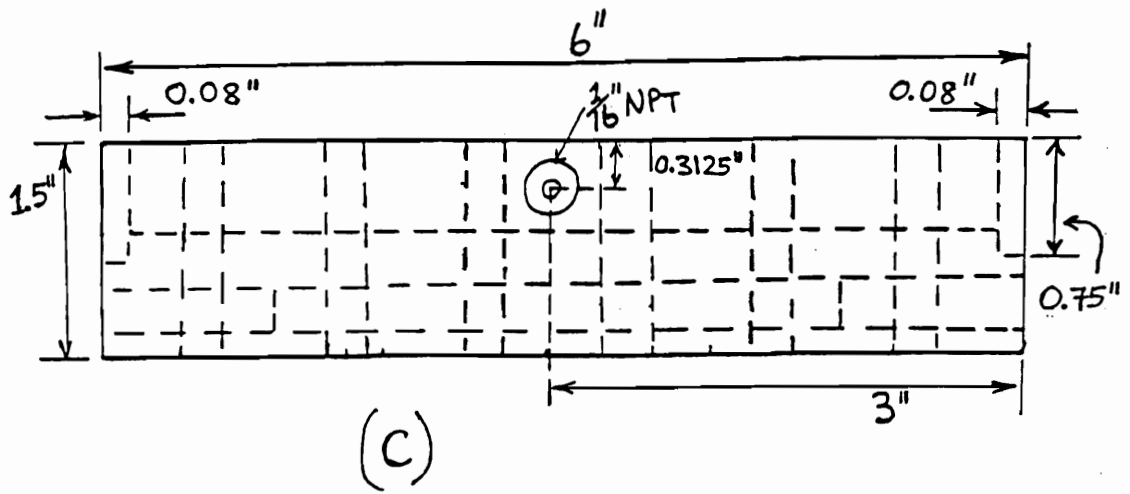


Figure 6.10: Side view (c) and Front view (d), of the bottom half of the middle section (viz. mid-bottom section).

Figure 6.11 presents views of the top half of the inlet section (viz. inlet-top section) namely (a) Isometric view, (b) Top view, (c) Side view and (d) Front view.

Figure 6.12 indicates views of the bottom half of the inlet section (viz. inlet-bottom section) namely (a) Isometric view, (b) Top view, (c) Side view and (d) Front view.

6.3.2 MATERIAL SELECTION

The microreactor would be heated to 482 C and maintained at this temperature for the duration of the experiment and cooled down to room temperature at the end of the experiment. Several experiments would be conducted in the microreactor.

Many of the brainstormed ideas on how the Vibrated Bed Microreactor could be designed had shortcomings on the following questions:

- (i) can the material be heated to a temperature of 482 C ?
- (ii) will the material maintain its integrity over a long period of time at this temperature ?
- (iii) is the material machinable ?
- (iv) since the microreactor could not be machined from a single piece, how will various pieces be put together to be leakproof and airtight ?

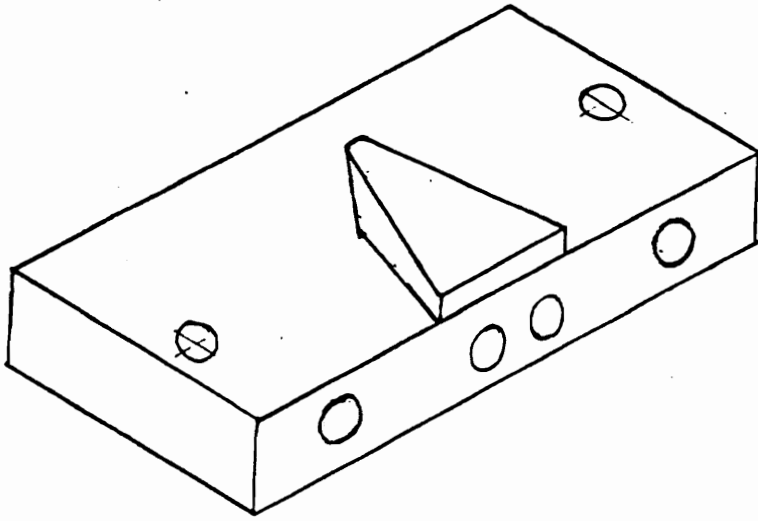


Figure 6.11 (a): Isometric view of the top half of the inlet section (viz. inlet-top section).

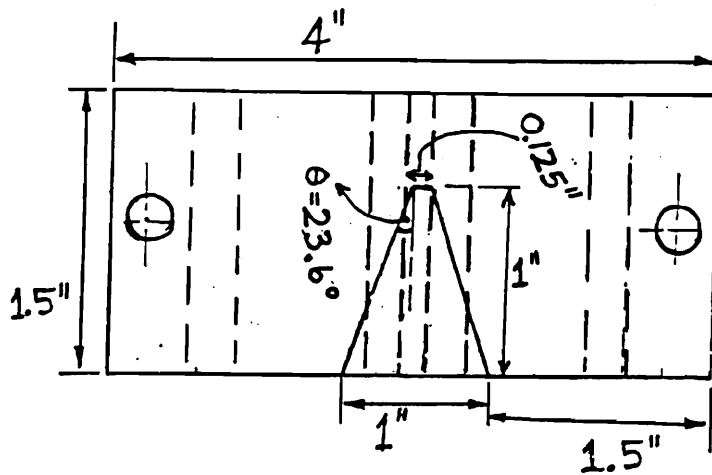
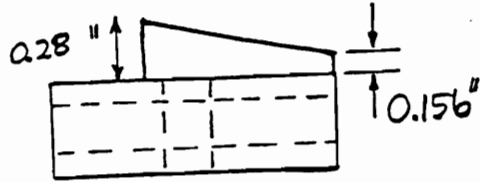
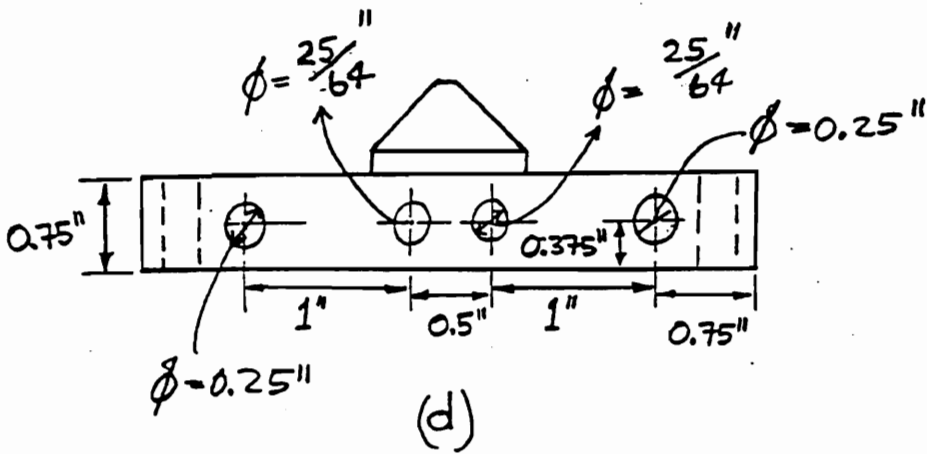


Figure 6.11 (b): Top view of the top half of the inlet section (viz. inlet-top section).



(c)



(d)

Figure 6.11: Side view (c) and Front view (d) of the top half of the inlet section (viz. inlet-top section).

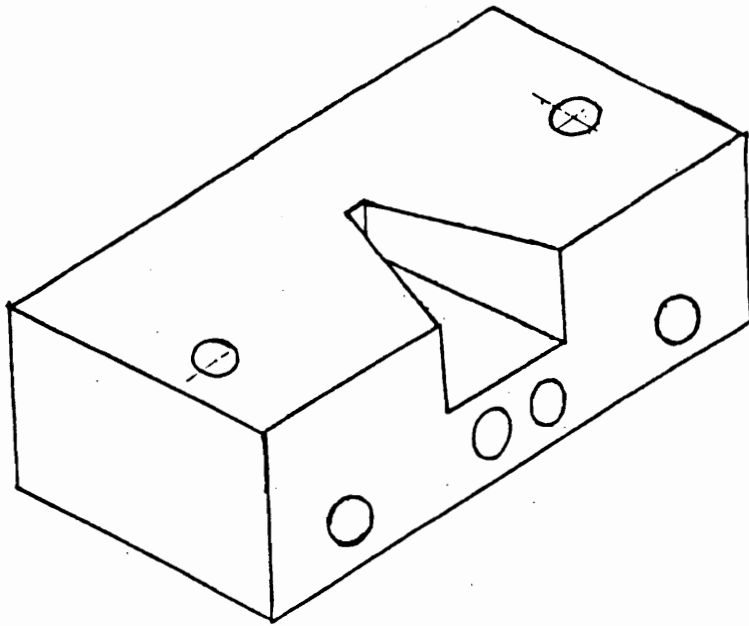


Figure 6.12 (a): Isometric view of the bottom half of the inlet section (viz. inlet-bottom section).

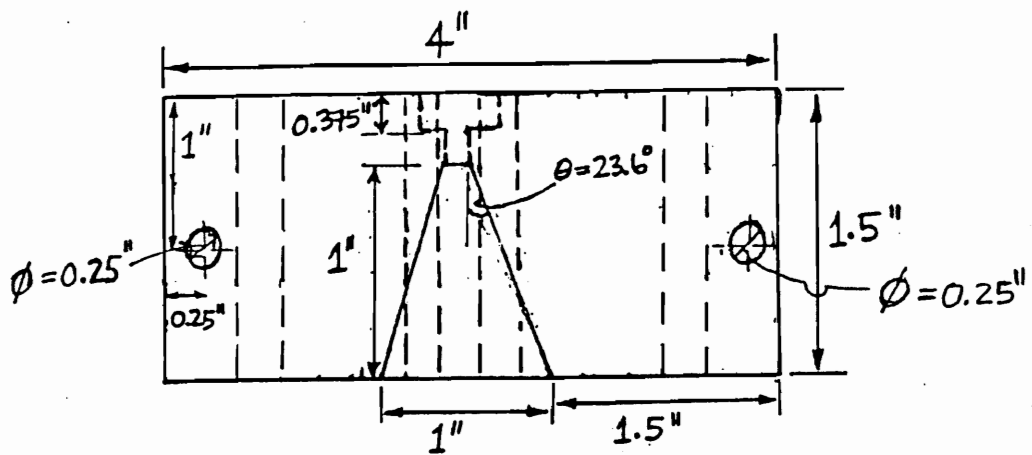
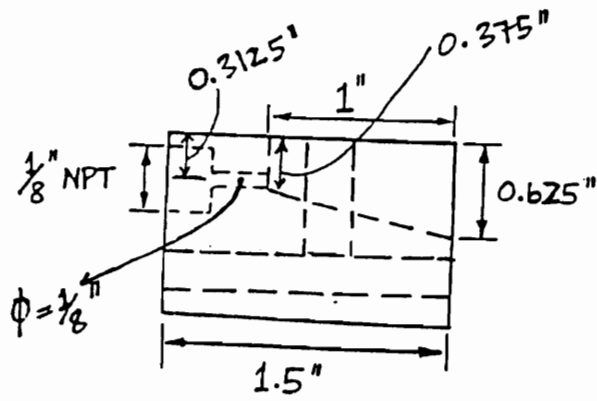
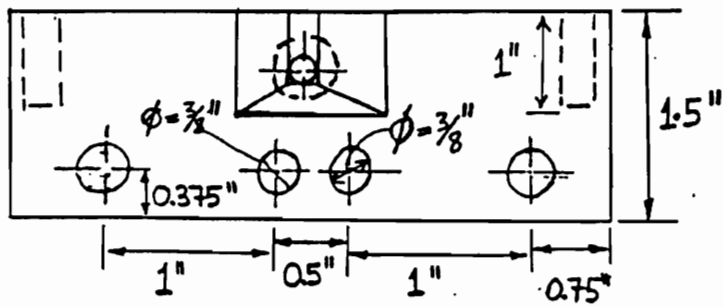


Figure 6.12 (b): Top view of the bottom half of the inlet section (viz. inlet-bottom section).



(c)



(d)

Figure 6.12: Side view (c) and Front view (d) of the bottom half of the inlet section (viz. inlet-bottom section).

(v) will a visual inspection of the C-E vibration state in the microreactor be possible ?

The challenges in the selection of the material of construction for the Vibrated Bed Microreactor were:

(i) finding the material which is suitable for operating at high temperatures for long periods of time and able to withstand cyclic Thermal Stress and Shock without losing its integrity and altering its physical properties. The heating and cooling cycles during and after the experiment would cause severe thermal stress and shock to the material.

(ii) the material should have a high Thermal Conductivity. It is imperative that the 482 C temperature be uniform throughout the horizontal duct length of the Vibrated Bed Microreactor. Material of low Thermal Conductivity would not be suitable because heating it would result in non-uniform temperature distribution (i.e. hot spots) which would adversely affect the performance of the MTO reaction.

(iii) the material would have a low Coefficient of Thermal Expansion. The microreactor is mounted and held on the Vibration Table with cap screws. It is heated to 482 C whilst the Vibration Table is kept at a temperature lower than 120 C, the Accelerometer maximum operating temperature. Material with high coefficient of thermal expansion would be unsuitable for the Vibrated Bed Microreactor because the temperature difference (i.e. 362 C)

between the Vibrated Bed Microreactor and the Vibration Table would create excess strain on the cap screws and most probably lead to their snapping in the middle of an experiment.

(iv) the material of construction should have low Density so that the microreactor will be as light as possible. Vibrational frequency and intensity required to yield vibration of HZSM-5 catalyst in the C-E state depends on the total load which the electromagnetic vibrator has to drive. This load includes the Vibration Table, six stiff Leaf Springs and the Microreactor. The higher this load is, the higher the vibrational intensity required to achieve the C-E state in the vibration of the catalyst. High vibrational intensity is very destructive and stressful on the surrounding equipment and the building too as it becomes impossible to cushion and dampen the vibrations.

(v) Lastly the material would have to be machinable and widely available. Special material requires special machining tools. Since the initial design is never perfect it has to go through several modifications and refinements, which are much cheaper and quicker if the material of construction is machinable and widely available in the first place.

6.3.2.1 Material of Construction for the Microreactor

Aluminum was chosen as material of construction for Vibrated Bed Microreactor. Table 6.1 presents Mechanical Properties of Aluminum in comparison with Stainless Steel. As shown in the table, Aluminum proved to be better suited for our application than Stainless Steel because;

(i) it has higher Thermal Conductivity

(ii) it has lower Density

(iii) its Melting Point is much higher than the operating temperature

Table 6.2 presents the Chemical Composition of the selected Aluminum Alloy, 6061-T6. As shown in the table the Alloy is made up of 99.45 percent Aluminum and the remaining 0.55 percent consists of alloying elements such as Magnesium, Iron, Silicon, Copper, Chromium, Zinc, Manganese and Titanium.

The alloy combines relatively high strength, good workability, high resistance to corrosion and is widely available (Williams and Company Inc., catalogue).

6.3.2.2 Distributor Material

Distributor Plates were put at both ends of the Reaction Zone. Their role and function was twofold (i) to keep HZSM-5 catalyst in place and (ii) to present a slight pressure drop in order to have Methanol Vapor flow into the reaction zone as a uniform plug which covers the entire cross sectional area.

Table 6.1: Mechanical Properties of Aluminum in comparison with Stainless Steel and Copper.

	Aluminum	Stainless Steel	Copper
Density, lb/ft ³	169	500	559
Melting Point, F	1190	2550	1981
Specific Heat, BTU/(lb F)	0.24	0.12	0.10
Thermal Expansion (#)	12.6	9.6	9.8
Thermal Conductivity (*)	1536	105.6	2688

(*) BTU in ft²/(hr F)

(#) in/in/F x 10⁻⁶

Table 6.2: Chemical Composition of the Aluminum Alloy, 6061-T6. Alloy is 99.45 percent Aluminum and the remaining 0.55 percent consists of alloying elements such as Magnesium, Iron, Silicon, Copper, Chromium, Zinc, Manganese and Titanium in the compositions shown in the table.

Element	Component Percent
Aluminum	99.45
Silicon	0.40 - 0.80
Iron	0.70
Copper	0.15 - 0.40
Manganese	0.15
Magnesium	0.80 - 1.20
Chromium	0.15 - 0.35
Zinc	0.25
Titanium	0.15
Others	0.05 - 0.15

The distributor material had to have similar properties as the material of construction for the Vibrated Bed Microreactor. The choice, which was available commercially, was between a wire cloth and a porous metal plate, both made from Stainless Steel.

Stainless Steel Porous Metal Plate was selected because it was rigid (i.e. inflexible) and would stay in place during the vigorous vibration of the Vibrated Bed Microreactor. It could also be machined with exact precision and be made to fit snugly.

6.3.2.3 Gasket Material

It was necessary to place a gasket between mating surfaces of the Vibrated Bed Microreactor in order to provide an airtight seal. GRAFOIL Flexible Graphite was chosen as a gasket for mating surfaces between the top and bottom pieces of the sections of the Vibrated Bed Microreactor. GRAFOIL gasket was suitable for the application because it has a high Thermal Conductivity, can withstand high temperature, has a good Leak Pressure and is easy to cut into shape (Norton Performance Plastics Corporation catalogue).

GRAFOIL material was not used on the mating surfaces between: (i) Reaction Zone and Inlet Section, and (ii) Reaction Zone and Outlet Section

because of an uncertainty on the catalytic activity of this material on Methanol Vapor at high temperature.

Soft Copper was chosen instead as gasket material for these surfaces because: (i) it had been observed not to have catalytic activity on Methanol at high temperature (Chen and Reagan, 1979), and (ii) it has a high thermal conductivity. The main reason why soft copper was not used entirely in the Vibrated Bed Microreactor as a gasket material was that it showed signs of severe corrosion at high temperature and its machining required special care and tools. A new copper gasket was used in each experiment.

6.3.2.4 Insulation Material

Alumina-Silica Bulk Ceramic Fiber, with a trademark Inswool-HP Bulk, was chosen for use as insulation material for the Vibrated Bed Microreactor. The material is light weight, easily packed, fitted and formed for rapid installation, can be used continuously at temperatures to 1230 C, has high temperature resistance, thermal stability and low heat storage, has excellent resistance to vibration, low thermal conductivity (0.9 BTU-in/ft² hr F) and a density of 6 lb/ft³ which can be hand packed to 12 lb/ft³ (A.P. Green Industries Inc., catalogue).

Insulation is used in order to reduce heat loss by radiation and convection. It is also used to keep high temperature away from heat sensitive

accelerometer (120 C max) and GE silicone adhesive (204 C max). The application of GE silicone adhesive is described in the later section.

6.3.3 METHOD OF HEATING

The MTO reaction requires a temperature of 482 C over HZSM-5 catalyst to yield maximum amounts of Light Olefins.

Heating the Vibrated Bed Microreactor to this temperature was accomplished with the use of a set of four (3/8 inch) Cartridge Heaters rated at 600 Watts and 120 Volts each. The cartridge heaters of 25.4 cm length were used to heat horizontal duct of 15.4 cm and the inlet and outlet sections to a temperature of 482 C. The Cartridge Heaters were connected in series. Two of them were located in the bottom plate whilst two were in the top plate, in a symmetrical fashion. The Cartridge Heaters were fitted with straight Stainless Steel Braid to protect the leads from snapping during vigorous vibration.

A high performance Temperature and Process Controller, OMEGA CN3201 was used to ramp and maintain the temperature at a setpoint of 482 C. The Controller offered selectable Proportional, PID or ON/OFF control modes and with an input for a J (Iron-Constantan) thermocouple with a range of -73 to 760 C. A J thermocouple with an ungrounded junction was connected

to the Controller and used to monitor temperature directly in the Reaction Zone of Vibrated Bed Microreactor. The ungrounded junction was selected for its abrasion resistance, vibration resistance and chemical resistance since the thermocouple tip was located to look only slightly into the Reaction Zone of the Vibrated Bed Microreactor through a (1/16 inch) hole.

6.3.4 GLASS REFERENCE DUCT

The intimate gas-solid contacting in the Vibrated Bed Microreactor depends entirely on the catalyst vibrating in the C-E state. It is therefore crucial to check and ensure that the catalyst continues to vibrate in the C-E state during the experiment.

The most difficult challenge in the design of the Vibrated Bed Microreactor was to find a design allowing a visual inspection of the state of vibration of the HZSM-5 catalyst in the Horizontal Duct (i.e. Reaction Zone). Quartz glass was considered as a possible material of construction for the Vibrated Bed Microreactor because it is transparent and heat resistant. Quartz glass is very brittle and machining of it could not be handled by the Department Machine Workshop, as this would require special tools and blocks of the thickness required for the design were not easily available. They would have had to be specially fabricated by an outside commercial manufacturer.

It was out of financial prudence that Aluminum was selected as material of construction for Vibrated Bed Microreactor.

Selecting Aluminum metal as material of construction for the Vibrated Bed Microreactor completely ruled out the possibility of a visual inspection of the state of vibration of the catalyst. Several ideas were advanced on how to get around this, including the notion of making a window on the side of the Reaction Zone. Such a window would have to be made: (i) on both sides of the Reaction Zone in order to maintain a symmetrical load distribution, and (ii) out of Quartz material. This meant that a way would have had to be found of ensuring good airtight contact between Aluminum and Quartz; and (iii) a window would require an insulating cover to reduce heat loss by radiation. Moreover, opening and closing the window to check on the state of vibration of the catalyst would upset the stability of the uniform temperature in the Reaction Zone.

The best idea was to construct a Glass Reference Duct that could be suspended directly above the Vibrated Bed Microreactor. The Glass Reference Duct was made out of a rectangular duct of heat resistant Borosilicate Glass attached symmetrically on an Aluminum plate. Figure 6.13 (a) shows a simplified sketch of the assembled Glass Reference Duct and Figure 6.13 (b) shows the dimensions of the aluminum plate where in the borosilicate glass is placed in symmetry.

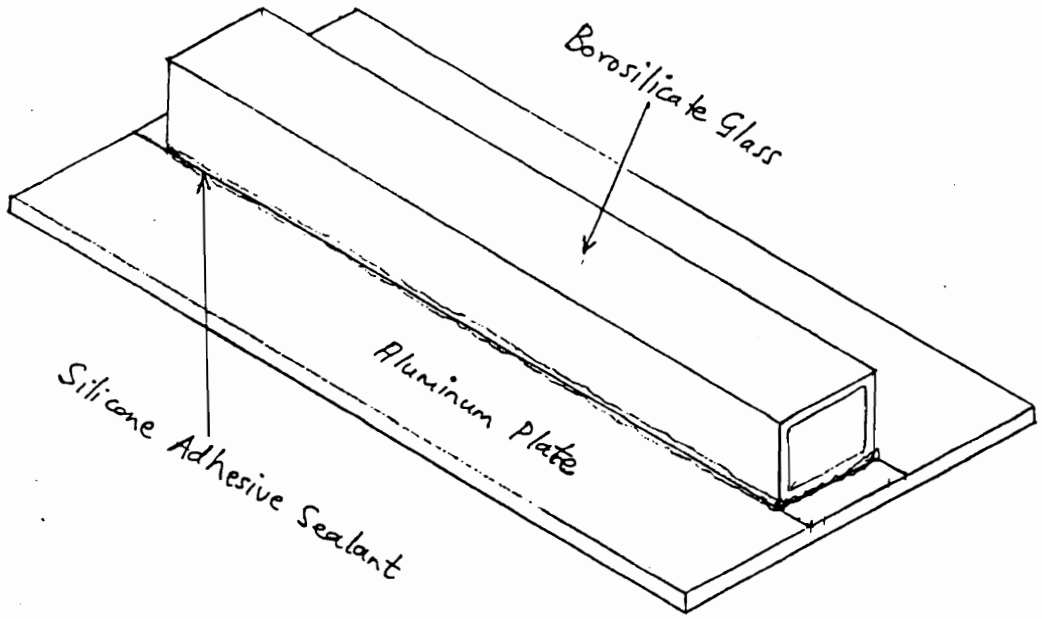


Figure 6.13 (a): Isometric view of assembled Glass Reference Duct.

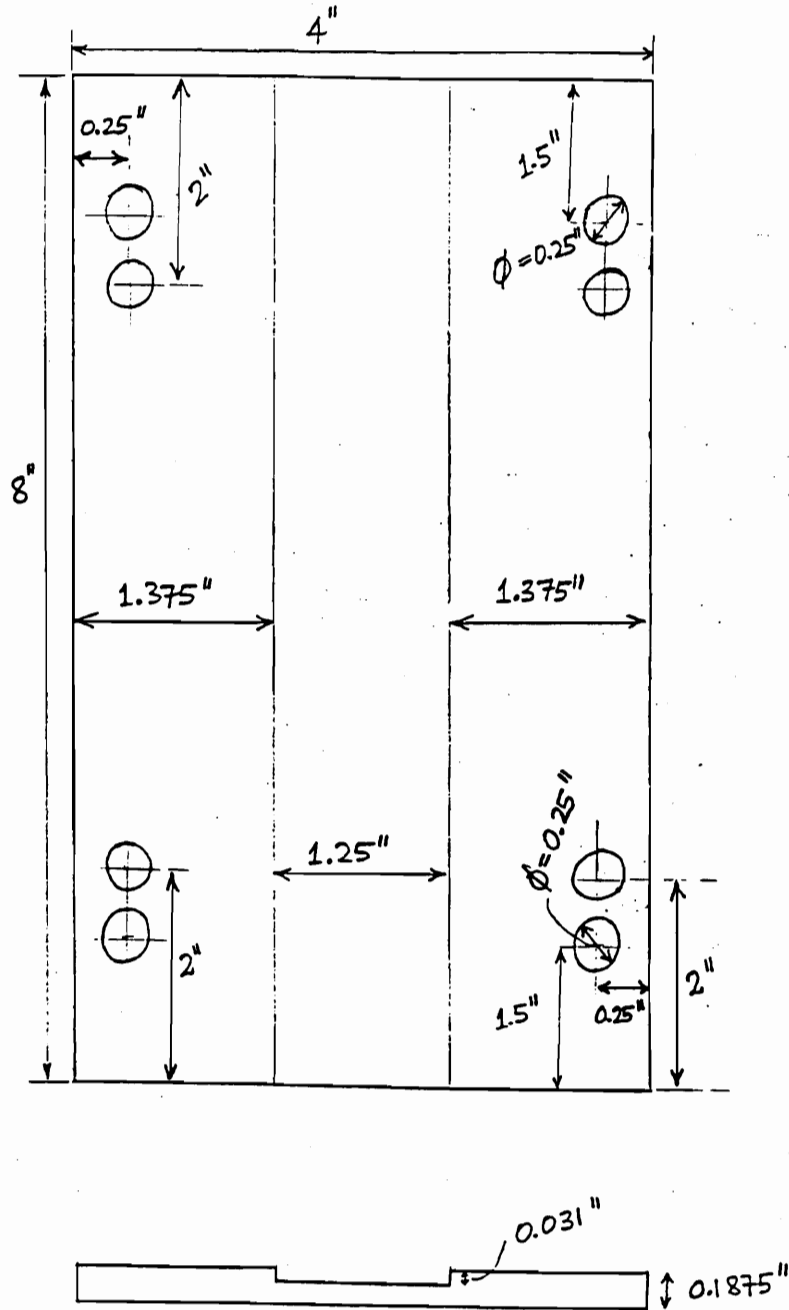


Figure 6.13 (b): Design dimensions of the aluminum plate onto which the borosilicate glass is attached.

Dimensions of the Borosilicate Glass rectangular duct were exactly the same as those in the Horizontal Duct of the Vibrated Bed microreactor (i.e. 2.54 cm in width and 1.27 cm in height). The Glass Reference Duct is 17.8 cm long. As with the Vibrated Bed Microreactor the duct would be loaded with a 1-mm layer of the HZSM-5 catalyst.

Attaching borosilicate glass to aluminum metal plate was an unfamiliar problem since the resulting bond would have to be strong to withstand the vigorous vibration and high temperature. A number of adhesives were tried including Super Glue, Epoxy, Double-sided Tape, Sauereisen Insa-lute Adhesive Cement and Silicone Adhesive Sealant with maximum operating temperatures of 82, 93, 121, 982 and 204 C, respectively. Super Glue, Epoxy and Double Sided Tape failed because they could not stand up at the necessary temperature. Sauereisen Insa-lute Adhesive Cement was tried, but it cured to a very hard crust which does not allow for thermal expansion of the glass. This led to the glass cracking during an actual experiment. Silicone Adhesive Sealant from General Electric provided an excellent bond which survived the vigorous vibration, high temperature and allowed thermal expansion of the glass.

6.3.5 VIBRATED BED MICROREACTOR SETUP

Setting the Vibrated Bed Microreactor in preparation for an experiment involved mounting it on the Vibration Table and mounting the Glass Reference Duct directly above it, as shown schematically in Figure 6.14.

The Accelerometer which monitors the vibration of the load (i.e. Vibration Table, Vibrated Bed Microreactor and Glass Reference Duct) has a maximum operating temperature of 120 C. In order to prevent exceeding this temperature the Vibrated Bed Microreactor was mounted onto the Vibration Table with 12.7 cm long hardened cap screws which went through it, through 5 cm long metal spacers, and were screwed tightly onto the Vibration Table.

The Silicone Adhesive Sealant used in the Glass Reference Duct has a maximum operating temperature of 204 degree Celsius. The Glass Reference Duct was mounted onto the Vibrated Bed Microreactor with 12.7 cm long cap screws which went through its Aluminum Plate, 5 cm long metal spacers and through the top and bottom aluminum microreactor pieces and held tightly with nuts.

Inswool material was stuffed in the open space between: (i) the microreactor and vibration table and (ii) the microreactor and the glass reference duct. It succeeded in keeping the temperature at: (i) the Vibration Table not higher than 80 degree Celsius and (ii) the glass reference duct not higher than 180 degree Celsius during the experiment.

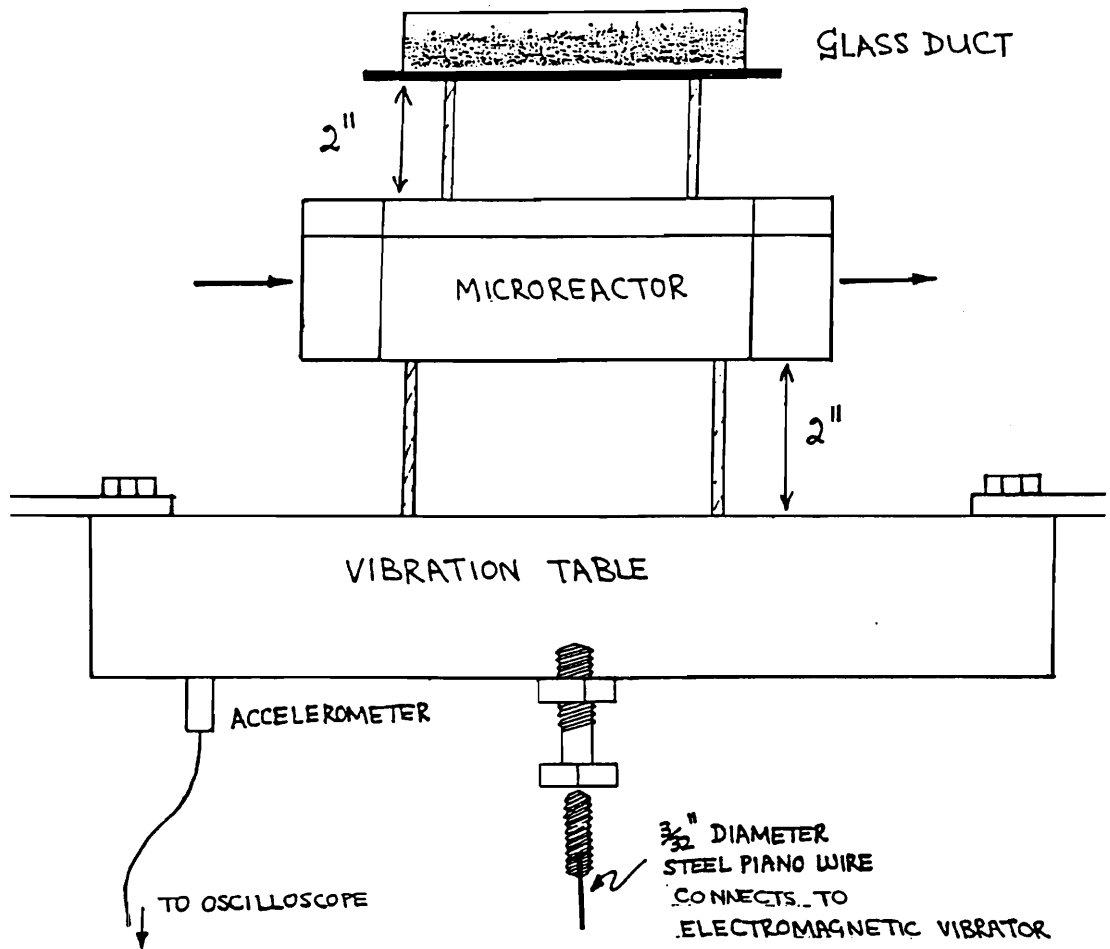


Figure 6.14: Sketch of apparatus setup in preparation for an experiment.

Extra insulation was also packed on all of the sides of the microreactor. This arrangement was found to be effective in reducing heat radiation and convection from the hot microreactor. An aluminum sheet cover (0.24 mm thickness) was designed to cover the insulation and keep it in place during the vibration.

This concludes a description of a design for the microreactor which satisfactorily met the challenges posed by high temperature work.

6.4 PRODUCT ANALYTICAL SCHEME

The product analytical scheme employed in this work is much simpler than that used by MRDC, described in chapter 5. Our scheme consists of a sampling valve, a gas chromatograph and two integrators as shown in Figure 6.15.

6.4.1 SAMPLING VALVE

A 10-port, 1/8 inch, zero volume, gas sampling Valco Valve is used to sample the hot reaction product gases. The valve can withstand a temperature of 350 C and pressure of 400 psi. The valve is driven with an Air Actuator coupled to a pair of 3-way solenoid air valves. Figure 6.16 shows the block diagram of the operation of the sampling valve.

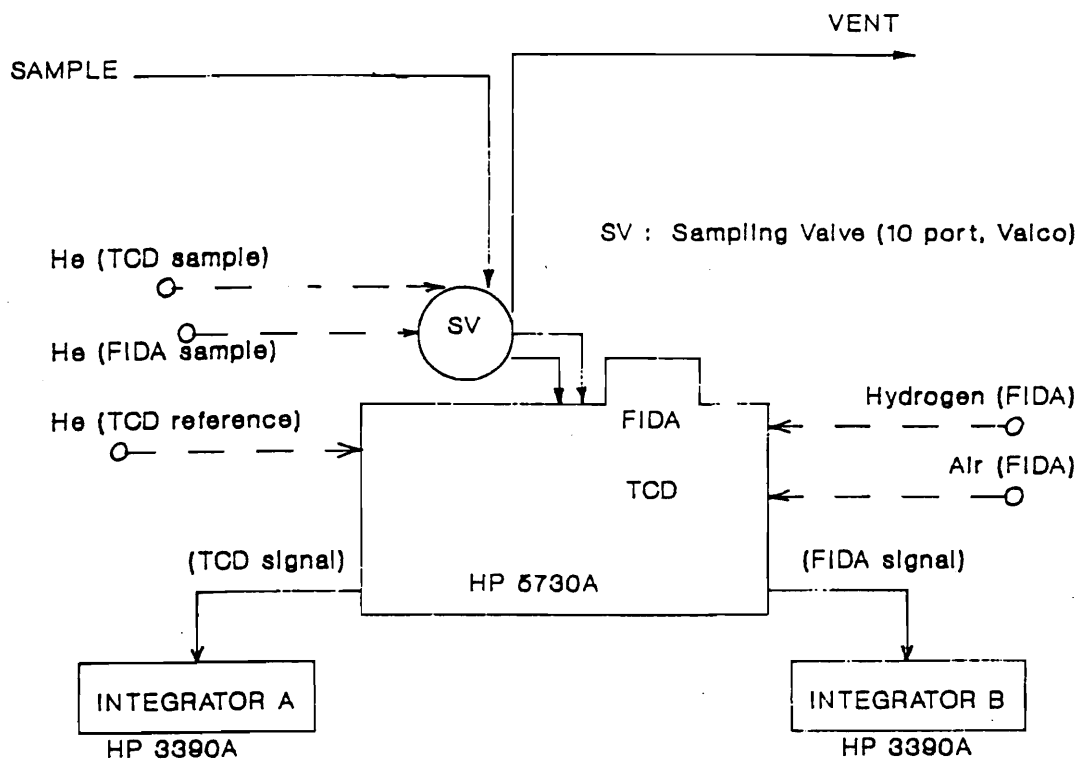


Figure 6.15: Product sampling scheme.

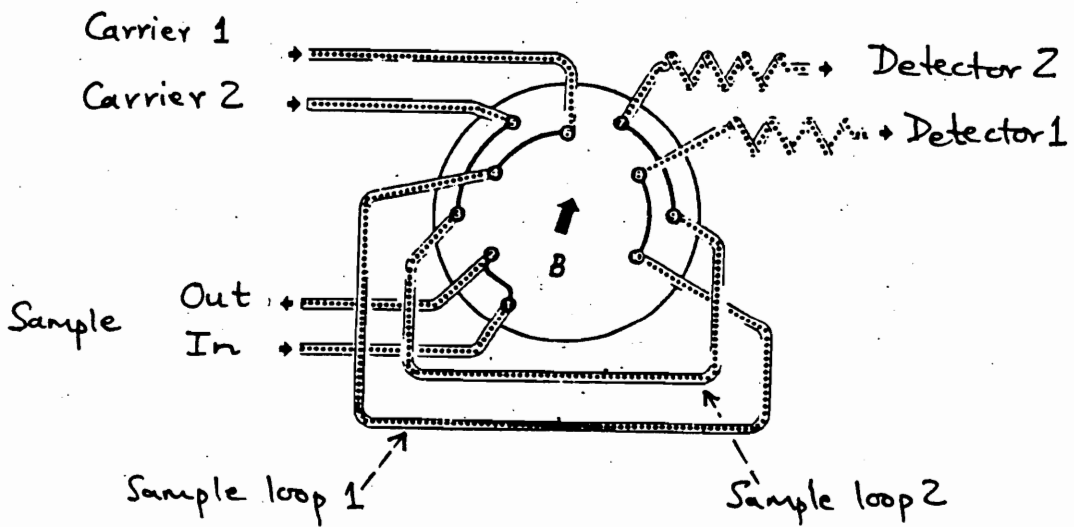
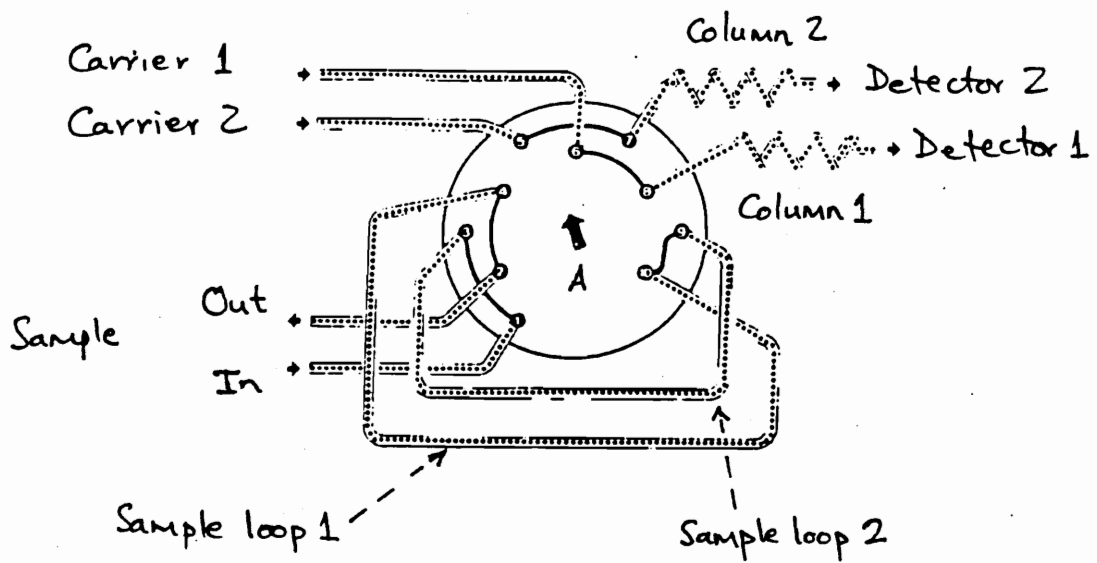


Figure 6.16: Block diagram of operation of the sampling valve.

To reduce problems associated with dead volume, the valve is mounted in close proximity to the column oven. This valve is fitted with two 100 microliter sample loops.

6.4.2 GAS CHROMATOGRAPH

An HP 5730A Gas Chromatograph with a flame ionization detector (FID) and a thermal conductivity detector (TCD) is used for analysing the product sample. Hewlett Packard ceased the manufacture of this model and phased out the support for it (i.e. carrying and supplying replacement parts and providing service for it). It was a long arduous task to restore the Gas Chromatograph to a reasonable working order. Missing parts were replaced. The TCD and FID detectors were overhauled and made operational.

We are using two Hewlett Packard Integrators, Model 3390A, to receive and integrate the signals from the TCD and the FID detectors. One is borrowed from Dr Cox and the other is borrowed from Dr McNair.

6.4.3 PACKED COLUMN

The MTO reaction product contains a mixture of water and hydrocarbons. The majority of GC packed columns though cannot handle a hydrocarbon-water mixture with a high fraction of water (viz. 56 weight percent). We

searched for the appropriate GC packed column to effectively separate the reaction product spectrum and settled for a HayeSep D column whose characteristics are shown in Table 6.3.

A packed column has a higher sample loading capability and can operate without deterioration from large amount of water making it better suited for our application than a capillary column.

Separation of the components in a sample depends on selection of column parameters and column efficiency. Columns obtained from different sources tend to vary in dimension, material and liquid phase coating. These variations result in columns having differences in their retention capacity and thus cause different elution patterns if identical operating conditions are employed (Hollis, 1973; Pollock et al., 1984). It was primarily for this reason that we have always obtained our HayeSep D packed columns from a single source, the manufacturer, Hayes Separations Inc..

HayeSep D packed columns were conditioned before initial use, at 270 C with helium flow overnight (18 hours).

Table 6.3: Characteristics of the HayeSep D packed column.

Mesh Size	100/120 mesh
Dimension	1/8 inch by 10 ft
Max Operating Temperature	290 degree Celsius
Surface Area	803 m²/g
Bulk Density	0.3311 g/cm³
Polymer Composition	DVB (high purity)
Polarity	1
Porosity	70.35 %
Average Pore Diameter	0.0308 micron

6.4.4 CARRIER GAS

When a thermal conductivity cell is used as the detector, it is advantageous to use a carrier gas that has a thermal conductivity and molecular weight vastly different from any compounds to be determined. Helium was chosen as a carrier gas because it has a low molecular weight and is safe to handle. Helium gas, (Grade 5.0), is used as the carrier gas in both the FID and the TCD detectors.

The composition of grade 5.0 helium is presented in Table 6.4. The carrier gas flow to both the detectors is maintained at 30 ml/min.

6.5 OTHER MATERIALS AND SYSTEMS

This section will briefly describe the ZSM-5 catalyst samples and a number of miscellaneous items such as valves, process tubing and heating tapes, which are used in the research. The layout of the laboratory will also be described. The section will also describe the means of reducing risks, damage and/or injury to both equipment and human involved in handling toxic materials, dusts and high voltages.

Table 6.4: Composition of grade 5.0 helium.

Helium	99.999 %
Moisture	1 ppm
C. Monoxide, C. Dioxide	0.5 ppm
Oxygen	0.1 ppm
Nitrogen	4 ppm

6.5.1 CATALYST USED

Three batches of ZSM-5 catalyst were supplied by Dr Amos Avidan at Mobil Research and Development Corporation. These were batches of (i) Fresh ZSM-5 as received, uncalcined, (ii) ZSM-5 decoked at 500 C for 5 hours and (iii) Calcined fresh ZSM-5. We have entered into a legal agreement not to investigate the catalyst (i.e. Silica/Alumina ratio, Catalyst binder, form of the catalyst for example Hydrogen or Ammonium, Density, etc). The only information of value supplied about the catalyst is that it is identical to the catalyst used in the 100 BPD Demonstration Plant. The catalyst particle size is lower than 180 microns, and its true density and bulk density are 1.7924 g/ml and 0.7534 g/ml, respectively.

Permission was granted to calcine the catalyst (i.e. fresh ZSM-5 as received, uncalcined) and generate the active hydrogen form of it. A sample was calcined at 538 C for 12 hours with 10 ml/min of air flowing through.

6.5.2 MISCELLANEOUS

Most of the valves used in the system are the Whitey "83" Series Multi Service Trunnion Ball Valve, 3 way switching model. The valves can withstand maximum temperature of 232 C and pressure of 1500 psi.

An approximate length of 20 feet of tubing is used in the setup. Part of the tubing carries hot gaseous reaction product to the GC for analysis and to the vent in the Fume Hood. We required tubing material that would be able to withstand thermal stress over a long period of time and that would not catalytically react with the hot gaseous reaction products. The tubing selected was a stainless steel with an outside diameter, of 1/8 inch (ID = 0.085 inch), and can operate at a temperature of 450 C and pressure of 6400 psi.

This section of the tubing is heated with Calcords to a temperature of 200 C to prevent condensation of the reaction products with boiling point ranging between -161 C (methane) and 176 C (1,2,3-Trimethylbenzene). The Calcords Heating Tapes can reach a maximum temperature of 400 C. We use a combination of Calcords with wattages of 120, 240 and 340 Watts, controlled with Variable Autotransformers.

6.5.3 LAYOUT OF THE LABORATORY

Figure 6.17 gives a layout of the laboratory in which the research was conducted. It has to be noted that the fume hood housing the vibrated bed system, is against the wall.

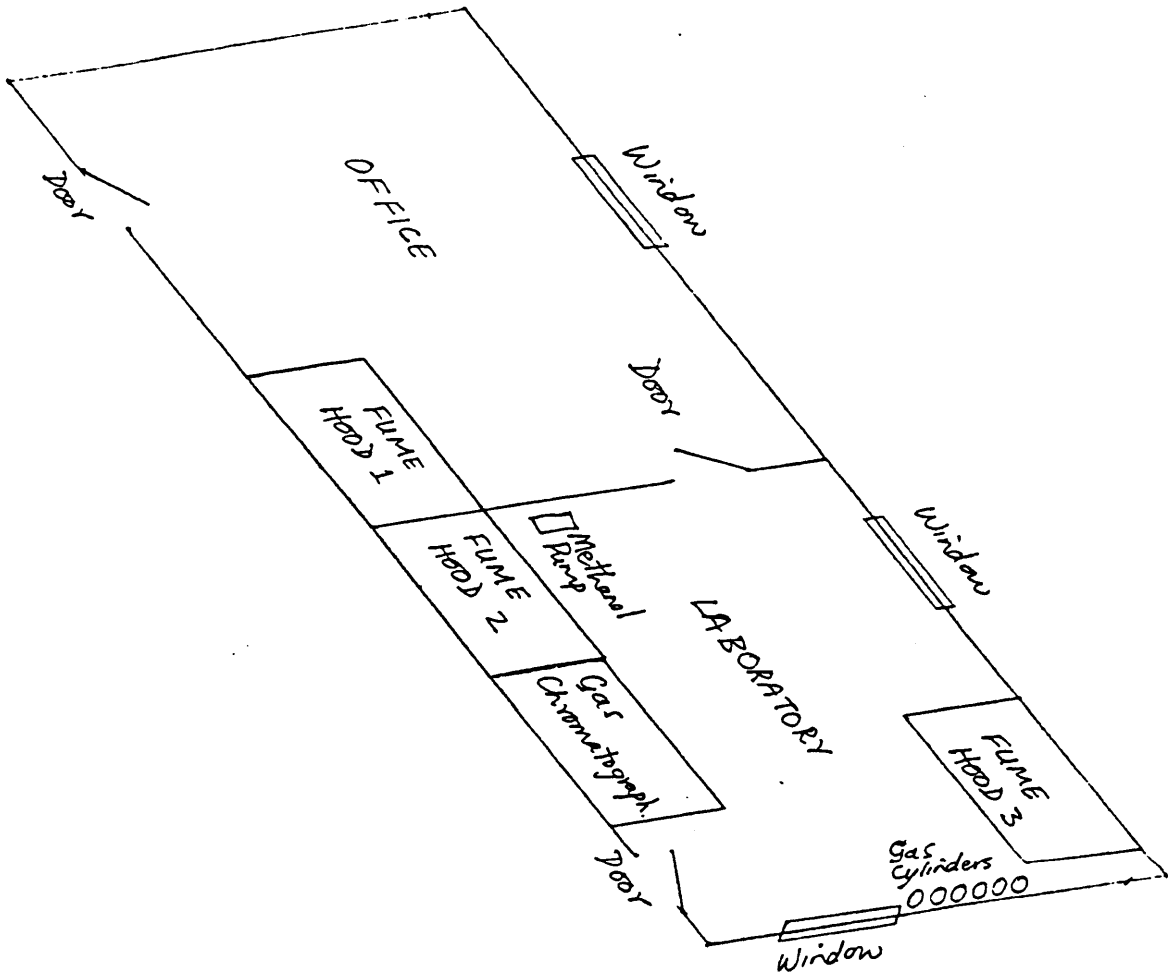


Figure 6.17: Layout of the laboratory.

This was a disadvantage because it was difficult and in some instances impossible to access the back of the vibrator during an experiment when the microreactor was at 482 C.

6.5.4 SAFETY PRECAUTIONS AND EQUIPMENT

This section will describe the means of reducing risks, damage and/or injury to both equipment and human involved in handling toxic materials, dusts and high voltages.

An electrical fuse was installed in the electrical supply line to the electromagnetic vibrator in order to protect it against an overload since it is not equipped with a fuse an overload safety switch. The load power which supply the cartridge heaters was also fitted with a fuse to protect the heaters from an electrical overload. This fuse blew several times. It was easier to replace the fuse than a shorted cartridge heater.

The TECHRON amplifier is fitted with cooling fans which draw room air in, to cool the amplifier. The cooling fans are electrically connected to come on everytime the amplifier is turned on. During the experiment the electromagnetic vibrator is also kept cool with a continuous stream of cold compressed air from the building.

Helium flows through the system overnight after an experiment, before the microreactor is disconnected. The lines are kept at 200 C during the helium flow. This helps to flush out into the vent any toxic material remaining in the microreactor and lines. Doing this helps in cleaning the lines and reducing possible contamination of the product in the next experimental run.

The vibration system used in the research is placed in a GE fume hood because the work involved catalytic conversion of methanol which produces toxic reaction products. The GE Fume Hood is equipped with an exhaust fan. The average face velocity of the exhaust fan was determined to be 124 fpm by Virginia Tech Environmental Health and Safety Services. The exhaust fan is always turned on during an experiment to ensure complete withdrawal of the toxic materials from the reactor outlet line. The TCD exhaust is also put directly into the fume hood for immediate withdrawal because the TCD does not destroy the toxic material in the sample. The FID destroys the sample by burning in air at high temperature.

Latex hand gloves and a Respirator with replaceable cartridges are always worn when: (i) handling methanol (i.e. filling the pump), (ii) doing a task that requires leaning directly into the fume hood during an experiment and (iii) disassembling the microreactor after an experiment.

Disposable dust masks are always worn when handling: (i) the fine HZSM-5 catalyst powder and (ii) Inswool which is an insulation material made of fine glass fibres.

It is imperative to ensure the microreactor is leakproof and is therefore tested for leaks by pressurizing with compressed air and monitoring the rate of pressure drop.

The microreactor is heated to a temperature of 482 C with four cartridge heaters, each with a set of two electrical leads. The product carrying tubing is kept at 200 C with heating from calcord heaters. The experimental apparatus has rather a lot of voltage carrying electrical wires. A fire extinguisher is always kept on hand just in case of electrical fire. Riley Chan, electrical engineer in the department, has been helpful in providing ways for proper electrical grounding.

6.6 EXPERIMENTAL PROCEDURE

Some calculations required the density of methanol (e.g. weight hourly space velocity). Literature quoted a density of 0.796 g/ml at 20 C whilst the density determined in the laboratory was found to be 0.7741 g/ml at 24 C. This was done by measuring a volume of methanol in a measuring cylinder and determining its mass using Mettler AJ 100 measuring scale. The

laboratory determined value of 0.7741 g/ml was used in all computations that required the density of methanol.

All runs will be made at WHSV in the vicinity of 1, with complete conversion of methanol, as commercial practice requires. Blank runs will also be done to check if methanol cracks on metal surfaces of the microreactor at 482 C.

6.6.1 QUALITATIVE ANALYSIS OF MTO PRODUCTS

Primary products of the MTO process are hydrocarbons and water. The hydrocarbons consists of paraffins, olefins and aromatics. In this research work we are interested in olefins and paraffins.

Aromatics are produced in very small amounts if at all, and besides they take a lot longer time to elute from the HayeSep D packed column used. MRDC used an aromatics precutter column to separate aromatics from the paraffins and olefins (Bloch et al., 1977). Such an arrangement was not feasible because our Gas Chromatograph has a single oven with a simple temperature programming capability. One could not for instance use multiple temperature programming rates within a single analysis.

There is also in some cases minor concentrations of hydrogen, carbon monoxide, carbon dioxide, methanol and dimethylether. The absence of these components from MTO reaction when conducted at 482 C made the overall analysis of the reaction products manageable.

6.6.1.1 IDENTIFICATION OF PEAKS

Olefins considered important in this work are ethylene, propene, 1-butene, 1-pentene and 1-hexene ; paraffins are methane, ethane, propane, n-butane, n-pentane and n-hexane. Standard gas samples which contained olefins and paraffins were purchased. Table 6.5 and Table 6.6 indicates the standard gas samples of olefins and paraffins respectively.

Gas calibration was attempted using an isothermal oven condition. Results obtained indicated that the analysis cannot be done under isothermal oven conditions because not all of the compounds were eluted from the column under isothermal condition.

The oven was capable of temperature programming since it offered (i) program rates in steps of 1, 2, 4, 8, 16 and 32 and (ii) capability to time its entire operation for periods of 2, 4, 8, 16, 32 min and infinity, stop and cool down to the initial temperature. Temperature programming by itself was tried and found to elute higher molecular weight hydrocarbons successfully but gave a poor resolution of the C₁ to C₃ paraffins and olefins.

Table 6.5: Standard gas sample of olefins.

Concentration	Scotty Can Mix 223 by volume	Scotty Can Mix 856 by volume
Ethylene	1000 ppm	9.92 %
Propylene	1000 ppm	
1-Butene	1000 ppm	
1-Pentene	986 ppm	
1-Hexene	953 ppm	
Balance	Helium	Helium

Table 6.6: Standard gas sample of paraffins.

Concentration	Scotty Can Mix 236 by volume	Scotty Can Mix 367 by volume	Scotty Can Mix 4445 by volume
Methane	973 ppm		
Ethane	1040 ppm	9.97 %	
Propane	995 ppm		989.8 ppm
n-Butane	1000 ppm		
n-Pentane	1010 ppm		
n-Hexane	999 ppm		
Balance	Helium	Helium	Helium

It became clear that in order to elute all of the C₁ to C₆ hydrocarbons in the standard gas sample, a combination of isothermal and programmed temperature steps should be utilized.

Various combinations of isothermal and programmed steps were attempted. Adjustments were made in the initial temperature, program rate and final temperature in order to exactly position particular peaks.

Table 6.7 presents the retention times of the peaks which were eluted from the HayeSep D column using isothermal temperatures of 80 C and 120 C. The table also shows the optimum condition which involved a combination of isothermal and temperature programming conditions. The optimum oven conditions used are shown in Table 6.8.

This optimised oven operating condition achieves adequate separation of the main important components (e.g. olefins and paraffins) and sacrifices resolution between minor components in the MTO reaction product. The minor components in the MTO reaction product consists of highly branched paraffins and aromatics which tend to be retained longer relative to the n-paraffins or paraffins with little substitution.

Table 6.7: Retention times obtained using isothermal temperatures and optimum oven condition which combined isothermal and temperature programmed steps.

ELEMENT	Carbon Number	Bolling Pt degree C	80 degC	120 degC	Optimum Condition
Methane	1	-161.0	1.15	1.09	1.07
Ethylene	2	-104.0	3.15	2.05	2.10
Ethane	2	-88.0		2.52	2.45
Propene	3	-47.7		6.14	5.90
Propane	3	-42.0		7.03	6.57
1-Butene	4	-6.3		19.48	11.27
n-Butane	4	0.0		22.81	12.74
1-Pentene	5	30.0		64.03	15.43
n-Pentane	5	36.0			16.41
1-Hexene	6	64.0			19.68
n-Hexane	6	69.0			20.45

Table 6.8: Optimum oven conditions used.

Initial Temperature	120 degree Celsius
Hold-up Time	2 minutes
Program Rate	8 degree Celsius/minute
Final Temperature	250 degree Celsius
Duration of Analysis	32 minutes

Figure 6.18 presents typical FID chromatogram for paraffins standard gas sample. Figure 6.19 presents typical chromatogram for a mixture of olefins and paraffins standard gas sample. Both chromatograms show good resolution of olefin peaks and paraffin peaks.

Resolution of peaks such as olefins and paraffins on HayeSep D packed column is accomplished by the boiling point difference (i.e. carbon number). Since the oven operating condition for resolving the components involves a combination of isothermal- and temperature programmed- steps, the best way of making a proper identification of the resolved peaks of olefins and paraffins is to make plots of: (i) adjusted retention times versus boiling point (which should come out as a straight line), and (ii) $\log(\text{adjusted retention time})$ versus carbon number (which should come out as a smooth curved line) (McNair, personal communication; Dave, 1969). An adjusted retention time for each component is the difference between the retention time of the component and the retention time of the methane peak.

Figure 6.20 presents a plot of adjusted retention time against boiling point for the standard gas samples of paraffins and olefins. The figure shows the data approaching a straight line for olefins and paraffins at higher molecular weights.

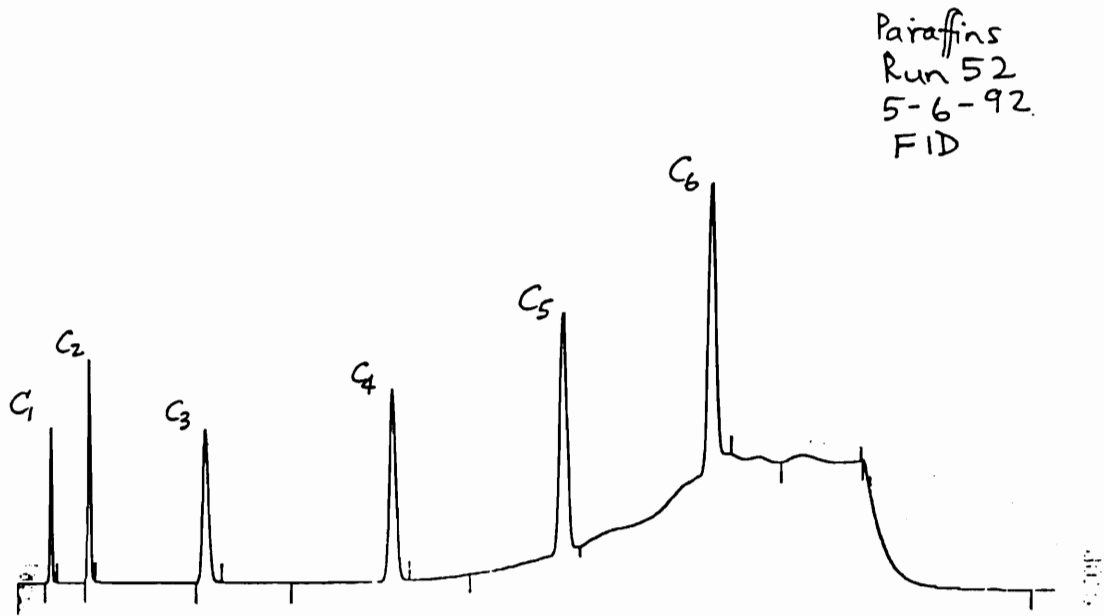


Figure 6.18: Typical Chromatogram (FID) for paraffins standard gas sample.

STDGAS
Run 56
5-7-92
FID

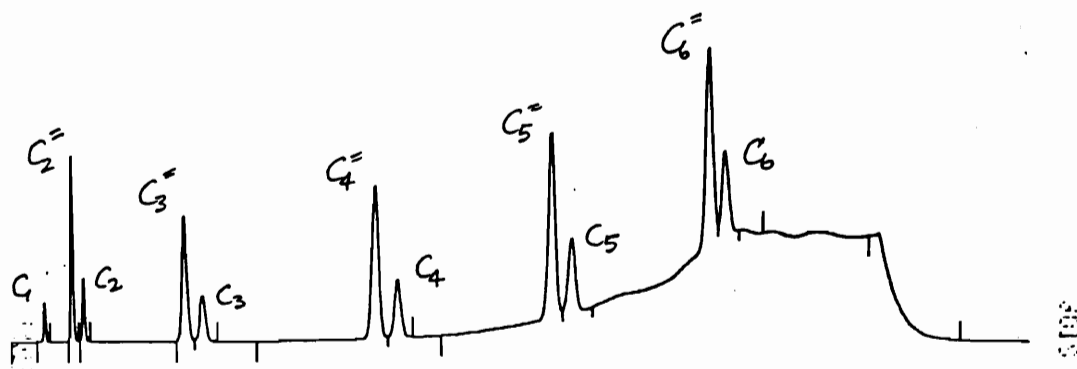


Figure 6.19: Typical Chromatograph (FID) for a mixture of paraffins and olefins standard gas sample.

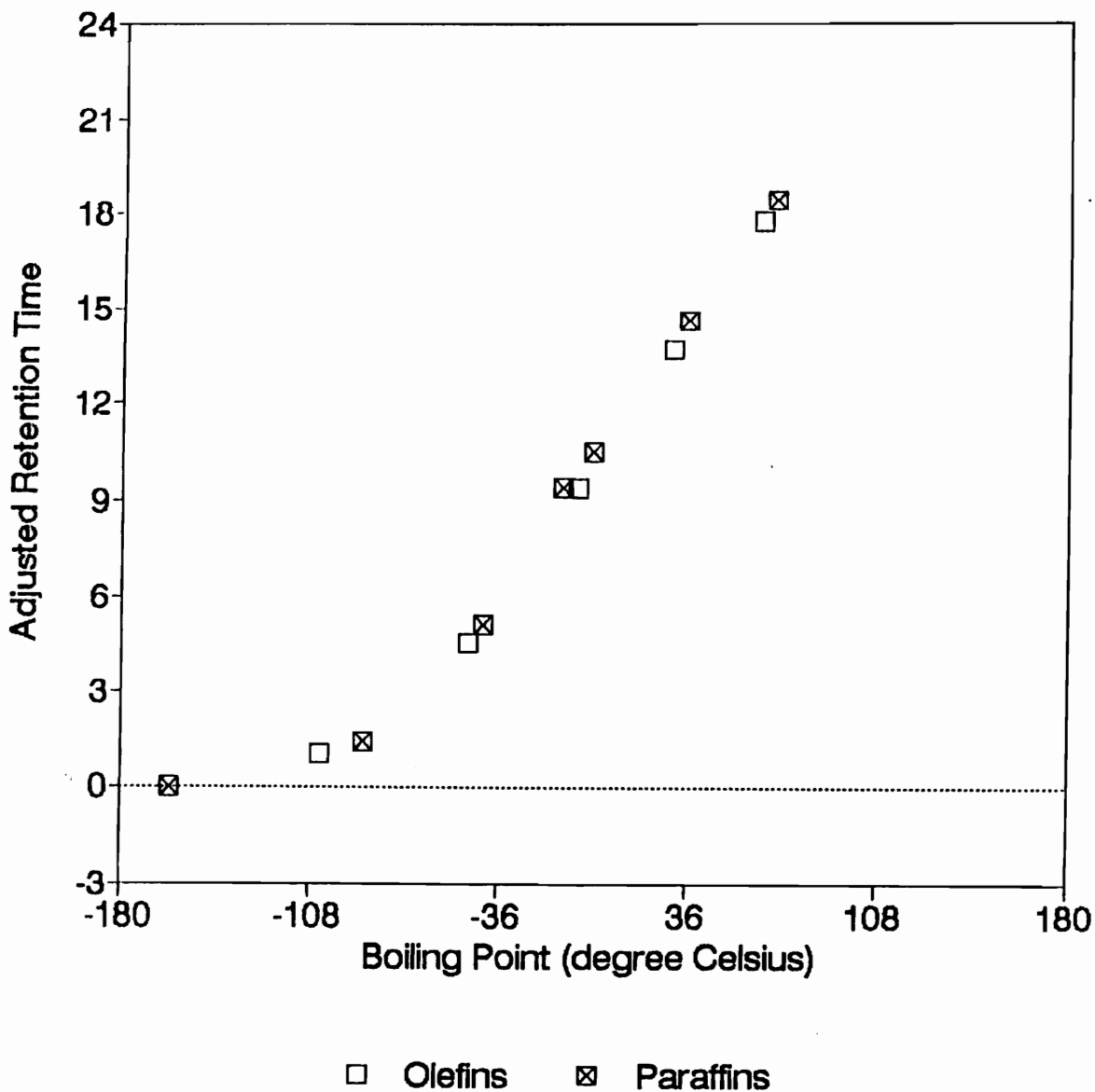


Figure 6.20: Plot of Adjusted Retention Time against Boiling Point for the standard gas samples of paraffins and olefins. The figure shows how data approaches a straight line for olefins and paraffins at higher molecular weight.

A plot of $\log(\text{Adjusted Retention Time})$ against Carbon Number for the paraffins and olefins standard gas samples in Figure 6.21 shows a smooth curved line. Both olefins and paraffins describe an identical trend.

6.6.1.2 REPRODUCIBILITY OF RETENTION TIMES

Identification of components in a sample assumes that retention data are accurately reproduced. A test was done to check the reproducibility of the retention times obtained from HP 5730A GC we are using. We took the HayeSep D packed column used in our HP 5730A GC and connected it to a Perkin Elmer Autosystem Gas Chromatograph (PEA GC), which belonged to Dr McNair's research group. We ran the PEA GC at the same optimised oven conditions used in HP 5730A GC.

Analysis of more hydrocarbon compounds was done in the PEA GC. The compounds investigated covered boiling point range from -161 C (methane) up to 142 C (o-xylene).

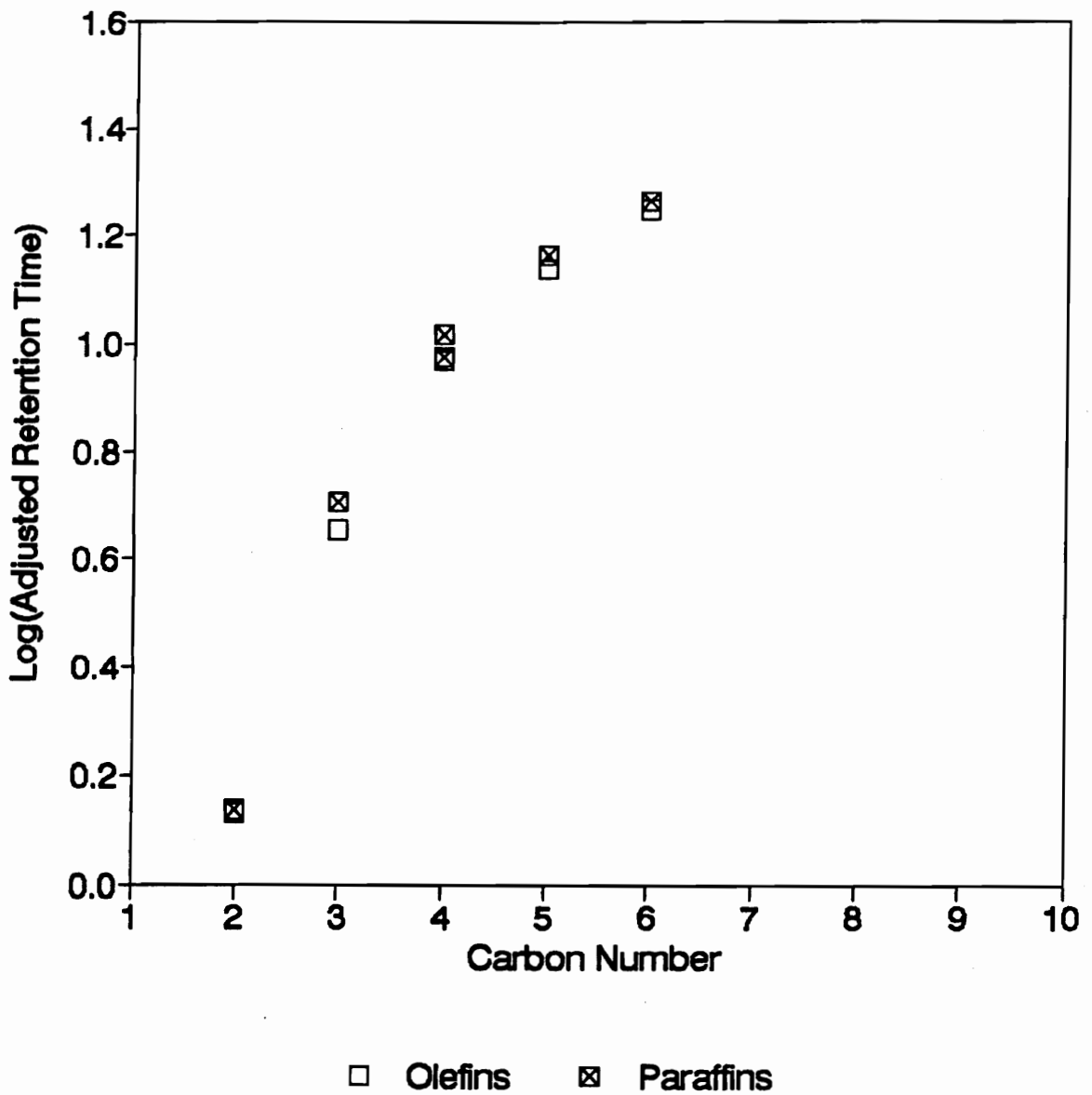


Figure 6.21: Plot of $\log(\text{Adjusted Retention Time})$ against Carbon Number for the paraffins and olefins standard gas samples. The figure shows a smooth curved line.

Table 6.9 presents the retention times obtained from HP 5730A GC, and from PEA GC. The difference in retention times observed in HP 5730A GC during Phase I and Phase II, was due to the helium flow arrangement. During Phase I, helium flow was supplied from a single cylinder and split between the packed columns and their detectors. With this arrangement, a severe baseline drift for both detectors was observed to occur during the temperature programming step. A better control was achieved when helium flow to the detectors was not split and each detector and its packed column was supplied from its own helium gas cylinder.

The table also indicates that retention times from PEA GC is shorter than retention times observed in our HP 5730A GC. This difference could have been due to the superior control of operating conditions (viz. carrier gas flow, oven temperature and programming) in PEA GC.

Figure 6.22 shows a plot of adjusted retention time against boiling point for data obtained from HP 5730A GC and PEA GC. The figure revealed a straight line; both data appear to merge at lower molecular hydrocarbons such as ethylene and ethane which did not fall on the straight line.

Table 6.9: Retention times obtained from HP 5730A GC and from PEA GC.

ELEMENT	Carbon Number	Bolling Pt degree C	HP 5730A Phase I Average	HP 5730A Phase II Average	PEA GC
Methane	1	-161.0	1.07	1.04	0.68
Ethylene	2	-104.0	2.10	2.00	1.00
Ethane	2	-88.0	2.45	2.42	1.14
Propene	3	-47.7	5.90	5.09	2.32
Propane	3	-42.0	6.57	5.54	2.42
iso-Butane	4	-11.7	10.48		5.09
1-Butene	4	-6.3	11.27	9.11	5.33
n-Butane	4	0.0	12.74	9.95	5.79
1-Pentene	5	30.0	15.43	13.83	9.31
n-Pentane	5	36.0	16.41	14.43	9.81
1-Hexene	6	64.0	19.68	17.74	13.28
n-Hexane	6	69.0	20.45	18.18	13.74
Methylcyclopentane	6	72.0			13.74
Cyclohexane	6	81.0			14.55
Methylcyclohexane	7	101.0			17.56
Toluene	7	111.0			17.63
iso-Octane	8	99.0			18.50
Ethylbenzene	8	136.0			20.85
o-Xylene	8	142.0			21.80

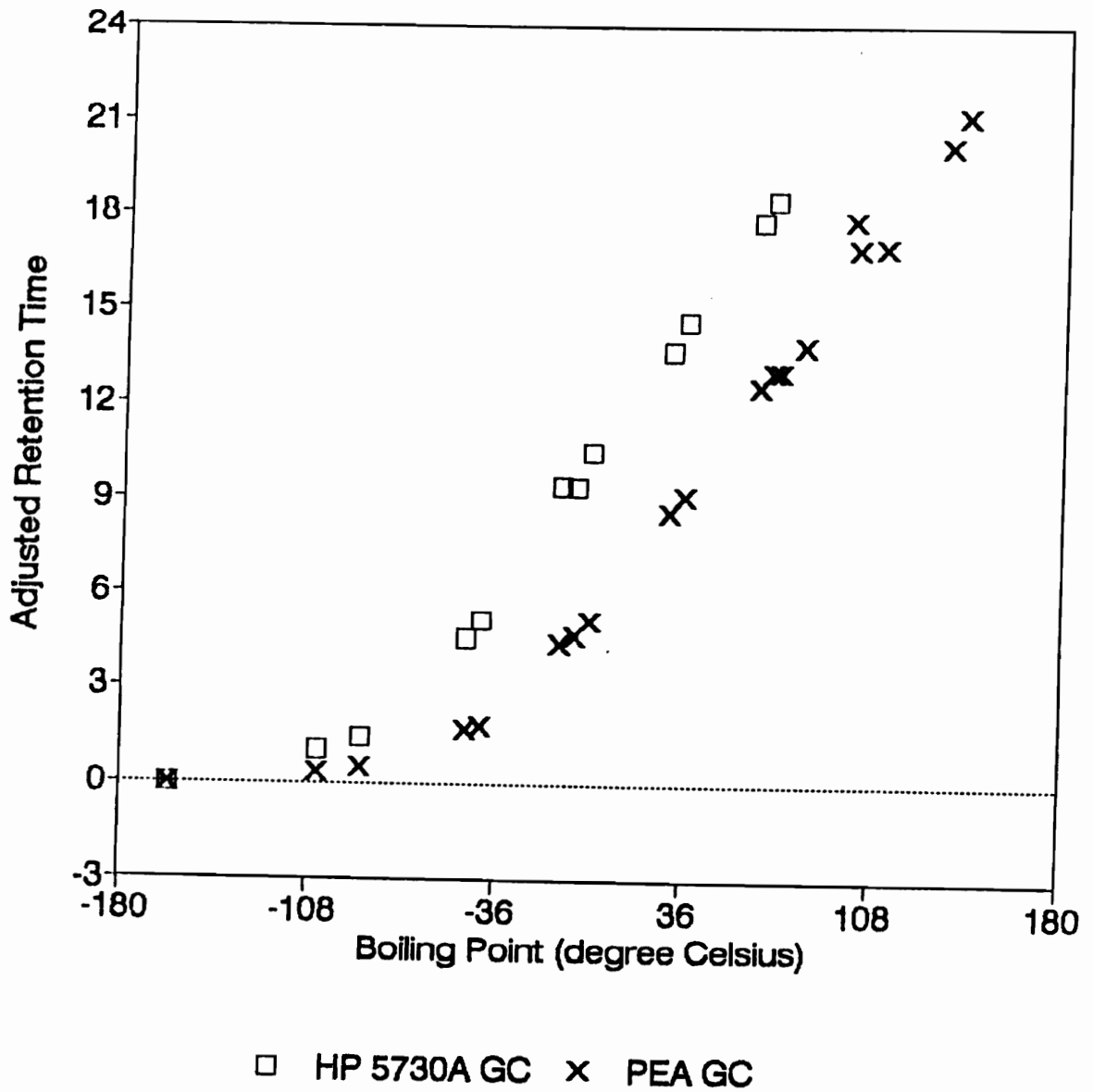


Figure 6.22: Plot of Adjusted Retention Time against Boiling Point for data obtained from HP 5730A GC and PEA GC. The figure revealed a straight line and both data appear to merge at lower molecular hydrocarbons.

Figure 6.23 shows a plot of $\log(\text{adjusted retention time})$ against carbon number for data obtained from HP 5730A GC and PEA GC. The figure shows a similar trend. The figure revealed the characteristic smooth curve; both data appear to approach the same asymptote at higher molecular hydrocarbons.

Although the retention times obtained from PEA GC and HP 5730A GC were not the same, the retention times obtained from HP 5730A GC were reproducible when comparing all the analyses done on it. HP 5730A GC appeared to be a reliable piece of equipment in spite of its age and years of operation.

6.6.2 QUANTITATIVE ANALYSIS OF MTO PRODUCTS

Standard gas samples with known concentrations were used in the HP 5730A GC calibration. Peak areas obtained from HP integrators were found not to be a reliable indicator of weight percent. Correlations were derived which related the peak area count from the HP integrator with the amount in nanograms of the components.

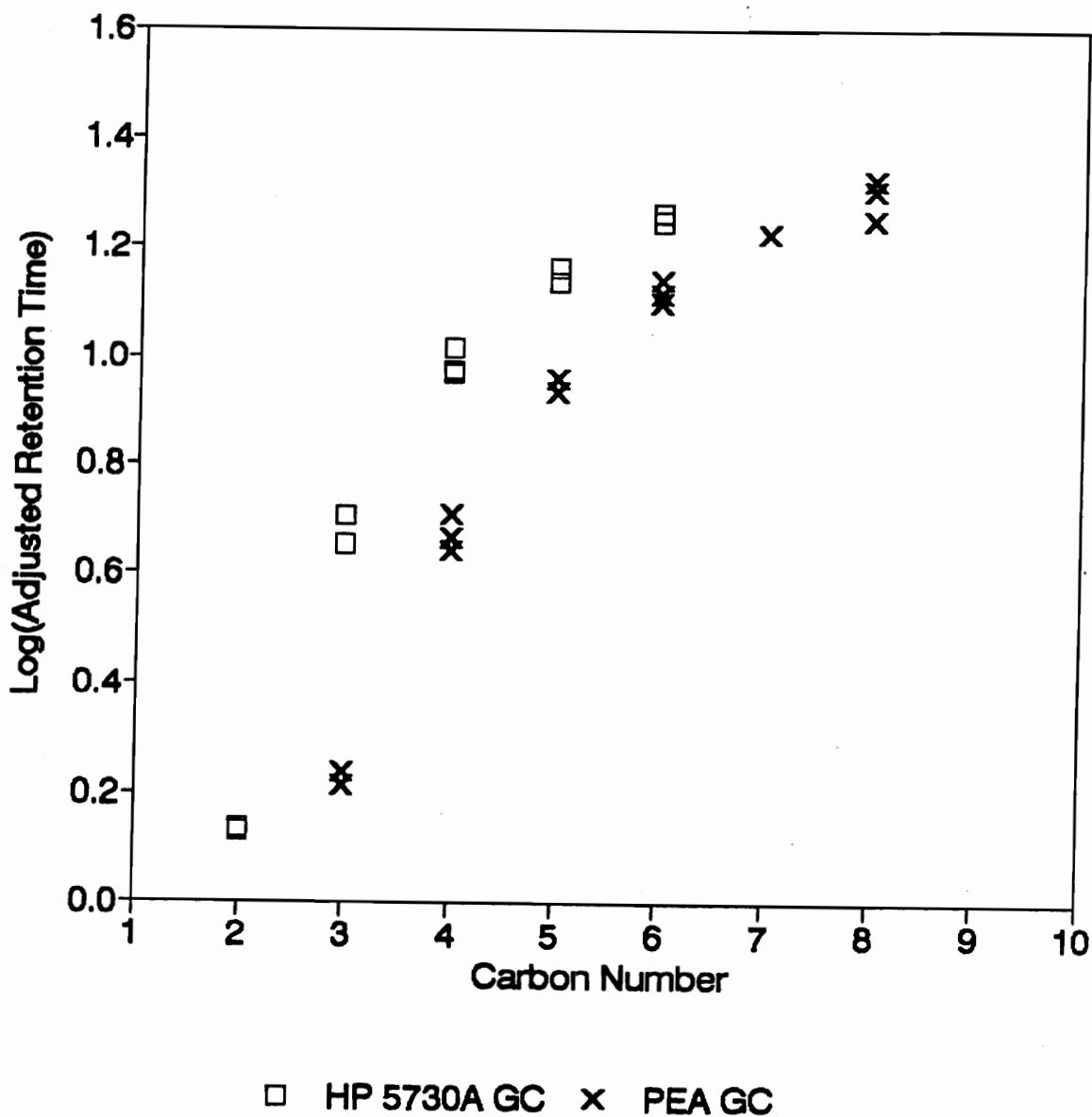


Figure 6.23: Plot of $\log(\text{Adjusted Retention Time})$ against Carbon Number for data obtained from HP 5730A GC and PEA GC. The figure revealed a smooth curve and both appear to approach the same asymptote at higher molecular hydrocarbons.

Figure 6.24 shows the plot of Peak Area against Amount for the standard gas sample which contained only olefins. Figure 6.25 shows the plot of Peak Area against amount for a more concentrated (9.92 % by volume in helium) sample of ethylene. Both Figure 6.24 and Figure 6.25 indicate a linear correlation between Peak Area and amount.

Table 6.10 presents the correlations for the olefinic species investigated. It can be seen from this table that the correlations are similar for the various olefinic species. A general correlation for the olefins is given by:

$$\text{Amount in Nanograms} = \text{Peak Area} / 17369 \quad (6.1)$$

Figure 6.26 shows the plot of Peak Area against Amount for the standard gas sample which contained only paraffins.

Figure 6.27 shows the plot of Peak Area against amount for a more concentrated (9.97 % by volume in helium) sample of ethane. Both figures indicate a linear correlation between Peak Area from HP integrator and amount.

Table 6.11 presents the correlations for the paraffinic species investigated. It can be seen from this table that the correlations are similar between the paraffinic species.

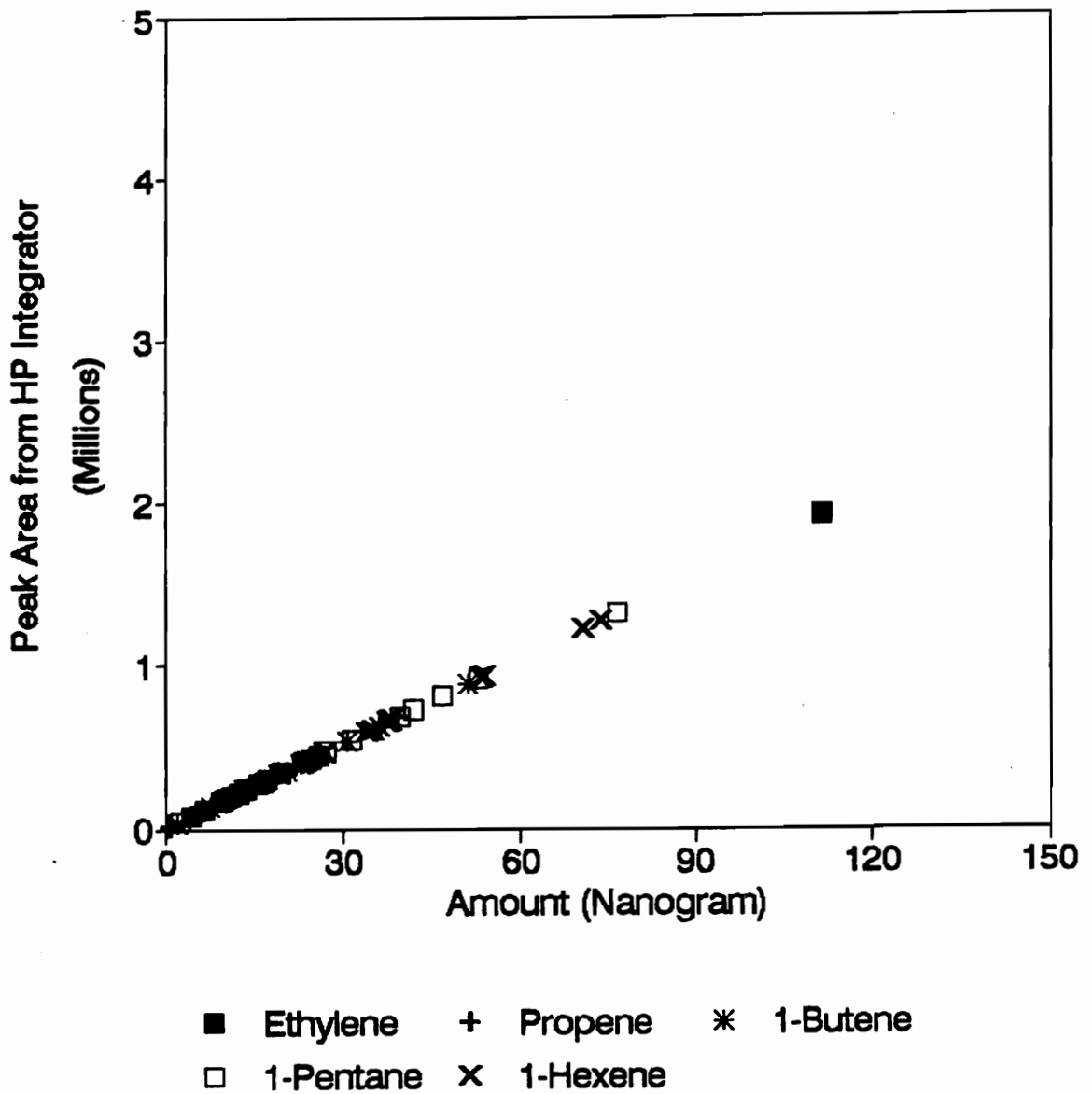


Figure 6.24: Plot of Peak Area against Amount for the standard gas sample which contained only olefins.

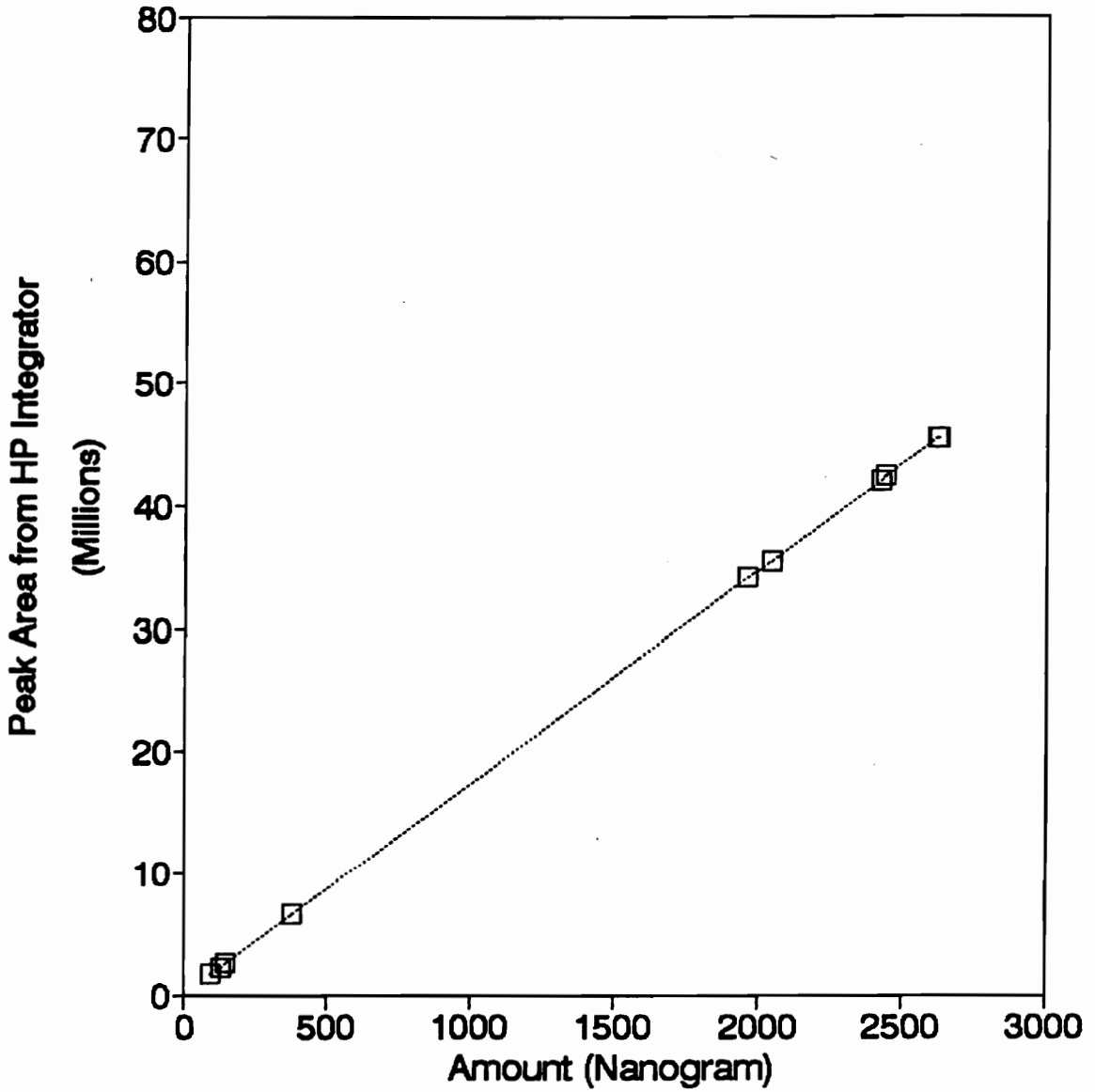


Figure 6.25: Plot of Peak Area against Amount for a more concentrated (9.92 % by volume in helium) sample of ethylene.

Table 6.10: Correlations for the olefinic species investigated. Correlations are similar between the olefinic species.

ELEMENT	Gradient	Intercept	Corr. Factor	Data Points
Ethylene	17371.2	31.31	1.00	13
Propene	17370.4	18.33	1.00	13
1-Butene	17373.4	-29.70	1.00	13
1-Pentene	17363.9	-42.57	1.00	13
1-Hexene	17366.5	15.21	1.00	10
Ethylene (*)	17371.2	27.53	1.00	11

(*) concentrated sample, see Table 6.5

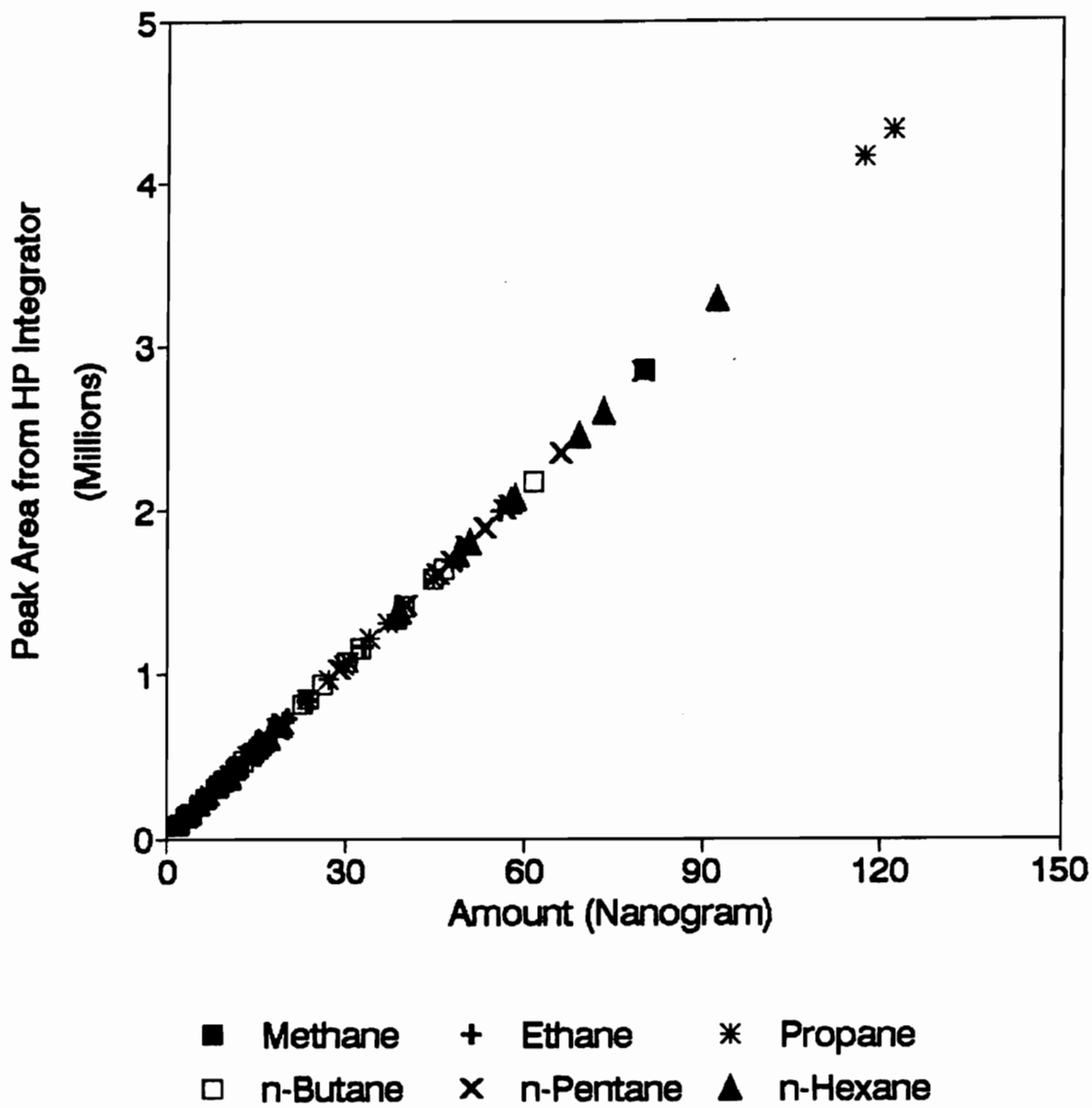


Figure 6.26: Plot of Peak Area against Amount for the standard gas sample which contained only paraffins.

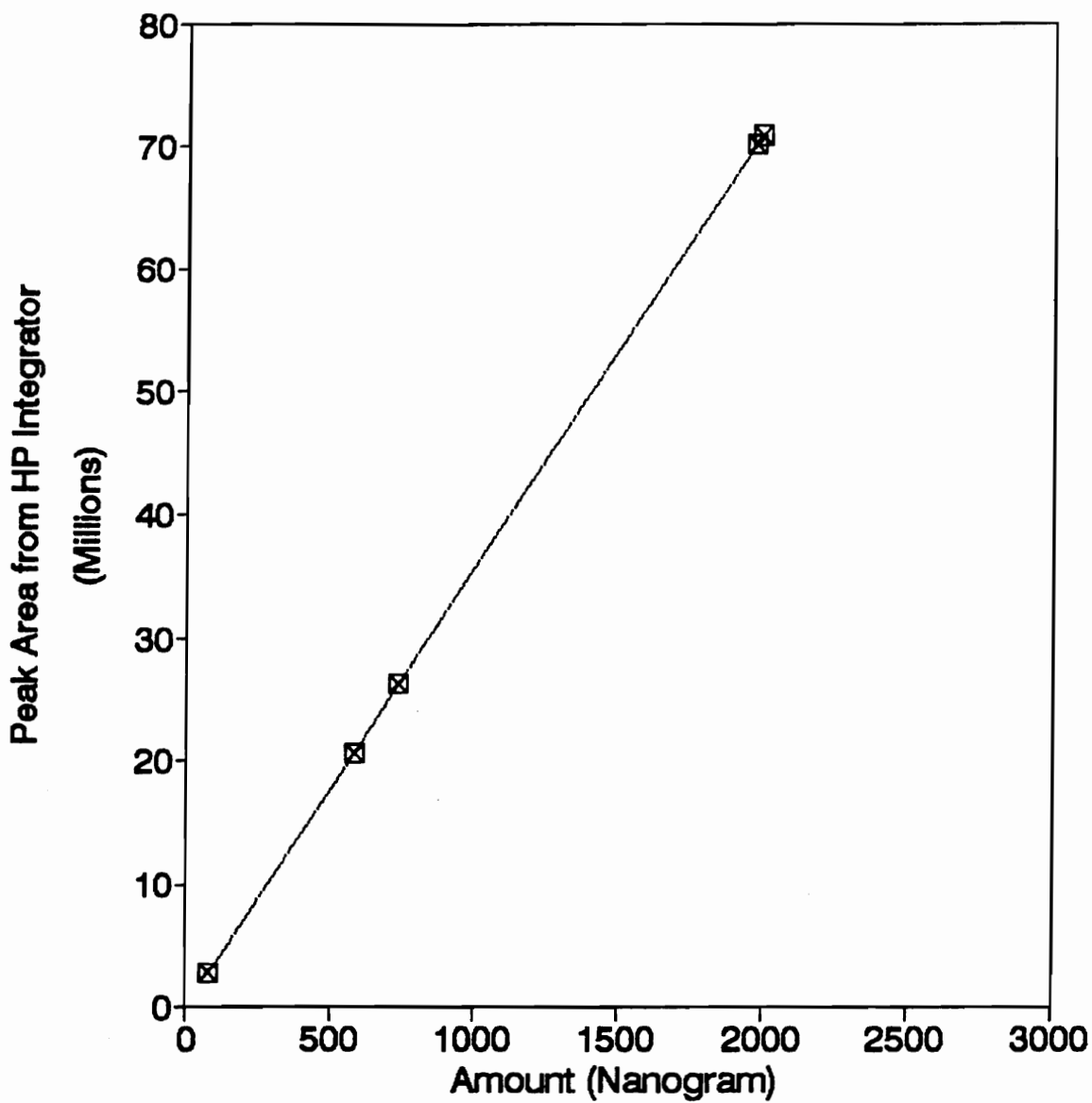


Figure 6.27: Plot of Peak Area against Amount for a more concentrated (9.97 % by volume in helium) sample of ethane.

Table 6.11: Correlations for the paraffinic species investigated. Correlations are similar between the paraffinic species.

ELEMENT	Gradient	Intercept	Corr. Factor	Data Points
Methane	35526.5	-1.58	1.00	20
Ethane	35536.7	0.37	1.00	20
Propane	35534.5	0.10	1.00	20
n-Butane	35549.3	-1.45	1.00	19
n-Pentane	35539.3	-6.55	1.00	15
n-Hexane	35548.0	-16.05	1.00	11
Ethane (*)	35536.7	-44.93	1.00	6

(*) concentrated sample, see Table 6.6

A general correlation for the paraffins is given by:

$$\text{Amount in Nanograms} = \text{Peak Area} / 35539 \quad (6.2)$$

As discussed earlier on, the MTO product slate is wide and we were not equipped to quantify each and every component in the MTO product stream individually. In calculating the weight percent of the olefins and paraffins from MTO reaction, their weights have to be calculated using correlations derived by standard gas calibration described above.

The ratio of the sum of calculated weights to the sum of the areas, for olefins and paraffins, was calculated. This ratio is multiplied by the total peak area of all components given by the HP integrator, to give a best estimate of the total weight of all the hydrocarbon components from MTO product stream.

The weight percent is given by dividing the calculated weight of the known component with the estimated total weight of all components.

6.6.3 OVERALL PROCEDURE FOR EXPERIMENTAL DATA ANALYSIS

This section will give a summary of the steps necessary for conducting an experiment and for doing the data analysis after taking a sample.

In conducting an experiment the following steps are involved:

(i) Setting up the microreactor

- assemble the microreactor
- load it with the right amount of HZSM-5 catalyst
- ensure that gaskets sit tightly and are leakproof
- mount the microreactor and glass reference duct on vibration table, ensure horizontal/vertical alignment and symmetrical weight distribution
- insert the cartridge heaters
- connect the methanol inlet line and the product outlet line
- pack insulation all around the microreactor and cover it so that it will stay in place during vibration
- vibrate entire setup and check for C-E state in the glass reference duct
- flow helium gas at a small rate to flush air out of the system

(ii) Product Analytical Scheme

- establish correct carrier gas flow to the FID and TCD
- establish operating temperature in the FID, TCD and injection port
- heat product lines and the sampling valve to desired temperature
- ensure sufficient air pressure is available for operating sampling valve, GC oven door and cooling of vibrator
- enter appropriate parameters in the HP integrators, FID and TCD

- check for excessive line noise in the integrators, FID and TCD
- check for "ghost peaks" in the columns
- ensure fume hood fan works

(iii) Experimental Run

- vibrate microreactor in the C-E state and monitor it constantly
- heat the microreactor to 482 C
- replace helium flow with required methanol flow
- take sample every 45 minutes
- monitor temperatures in the reactor, product lines and sampling valve

The experiment requires constant supervision because it involves vigorous vibration, high temperatures, toxic materials and taking samples is done manually. The typical length of an experiment was 35 hours.

Figure 6.28 shows the block diagram of steps taken in analysis of each sample of MTO product stream. A listing of sample ID, sample time, retention times and peak area count is obtained from the HP integrator. Retention times are checked for proper identification, and peak area count of the identified peak is quantified by using the correlations from standard gas calibration. Sample times, yield of olefins, and reaction index are collected and plotted.

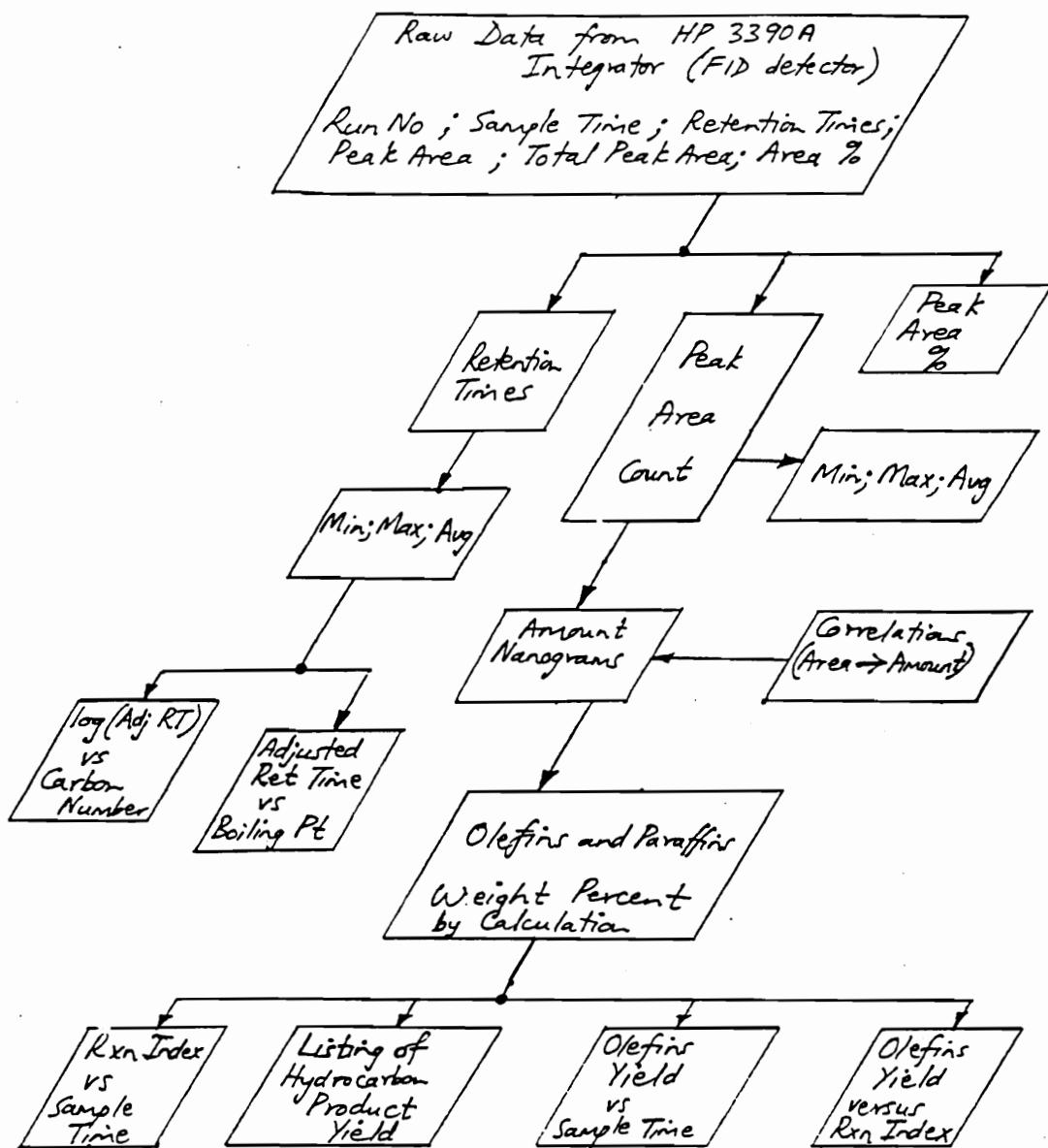


Figure 6.28: Block diagram of steps taken in the analysis of each product sample taken during an experiment.

7. RESULTS AND DISCUSSION

As discussed in chapter 4, the Coherent-Expanded vibrated-bed (C-E) state, discovered in the study of bed dynamics of shallow vibrated beds, showed promise of excellent gas-solid contacting. The C-E state is achieved by subjecting a horizontal duct on whose floor rests Group A catalyst powder, less than about 1 mm in depth, to vertical sinusoidal vibration. The catalyst powder can be made to expand to a height of 12.7 mm, during a portion of each vibration cycle. This results in an intense mixing of the catalyst powder in the vertical direction and little or none in the horizontal (axial) direction.

This brought about the Vibrated Bed Microreactor Concept in which the catalyst would be vibrated in the C-E state. The microreactor comprises a rectangular horizontal duct, 12.7 mm in height, 25.4 mm in width and variable length, charged with a shallow layer (1 mm deep) of Group A catalyst powder. A concerted effort was committed to developing the microreactor and studying its feasibility.

Earlier research on cold-flow model of the microreactor indicated that: (i) shifting of catalyst powder from inlet toward the outlet was negligible at horizontal superficial air velocities up to approx 20 mm/s, (ii) there is no gas bypassing and (iii) axial gas dispersion coefficient varies linearly with

superficial gas velocity, revealing a capability to vary axial Peclet Number in the microreactor by simply varying the horizontal duct length while holding weight hourly space velocity constant. The ultimate test of the idea is to conduct a known gas-solid catalytic reaction in the microreactor and study its sensitivity to axial gas dispersion. This is the subject of the present research work.

Mobil Research and Development Corporation (MRDC) who was associated with earlier work in the group, had discovered and scaled-up Methanol-To-Olefin (MTO) reaction as a fluid-bed process. Data from the fluid-bed scale-up had been reported. Accordingly, MTO reaction was chosen for this study. The main goal of the present research work was to conduct the MTO reaction in the microreactor in order to study its sensitivity to axial gas dispersion.

This chapter will describe results obtained from conducting MTO reaction in microreactors of three lengths, affording a wide range of axial Peclet Number. Three vibrated bed microreactors, referred to as VBMR-3, VBMR-6 and VBMR-9 were designed with a horizontal duct length of 7.62 cm, 15.24 cm and 22.86 cm respectively. These were essentially of the same basic design with the main difference in their horizontal duct lengths. The MTO reaction was conducted in each of the three microreactors in turn. Table 7.1 shows dimensions of the microreactors and vibrational conditions used to obtain C-E state.

Table 7.1: Dimensions of the Vibrated Bed Microreactors.

	VBMR-3	VBMR-6	VBMR-9
Duct Length, cm	7.62	15.24	22.86
Duct Width, cm	2.54	2.54	2.54
Duct Height, cm	1.27	1.27	1.27
Empty Mass, kg	2.72	3.63	4.54
Frequency, Hz	24	24	24
Vibrational Intensity	10	10	10

A microreactor was loaded with fresh HZSM-5 catalyst to a bed depth of 1 mm for each experimental run. The entire apparatus was vibrated at a frequency of 24 hertz and vibrational intensity of 10 to yield vibration of HZSM-5 catalyst in the C-E state, as observed in the Glass Reference Duct.

Confirmation of Existence of C-E State in Experiments

Thomas et al. (1989) described how a vibrated bed of particles, at very low inventory, displays a Newtonian state. As one adds particles, building up a deeper vibrated bed, a transition is observed to the coherent-expanded (C-E) state. In general, this transition occurs at a bed depth amounting to coverage of the floor by about 1-1/2 layers of particles. As one adds still more particles, a second transition occurs, from the C-E state to the coherent-condensed (C-C) state. This transition is to be avoided, since it is desired to operate the microreactor in the C-E state. Figure 7.1 shows Thomas et al.'s data for the C-E to C-C transition in glass beads at three particle sizes in air at one atmosphere and room temperature.

In the figure, a parameter, ψ , is plotted versus bed depth (expressed as number of particle layers). The parameter ψ is given by:

$$\psi = \left[\frac{P_o \epsilon^3}{180 \mu \omega (1 - \epsilon)^2} \right] \frac{d_p}{L} \frac{d_p}{z_o} \quad (7.1)$$

For a given type of glass beads, the C-E state appears at conditions to the left of the appropriate solid line in the Figure. Density of the glass, high (H) or low (L), had no significant effect upon the transition to the C-C state; Thomas et al. (1989) believed that static electricity effects caused the small difference between H and L glass beads at the smallest size that they studied. The authors studied beds at K-values from 2.5 to 6. At higher K, one can add more particles to a vibrated bed before the transition to the C-C state appears.

Thomas et al. (1989) found it difficult to obtain quantitative data for the C-E to C-C transition in fluid catalytic cracking (FCC) catalyst. Thomas believes a curve for FCC catalyst would fall close to those for the 88 micron glass beads in Figure 7.1.

In the present study, using HZSM-5 powder of particle size and density similar to FCC catalyst, we found it advisable to operate at $K = 10$ to ensure existence of the C-E state in the glass reference duct mounted above the hot microreactor. The star in Figure 7.1 indicates the approximate value of ψ for the glass reference duct. There is a relatively large separation between the star and the curves for 88 micron glass beads. The Maltese cross in Figure 7.1 shows the approximate value of ψ for the hot microreactor duct. The higher viscosity in hot gases undergoing the MTO reaction accounts for the separation between star and Maltese cross.

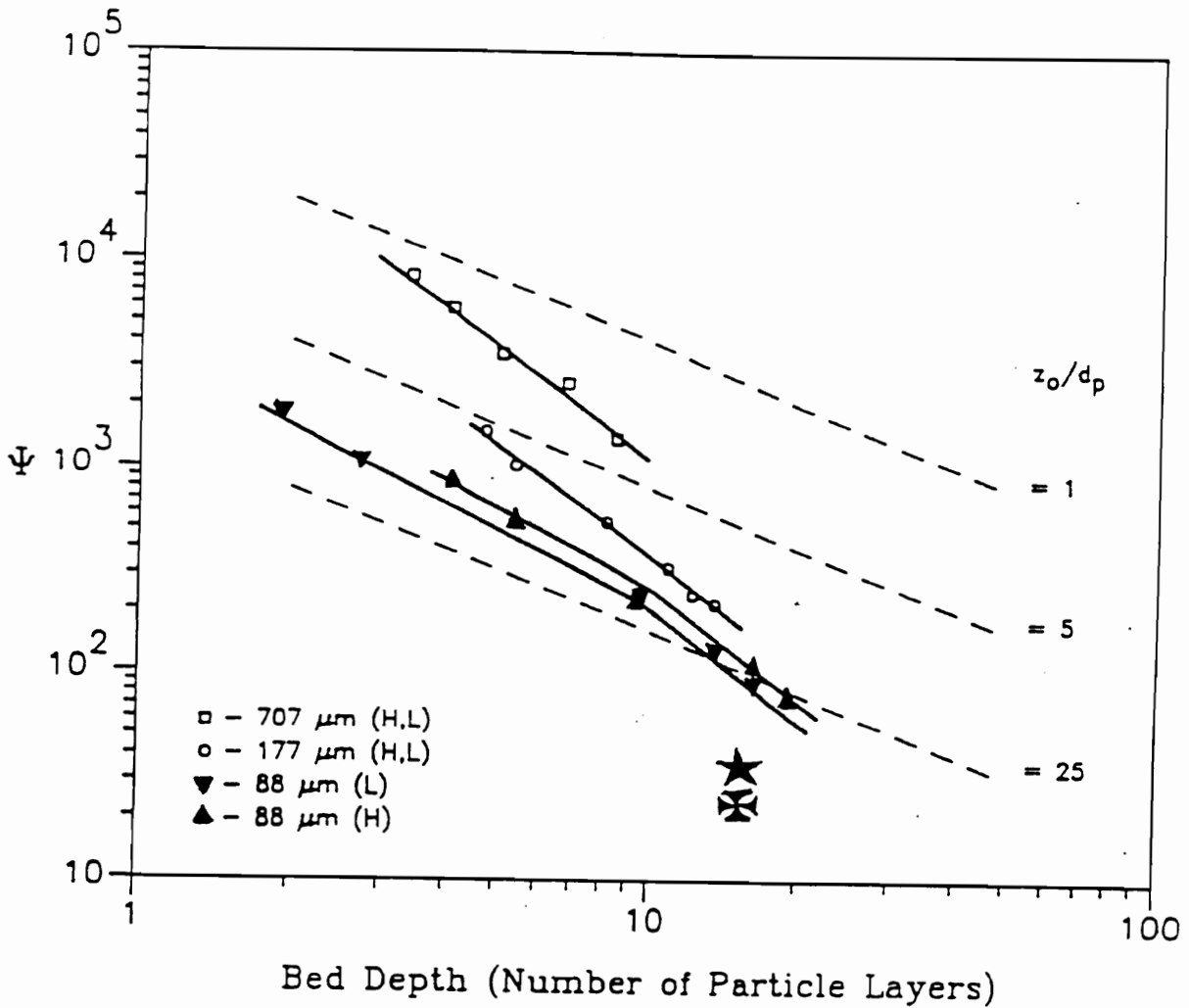


Figure 7.1: Data of Thomas et al. (1989) for transition from C-E to C-C state in high (H) and low (L) density glass beads. The C-E state is obtained on the left side of the solid lines showing transitions. Moving to the right along a transition line represents movement toward higher K (i.e. higher value of z_0/d_p , where z_0 is maximum vessel displacement and d_p is particle diameter). Star and Maltese cross are ψ -values for glass reference duct and hot microreactor duct, respectively. Their locations provide assurance that the C-E state existed in microreactor duct during the experiments.

Although existence of the C-E state in the hot microreactor duct could not be verified by visual observation, it may be concluded, with high probability, that this state did exist under the conditions of the experiments.

Continuous vibration at an intensity of 10 turned out to be destructive on the apparatus setup, no matter how tightly secured it was. This made it impossible to conduct an experimental run continuously for longer than 34 hours because of a variety of problems cropping up (e.g. insulation falling apart, bolts running loose, etc).

The microreactor is heated with four 600 Watts cartridge heaters, each one as long as to cover the horizontal length of the microreactor. The desired temperature is maintained by a process controller using a thermocouple looking into the middle of the horizontal duct length. Three thermocouples looking into the inlet section, middle of the horizontal duct length and the outlet section of the microreactor showed the same temperature. This revealed that this heating arrangement produced a uniform temperature throughout the microreactor.

Methanol was fed into the microreactor with an ISCO Syringe Pump once (i) the reactor was consistently maintained at 482 C, (ii) HZSM-5 catalyst in the Glass Reference Duct was observed to vibrate in the C-E state, (iii) Gas Chromatograph Detectors were giving a steady “ghost-peak-free baseline”, and (iv) the product line was heated and maintained at a steady uniform

temperature of 200 C in order to prevent condensation of gaseous reaction products.

An ISCO Model 314 Metering Pump was used to deliver methanol into the microreactor at a chosen flowrate. The pump can hold 375 ml of liquid methanol and deliver flowrates from 0.08 ml/hr up to a maximum of 200 ml/hr. All of our flowrates were in the lower range for the pump and were also below 5 ml/hr. The pump stem is graduated in divisions of 5 ml and turned out to be too large, making it difficult to measure our low flowrates accurately. Observed flowrates from the pump ranged between 4 to 15 percent more than the required, resulting in Weight Hourly Space Velocity (WHSV) variation of 1.04 to 1.15.

Table 7.2, Table 7.3 and Table 7.4 present conditions regarding all experiments conducted in VBMR-3, VBMR-6 and VBMR-9 respectively.

Product samples were taken soon after the introduction of Methanol into the microreactor. Main products from the MTO reaction are water and hydrocarbons, of which the maximum yields are at a stoichiometric ratio of 56.4 and 43.6 weight percent respectively. The hydrocarbon product consists of varying amounts of Olefins, Paraffins, Cycloparaffins and Aromatics.

Table 7.2: Operational conditions for experiments conducted in VBMR-3 (horizontal duct length = 7.62 cm).

Experiment	I	II	III
HZSM-5 gram	1.3757	1.3669	1.3608
Methanol, ml/hr	0.97	1.96	1.88
WHSV, /hr	0.54	1.11	1.06
Duration, hour	32	19	29
Peclet Number	1.27	2.5	2.4

Table 7.3: Operational conditions for experiments conducted in VBMR-6 (horizontal duct length = 15.24 cm).

Experiment	I	II
HZSM-5 gram	2.8298	2.8107
Methanol, ml/hr	4.05	3.79
WHSV, /hr	1.10	1.04
Duration, hour	34	25
Peclet Number	9.16	8.73

Table 7.4: Operational conditions for experiments conducted in VBMR-9 (horizontal duct length = 22.86 cm).

Experiment	I	II
HZSM-5 gram	4.3860	4.3451
Methanol, ml/hr	6.50	6.20
WHSV, /hr	1.15	1.10
Duration, hour	33	24
Peclet Number	19.81	19.13

In this research, we were only interested in quantifying olefins in the range $C_2^=$ to $C_6^=$, (which make up a major portion of the hydrocarbon product), and paraffins in the range, C_1 to C_6 . The composition of the remainder portion of hydrocarbon product, which consisted of cycloparaffins and aromatics, was not determined. It was lumped together as unidentified material.

A complete description of the experimental procedure adopted in taking and analyzing a sample, is presented in chapter 6. Figure 7.2, Figure 7.3 and Figure 7.4 show typical chromatogram from a flame ionisation detector (FID) of a product sample taken during an MTO reaction experiment in VBMR-3, VBMR-6 and VBMR-9 respectively. Identification of olefinic and paraffinic peaks was done by retention times.

Retention times of the olefinic and paraffinic peaks seen in the analysis of product sample from VBMR-3, VBMR-6 and VBMR-9, was the same. Figure 7.5 presents a plot of adjusted retention times against boiling point for the olefins and paraffins present in the product samples. Data in the figure clearly approaches a straight line for both olefins and paraffins at higher molecular weights, confirming proper identification.

Figure 7.6 indicates a plot of $\log(\text{adjusted retention time})$ against carbon number for the olefins and paraffins in the product sample. The figure shows a smooth curved line, confirming proper identification as well.

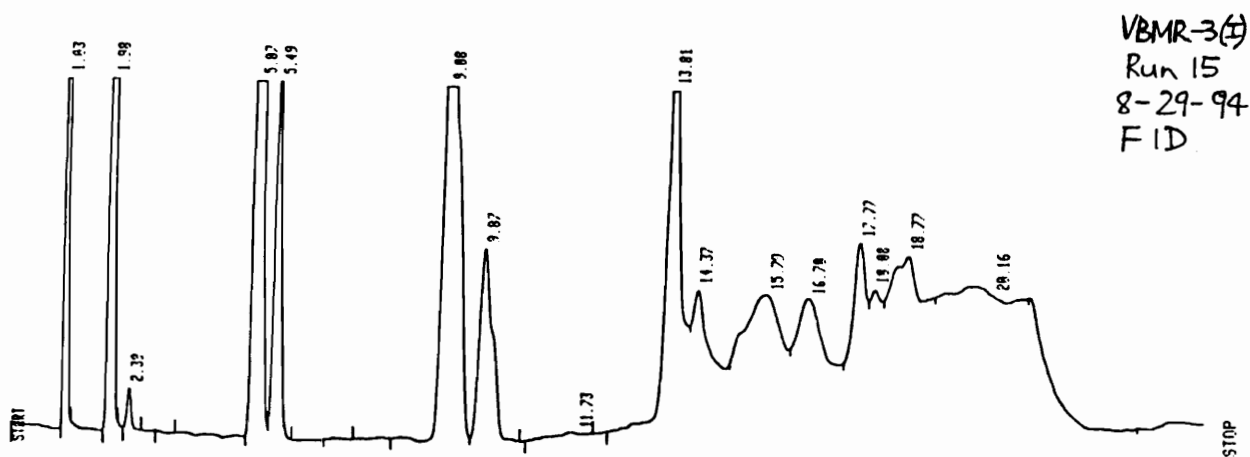


Figure 7.2: Typical FID chromatogram of a product sample taken during an MTO reaction experiment in VBMR-3.

VBMR-6 Run 22
5-10-95
FID

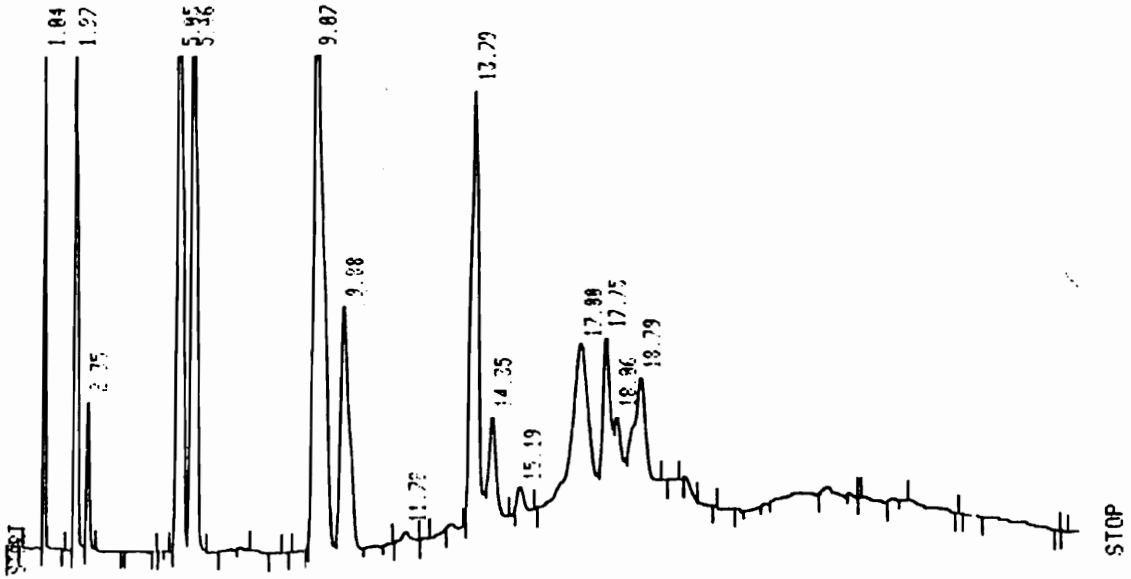


Figure 7.3: Typical FID chromatogram of a product sample taken during an MTO reaction experiment in VBMR-6.

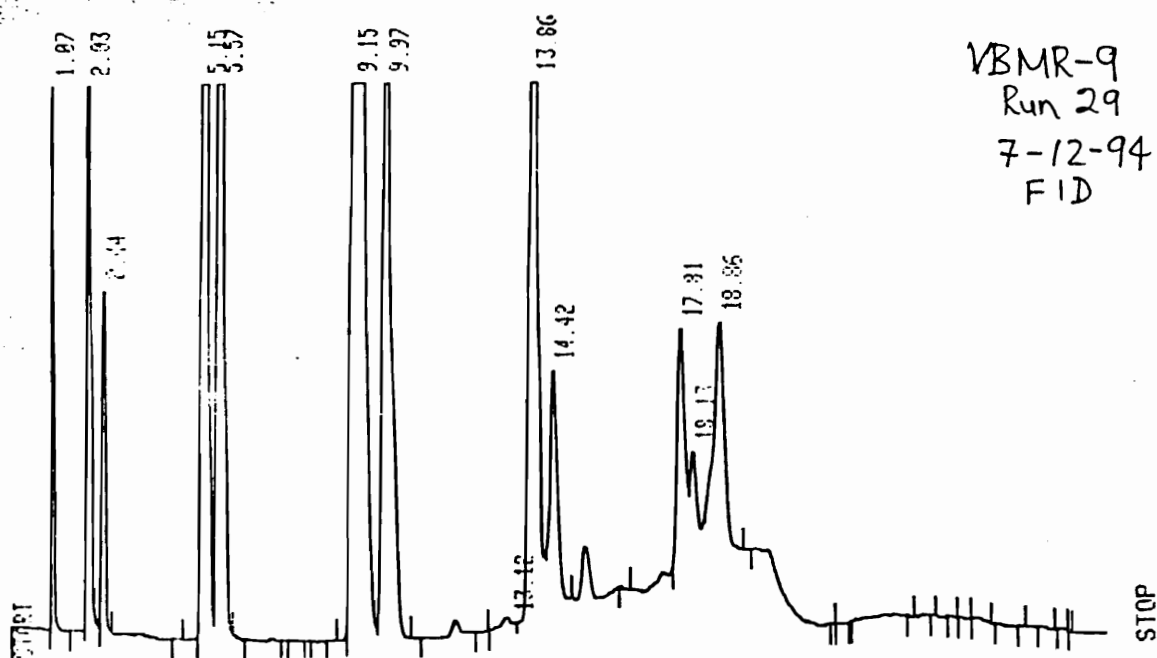


Figure 7.4: Typical FID chromatogram of a product sample taken during an MTO reaction experiment in VBMR-9.

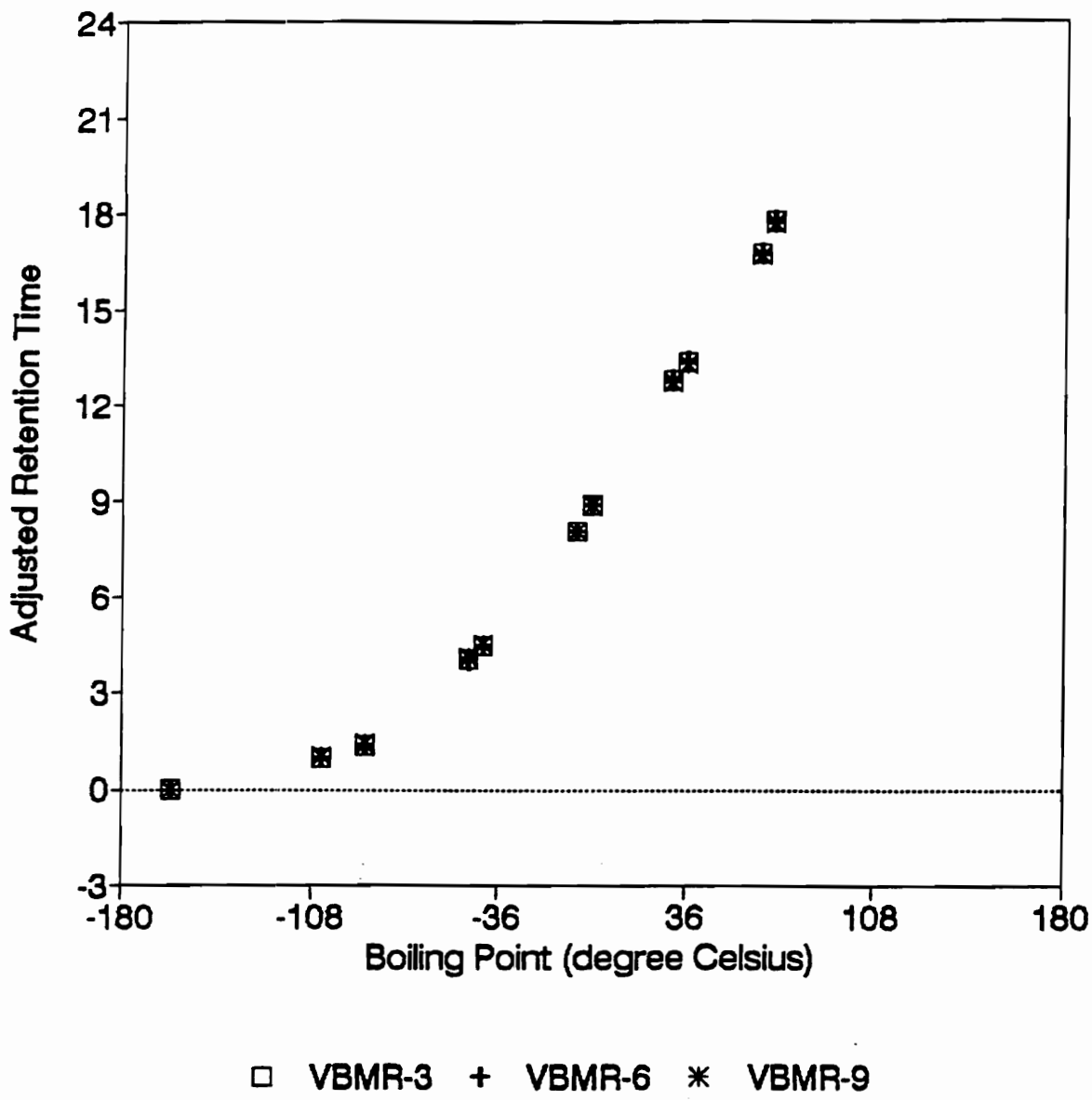


Figure 7.5: Plot of adjusted retention times against boiling point for olefins and paraffins in the product samples from the three microreactors (VBMR-3, VBMR-6 and VBMR-9). The data approach a straight line for both olefins and paraffins at higher boiling points.

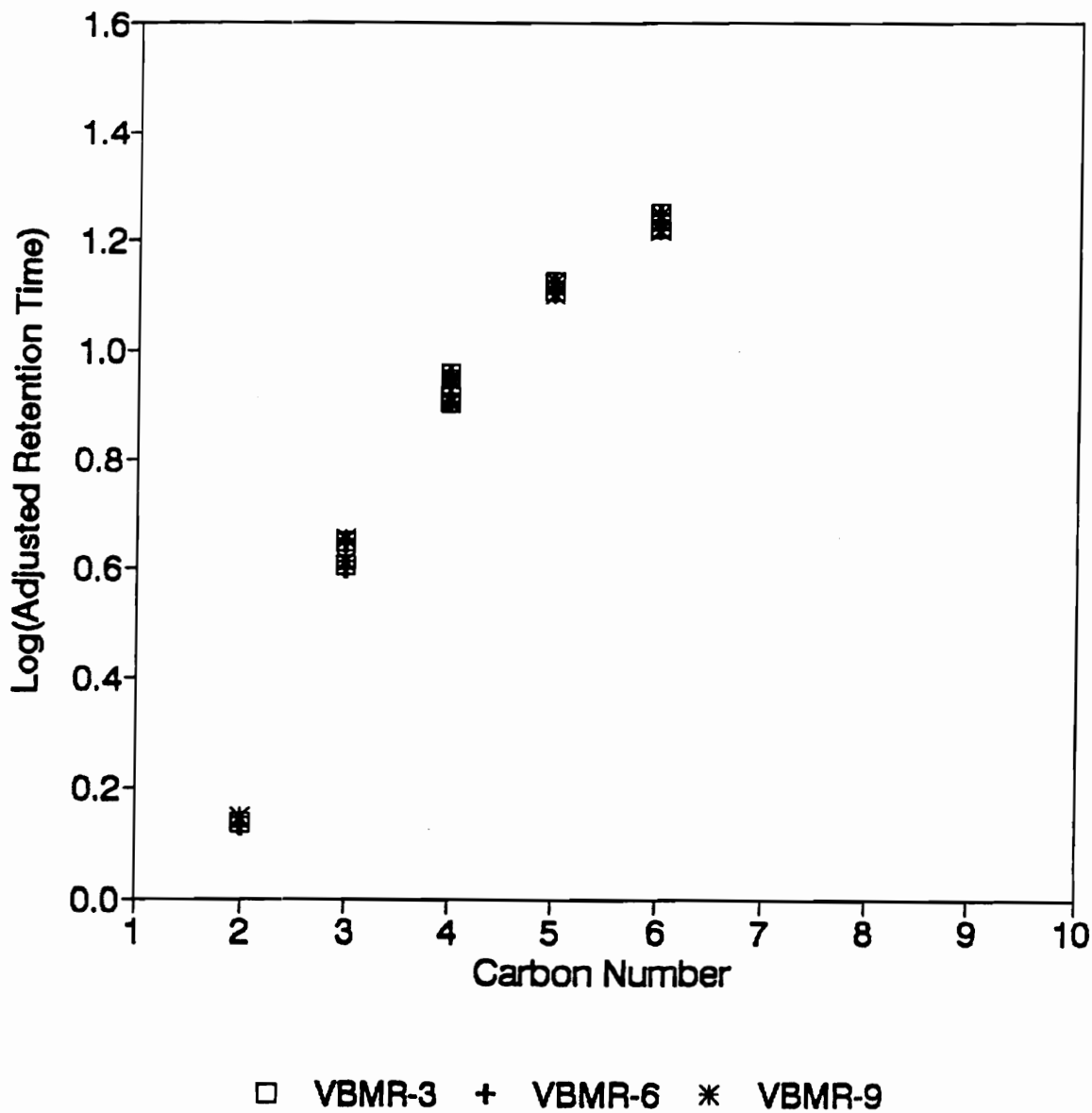


Figure 7.6: Plot of log(adjusted retention time) against carbon number for olefins and paraffins in the product samples from the three microreactors (VBMR-3, VBMR-6 and VBMR-9). The figure shows a smooth curved line, confirming a proper identification as well.

The area count of olefinic and paraffinic species was converted to an equivalent mass in nanograms with the use of equations 6.1 and 6.2, derived from standard gas calibration. The sum of the masses gave the best estimate of the total mass of all hydrocarbon species in the product stream.

Individual masses of olefinic and paraffinic species were finally converted by computation to a mass fraction of methanol carbon reporting to each species. The mass fraction was given by dividing the calculated mass of the known species with the estimated total mass of all hydrocarbon species in the product stream.

7.1 SENSITIVITY OF MTO REACTION TO AXIAL GAS DISPERSION IN THE MICROREACTOR

Results obtained from conducting MTO reaction in microreactors at 482 C and 712 mm Hg are presented in this section.

Experimental runs done in microreactors did not last more than 34 hours (during which data gathering was 20 hours) due to problems inherent with continuous vibration at an intensity of 10. Sample Time is the actual time during an experiment when a product sample from MTO reaction was taken for analysis.

This section will present:

- (i) the yield of Light Olefins and examines how it varies with Sample Time, Reaction Index and Peclet Number, and
- (ii) the composition of the Hydrocarbon Product from MTO reaction.

The section will also present subsections described below and conclude with a summary of observations presented in the section.

Reported Data from Fluid Bed

Mobil Research and Development Corporation (MRDC) reported results from scale-up of MTO process in Bench Scale, 4 BPD Pilot Plant and 100 BPD Demonstration Plant. Results reported by MRDC which cover the parameter in discussion will be presented in this section.

Comparing Vibrated Bed Microreactor Data with Fluid Bed Data

This section will compare results obtained from the microreactor with those reported by MRDC in their fluid bed scale-up. An attempt will be made to draw conclusions on how the MTO reaction performed in the different reaction environments exhibited by the microreactor and fluid bed.

7.1.1 YIELD OF LIGHT OLEFINS

Hydrocarbon product from MTO reaction is Olefins, Paraffins, Cycloparaffins and Aromatics.

The following section presents plots of Reaction Index with respect to Sample Time and with respect to Peclet Number.

The primary goal in MTO reaction is to maximize Yield of Light Olefins. Yield of Light Olefins is computed as a percentage of methanol carbon reporting to light olefins. Here, this is taken to be the light olefin percentage of the hydrocarbon product stream.

Yield of Light Olefins observed from experimental runs done in microreactors is the sum of Ethylene, 1-Propene, 1-Butene, 1-Pentene and 1-Hexene.

This section presents plots of Yield of Light Olefins with respect to Sample Time, Reaction Index and Peclet Number.

7.1.1.1 SAMPLE TIME

The following figures show Yield of Light Olefins plotted against Sample Time of 20 hours, for experimental runs done in the microreactors.

Figure 7.7 reveals that Yield of Light Olefins from experimental runs done in VBMR-3 (horizontal duct length = 7.62 cm) varies between 49.0 and 59.7 percent throughout Sample Time. The experiments were conducted at weight hourly space velocity of 0.54, 1.11, and 1.06.

Figure 7.8 shows that Yield of Light Olefins obtained from experimental runs done in VBMR-6 (horizontal duct length = 15.24 cm) varies between 68.0 and 72.9 percent throughout Sample Time. The experiments were conducted at WHSV of 1.10 and 1.04.

Figure 7.9 indicates Yield of Light Olefins obtained from experimental runs done in VBMR-9 (horizontal duct length = 22.86 cm) varies between 78.3 and 88.5 percent throughout Sample Time. The experiments were conducted at WHSV of 1.15 and 1.10.

In summary, yield of Light Olefins obtained from experimental runs done in microreactors does not vary widely with Sample Time. From the one comparison that is available, it appears that yield of Light Olefins obtained from microreactors did not vary with WHSV.

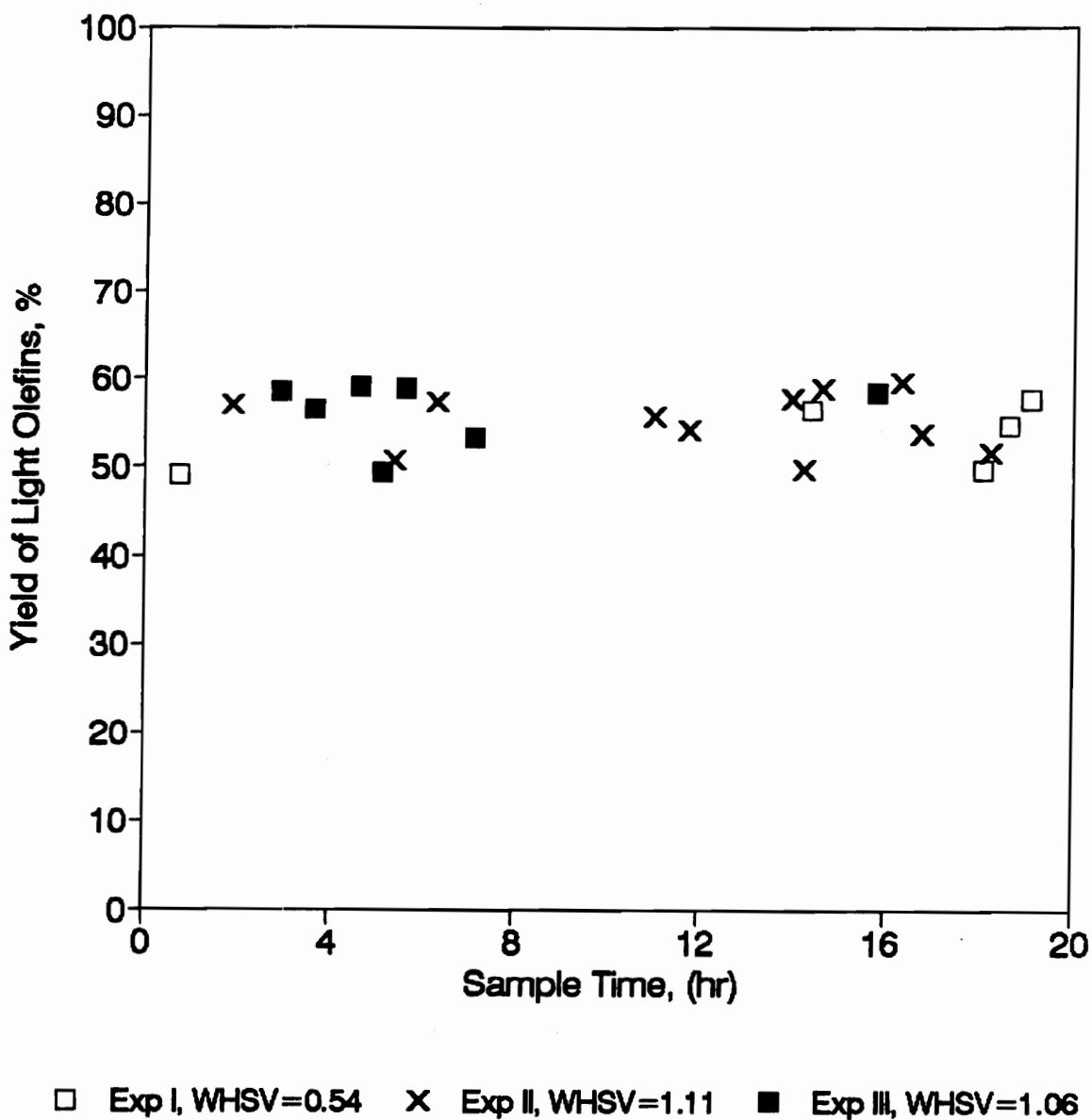


Figure 7.7: Yield of Light Olefins from runs done in VBMR-3 (horizontal duct length = 7.62 cm) varies between 49.0 and 59.7 percent. Experiments were conducted at weight hourly space velocity of 0.54, 1.11 and 1.06.

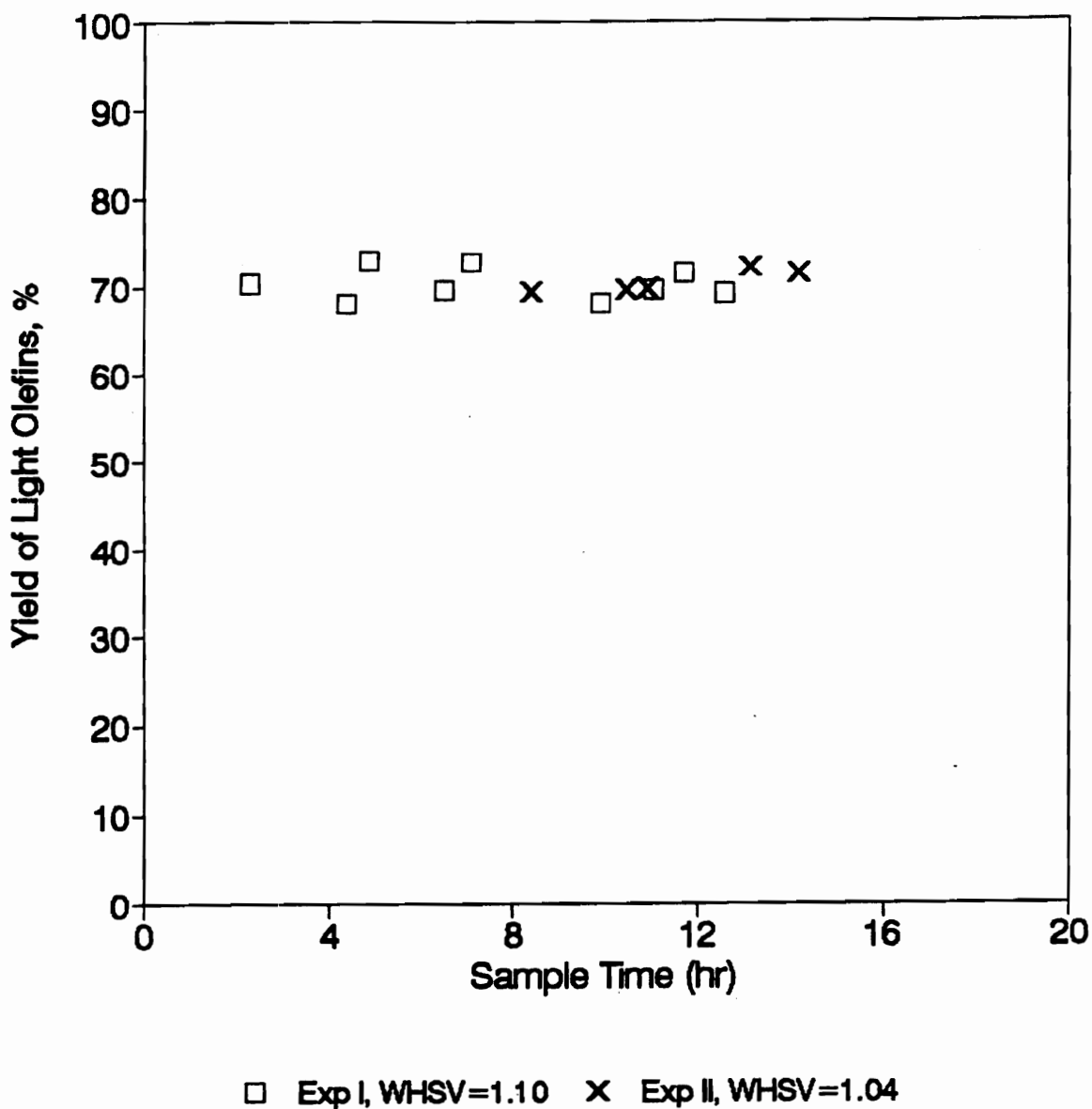
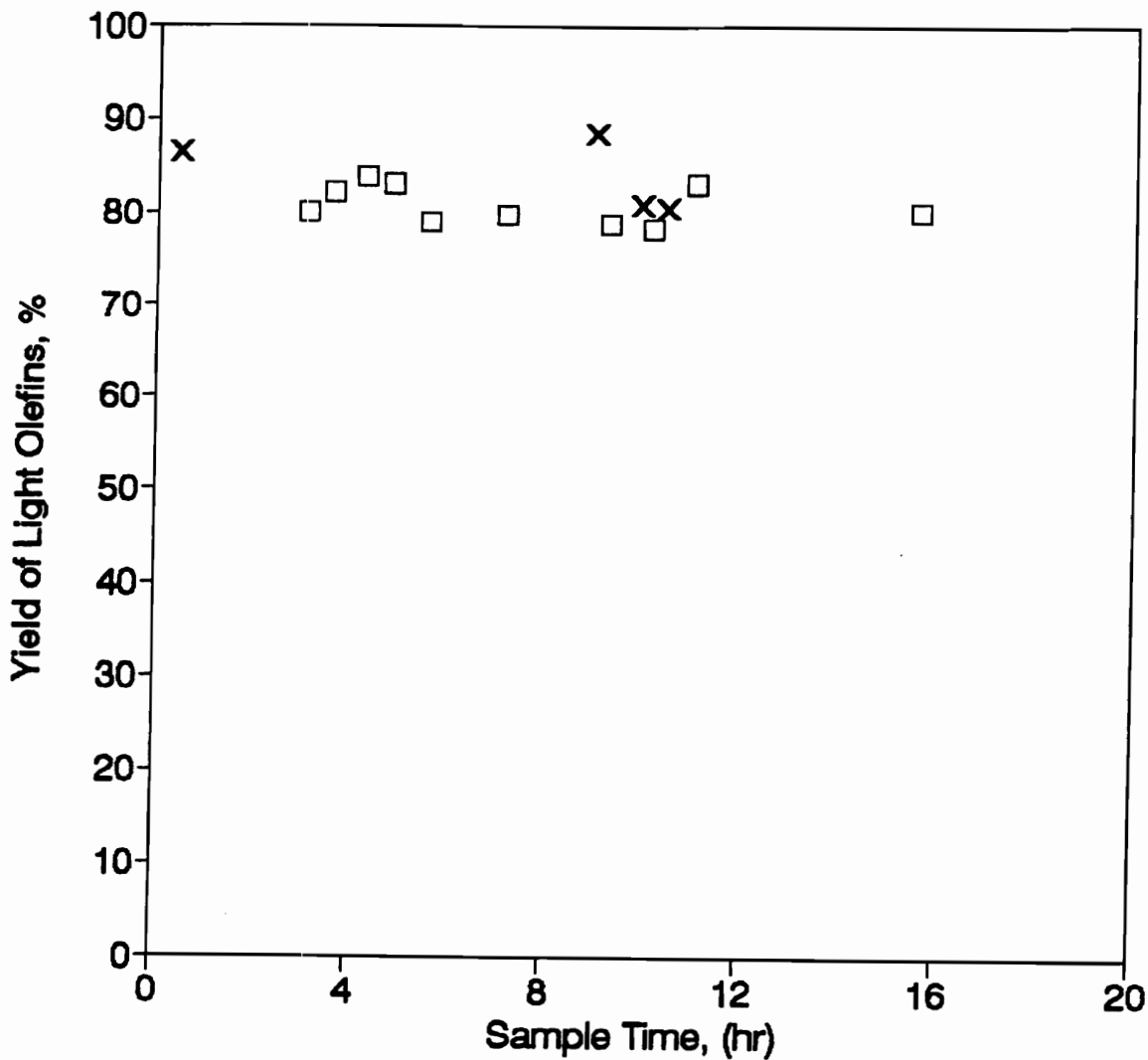


Figure 7.8: Yield of Light Olefins from runs done in VBMR-6 (horizontal duct length = 15.24 cm) varies between 68.0 and 72.9 percent. Experiments were conducted at WHSV of 1.10 and 1.04.



□ Exp I, WHSV=1.15 x Exp II, WHSV=1.10

Figure 7.9: Yield of Light Olefins from runs done in VBMR-9 (horizontal duct length = 22.86 cm) varies between 78.3 and 88.5 percent. Experiments were conducted at WHSV of 1.15 and 1.10.

Reported Data from Fluid Bed

Data were available on the yield of light olefins versus sample time only for the MRDC 100 BPD Demonstration plant. Figure 7.10 indicates yield of Light Olefins obtained from two experimental runs done at WHSV of 1.0 in the 100 BPD Demonstration Plant reported by MRDC. Yield of Light Olefin species reported by MRDC includes Ethylene, Propene, Butenes, Pentenes, Hexenes and C₇ olefins. The types of Butenes, Pentenes, Hexenes and C₇ olefins considered were not specified.

Yield of Light Olefins started off at 36.7 % and took 210 hours (i.e. 8.75 days) of continuous operation to rise up to 61.1. It then varied between 61.1 and 56.7 through 798 hours (33.25 days) of continuous operation.

Comparing Vibrated Bed Microreactor Data with Fluid Bed Data

Although Yield of Light Olefins obtained from microreactors does not include all of the olefinic species reported by MRDC, the value amount does not seem very different. This is because the bulk of Light Olefins produced by MTO reaction is in the C₄⁻ range and significantly drops to negligible amounts after this range, so that inclusion of C₆⁺ olefinic species does not change the total of Yield of Light Olefins by much.

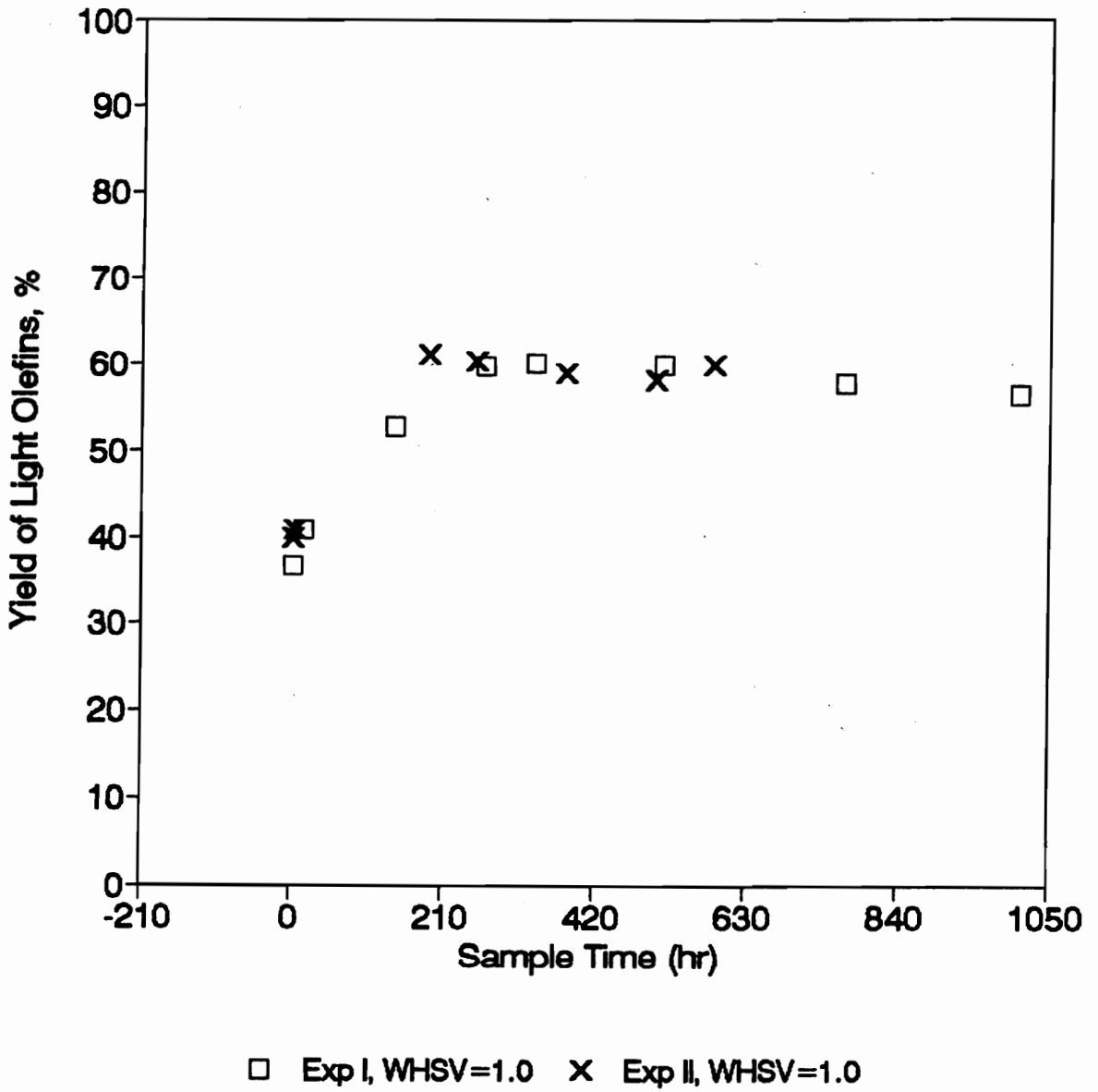


Figure 7.10: Yield of Light Olefins from runs done at WHSV of 1.0 in the 100 BPD Demonstration Plant reported by MRDC. Experiments were conducted at WHSV of 1 (Keim et al, 1987).

In comparing the Yield of Light Olefins obtained from the microreactors with that reported by MRDC, it needs to be pointed out that ;

(i) Yield of Light Olefins observed by MRDC in the 100 BPD

Demonstration Plant took a substantial amount of time (i.e. 210 hours or 8.75 days) of continuous operation before it reached a steady state value which ranged between 61.1 and 56.7 percent.

(ii) Yield of Light Olefins observed in the microreactors almost

immediately reached the steady state value which ranged between: (a) 49.0 and 59.7 percent for VBMR-3, (b) 68.0 and 72.9 percent for VBMR-6, (c) 78.3 and 88.5 percent for VBMR-9, and remained within this range for the entire 20 hours of continuous operation.

7.1.1.2 REACTION INDEX

Reaction Index (RI) is defined by the propane/propene ratio and is a criterion of catalyst activity chosen by MRDC to correlate their fluid bed data. Avidan writes, “ since the measurement of on-line catalyst activity is difficult, we found it convenient to follow an on-line reaction index (RI), which is a selectivity ratio. The propane/propene RI can be easily monitored by an on-line Gas Chromatograph.”.

Careful examination of Reaction Index was done and found not to reveal any interesting, conclusive information about catalyst activity in the

microreactor reaction environment. Plots of how the Reaction Index varied with Sample Time and with Peclet Number are shown in Appendix C.

Figure 7.11 indicates that Yield of Light Olefins observed in VBMR-3 (horizontal duct length = 7.62 cm) when plotted against Reaction Index remained relatively steady between 49.0 and 59.7 percent. Experimental run (WHSV = 1.06) produced Light Olefins at higher Reaction Index than the other two experimental runs (WHSV = 0.54, and WHSV = 1.11).

Figure 7.12 indicates that Yield of Light Olefins observed in VBMR-6 (horizontal duct length = 15.24 cm) when plotted against Reaction Index remained relatively steady between 68.0 and 72.9 percent. Both experimental runs (WHSV = 1.04, and WHSV = 1.10) produced Light Olefins at the same Reaction Index range.

Figure 7.13 indicates that Yield of Light Olefins observed in VBMR-9 (horizontal duct length = 22.86 cm) when plotted against Reaction Index remained relatively steady between 78.3 and 88.5 percent. Experimental run (WHSV = 1.15) produced Light Olefins at higher Reaction Index than the experimental run (WHSV = 1.10) which produced Light Olefins mainly in the lower range.

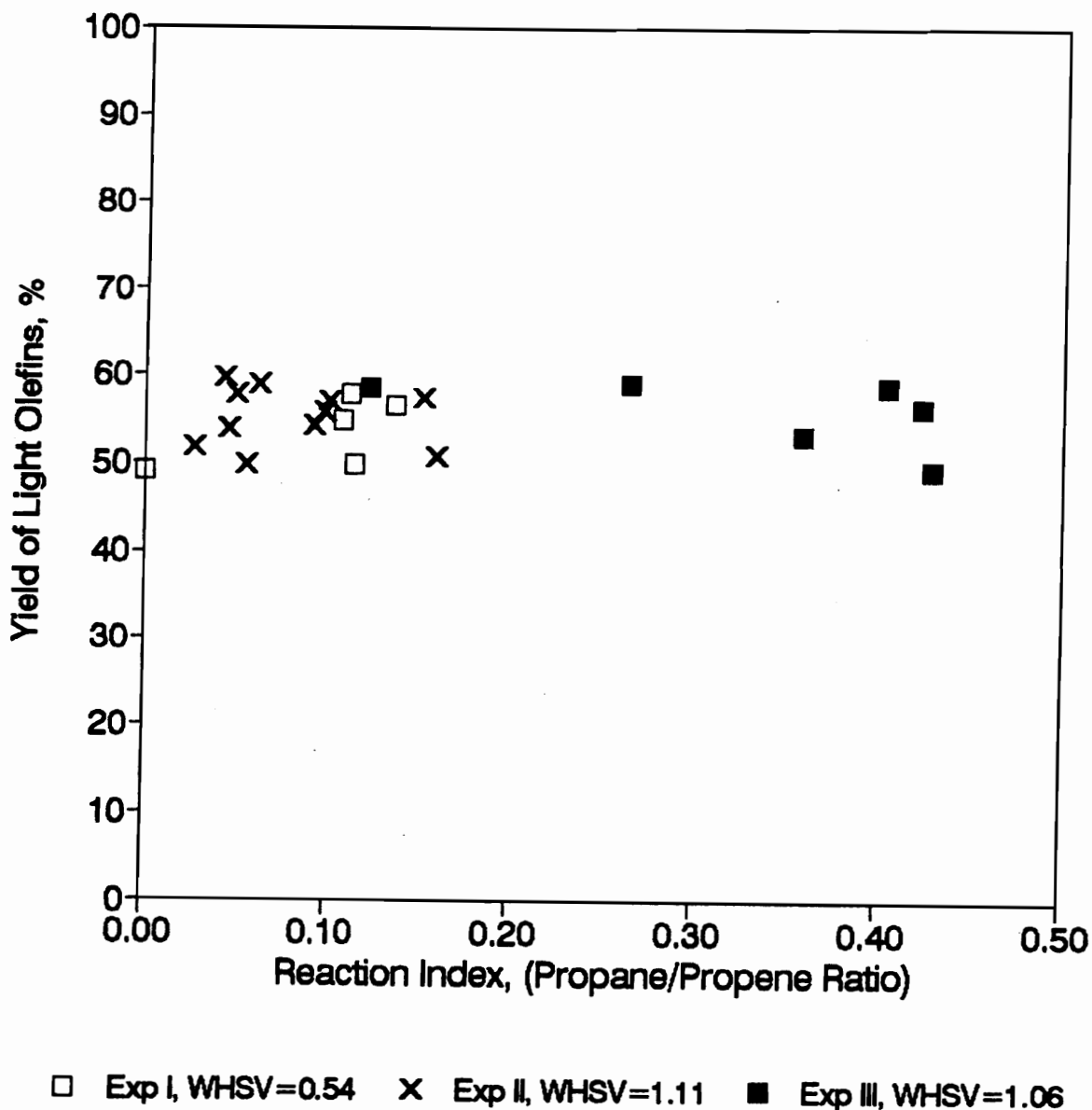


Figure 7.11: Yield of Light Olefins observed in VBMR-3 (horizontal duct length = 7.62 cm) when plotted against Reaction Index remained between 49.0 and 59.7 percent. Experimental run (WHSV = 1.06) produced Light Olefins at higher Reaction Index than the other two runs (WHSV = 0.54, and WHSV = 1.11).

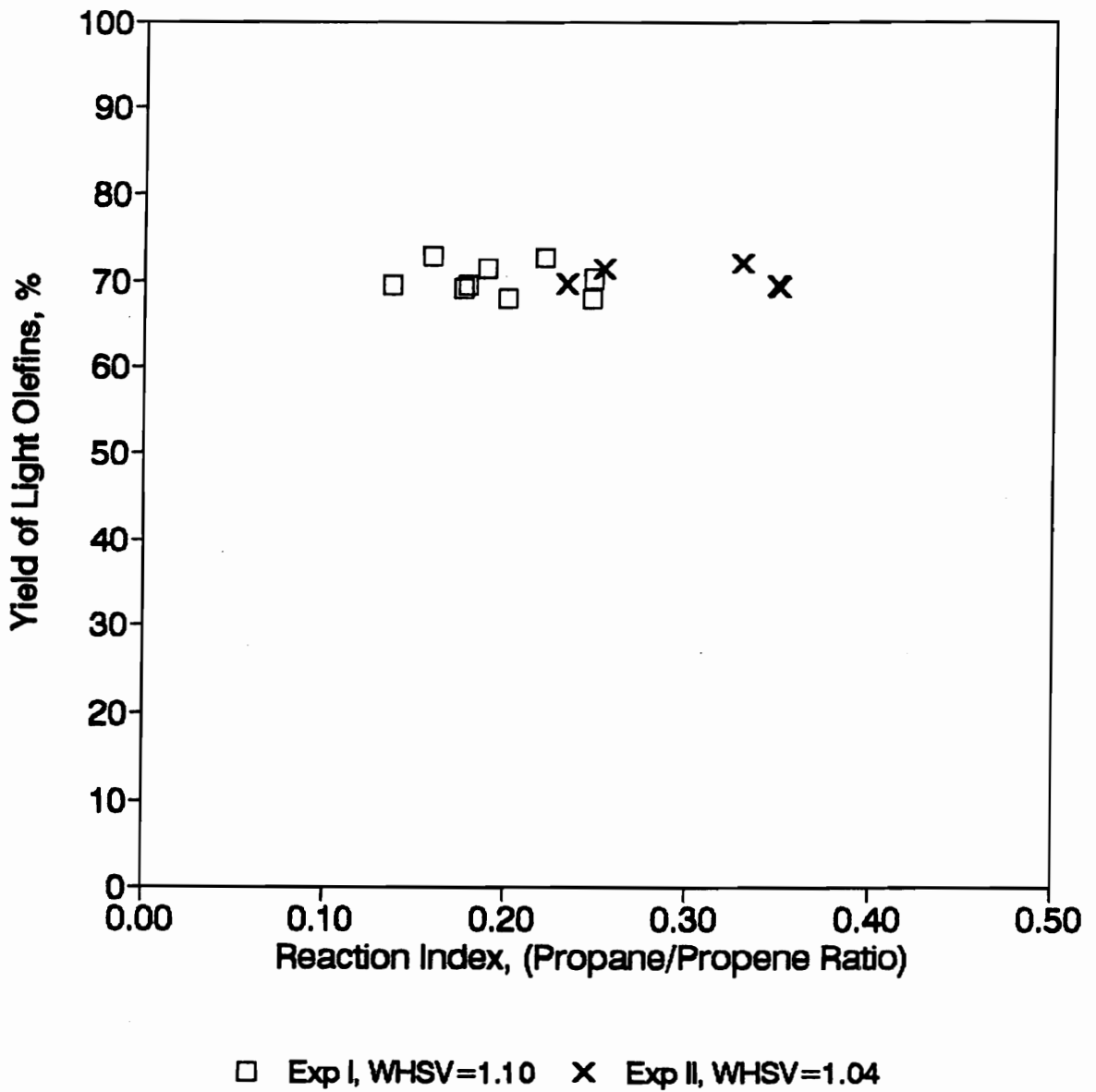


Figure 7.12: Yield of Light Olefins observed in VBMR-6 (horizontal duct length = 15.24 cm) when plotted against Reaction Index remained between 68.0 and 72.9 percent. Both experimental runs (WHSV = 1.04, and WHSV = 1.10) produced Light Olefins at the same Reaction Index range.

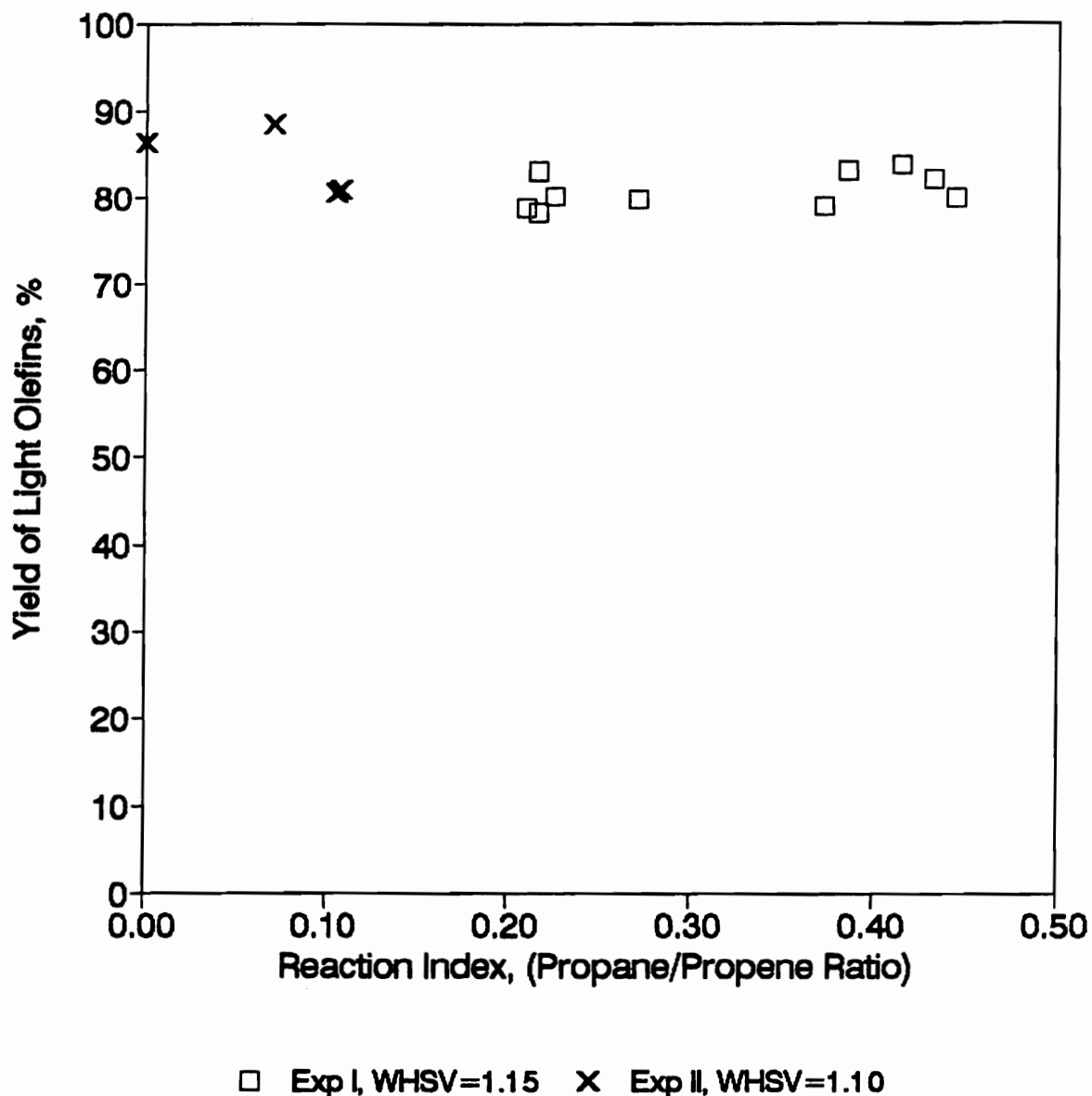


Figure 7.13: Yield of Light Olefins observed in VBMR-9 (horizontal duct length = 22.86 cm) when plotted against Reaction Index remained between 78.3 and 88.5 percent. Experimental run (WHSV = 1.15) produced Light Olefins at higher Reaction Index than the run (WHSV = 1.10).

In summary, yield of Light Olefins obtained from experimental runs done in microreactors when plotted against Reaction Index did not vary widely with increase in Reaction Index in the range of 0.0 up to 0.5. Another point can be made here, that when considering runs conducted in the same microreactor, there were clearly some runs which produced Light Olefins at higher Reaction Index than others. No well defined pattern could be established as to why this was the case. This observation could not be attributed to the variation in WHSV.

Reported Data from Fluid Bed Scale-Up

Experimental runs were done in Bench Scale Unit and 4 BPD Pilot Plant at 482 C and 103 kiloPascal pressure. The reported Yield of Light Olefins consisted of Ethylene, Propene, Butenes and Pentenes. The types of Butenes and Pentenes considered were not specified.

Figure 7.14 indicates a Yield of Light Olefins from Bench-scale unit against Reaction Index in the range between 0.017 and 0.147. Yield of light olefins shows a drop from 74.5 to 63.1 percent.

Figure 7.15 indicates a Yield of Light Olefins from 4 BPD Pilot plant against a Reaction Index in the range between 0.077 and 0.222. Yield of light olefins shows a drop from 71.6 to 57.6 percent.

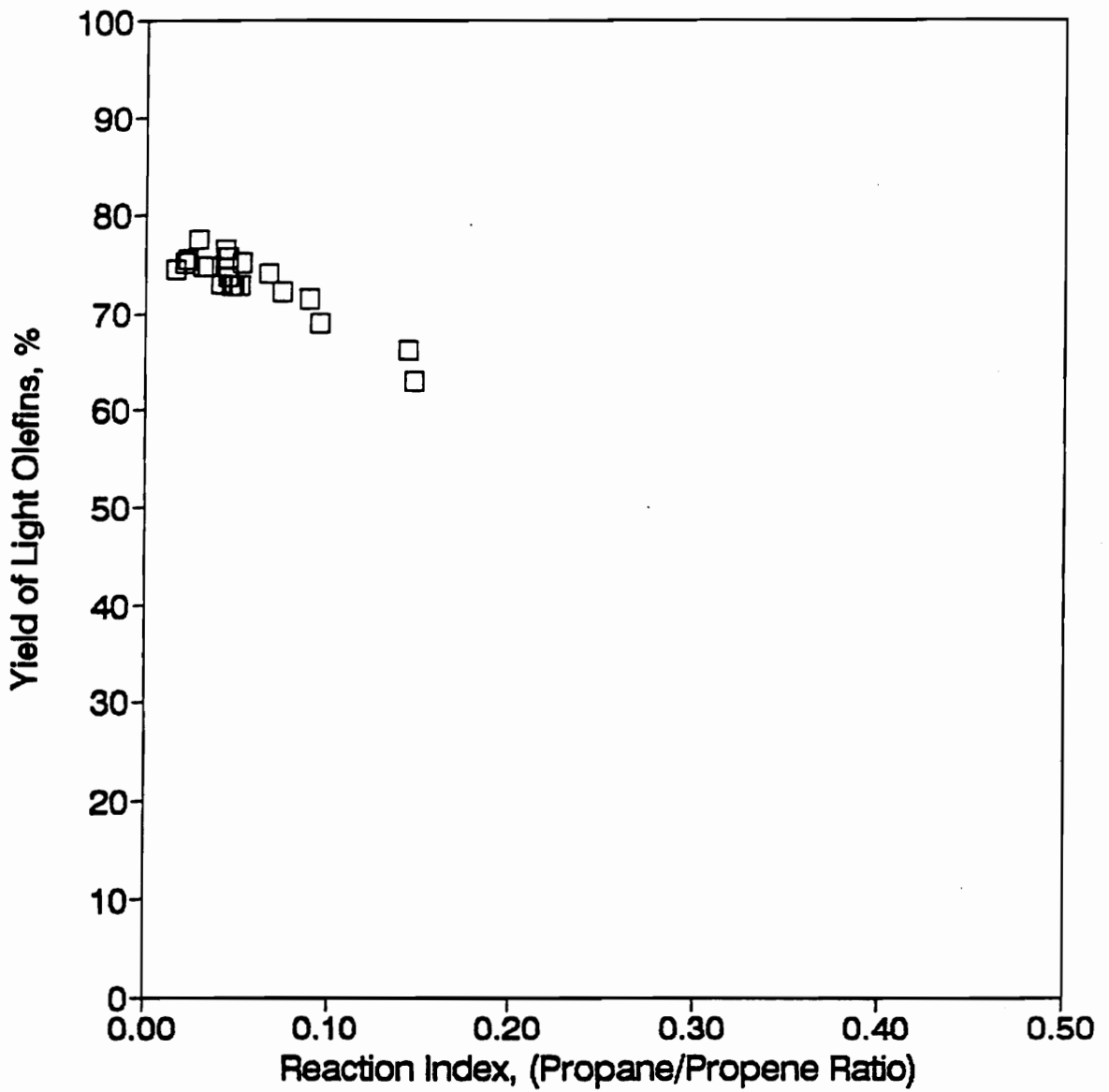


Figure 7.14: Yield of Light Olefins from MRDC Bench-scale fluid-bed unit against Reaction Index in the range between 0.017 and 0.147. Yield of light olefins shows a sharp drop from 74.5 down to 63.1 percent.

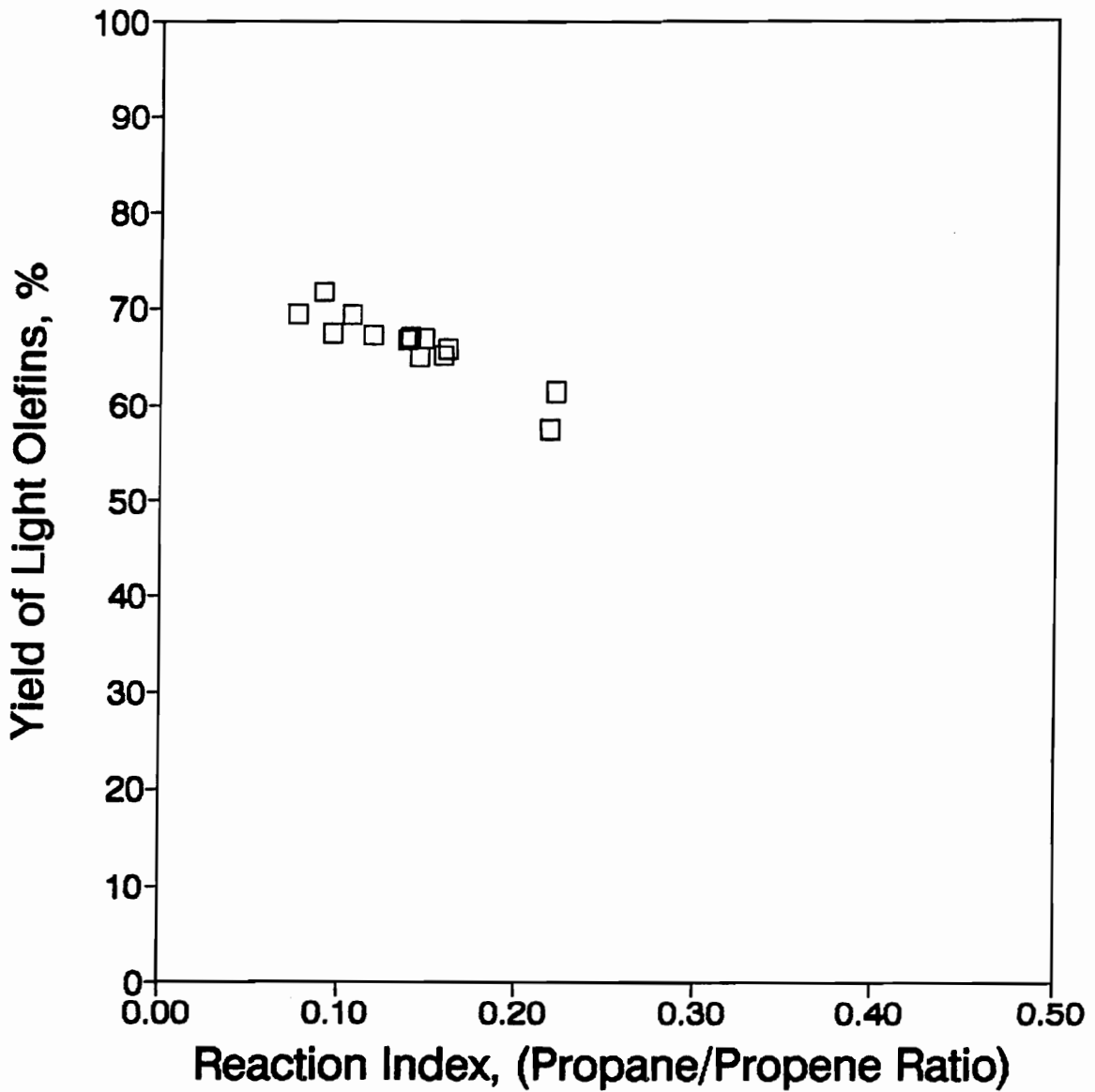


Figure 7.15: Yield of Light Olefins from MRDC 4 BPD Pilot plant against a Reaction Index in the range between 0.077 and 0.222. Yield of light olefins shows a drop from 71.6 to 57.6 percent.

In summary, the yield of Light Olefins observed by MRDC in their Bench Scale and 4 BPD Pilot Plant described above, show a drop with an increase in Reaction Index.

Experimental runs were done in 4 BPD Pilot Plant and 100 BPD Demonstration Plant at 500 C and 250 kiloPascal pressure. The reported Yield of Light Olefins consisted of Ethylene, Propene, Butenes, Pentenes, Hexenes and C₇ olefins. The types of Butenes, Pentenes, Hexenes and C₇ olefins considered were not specified.

Figure 7.16 indicates a Yield of Light Olefins from 4 BPD Pilot plant against a Reaction Index in the range between 0.10 and 0.375. Yield of light olefins shows a drop from 67.5 to 49.5 percent.

Figure 7.17 indicates a Yield of Light Olefins from 100 BPD Demonstration plant against a Reaction Index in the range between 0.175 and 0.445. Yield of light olefins shows a drop from 61.1 to 36.7 percent (Keim et al, 1987).

In summary, the yield of Light Olefins observed by MRDC in the 4 BPD Pilot Plant and 100 BPD Demonstration Plant described above, dropped significantly with increase in Reaction Index.

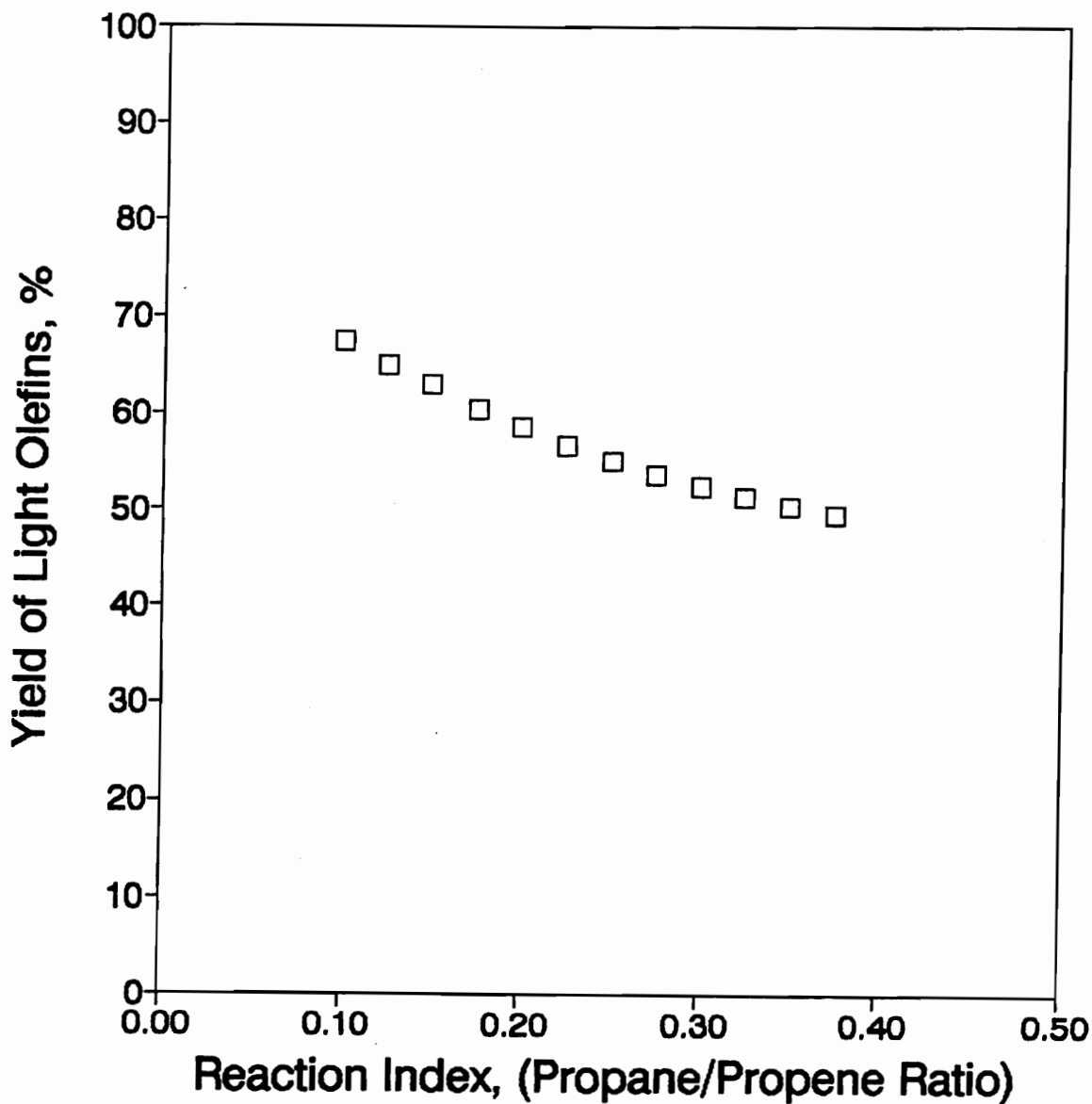


Figure 7.16: Yield of Light Olefins from MRDC 4 BPD Pilot plant against a Reaction Index in the range between 0.10 and 0.375. Yield of light olefins shows a drop from 67.5 to 49.5 percent.

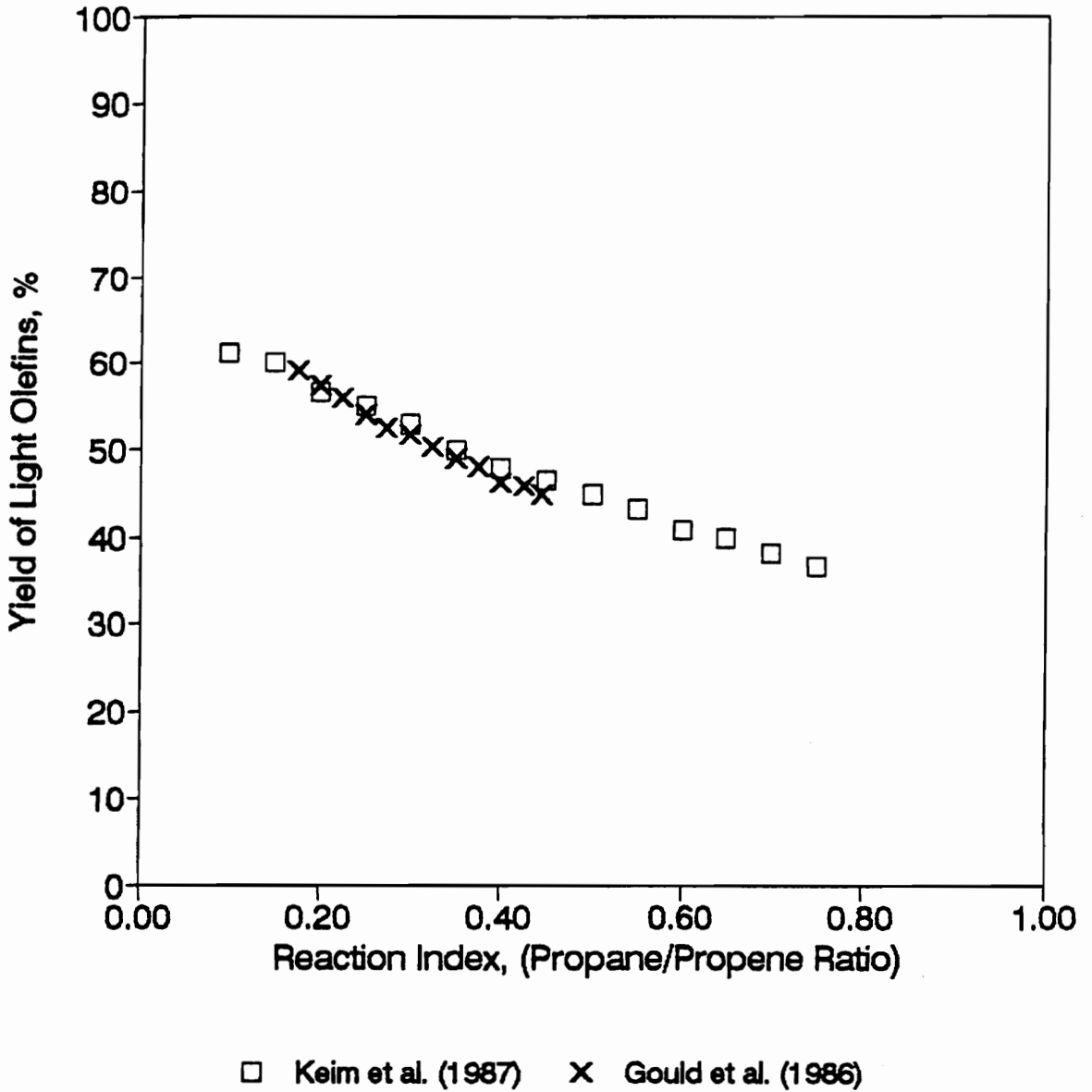


Figure 7.17: Yield of Light Olefins from MRDC 100 BPD Demonstration plant against a Reaction Index in the range between 0.175 and 0.445. Yield of light olefins shows a drop from 61.1 to 36.7 percent (Keim et al, 1987).

Yield of light olefins observed by MRDC from each of their fluid bed units, dropped with increase in Reaction Index regardless of the operating conditions in the fluid bed.

Comparing Vibrated Bed Microreactor Data with Fluid Bed Data

Yield of Light Olefins obtained from experimental runs done in the microreactors when plotted against Reaction Index did not vary with an increase in Reaction Index.

Yield of Light Olefins observed by MRDC in their fluid bed units showed a marked drop with an increase in Reaction Index. This trend was observed in all of the units regardless of the difference in their operating conditions.

7.1.1.3 PECKET NUMBER

Figure 7.18 indicates a plot of Yield of Light Olefins (maximum and minimum values) obtained from microreactors against Peclet Number.

The range of yield of Light Olefins in VBMR-3 is:

- (i) between 49 and 57.8 at Peclet Number of 1.27
- (ii) between 49.4 and 59.1 at Peclet Number of 2.4
- (iii) between 49.9 and 59.7 at Peclet Number of 2.5.

The range of yield of Light Olefins in VBMR-6 is:

- (i) between 69.4 and 72.2 at Peclet Number of 8.7
- (ii) between 68 and 72.9 at Peclet Number of 9.2.

The range of yield of Light Olefins in VBMR-9 is:

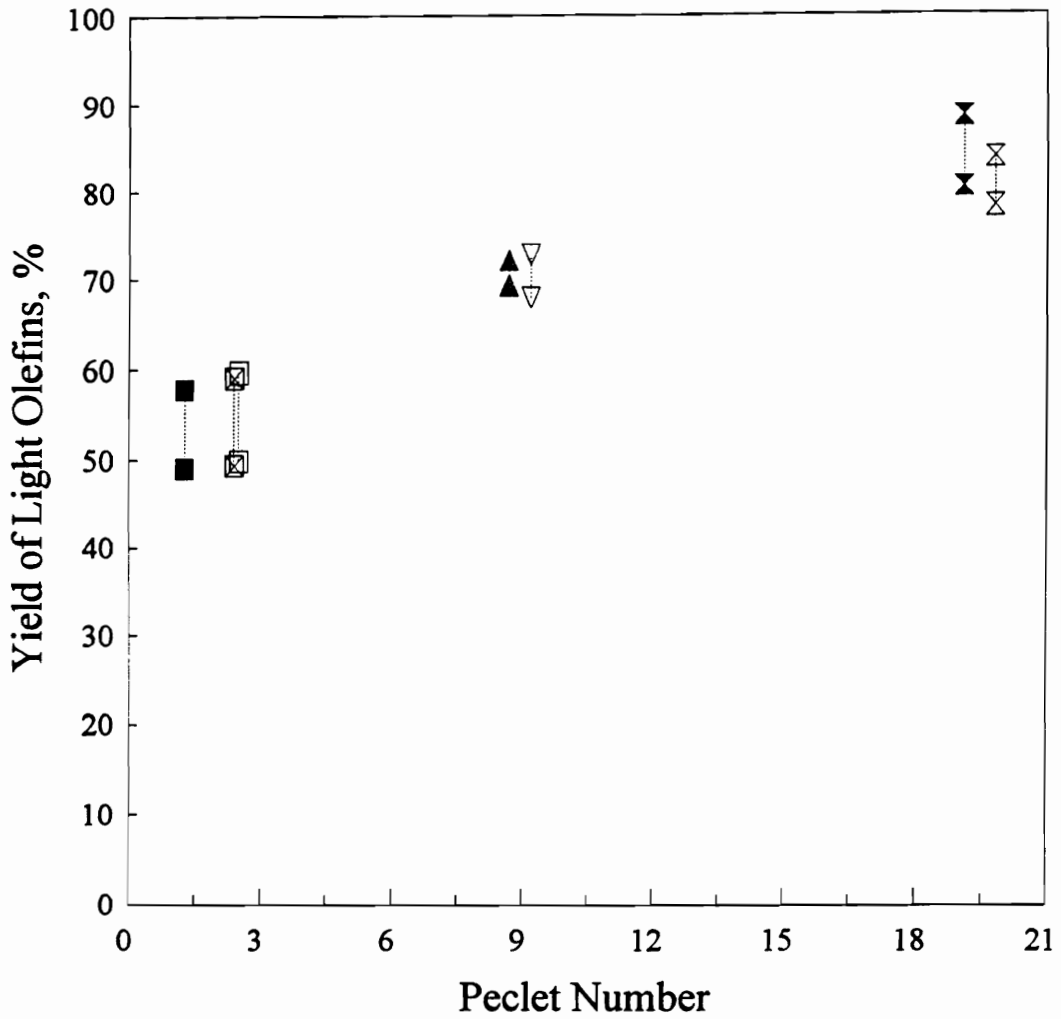
- (i) between 80.5 and 88.5 at Peclet Number of 19.1
- (ii) between 78.3 and 83.8 at Peclet Number of 19.8.

In summary, yield of Light Olefins obtained from experimental runs done in microreactors, at 482 C and 103 kPa pressure, increased with an increase in Peclet Number.

The variation in light olefins (difference between maximum and minimum values) does not appear to vary with variation in WHSV or Peclet Number.

Reported Data from Fluid Bed Scale-Up

Figure 7.19 presents Yield of Light Olefins (maximum and minimum values) reported by MRDC, when plotted against Peclet Number. Data obtained at 482 C was obtained at 103 kiloPascal pressure whilst that obtained at 500 C was done at 250 kiloPascal pressure. All of this data was obtained at WHSV of 1.0.



■ (7.6 cm), Exp I ⊠ (7.6 cm), Exp III □ (7.6 cm), Exp II ▲ (15.2 cm), Exp II
 ▽ (15.2 cm), Exp I × (22.9 cm), Exp II ⊗ (22.9 cm), Exp I

Figure 7.18: Yield of Light Olefins (maximum and minimum values) obtained from microreactors against Peclet Number. Yield of Light Olefins from: (i) 7.6 cm duct length, is between 49.0 and 59.7 percent, (ii) 15.2 cm duct length, is between 68.0 and 72.9 percent and (iii) 22.9 cm duct length, is between 78.3 and 88.5 percent.

Yield of Light Olefins at Peclet number of:

- (i) 7 is between 36.7 and 61.1,
- (ii) 10 is between 49.5 and 67.5,
- (iii) 10 is between 57.6 and 71.6,
- (iv) 14 is between 63.1 and 74.5.

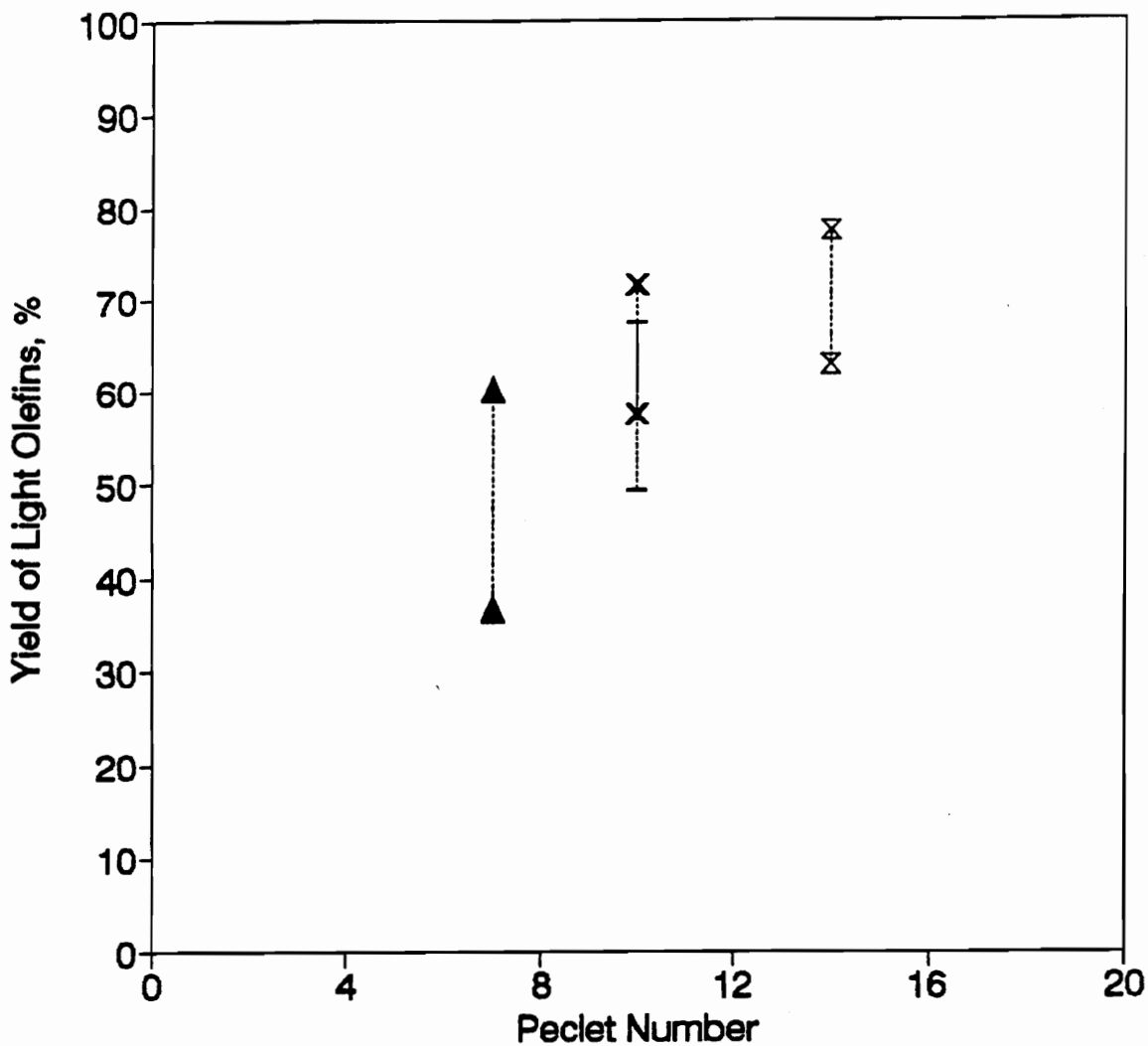
In summary, yield of Light Olefins observed by MRDC in the fluid bed scale up of MTO reaction increased with an increase in Peclet Number.

The variation points in Yield of Light Olefins observed appears to vary with:

- (i) Peclet Number by decreasing with an increase in Peclet Number;
- (ii) operating conditions. The difference in variation points observed from 4 BPD Pilot Plant suggests that the increase of both reaction temperature from 482 to 500 C and pressure from 103 to 250 kiloPascal increased the range of Yield of Light Olefins observed from 14.0 to 18.0 points.

Comparing Vibrated Bed Microreactor Data with Fluid Bed Data

Yield of Light Olefins observed by MRDC in the fluid bed scale up of MTO reaction increased with an increase in Peclet Number.



--x-- Micro (482 C) --x-- Pilot (482 C) --- Pilot (500 C) --▲-- Demo (500 C)

Figure 7.19: Yield of Light Olefins (maximum and minimum values) reported by MRDC, when plotted against Peclet Number. Data obtained at 482 C was done at 103 kiloPascal pressure whilst that obtained at 500 C was done at 250 kiloPascal pressure. All of this data was obtained at WHSV of 1.0.

Yield of Light Olefins obtained from experimental runs done in microreactors, also increased with an increase in Peclet Number, indicating the ability for the microreactor to determine the sensitivity of MTO reaction to axial gas dispersion.

7.1.1.4 SUMMARY OF OBSERVATION ON RESULTS

Yield of Light Olefin species reported by MRDC includes Ethylene, Propene, Butenes, Pentenes, Hexenes and C₇ olefins. The types of Butenes, Pentenes, Hexenes and C₇ olefins considered were not specified. Yield of Light Olefins presented by us in our work with MTO reaction in the microreactors includes Ethylene, 1-Propene, 1-Butene, 1-Pentene and 1-Hexene. Although Yield of Light Olefins presented for MTO reaction conducted in microreactors does not include all of the olefinic species reported by MRDC, the amount does not seem very different. This is because the bulk of Light Olefins produced by MTO reaction is in the C₄⁻ range and significantly drops to negligible amounts after this range, so that inclusion of C₆⁺ olefinic species does not change the total of Yield of Light Olefins by much.

Sample Time

Yield of Light Olefins obtained from experimental runs done in microreactors;

(i) did not appear to be a function of WHSV.
(ii) ranged between: (a) 49.0 and 59.7 percent for VBMR-3, (b) 68.0 and 72.9 percent for VBMR-6 and (c) 78.3 and 88.5 percent for VBMR-9. Yield of Olefins remained within this range for the 20 hours of operation.

Yield of Light Olefins observed by MRDC in the 100 BPD Demonstration Plant took 210 hours (i.e. 8.75 days) of continuous operation to rise from 36.7 to 61.1 percent. It then remained at a range between 61.1 and 56.7 percent.

Reaction Index

Yield of Light Olefins obtained from experimental runs done in microreactors when plotted against Reaction Index did not vary widely with increase in Reaction Index. Some runs conducted in the same microreactor produced Light Olefins at higher Reaction Index than others. This observation did not appear to be related to the variation of WHSV in the runs.

Yield of Light Olefins observed by MRDC in their fluid bed units showed a marked drop with an increase in Reaction Index. This trend was observed in all of the units regardless of the difference in their operating conditions.

Peclet Number

Yield of Light Olefins observed by MRDC in the fluid bed scale up of MTO reaction increased with an increase in Peclet Number.

Yield of Light Olefins obtained from experimental runs done in microreactors, also increased with an increase in Peclet Number, indicating the ability for the microreactor to determine the sensitivity of MTO reaction to axial gas dispersion.

7.1.2 COMPOSITION OF MTO HYDROCARBON PRODUCT

The hydrocarbon product from MTO reaction is composed of varying amounts of Olefins, Paraffins Cycloparaffins and Aromatics. The primary goal in MTO reaction is to maximize the yield of Light Olefins.

Our main interest in this investigation of the sensitivity of MTO reaction to axial gas dispersion has been to monitor the production of Light Olefins as well as the Paraffins. Several samples were taken during each experimental run conducted in Vibrated Bed Microreactor and analysed. The following Olefinic and Paraffinic species of hydrocarbons are identified and quantified in each sample taken;

(i) Light Olefins: Ethylene, 1-Propene, 1-Butene, 1-Pentene and 1-Hexene

(ii) Paraffins: Methane, Ethane, Propane, n-Butane, n-Pentane and n-Hexane

Since the yield of hydrocarbon product remained relatively constant with sample time, it is therefore possible to represent the product with a mean value. A mean of the yield of Light Olefins, Paraffins and unidentified portion of the product was computed for each experimental run.

Table 7.5, Table 7.6 and Table 7.7 present mean composition of the MTO hydrocarbon product obtained in the three microreactors (VBMR-3, VBMR-6 and VBMR-9) respectively. The tables indicate that:

- (i) Light Olefins increases with Peclet Number, and make up a major portion of hydrocarbon product at all Peclet Numbers.
- (ii) the Paraffin portion is very small when compared to the olefins, and does not appear to vary with Peclet Number. The slight variation observed is within experimental error margin.
- (ii) the amount of unidentified material drops with increase in Peclet Number.

It would have been costly to try and verify the exact make up of this unidentified material because it comprises of C_7^+ hydrocarbon product species which include a combination of heavy Olefins, Paraffins, Naphthenes and Aromatics, most of which are cyclic and branched and thus difficult to resolve on the packed column.

Table 7.5: Mean composition of the MTO hydrocarbon product obtained in VBMR-3 (horizontal duct length = 7.62 cm).

Experiment	I	II	III
PARAFFINS			
Methane	3.3	0.9	1.2
Ethane	0.1	0.2	0.4
Propane	2.0	2.0	4.8
n-Butane	2.0	2.1	3.3
n-Pentane	1.7	2.1	1.5
n-Hexane	1.1	0.7	0.9
Total	10.3	8.0	12.2
OLEFINS			
Ethylene	12.0	8.3	10.2
1-Propene	17.9	18.1	17.8
1-Butene	13.5	14.9	17.3
1-Pentene	6.7	9.5	8.2
1-Hexene	3.6	3.3	3.4
Total	53.6	54.1	56.9
Others (*)	36.1	37.9	30.8
Peclet Number	1.27	2.5	2.4

Others (*) represents Cycloparaffins and Aromatics

Table 7.6: Mean composition of the MTO hydrocarbon product obtained in VBMR-6 (horizontal duct length = 15.24 cm).

Experiment	I	II
PARAFFINS		
Methane	1.4	1.2
Ethane	0.4	0.7
Propane	3.5	5.7
n-Butane	3.4	4.0
n-Pentane	3.4	1.7
n-Hexane	1.2	0.7
Total	13.3	12.8
OLEFINS		
Ethylene	13.9	12.1
1-Propene	18.8	19.4
1-Butene	17.5	24.4
1-Pentene	14.7	11.1
1-Hexene	5.2	3.3
Total	70.2	70.2
Others (*)	16.5	17.0
Peclet Number	9.16	8.73

Others (*) represents Cycloparaffins and Aromatics

Table 7.7: Mean composition of the MTO hydrocarbon product obtained in VBMR-9 (horizontal duct length = 22.86 cm).

Experiment	I	II
PARAFFINS		
Methane	1.3	3.3
Ethane	0.7	0.0
Propane	7.4	4.5
n-Butane	4.5	0.9
n-Pentane	1.8	1.4
n-Hexane	1.4	0.5
Total	17.1	10.7
OLEFINS		
Ethylene	12.5	2.7
1-Propene	19.1	72.2
1-Butene	28.9	3.5
1-Pentene	14.8	2.3
1-Hexene	7.2	4.8
Total	82.5	85.5
Others (*)	0.4	3.8
Peclet Number	19.81	19.13

Others (*) represents Cycloparaffins and Aromatics

MRDC reported this portion to be relatively small, consisting of PON (i.e. Paraffin/Olefin/Naphthene) and a substantial variety of aromatics, as shown in Table 5.1 in chapter 5. We would have to buy standard samples of all of these species, most of which are available commercially only in large quantities (e.g. gallons). We decided that it was not worth the money and time to map the true nature of this portion, especially with the gas chromatograph we have.

Reported Data from Fluid Bed

Table 7.8 presents mean composition of the MTO hydrocarbon product from Fluid Beds. MRDC reported composition of hydrocarbon product obtained from conducting MTO reaction at 482 C and 103 kiloPascal pressure, in Micro-Fluid Bed and 4 BPD Pilot Plant. Composition of hydrocarbon product obtained from conducting MTO reaction at 500 C and 250 kiloPascal pressure, was not reported in full.

It is worth noting from this table that:

- (i) Propene makes up a major portion of the hydrocarbon product.
- (ii) C_6^+ olefins is in the least amount.
- (iii) Aromatics portion is very small.

Table 7.8: Mean composition of the MTO hydrocarbon product obtained by MRDC in the fluid-bed scale up of the reaction.

	MICRO	PILOT	PILOT	DEMO
PARAFFINS				
Methane	n/a	n/a	n/a	n/a
Ethane	n/a	n/a	n/a	n/a
Propane	n/a	n/a	7.0	7.0
n-Butane	n/a	n/a	n/a	n/a
n-Pentane	n/a	n/a	n/a	n/a
n-Hexane	n/a	n/a	n/a	n/a
Total	15.3	16.6	n/a	n/a
OLEFINS				
Ethylene	5.8	5.2	n/a	n/a
Propenes	33.7	32.9	n/a	n/a
Butenes	18.4	19.1	n/a	n/a
Pentenes	14.8	12.0	n/a	n/a
Hexenes	5.5	7.7	6.0	6.0
Total	78.2	76.9	63.0	61.0
Aromatics	6.5	6.5	n/a	n/a
Temp., degC	482	482	500	500
Pressure, kPa	103	103	250	250
Peclet No.	14	10	10	7

n/a, not reported

Comparing Vibrated Bed Microreactor Data with Fluid Bed Data

The following observations can be made when comparing yield of MTO hydrocarbon product obtained in microreactors and fluid beds:

(i) Both microreactors and fluid beds indicate an increase in the yield of Light Olefins with an increase in Peclet Number. However the yield of Light Olefins is higher in microreactors than in fluid beds.

(ii) Both microreactors and fluid beds indicate a small yield of Paraffins. The yield of Paraffins does not seem to vary with Peclet Number. The slight variations are within experimental error margin.

(iii) MRDC reported a yield of 6.5 percent for Aromatics at Peclet Numbers of 14 and 10. It would have been very interesting to see the yield of Aromatics at Peclet Number of 7 as this would give us some idea as to where the yield of Aromatics would be in our own results from the microreactors.

(iv) More Propene is produced in the fluid beds than in microreactors.

(v) More Ethylene is produced from microreactors than in fluid beds.

Schultz-Flory plots provided no interesting information.

7.2 ACCURACY OF MTO REACTION RESULTS

Two Detectors in the Gas Chromatograph were used to identify the presence of Hydrocarbons and Oxygenates.

Flame Ionisation Detector identified the presence of Hydrocarbon Product Species like Light Olefins, Paraffins, Cycloparaffins and Aromatics. On average for every reaction product sample, a total of 26 signal peaks showed up in the printout from the Integrator, which was hooked to the Flame Ionization Detector. Eleven signal peaks were sorted out by their Retention Times and quantified. Peaks of interest were Light Olefins such as Ethylene, Propene, 1-Butene, 1-Pentene and 1-Hexene; and Paraffins such as Methane, Ethane, Propane, Butane, Pentane and Hexane.

Thermal Conductivity Detector identified presence of oxygenates like water, unreacted methanol, hydrogen, carbon dioxide and carbon monoxide. It was very important to monitor the presence of:

- (i) water because it indicated that the reaction is going well,
- (ii) unreacted methanol in case there was incomplete conversion of methanol in the Vibrated Bed Microreactors,
- (iii) hydrogen, carbon dioxide and carbon monoxide to indicate in case methanol was decomposing.

Entering all of the data into a spreadsheet manually was quite a task. Extreme care was exercised to minimize the human error in entering the data by hand into a spreadsheet.

Products of Methanol decomposition include methane, hydrogen, water, carbon monoxide and carbon dioxide (Chang and Silvestri, 1977). No carbon monoxide, carbon dioxide, hydrogen were detected in the Thermal Conductivity Detector, indicating that no methanol was decomposing.

Methane observed in the product sample was small, in the range of 0.5 to 2 percent. We understand (Amos Avidan, personal communication) that methane can arise in our system only from methanol cracking. As will be seen shortly, we observed negligible carbon on catalyst at the end of runs.

Unreacted Methanol signal peak was not detected, which indicated that we were obtaining complete conversion of methanol to olefins.

Lastly two investigations were done:

- (i) analyzed used HZSM-5 catalyst to detect if any significant methanol carbon was deposited on the catalyst as coke,
- (ii) conducted a blank run (i.e. run without HZSM-5 catalyst).

Material balance was not attempted due to the problems associated with measuring the amounts of toxic, hot gaseous reaction products. Only the

composition of the reaction products was determined and the rest of the stream was sent out the vent. Moreover we were working with very small flow of methanol into the microreactor, in the range of 0.97 and 6.5 ml/hr.

7.2.1 ANALYSIS OF USED HZSM-5 CATALYST

Fresh HZSM-5 catalyst was used in each of experimental runs done in Vibrated Bed Microreactors.

Samples of used HZSM-5 catalyst directly from an experiment from each of the Vibrated Bed Microreactors was send to a commercial analytical laboratory. Table 7.9 shows the analysis of Carbon and Hydrogen contents in the used HZSM-5 catalyst sample perfomed by the commercial analytical laboratory. An insignificant percentage of Methanol Carbon deposited as coke on the HZSM-5 catalyst.

The interior of the Vibrated Bed Microreactors were also visually inspected after each experimental run. No carbon deposits were seen. Substantially all methanol carbon appeared to report to hydrocarbons.

Table 7.9: Analysis of Carbon and Hydrogen in the used HZSM-5 catalyst sample performed by a commercial analytical laboratory. The column “ % Carbon from Methanol” reflects the percentage of methanol carbon reporting to coke deposited on the HZSM-5 catalyst.

Sample ID	Laboratory Carbon %	Results Hydrogen %	Calculated % Carbon from Methanol
VBMR-3	1.42	< 0.5	0.22
VBMR-6	2.84	< 0.5	0.29
VBMR-9	1.44	< 0.5	0.21

7.2.2 BLANK RUN

A blank run was conducted by setting up the Vibrated Bed Microreactor the same as if it were an experiment, the only difference being that HZSM-5 catalyst was not loaded. Methanol was fed with a Syringe Pump when the reactor temperature was constant at 482 C.

Figure 7.20 (a) shows a typical gas chromatogram from flame ionisation detector depicting the unreacted/uncracked methanol obtained during a blank run. Figure 7.20 (b) shows a typical gas chromatogram from thermal conductivity detector depicting methanol and water peaks obtained during a Blank Run.

Signal Peak from the flame ionisation detector identified only methanol, while the signal peak from thermal conductivity detector showed water and methanol. Water peak is not a reaction product since methanol is known to contain some water.

This indicated that methanol did not crack on the hot Vibrated Bed Microreactor.

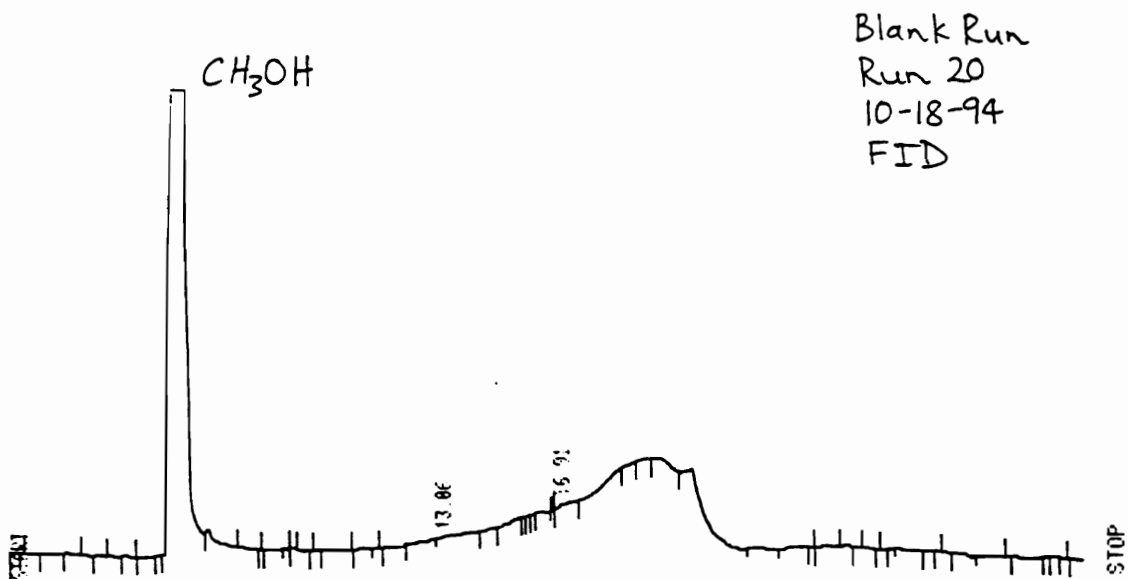


Figure 7.20 (a): A typical gas chromatogram from flame ionisation detector depicting the unreacted/uncracked methanol obtained during a blank run.

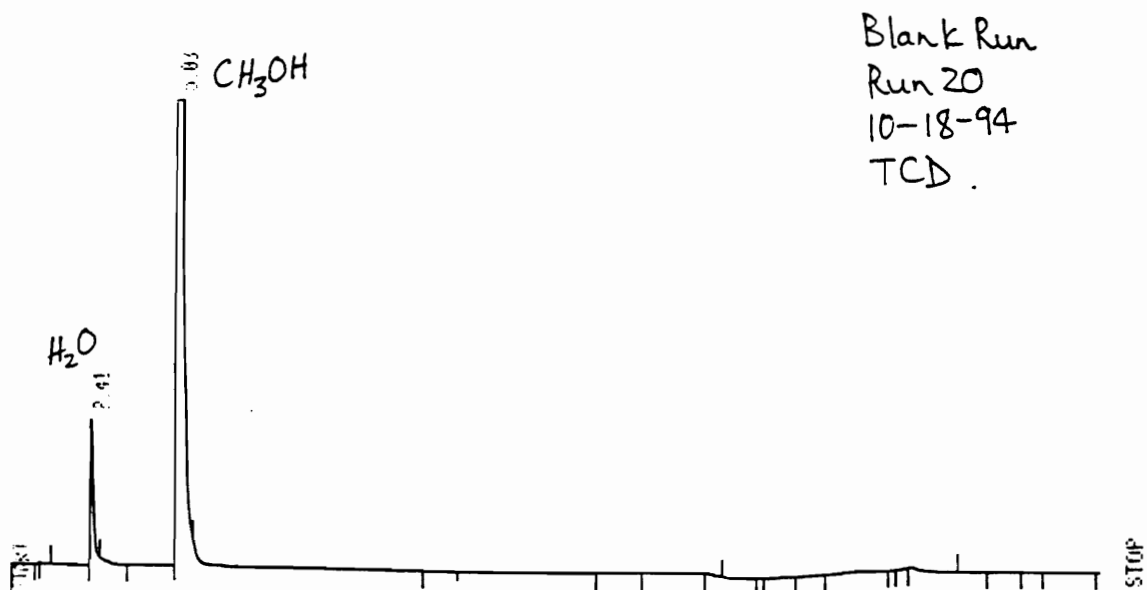


Figure 7.20 (b): A typical gas chromatogram from thermal conductivity detector depicting the unreacted/uncracked methanol and water peaks obtained during a blank run. The water peak represents water that is present in methanol and not a reaction product.

8. CONCLUSIONS

Discovery and elucidation of the coherent-expanded (C-E) vibrated-bed state has led to the design and development of a vibrated bed microreactor. The microreactor exploits the intense solid mixing of the C-E state to promote intimate contact between reactant gas and catalyst solid.

The C-E state is achieved by subjecting a horizontal duct on whose floor rests a shallow layer (1 mm deep) of Group A catalyst powder to vertical sinusoidal vibration at sufficient intensity. The catalyst powder can expand to a height of 12.7 mm during a portion of each vibration cycle. This results in an intense mixing of the catalyst powder in the vertical direction and little or none in the horizontal (axial) direction.

Earlier research on a cold-flow model of the microreactor showed that (i) shifting of catalyst powder from inlet toward the outlet was negligible at horizontal superficial air velocities up to approx 20 mm/s, (ii) there is no gas bypassing, and (iii) axial gas dispersion coefficient varies linearly with superficial gas velocity, revealing a capability to vary Peclet Number in the microreactor by simply varying horizontal duct length when holding WHSV constant. The object of the present research is to determine the sensitivity of Methanol-To-Olefins (MTO) reaction to axial gas dispersion.

8.1 VIBRATED BED MICROREACTOR DESIGN

A microreactor capable of operating at 482 C has been designed to study the sensitivity of MTO reaction to axial Peclet Number. It comprises a rectangular horizontal duct, 12.7 mm in height, 25.4 mm in width and variable length, charged with a shallow (1 mm deep) layer of HZSM-5 catalyst. The microreactor is constructed out of an aluminum alloy, 6061-T6, heated with four 600 Watts cartridge heaters; the desired temperature is maintained by a process controller using a thermocouple looking into the duct.

A glass reference duct with the same catalyst loading is mounted directly above the microreactor to provide a visual check of the C-E state when the setup is vibrated at 24 hertz and vibrational intensity of 10 (i.e. 4.3 mm vertical displacement).

8.2 SENSITIVITY OF MTO REACTION TO GAS DISPERSION IN THE MICROREACTOR

The ultimate goal of the present research was to determine the sensitivity of MTO reaction to axial gas dispersion represented herein by Peclet Number. Three microreactors were designed with horizontal duct lengths of 7.62 cm, 15.24 cm and 22.86 cm. The MTO reaction was conducted in each of the

three microreactors at temperature of 482 C, pressure of 712 mm Hg at a WHSV in the vicinity of 1, affording complete conversion of methanol. Main products from MTO reaction are water and hydrocarbons, of which the maximum yield is 56.4 and 43.6 weight percent by stoichiometry, respectively. The hydrocarbon product consists of varying amounts of Olefins, Paraffins, Cycloparaffins and Aromatics. Light olefins make up a major portion of the hydrocarbon product.

Figure 8.1 represents all of the hydrocarbon product from conducting MTO reaction in the microreactors. As shown in the figure:

- (i) yield of light olefins increased with an increase in Peclet Number, indicating that low gas dispersion favors production of light olefins which are a major product,
- (ii) yield of paraffins is low and did not vary with Peclet Number, indicating that gas dispersion does not affect production of paraffins,
- (iii) yield of cycloparaffins and aromatics is represented by the category “others”, and decreased with an increase in Peclet Number, indicating that high dispersion promoted production of cycloparaffins and aromatics. High gas dispersion represents a high level of gas backmixing, which tends to hold back the main product thus facilitating its further conversion into cycloparaffins and aromatics.

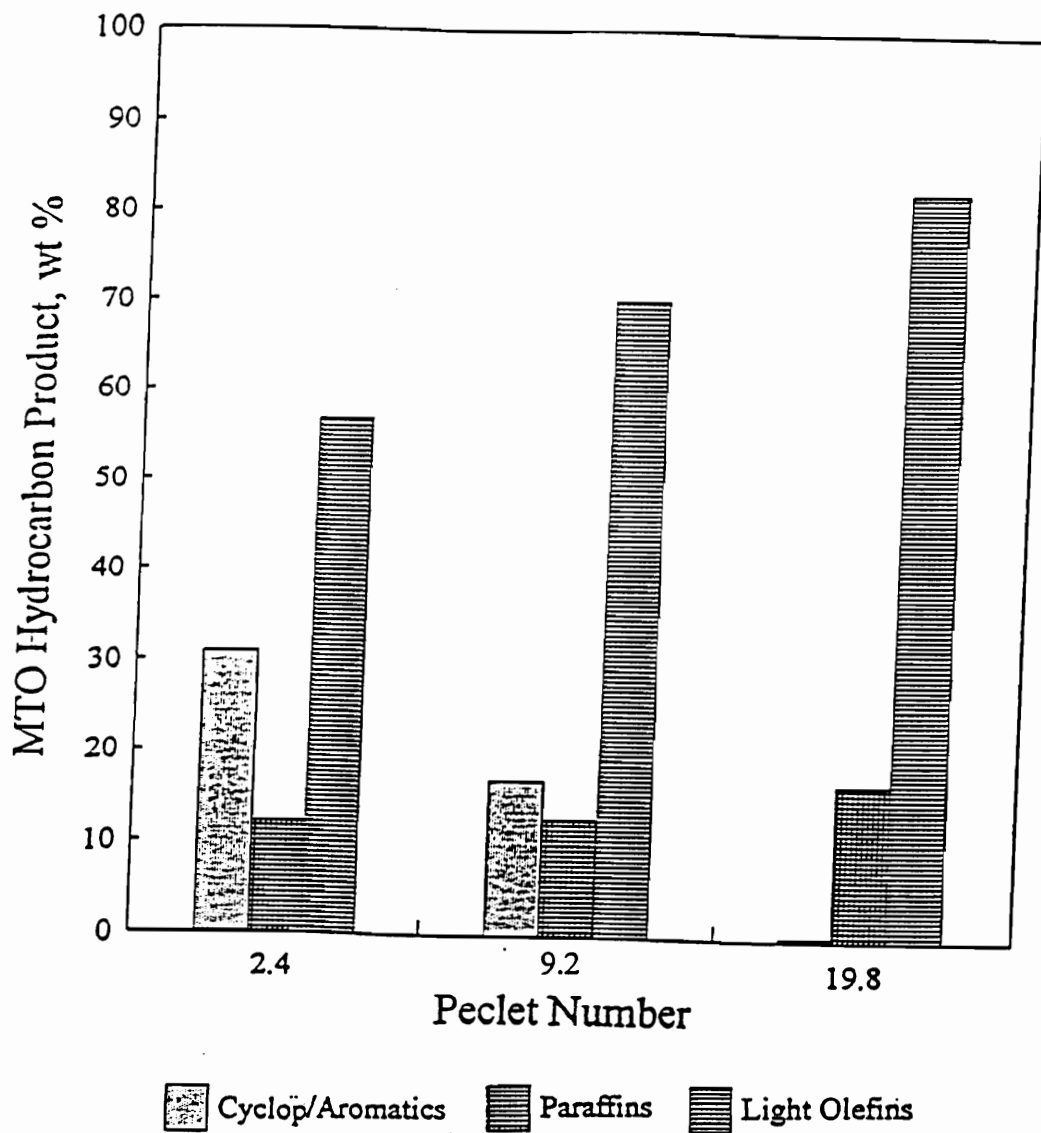


Figure 8.1: MTO hydrocarbon product plotted against Peclet Number. The data is from experiments done at Peclet Numbers of 2.4, 9.2 and 19.8 in the microreactor with duct length of 7.6 cm, 15.2 cm and 22.9 cm respectively. The figure shows that: (i) low gas dispersion (represented by high Peclet Number) favors production of light olefins which are a major product, (ii) gas dispersion shows little effect on production of paraffins, and (iii) high gas dispersion (i.e. high degree of gas backmixing represented by low Peclet Number) promotes production of cycloparaffins and aromatics.

Mobil Research and Development Corporation (MRDC) reported results from a fluid bed scale-up of MTO process in Bench Scale, 4 BPD Pilot Plant and 100 BPD Demonstration Plant.

Results obtained from the microreactors were compared with those reported by MRDC in their fluid bed scale-up. The comparison of the results will enable us to draw some conclusions on how the MTO reaction performs in the different reaction environments exhibited by the microreactor and a fluid bed. The microreactor offers a gas-solid contacting environment characterized by only gas dispersion and substantially devoid of solid mixing and/or circulation whilst the gas solid contacting environment in a fluid bed is characterised by both gas dispersion and top-to-bottom solid mixing and/or circulation.

8.2.1 YIELD OF LIGHT OLEFINS

In each of the microreactors the yield of Light Olefins remained substantially constant with (i) Sample Time in the range of 0.0 and 20 hours, and (ii) Reaction Index in the range of 0.0 and 0.5. Reaction Index does not appear to be as useful for characterizing microreactor data as MRDC found this parameter to be in analysis of fluid-bed data.

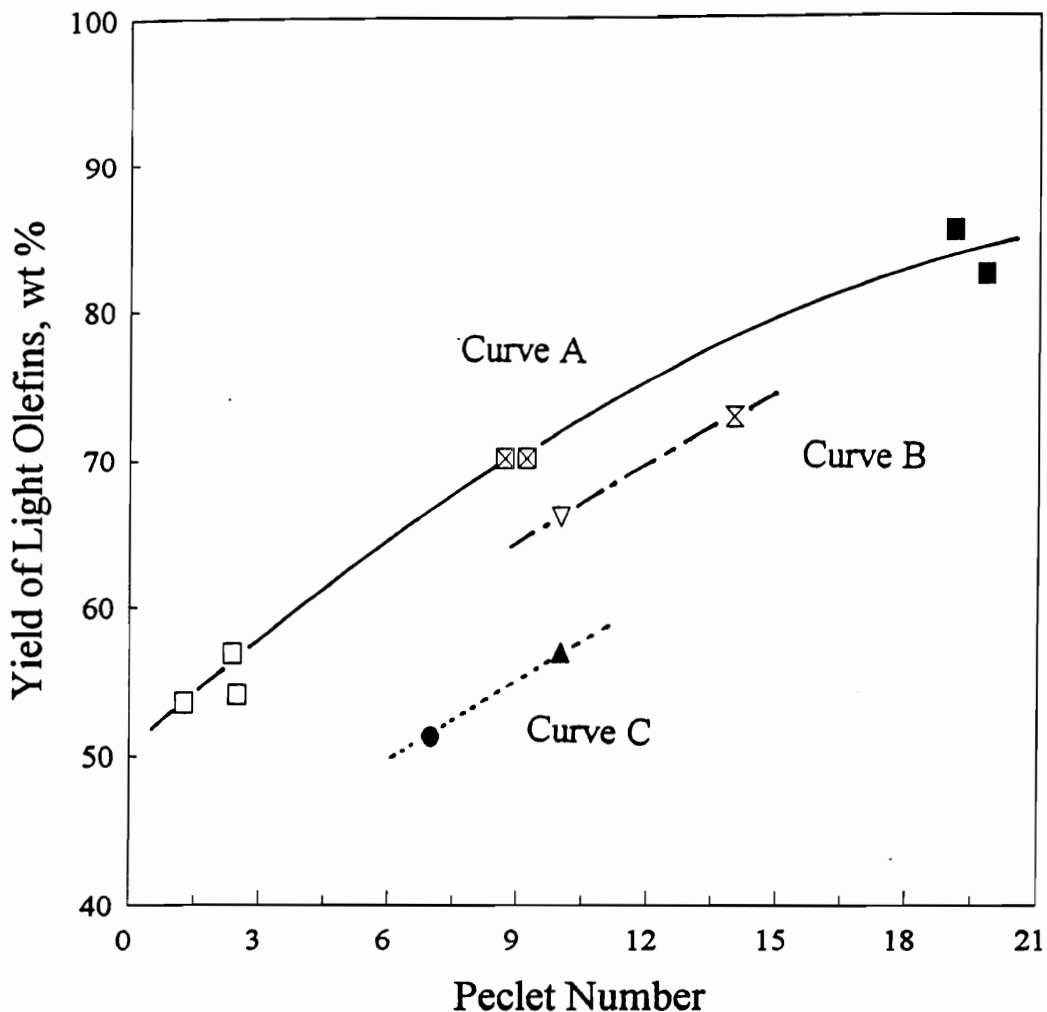
Yield of Light Olefins observed by MRDC from each of their fluid bed units, dropped significantly with an increase in Reaction Index in the range of 0.0 and 0.5.

Figure 8.2 indicates a plot of average yields of Light Olefins versus Peclet Number for runs done in the microreactors (data symbol, empty square) and runs done by MRDC in their fluid bed scale-up (data symbol, filled triangle). All of the data was obtained at WHSV of approximately 1. Yield of Light Olefins is percentage of methanol carbon reporting to C₂ to C₆ olefins.

Curve A represents data from microreactors (horizontal duct lengths of 7.62 cm, 15.24 cm and 22.86 cm.) where each point is a grand average from several experiments. All of the data was obtained at 482 C and 712 mm Hg.

Curve B represents data from Bench Scale (at Peclet Number of 10) and 4 BPD Pilot Plant (at Peclet Numbers of 10) operated by MRDC at 482 C and 772 mm Hg.

Curve C represents data from 100 BPD Demonstration Plant (at Peclet Number of 7) and 4 BPD Pilot Plant (at Peclet Number of 10) operated by MRDC at 500 C and 1 876 mm Hg.



□ 7.6 cm (482/95) ⊠ 15.2 cm (482/95) ■ 22.9 cm (482/95) ⊗ Micro(482/103)
 ▽ Pilot(482/103) ▲ Pilot(500/250) ● Demo(500/250)

Figure 8.2: Yield of Light Olefins from microreactors and from MRDC fluid-bed scale-up, plotted against Peclet Number. Curve A represents data from microreactors (horizontal duct lengths of 7.62 cm, 15.24 cm and 22.86 cm) where each point is a grand average from several experiments. All of the data was obtained at 482 C and 712 mm Hg. Curve B represents data from Bench Scale (at Peclet Number of 14) and 4 BPD Pilot Plant (at Peclet Numbers of 10) operated by MRDC, at 482 C and 772 mm Hg. Curve C represents data from 100 BPD Demonstration Plant (at Peclet Number of 7) and 4 BPD Pilot Plant (at Peclet Number of 10) operated by MRDC at 500 C and 1 876 mm Hg.

This figure shows clearly that the microreactor was able to determine the sensitivity of MTO reaction to axial gas dispersion. Yield of Light Olefins obtained in the microreactors was found to increase with an increase in Peclet Number. The trend of the microreactor data versus Peclet Number is the same as that of the earlier fluid-bed data. This is a major result. We have successfully designed and operated a microreactor capable of determining the sensitivity of a gas-solid catalytic reaction to axial gas dispersion.

The figure also shows that the yield of Light Olefins from the microreactor was higher by an average of 11 points to that obtained in a fluid bed at all Peclet Numbers.

Our somewhat higher yields may reflect: (1) our lower pressure; (2) uncertainties in Pe_{ax} , greatest for the two smaller fluid beds used by MRDC; (3) our microreactor's better gas-solid contacting at the micro-scale; (4) absence of front-to-back solid mixing in the microreactor, a phenomenon known to affect the kinetics of some reactions when conducted in a fluid bed (Squires et al., 1985); or (5) the fact that MRDC's fluid beds operated for hundreds of hours, with repeated catalyst regenerations that may have altered catalyst selectivities to olefinic products.

8.2.2 SUITABILITY OF TURBULENT FLUID BED FOR MTO REACTION

The demonstrated sensitivity of olefin yield to axial gas mixing raises doubts as to whether a conventional turbulent fluid bed, even if fitted with baffles to raise its Peclet Number, is a preferred reactor type for the MTO reaction.

A better choice may be the fast (circulating) fluid bed (Squires et al. 1985; Schoenfelder et al. 1994).

8.2.3 COMPOSITION OF MTO HYDROCARBON PRODUCT

This section examines how production of each hydrocarbon species varies with Peclet Number and gas-solid contacting environment by comparing the yields obtained from runs done in microreactors and fluid beds.

Table 8.1 indicates composition of the hydrocarbon product obtained from conducting MTO reaction in the microreactor. Olefinic species such as ethylene, 1-propene, 1-butene, 1-pentene and 1-hexene were identified and quantified. The sum of olefinic species increased with an increase in Peclet Number, indicating that low gas dispersion increases production of the sum of olefinic species. Both 1-propene and 1-butene are the largest component species whilst 1-hexene is the smallest species in the group.

Table 8.1: Composition of MTO hydrocarbon product from microreactors.

Duct Length	22.9 cm	15.2 cm	7.6 cm
OLEFINS			
Ethylene	12.5	13.9	10.2
1-Propene	19.1	18.8	17.8
1-Butene	28.9	17.5	17.3
1-Pentene	14.8	14.7	8.2
1-Hexene	7.2	5.2	3.4
Total	82.5	70.2	56.9
PARAFFINS			
Methane	1.3	1.4	1.2
Ethane	0.7	0.4	0.4
Propane	7.4	3.5	4.8
n-Butane	4.5	3.4	3.3
n-Pentane	1.8	3.4	1.5
n-Hexane	1.4	1.2	0.9
Total	17.1	13.3	12.2
Others (*)	0.4	16.5	30.8
Peclet Number	19.8	9.2	2.4

Others (*) represents Cycloparaffins and Paraffins

Paraffinic species such as methane, ethane, propane, butane, pentane and hexane were also identified and quantified. The slight increase observed in the sum of paraffinic species with an increase in Peclet Number is well within experimental error. Both propane and n-butane are the significant components in this group, whilst ethane is in the least amount.

Due to the inadequacy of our product analytical equipment, it was not possible to determine the composition of higher molecular weight hydrocarbon species such as cycloparaffins and aromatics. These are lumped into a category referred to as 'others'. This group decreased with an increase in Peclet Number.

Table 8.2 compares the hydrocarbon product obtained from the microreactors (VBMR-9, VBMR-6 and VBMR-3) with results from MRDC MicroFluid Bed and 4 BPD Pilot Plant. Data reported by MRDC did not specify the composition of paraffins observed. The table shows the composition of light olefins, the sum of paraffins and the group 'others'.

The table indicates that:

- (i) microreactors produced more Ethylene than the fluid beds.
- (ii) fluid beds produced more Propylenes than the microreactors.
- (iii) Butenes appear to drop with Peclet Number regardless of the geometry of the reaction environment (i.e. microreactor, fluid bed).

Table 8.2: Comparison of the MTO hydrocarbon product obtained from the microreactors (22.9 cm, 15.2 cm and 7.6 cm) with results from MRDC MicroFluid Bed and 4 BPD Pilot Plant.

	22.9 cm	MICRO	PILOT	15.2 cm	7.6 cm
OLEFINS					
Ethylene	12.5	5.8	5.2	13.9	10.2
Propene	19.1	33.7	32.9	18.8	17.8
Butenes	28.9	18.4	19.1	17.5	17.3
Pentenes	14.8	14.8	12.0	14.7	8.2
Hexenes	7.2	5.5	7.7	5.2	3.4
Total	82.5	78.2	76.9	70.2	56.9
PARAFFINS	17.1	15.3	16.6	13.3	12.2
Other (*)	0.4	6.5	6.5	16.5	30.8
Peclet Number	19.8	14	10	9.2	2.4

Other (*) represents Cycloparaffins and Aromatics

(iv) Pentenes appear to be constant between Peclet Number of 19.8 down to 9.2 and then drops significantly at Peclet Number of 2.4.

(v) very little amounts of Hexenes are produced overall and these appear to drop with Peclet Number.

It is interesting to note that the amount of Paraffins does not seem to vary with Peclet Number and is about the same in the microreactors and fluid beds.

8.2.4 SIGNIFICANCE OF THE RESULTS

A vibrated bed microreactor capable of (i) varying the level of axial gas dispersion (characterized by axial Peclet Number) at a fixed weight hourly space velocity (WHSV) and (ii) operating at high temperatures has been designed and tested. Researchers may use the microreactor with confidence in its ability to simulate one of the important features in a commercial-scale turbulent fluid bed, gas dispersion, and determine the sensitivity of a gas-solid catalytic reaction to this parameter, quickly and inexpensively. With the microreactor, a research engineer working at a laboratory bench can determine the sensitivity of a gas-solid catalytic reaction to fluid-bed gas dispersion.

The microreactor offers the following advantages which we believe will make it a useful tool in fluid bed design and scale-up as well as in catalyst screening studies: it

- (i) requires small amounts of catalyst, 1 mm layer,
- (ii) offers superb gas-solid contacting, with no gas bypassing,
- (iii) is able to operate with a wide range of superficial gas velocity and hence can be used to study weight hourly space velocity on the reaction,
- (iv) can be heated to a high temperature and therefore can be used to study the effect of temperature on the reaction, and
- (v) can be used to determine the sensitivity of a reaction to axial gas dispersion by simply varying the horizontal duct length while keeping weight hourly space velocity constant.

In the near future, our microreactor could help R&D managers to avoid expense of a fluid-bed R&D effort where an economically significant outcome of a reaction is acutely sensitive to axial gas dispersion, and where a fixed bed is an acceptable alternative. Our hope is that, over time, a body of microreactor data can grow to sufficient size, and represent sufficient variety of reaction type, such that, often, managers may use data for a new reaction to justify a decision to build plant around a fluid-bed reactor as soon as laboratory fluid-bed data become available.

9. RECOMMENDATIONS FOR FURTHER STUDY

The yield of Light Olefins obtained from microreactors was higher than the yield observed in fluid beds, suggesting that the Methanol-To-Olefin reaction is sensitive to other parameters which characterize the fluid bed reaction environment, which might include top-to-bottom solid mixing and/or circulation. The microreactor used in the present study had a duct with a flat floor. This arrangement affords little axial solid mixing.

An investigation was conducted on the possibility of initiating bulk solid movement in the microreactor. It was found that fitting the horizontal floor of the microreactor with a serrated bottom can create a front-to-back horizontal circulation of the catalyst powder. The bottom was divided in half longitudinally, with two sets of serrations causing solid to move in opposite directions in the two halves. The observed powder circulation in the microreactor occurs while maintaining the floor horizontal.

The ability to initiate front-to-back circulation of catalyst powder opens up another significant use for the microreactor. The front-to-back horizontal circulation of the catalyst powder observed in the microreactor can be used to simulate top-to-bottom mixing of the solid in a turbulent fluid bed reactor. The microreactor can be designed with a serrated bottom and be

used to determine the sensitivity of a gas-solid catalytic reaction to top-to-bottom solid mixing.

For any further work on the microreactor, the following recommendations are provided:

(i) Place the vibrator setup in the middle of the room with a hood over it, for withdrawing toxic fumes. This would make it easy to access all sides of the setup when problems arise that require immediate attention during an experimental run. It would also make it much easier to work with the setup.

(ii) Although it is recommended to put entire vibration equipment (housing and vibrator) on a sponge in order to dampen and absorb the vibrations, there is no guarantee that the equipment will be level at all times. It has been found that the sponge sags unevenly with time, resulting in the vibration setup losing level. It becomes very difficult to vibrate in the Coherent-Expanded (C-E) vibration state when the vibration setup is not level. A cork mat might be better in enduring the steady oscillations during experimental runs, and not sagging unevenly (Thomas, personal communication).

(iii) Obtaining perfect vertical vibration to stay in C-E state, is difficult with the rectangular vibration table. Proper alignment on the vibration table is very delicate in the sense that the load distribution and the leaf springs'

stiffness have to be symmetrical both lengthwise and widthwise. A simple overtightening of the screws on the table can move the drive shaft offcenter by a millimeter or so, and immediately causes solid bunkering making it impossible to return to C-E state. It may be better to use a circular vibration table as was done in other work at Virginia Tech, apparently with fewer alignment problems.

(iv) The capability of the HP 5730A Gas Chromatograph used in the present work was rather limited in detecting the full spectrum of products from the MTO reaction. It will have to be replaced with a modern one.

(v) The Gas Chromatograph and the sampling device should be brought as close to the microreactor as possible. An ideal situation would be to take the sample directly at the outlet of the microreactor.

(vi) It is imperative to do data acquisition through the computer because the data handling for the MTO reaction is overwhelming. Eleven important signal peaks (five Light Olefins and six Paraffins) were sorted out by their retention times, and quantified. Entering all of the data into a spreadsheet manually was a large task. It is recommended that for further studies on this reaction, data acquisition be done with a computer: (a) to cut down on the time of entering the data by hand into a spreadsheet, (b) to reduce the probability of human error in entering the data by hand into a spreadsheet,

and (c) to facilitate signal peak manipulation in the case when the integrator has erred (such as integrating area due to baseline drift).

BIBLIOGRAPHY

Argauer, R.J., and G.R. Landolt, "Crystalline Zeolite ZSM-5 and method of preparing the same", US Patent 3 702 886, 1972.

Avidan, A.A., "Turbulent Fluid Bed Reactors Using Fine Powder Catalysts," in Proc. J. Meet. Chem. Eng. Chem. Ind. Eng. Soc. China Am. Inst. Chem. Eng., (Beijing, China, Sept. 19-22, 1982), Chemical Industry Press, Beijing, China (1982), Vol. 1, pp. 411-423.

Avidan, A.A. and J. Yerushalmi, "Bed Expansion in High Velocity Fluidization", Powder Technology, 32 (1982), 223 - 232.

Avidan, A.A., "II. Fluid Bed Process Commercializations", 1990, personal notes.

Avidan, A.A., "Gasoline and Distillate from Methanol", Methane conversion Symposium, University of Auckland, New Zealand, Apr 27-May 1, 1987.

Avidan A.A., and R.Shinnar, "Development of Catalytic Cracking Technology. A Lesson in Chemical Reactor Design", Ind. Eng. Chem. Res., 1990, 29, pp 931 - 942.

Bem, J.Z., "From concept to concrete", Chemtech, 42, 1988.

Benge, G.G., "Cold model of vibrated bed microreactor capable of varying Peclet Number at Fixed Weight Hourly Space Velocity, Providing a Tool for Simulating an Important Feature of the Reaction Kinetic Scene in Large Catalytic Fluid Beds", Ph.D. thesis, Virginia Polytechnic Institute & State University, Blacksburg, 1992.

Bloch, M.G., R.B. Callen, and J.H. Stockinger, Journal of Chromatographic Science, 15, 504, 1977.

Chang, C.D., and W.H. Lang, "Process for manufacturing olefins", US Patent 4 025 575, May 24, 1977.

Chang, C.D., and W.H. Lang, "Process for manufacturing olefins", US Patent 4 025 576, May 24, 1977.

Chang, C.D., W.H. Lang, and A.J. Silvestri, "Conversion of Methanol to Olefinic Components", US Patent 4 052 479, Oct 4, 1977.

Chang, C.D., W.H. Lang, and A.J. Silvestri, "Manufacture of light olefins", US Patent 4 062 905, Dec 13, 1977.

Chang, C.D., C.T-W. Chu, and R.F. Socha, "Methanol Conversion to Olefins over ZSM-5: I. Effect of Temperature and Zeolite $\text{SiO}_2/\text{Al}_2\text{O}_3$ ", Journal of Catalysis, 86, 289, 1984.

Chang, C.D., and A.J. Silvestri, Journal of Catalysis, 47, 249, 1977.

Chang, C.D., Catal. Rev.-Sci. Eng., 25(1), 1 - 118, 1983.

Chang, C.D. and C.T-W., Chu, J of Catalysis 79, 244, 1983.

Chang, C.D., and A.J. Silvestri, CHEMTECH, 624, October 1987.

Chen, N.Y., J.N. Miale, and W.J.Reagan, "Method of producing a steam stable Aluminosilicate Zeolite catalyst", US Patent 4 231 899, 1980.

Chen, N.Y., and W. J. Reagan, Journal of Catalysis, 59, 123, 1979.

Dave, S.B., "A Comparison of the Chromatographic Properties of Porous Polymers," Journal of Chromatographic Science, vol 7, 1969, pp. 389-399.

Davis, M.E., "Zeolites and Molecular Sieves: Not Just Ordinary Catalysts," Ind. Eng. Chem. Res., 30 (1991), 1675 - 1683.

Dessau, R.M. and R.B. LaPierre, J of Catalysis 78, 136, 1982.

Edwards, M., and A.A. Avidan, "Conversion Model Aids Scale-Up of Mobil's Fluid-Bed MTG Process", *Chemical Engineering Science*, 41(4), 829-835, 1986.

Fogler, H.S., *Elements of Chemical Reaction Engineering*, Prentice Hall, Englewood Cliffs, New Jersey, 1986.

Geldart, D., "Types of Gas Fluidization", *Powder Technology*, 7, 1973.

Gierlich, H.H., K.H. Keim, N. Thiagarajan, E. Nitschke, A.Y. Kam, and N. Daviduk, "Successful Scale-up of the Fluid-Bed Methanol to Gasoline (MTG) process to 100 BPD Demonstration plant", Second EPRI Conference, San Francisco, USA, April 15-19, 1985.

Gould, R.M., A.A. Avidan, J.L. Soto, C.D. Chang, and R.F. Socha, 1986 AIChE Meeting, New Orleans, Los Angeles, April 6-10, 1986.

Gould, R.M., A.A. Avidan, J.L. Soto, C.D. Chang, R.F. Socha, "Scale-Up of a fluid-bed process for production of light olefins from methanol," presentation at AIChE meeting, New Orleans LA, April 6-10, 1986.

Hollis, O.L., "Porous Polymers Used in GC and LC," *Journal of Chromatographic Science*, vol 11, 1973, pp. 335-342.

Kaeding W.W. and S.A., Butter, "Production of Chemicals from Methanol. I. Low Molecular Weight Olefins", *J of Catalysis* 61, 155, 1980.

Kaufman, W.E., P. Chutoransky, and B.W. Finnerty, *Journal of Chromatographic Science*, 15, 1977.

Keim, K.H., J. Maziuk, and A. Tonnesmann, "The Methanol to Gasoline Process", *Erdol und Kohle-Erdgas-Petrochemie vereinigt mit Brennstoff Chemie*, 37(12), 559, 1984.

Keim, K.H., F.J. Krambeck, J. Maziuk, and A. Tonnesmann, "Olefin Production from Methanol", Erdol und Kohle-Erdgas-Petrochemie vereinigt mit Brennstoff Chemie, 103, 82, 1987.

Kokotailo, G.T., P. Chu, S.L. Lawton, and W.M. Meier, Nature, 275, 119, 1978.

Kokotailo G.T., S.L. Lawton, D.H. Olson and W.M. Meier, Nature, 272, 437, 1978.

Kunii, D. and O. Levenspiel, Fluidization Engineering, 2nd edition, Butterworth-Heinemann, 1991.

Levenspiel, O., Chemical Reaction Engineering, Wiley, New York, 2nd edition, 1972.

Liederman, D., S.M. Jacob, S.E. Voltz, and J.J. Wise, "Process Variable Effects in the Conversion of Methanol to Gasoline in a Fluid Bed Reactor", Ind. Eng. Chem. Proc. Des. Dev., 17, 3, 340, 1978.

Maiden, C.L., "A Project overview", Chemtech, 38, 1988.

Mason, M.O., "Bed Dynamics and Heat Transfer in Shallow Vibrated Particulate Beds," Ph.D. dissertation, VPI & SU, Blacksburg, VA (1990).

Meisel, S.L., J.P. McCullough, C.H. Lechthaler, and P.B. Weisz, "Gasoline from Methanol in one step", CHEMTECH, 86, 1976.

Meisel, S.L., "Catalysis research bears fruit", Chemtech, 32, 1988.

Morgan, C.R., J.P. Warner, and S. Yurchak, "Gasoline from Alcohols", Ind. Eng. Chem. Prod. Res. Dev., 20, 185-190, 1981.

Mujumdar A.S., "Vibrated Fluid Beds as Chemical Reactors", Frontiers in Chemical Reaction Engineering Vol II, L.K. Doraiswamy and R.A. Mashelkar, eds., Wiley Eastern Limited, New Delhi (1984), pp 419 - 427.

Nauman, E.B., and B.A. Buffham, *Mixing in Continuous Flow Systems*, John Wiley & Sons, New York, 1983.

Olson, D.H., W.O. Haag, and R.M. Lago, *Journal of Catalysis*, 61, 390-396, 1980.

Penick, J.E., W. Lee, and J. Maziuk, "Development of the Methanol-to-Gasoline Process", *Chemical Reaction Engineering*, 19, 1983.

Pollock, G.E., D. O'Hara and O.L. Hollis, *Journal of Chromatographic Science*, vol. 22, 1984, pp. 343-347.

Socha, R.F., C.T-W. Chu, and A.A. Avidan, *State of the Art Symposium, "Methanol as a raw material for Fuels and Chemicals"*, Marco Island, Florida, June 15-18, 1986.

Socha, R.F., C.D. Chang, R.M. Gould, S.E. Kane, and A.A. Avidan, "Fluid Bed Studies of Olefin Production from Methanol", *ACS Symposium Series* 328, 34-41, 1987.

Soto, J.L., and A.A. Avidan, "Status of the 100 BPD Fluid Bed Methanol to Olefins Demonstration Plant", 1985 DOE/FE Indirect Liquefaction Contractor's Review Meeting, Houston, Texas, December 2-5, 1985.

Squires, A.M., "The Story of Fluid Catalytic Cracking: The First Circulating Fluid Bed", *Proceedings of First International Conference on Circulating Fluid Beds*, Halifax, Nova Scotia, November 1985, Prabir Basu, ed. Pergamon Press, pp. 1 - 19.

Squires, A.M., M. Kwauk, and A.A. Avidan, *Science*, 230(1985): 1329-1337.

Stockinger, J.H., *Journal of Chromatographic Science*, 15, 198, 1977.

Suzuki, M., and J.M. Smith, *Chem. Eng. J.*, 3(1972): 256-264.

Tabak, S.A., A.A. Avidan, and F.J. Krambeck, Symposium of Status of Synfuels Commercialization, ACS National Meeting, New York City, April 13-15, 1986.

Thomas, B. and A.M. Squires, "Vibrated-Bed Microreactors Simulating Catalytic Fluid Beds: A Feasibility Study", International Fluidization Conference, Banff, Canada, May 7 - 12, 1989.

Thomas, B., and A.M. Squires, "Vibrated-Bed Microreactors Simulating Catalytic Fluid Beds: A Feasibility Study" in Fluidization VI, J.R. Grace, L.W. Shemilt, and M. Bergougnou (Eds.), Engineering Foundation, New York, 1989, pp. 375-382.

Thomas, B., "Shallow Vibrated Particulate Beds - Bed Dynamics and Heat Transfer," Ph.D. Dissertation, VPI & SU, Blacksburg, VA (1988).

Thomas B., Y.A. Liu, R. Chan, and A.M. Squires, "A Method for Observing Phase-Dependent Phenomena in Cyclic Systems: Application to Study of Dynamics of Vibrated Beds of Granular Solids", Powder Technology, 52 (1987), pp 77 - 92.

Thomas B., M.O. Mason, Y.A. Liu, and A.M. Squires, "Mapping the States of Vibrated Beds", AIChE Annual Meeting, Symposium on Fundamentals of Fluidization and Fluid-Particle Systems, New York, New York, November 15 - 20, 1987.

Thomas B., Y.A. Liu, M.O. Mason, and A.M. Squires, "Vibrated Beds: New Tools for Heat Transfer", Chemical Engineering Progress, June 1988, pp 65 - 75.

Thomas B., M.O. Mason, Y.A. Liu, and A.M. Squires, "Identifying States in Shallow Vibrated Beds", Powder Technology, 57 (1989), 267 - 280.

Trimm D.L., Design of Industrial Catalysts, Elsevier, 1980.

van Hooff, J.H.C., *J. of Catalysis* 79, 242, 1983.

Venuto, P.B., and P.S. Landis, *Journal of Catalysis*, 21, 330, 1971.

Wen, C.Y., and L.T. Fan, *Models for Flow Systems and Chemical Reactors*, Marcel Dekker, New York, 1975.

Wu, M.M. and W.W. Kaeding, "Conversion of Methanol to Hydrocarbons. II. Reaction Paths for Olefin Formation over HZSM-5 Zeolite Catalyst", *J. of Catalysis* 88, 478, 1984.

Yerushalmi, J. and A. Avidan, "High-Velocity Fluidization," Chapter 7 in *Fluidization, Second Edition*, J.F. Davidson, R. Clift, and D. Harrison, eds., Academic Press, New York (1985) pp. 225-291.

Yerushalmi, J., "High Velocity Fluidized Beds," Chapter 7 in *Gas Fluidization Technology*, D. Geldart, ed., Wiley, New York (1986) pp. 155-198.

APPENDIX A : DETAILED DRAWINGS OF VIBRATION SUPPORT STRUCTURE

This appendix presents the detailed drawings of the vibration support structure used in this research.

The drawings of the support structure, presented in Figure A.1 - Figure A.10 was prepared by Benku Thomas.

The vibration table, presented in Figure A.11 - Figure A.18 was also prepared by Benku Thomas.

APPENDIX A : DETAILED DRAWINGS OF VIBRATION SUPPORT STRUCTURE

This appendix presents the detailed drawings of the vibration support structure used in this research.

The drawings of the support structure, presented in Figure A.1 - Figure A.10 was prepared by Benku Thomas.

The vibration table, presented in Figure A.11 - Figure A.18 was also prepared by Benku Thomas.

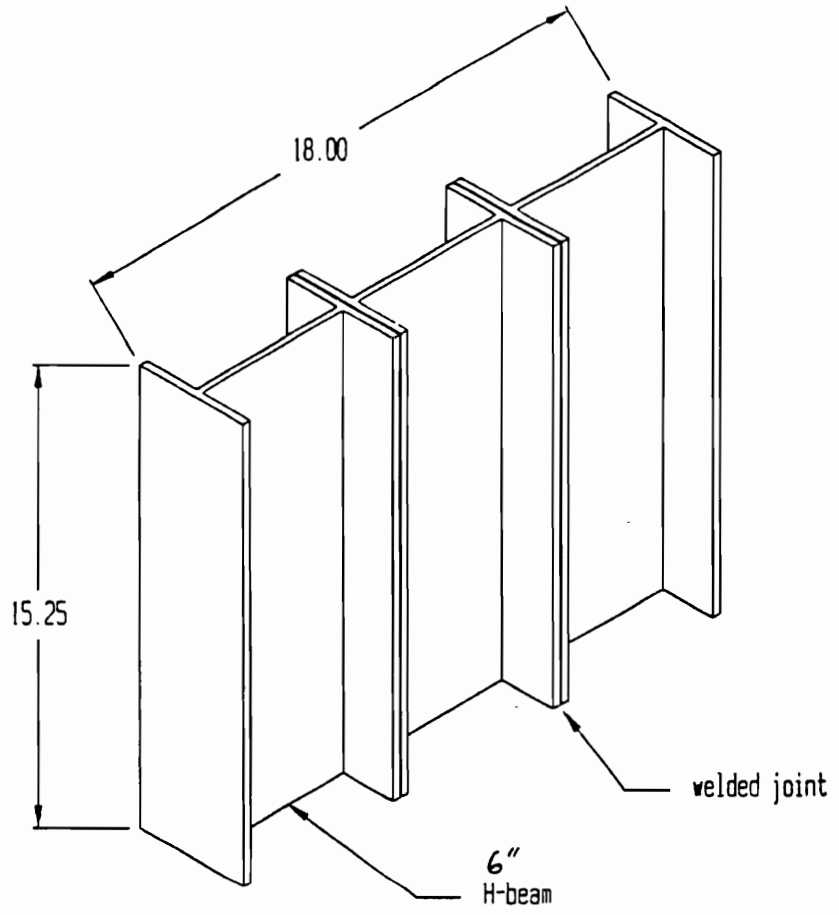
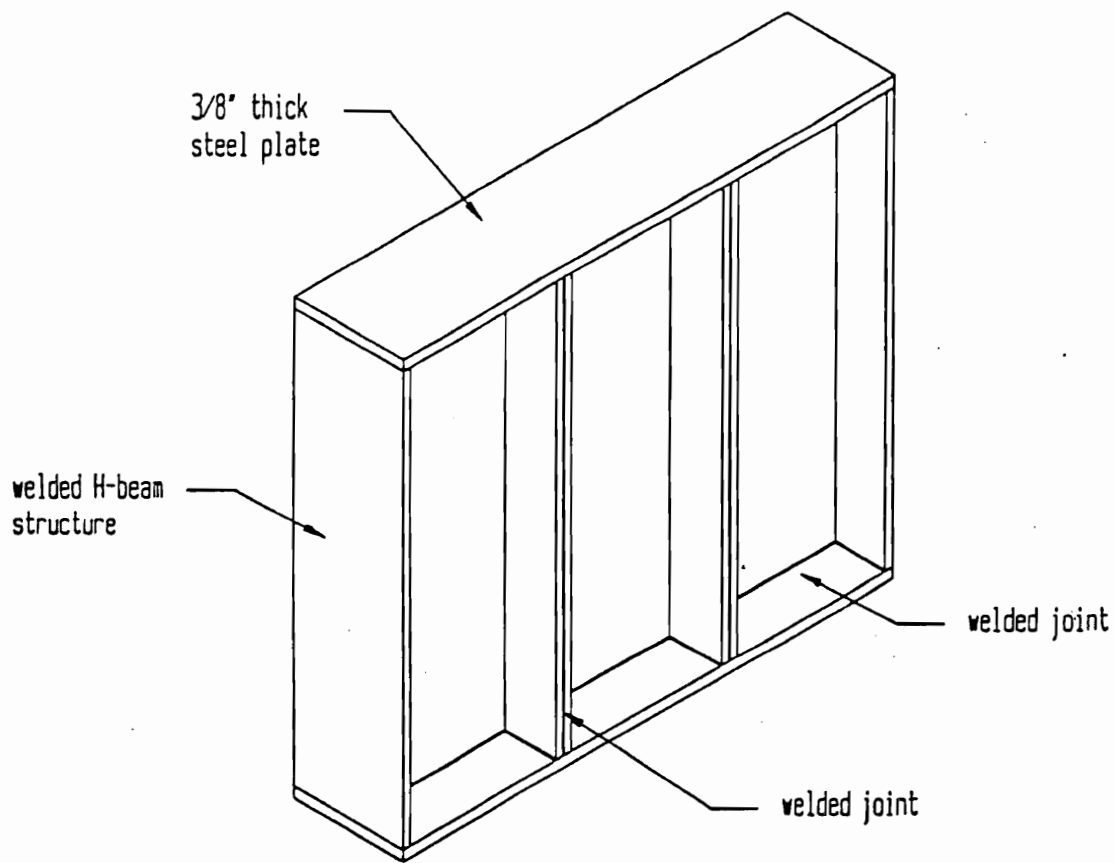


Figure A.2: Welded H-beam structure for side walls



NOTE: No bolt holes are shown in this figure

Figure A.3: Side walls for vibration support structure

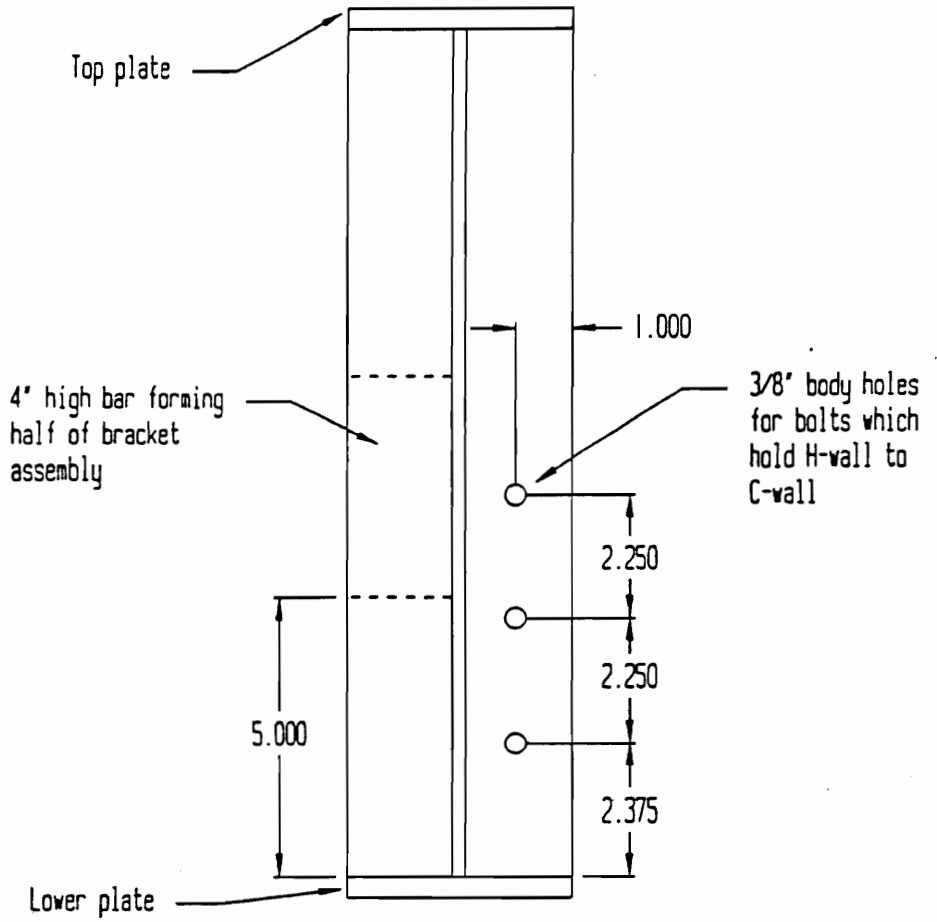
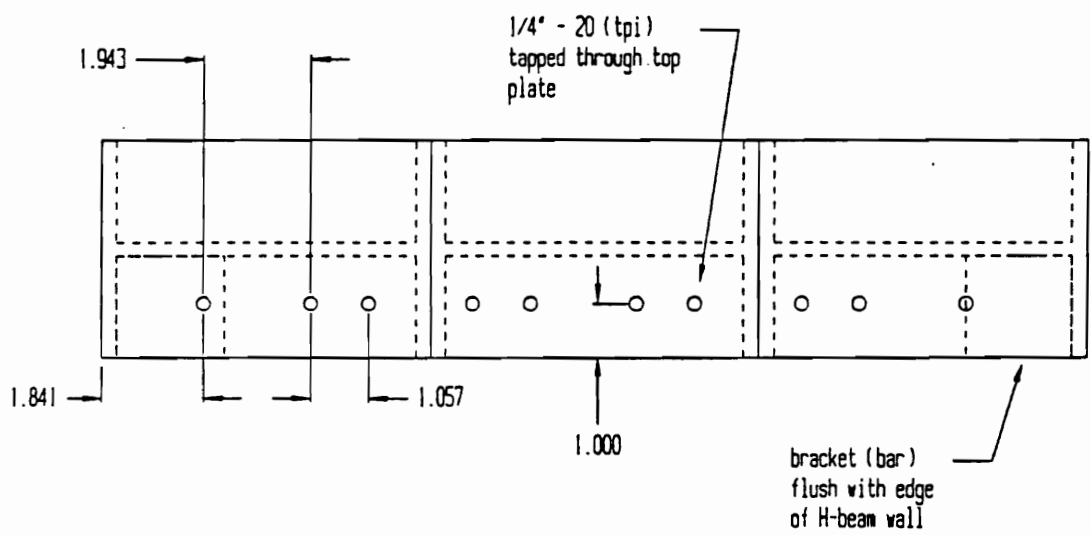
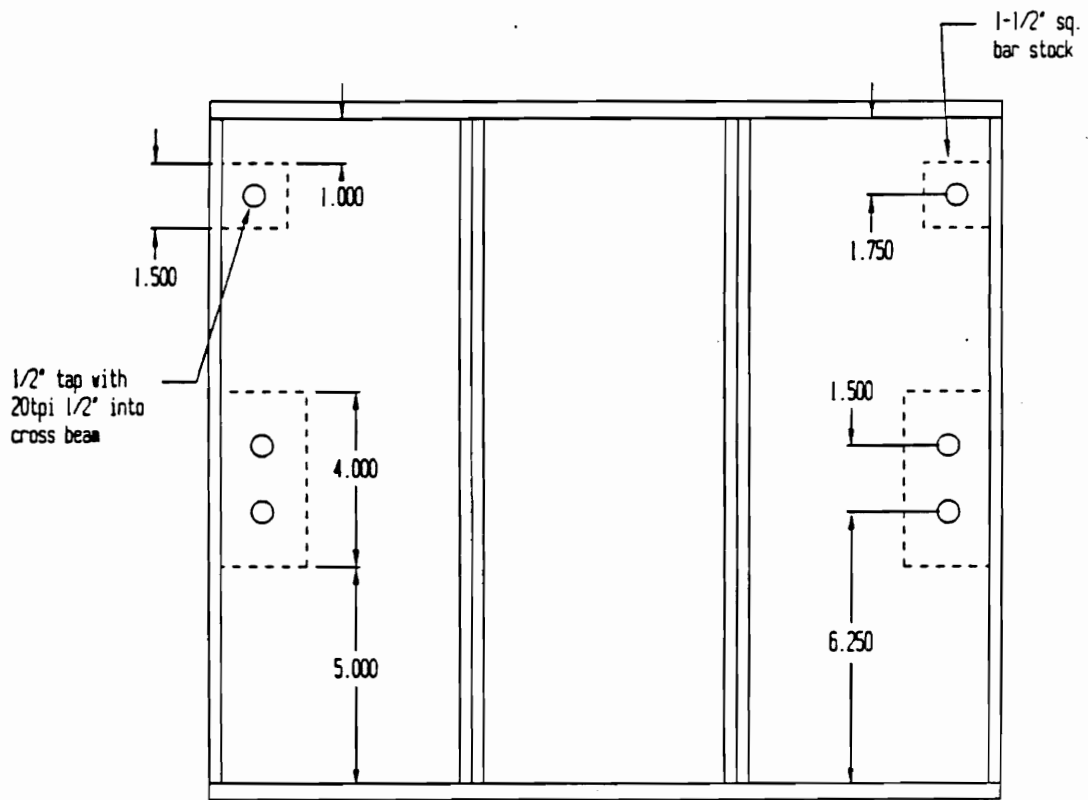


Figure A.4: Side view of H-beam side walls



Details of 1/4"-20 tapped holes on top are shown
 Holes on bottom are NOT shown
 H-beam structure is shown as dotted lines

Figure A.5: Top view of H-beam side walls



Shows locations of brackets and cross-beams

Figure A.6: Front view of H-beam side walls

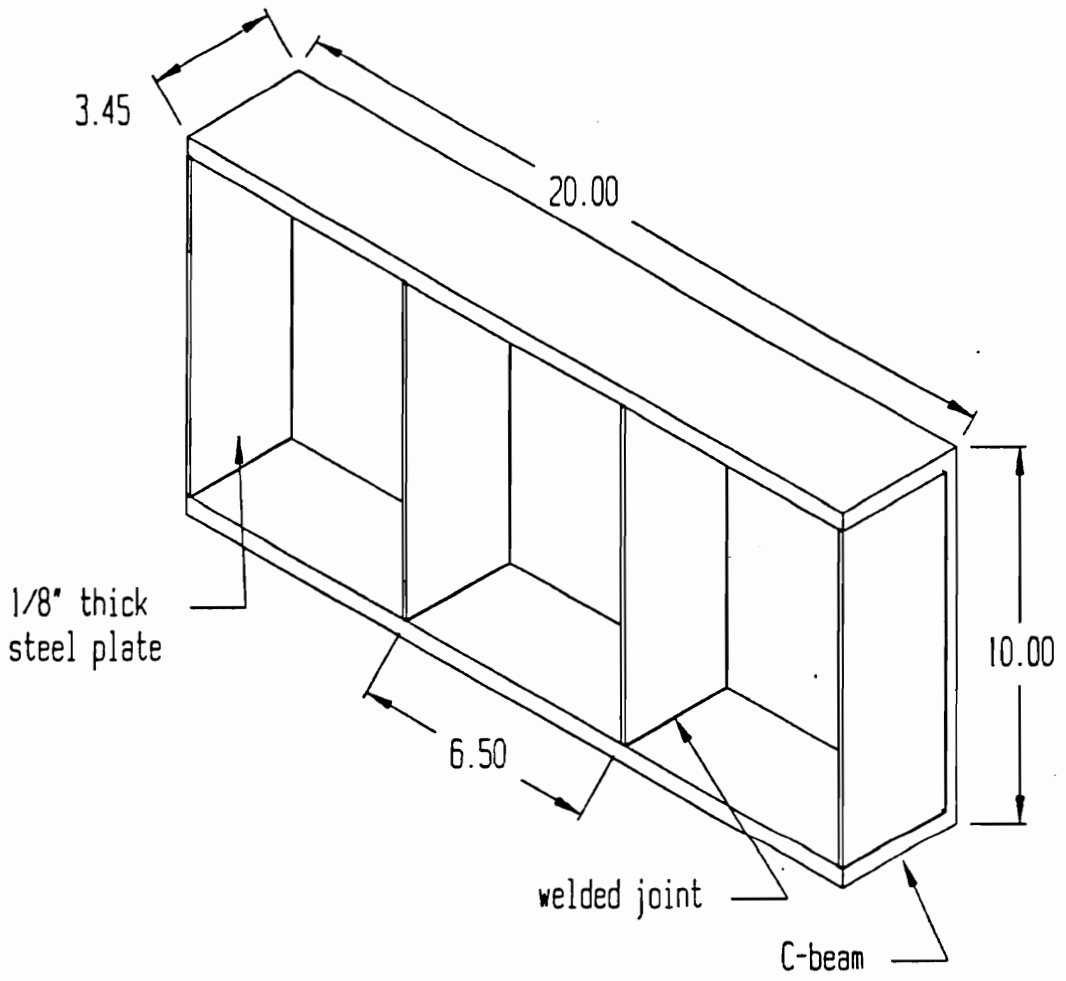


Figure A.7: Front and back walls made from C-beams

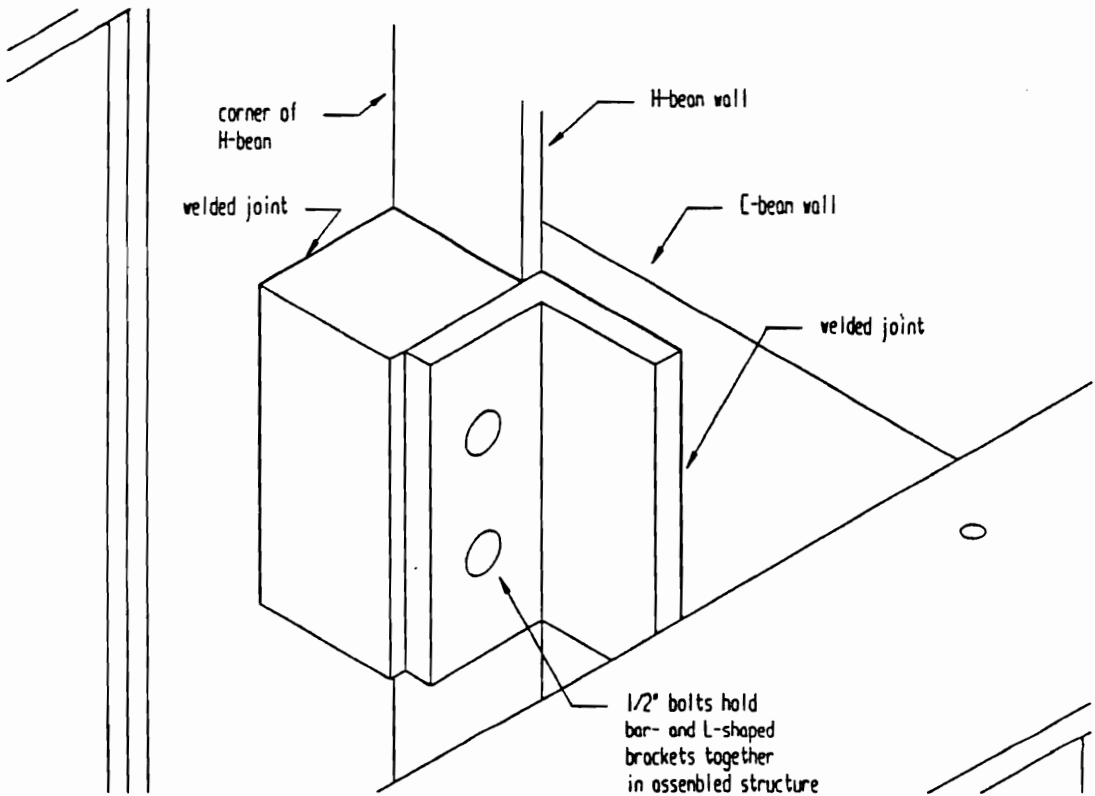


Figure A.8: Attachment of brackets to walls

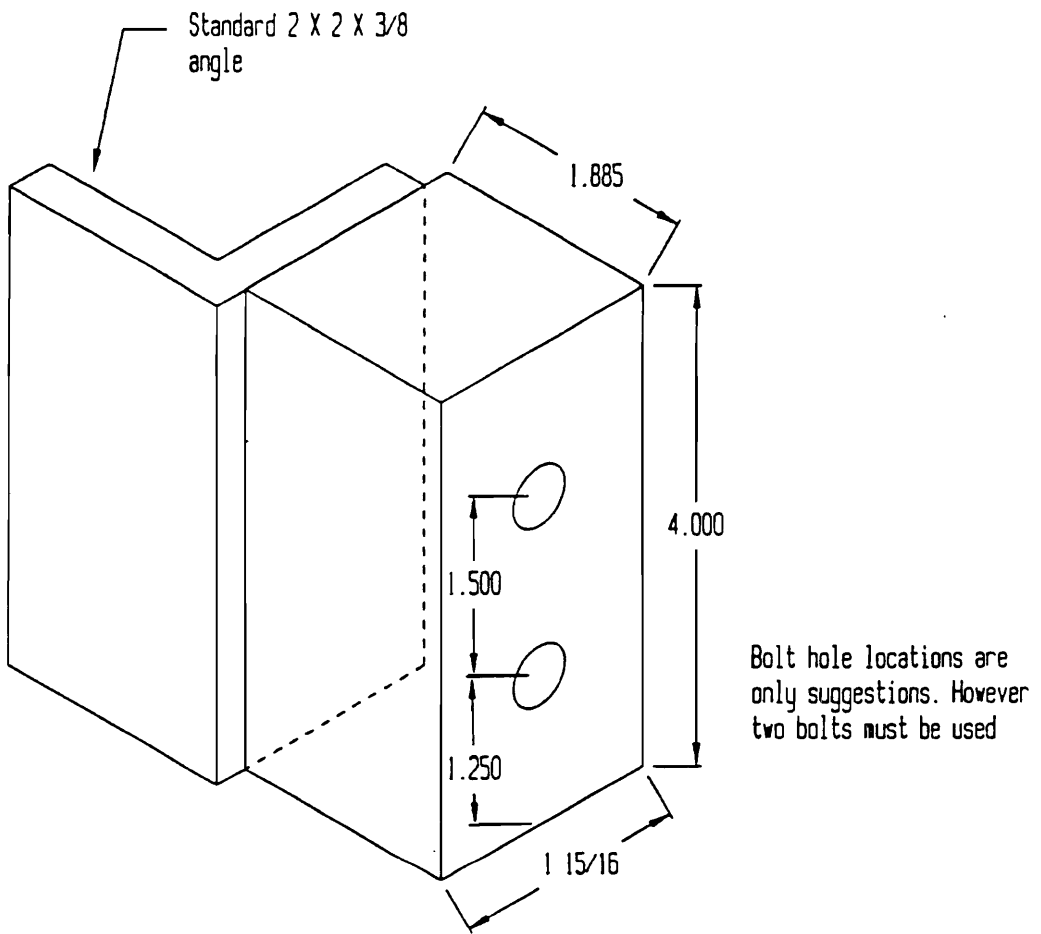
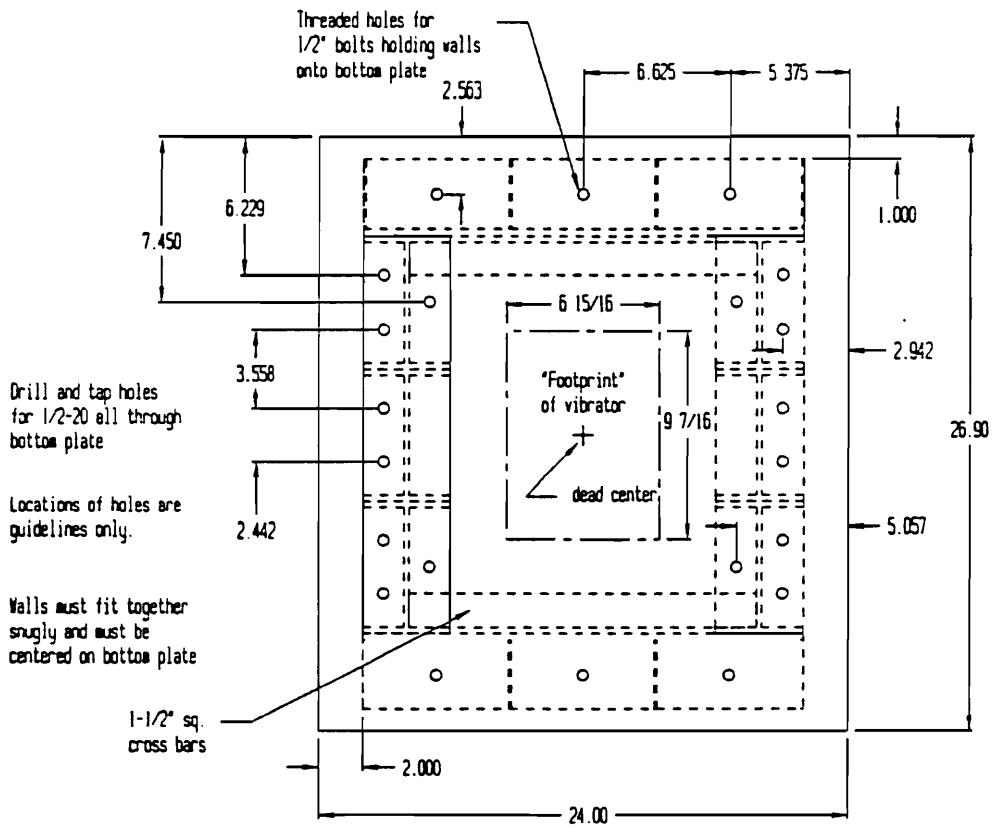


Figure A.9: Details of bracket assembly



Bottom plate is 0.75" thick.

Figure A.10: Bottom plate showing hole pattern

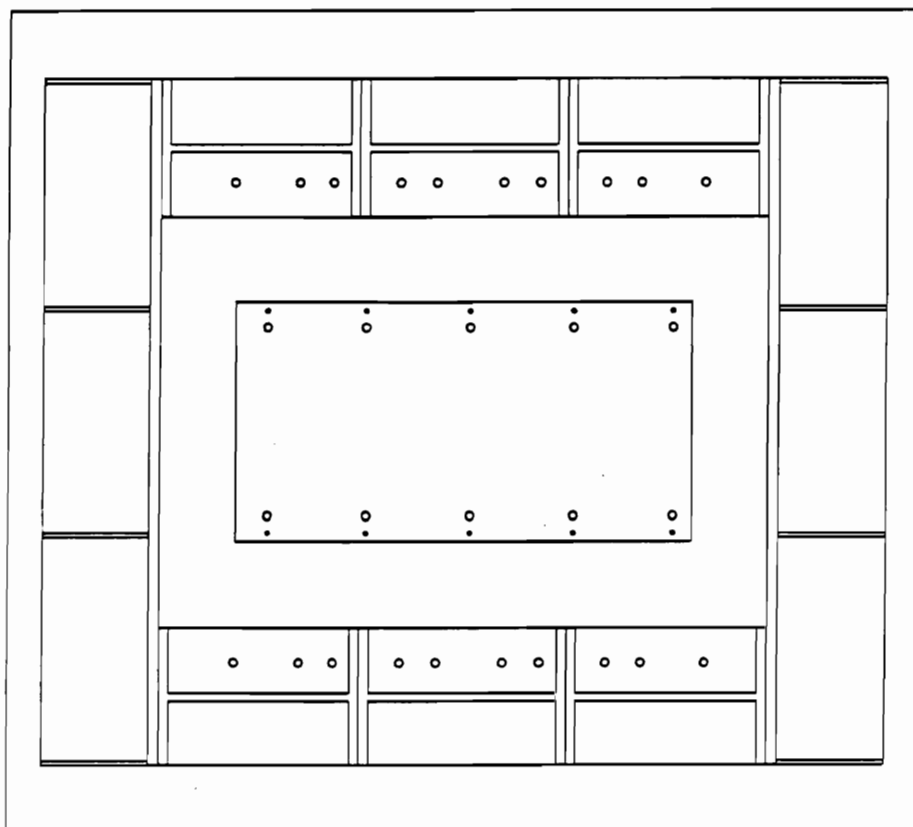


Figure A.11: Top view of assembled vibration support structure, with vibration table shown in center

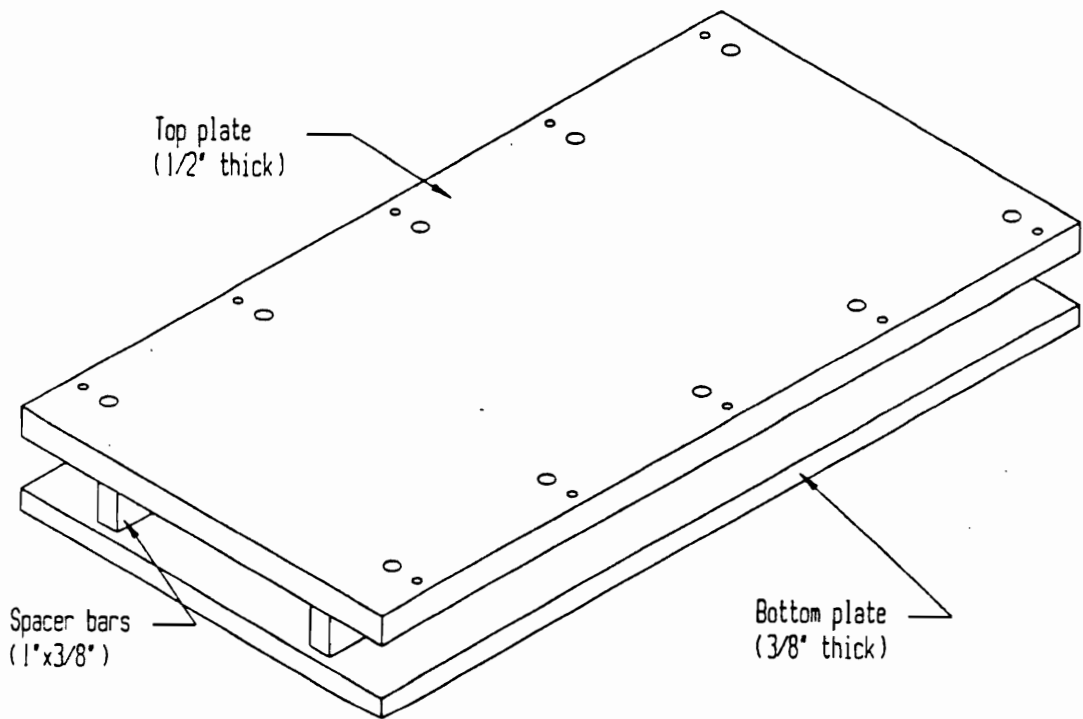


Figure A.12: Vibration table (end plates not shown)

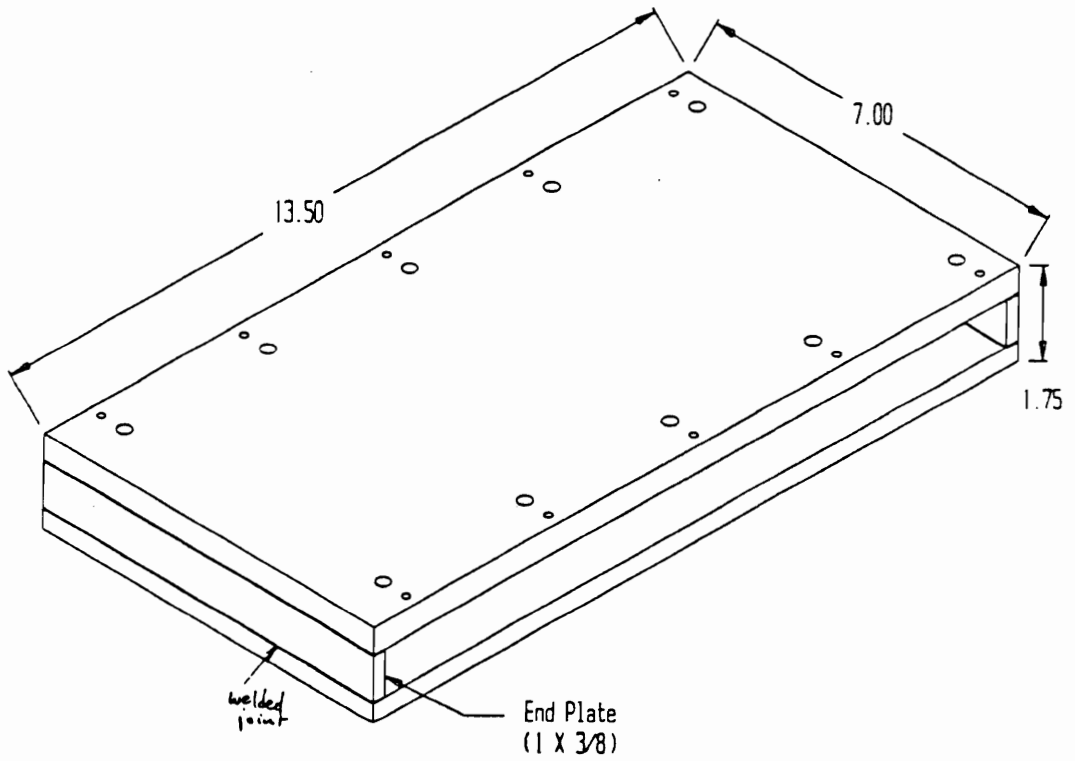


Figure A.13: Vibration table (shown with end plates)

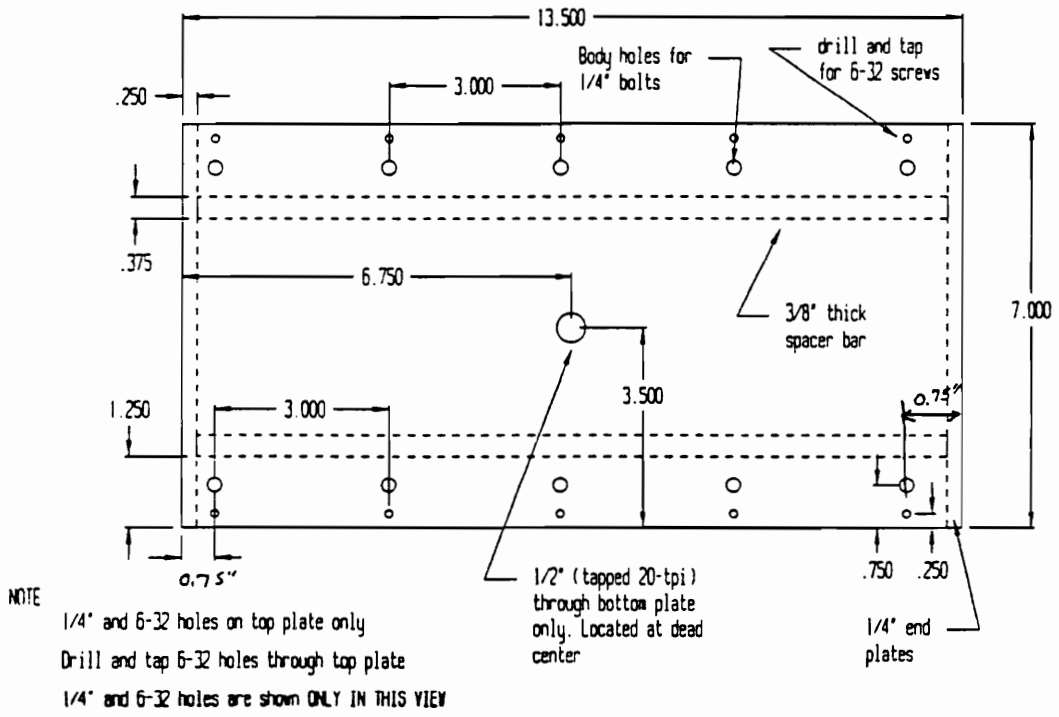


Figure A.14: Vibration table (top view)

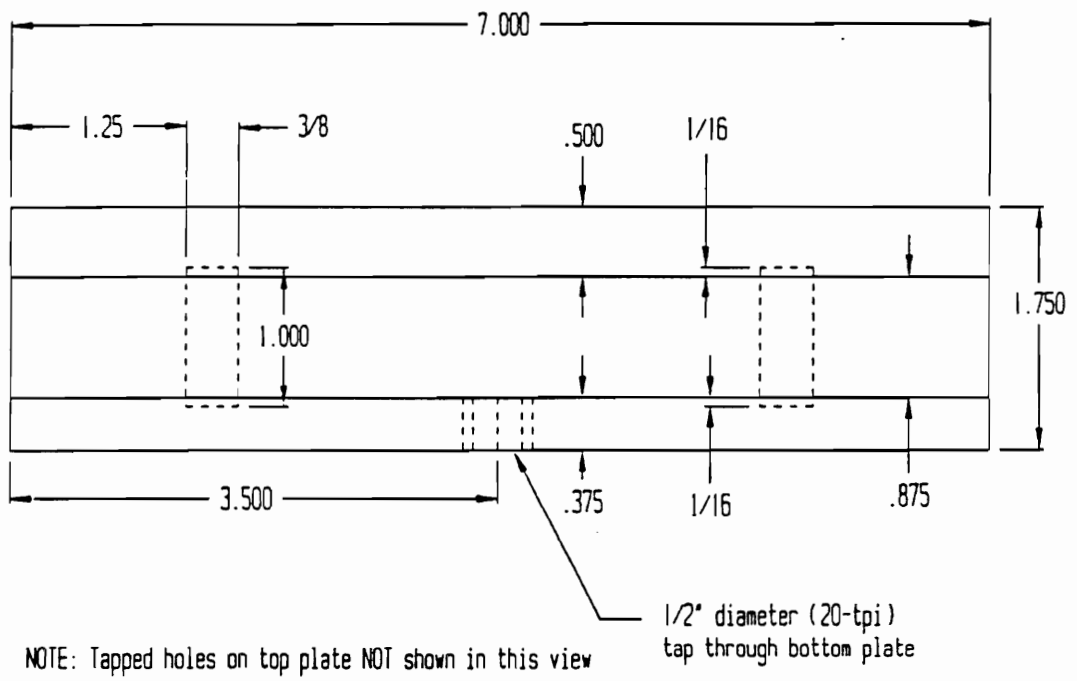
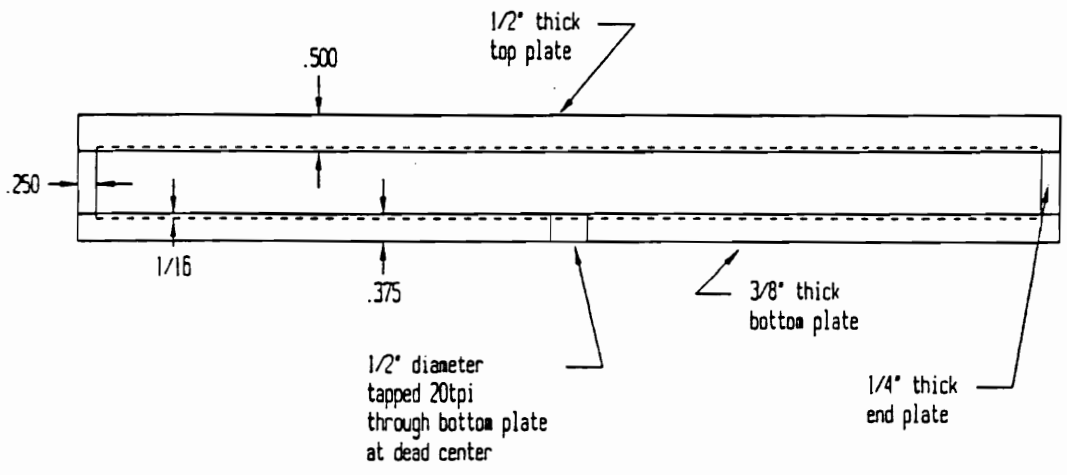


Figure A.15: Vibration table (front view)



NOTE Holes through top plate NOT shown in this view

Figure A.16: Vibration table (side view)

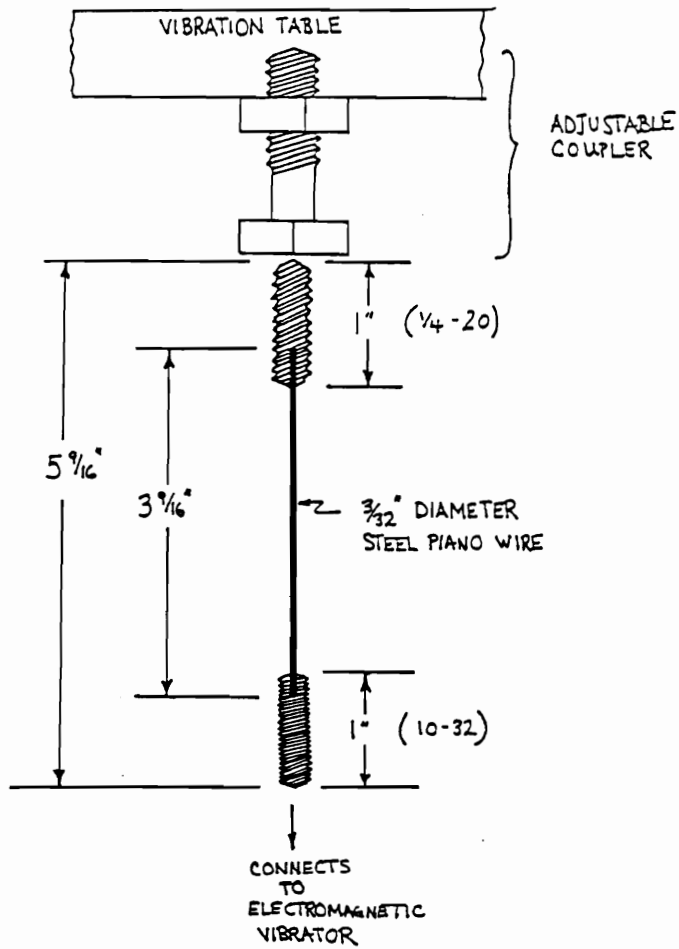


Figure A.17: Steel drive shaft

APPENDIX B : DESIGNS OF VIBRATED BED MICROREACTOR

Chapter 6 presented the design dimensions of the vibrated bed microreactor of horizontal duct length of 15.24 cm. This appendix contains design dimensions of the vibrated bed microreactor of horizontal duct lengths of 7.62 cm and 22.86 cm.

B.1: Horizontal Duct Length of 7.62 cm

Figure B.1 shows the basic design of the vibrated bed microreactor. The microreactor is made up of three main sections, namely the inlet section, middle section and outlet section. Each of these sections has two parts, namely the top and the bottom.

Figure B.2 shows all of the six individual pieces making up the microreactor. The two middle pieces make up the reaction zone at a horizontal duct length of 7.62 cm. The inlet section and outlet section are similar. Design dimensions of the middle section (both top and bottom parts) and the inlet section (both top and bottom parts) are presented in the following figures.

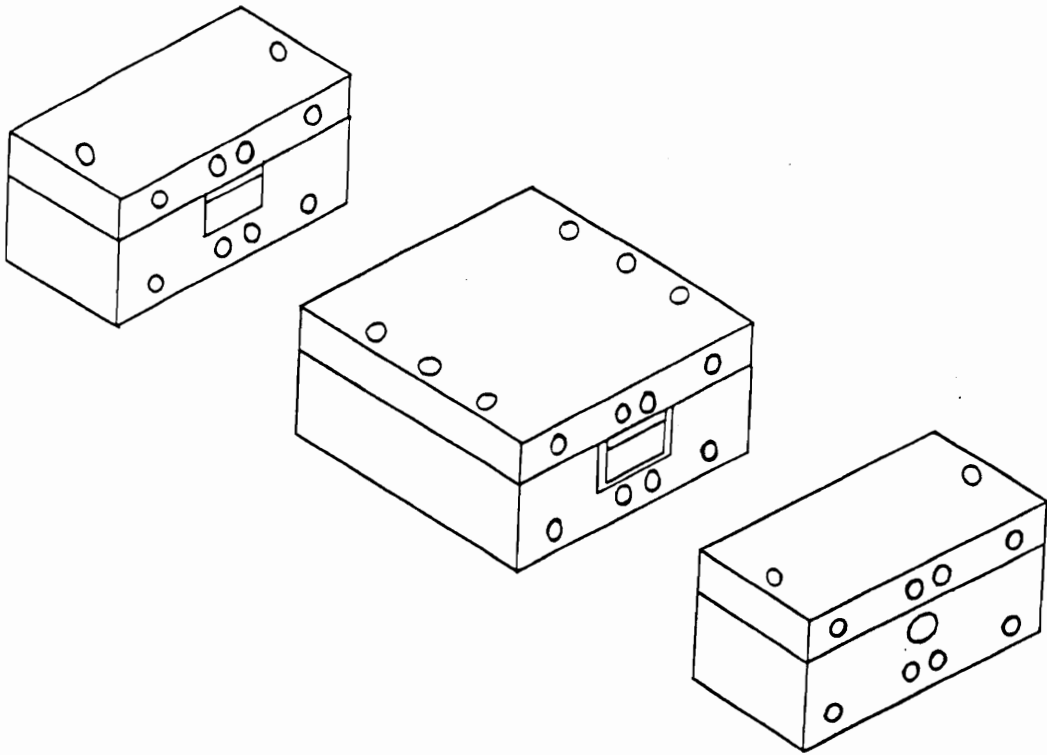


Figure B.1: Isometric drawing of the microreactor at 7.62-cm horizontal duct length. The figure shows three main sections of the microreactor, Inlet section, Middle section and Outlet section.

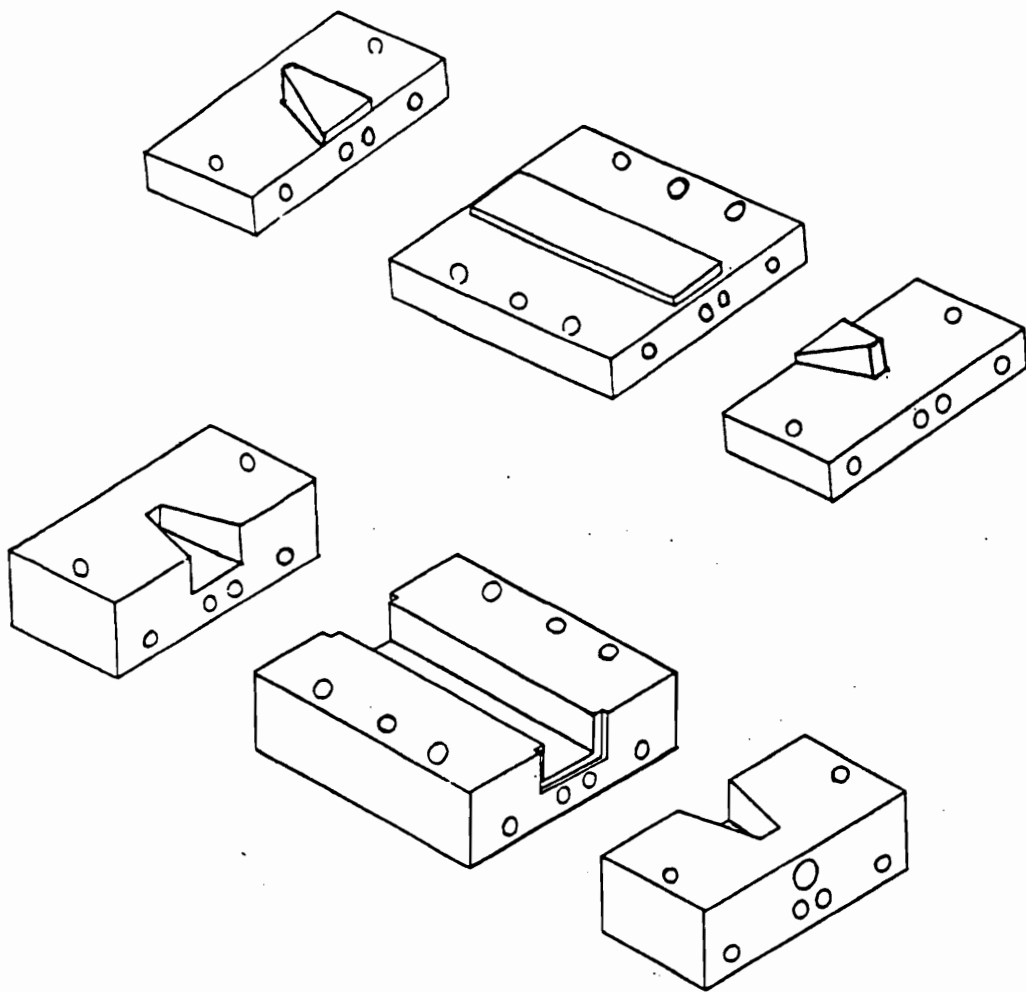


Figure B.2: Individual pieces making up the microreactor. Center pieces are for horizontal duct at a length of 7.62-cm. Inlet section and Outlet section are similar.

B.1.1 Middle Section

Several views of the top half of the middle section (viz. mid-top section) are shown in Figure B.3 namely (a) Isometric view, (b) Top view, (c) Side view and (d) Front view.

Several views of the bottom half of the middle section (viz. mid-bottom section) are shown in Figure B.4 namely (a) Isometric view, (b) Top view, (c) Side view and (d) Front view.

B.1.2 Inlet Section

Several views of the top half of the inlet section (viz. inlet-top section) are shown in Figure B.5 namely (a) Isometric view, (b) Top view, (c) Side view and (d) Front view.

Several views of the bottom half of the inlet section (viz. inlet-bottom section) are shown in Figure B.6 namely (a) Isometric view, (b) Top view, (c) Side view and (d) Front view.

Figure B.7 shows the complete assembled microreactor.

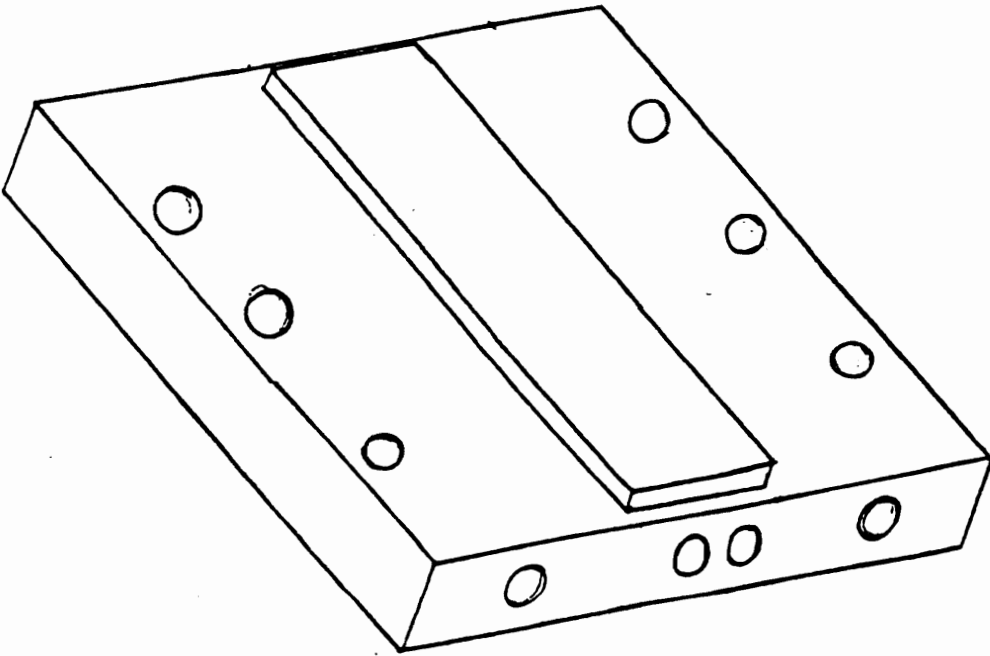


Figure B.3 (a): Isometric view of the top half of the middle section

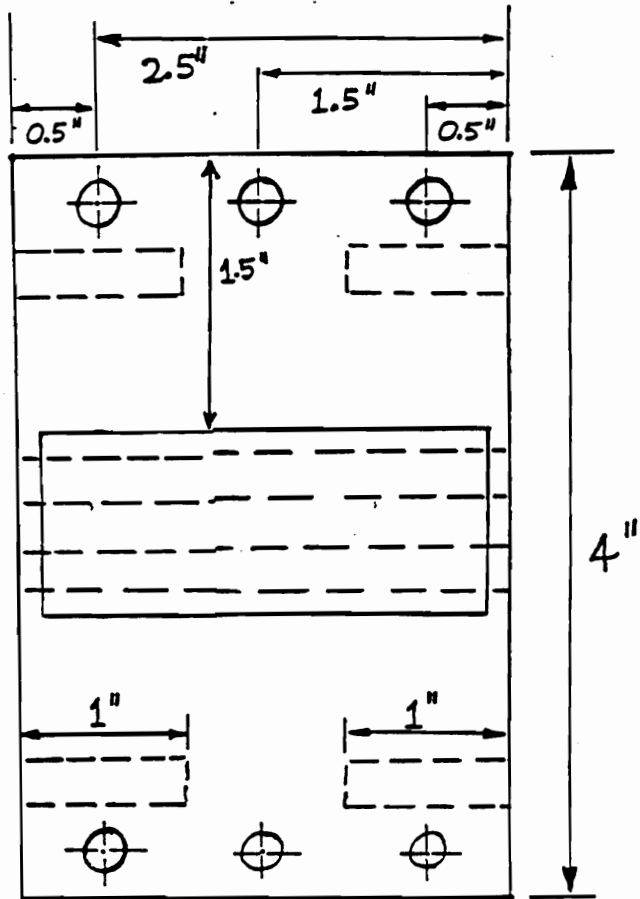
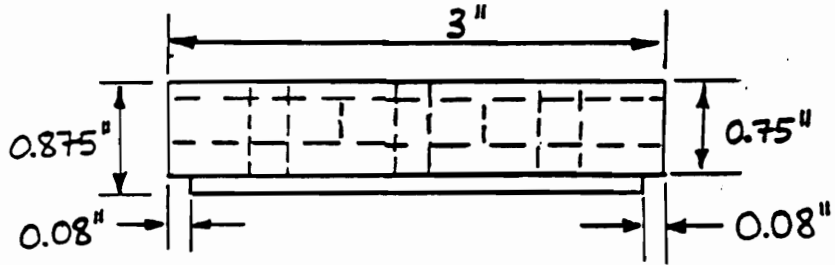
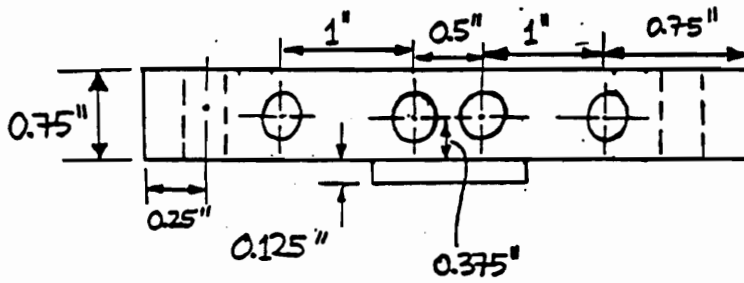


Figure B.3 (b): Top view of the top half of the middle section



(c)



(d)

Figure B.3: Side view (c), and Front view (d), of the top half of the middle section

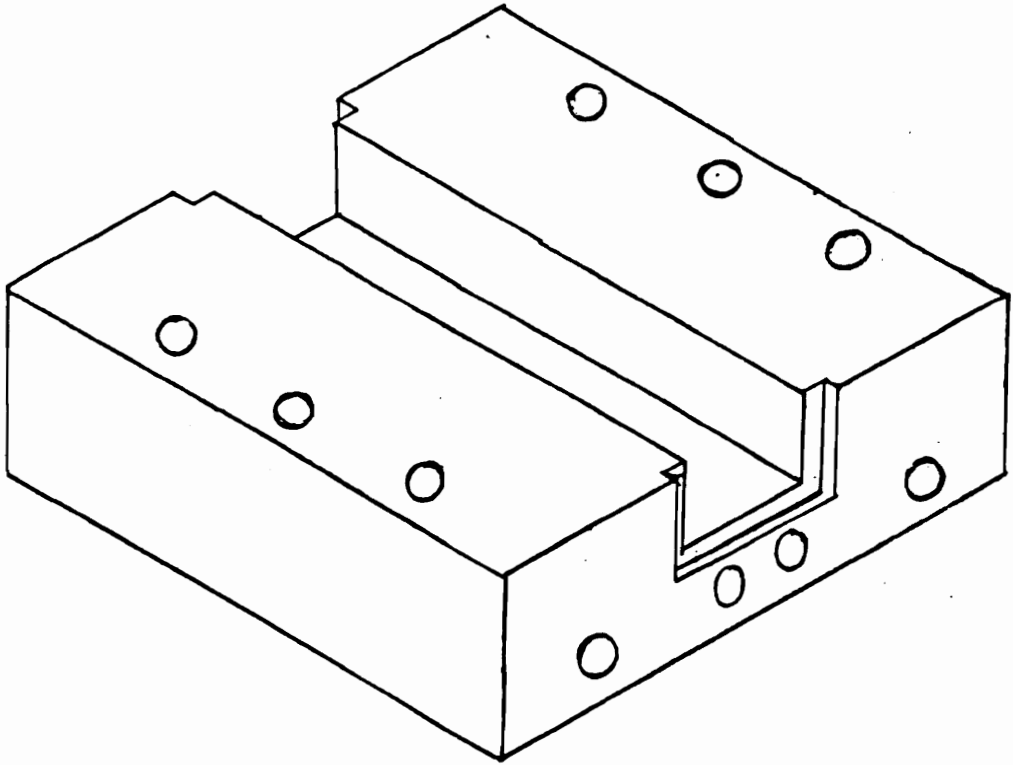


Figure B.4 (a): Isometric view of the bottom half of the middle section

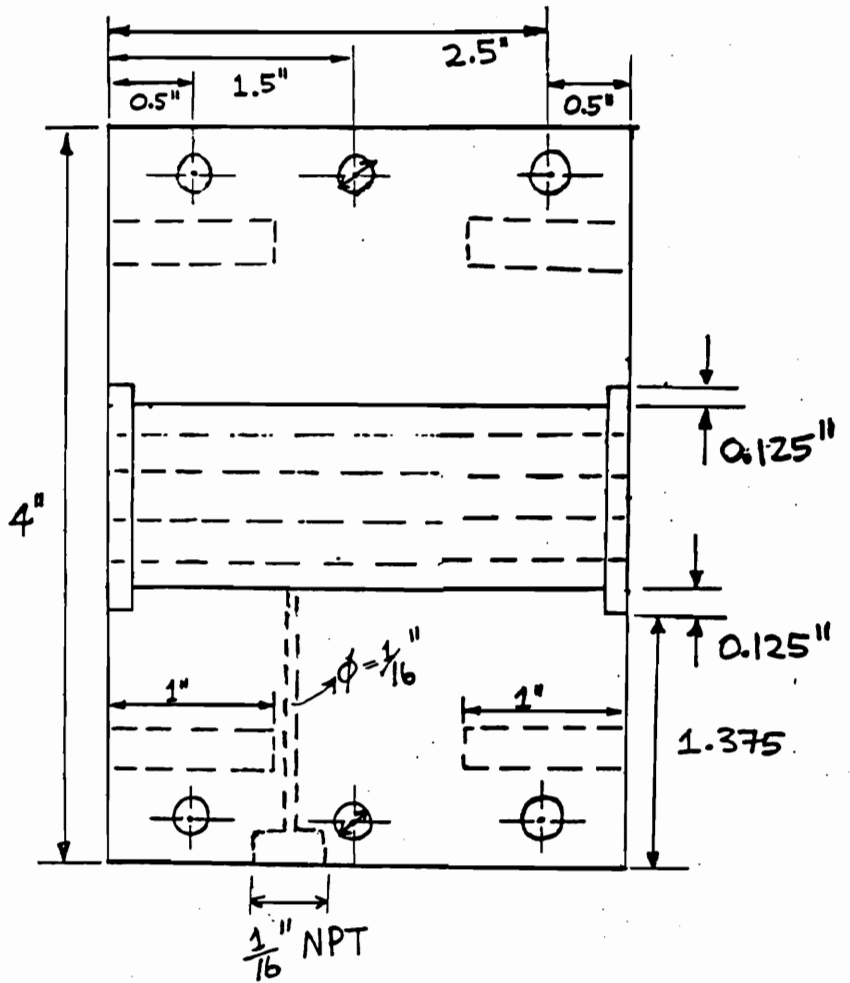


Figure B.4 (b): Top view of the bottom half of the middle section

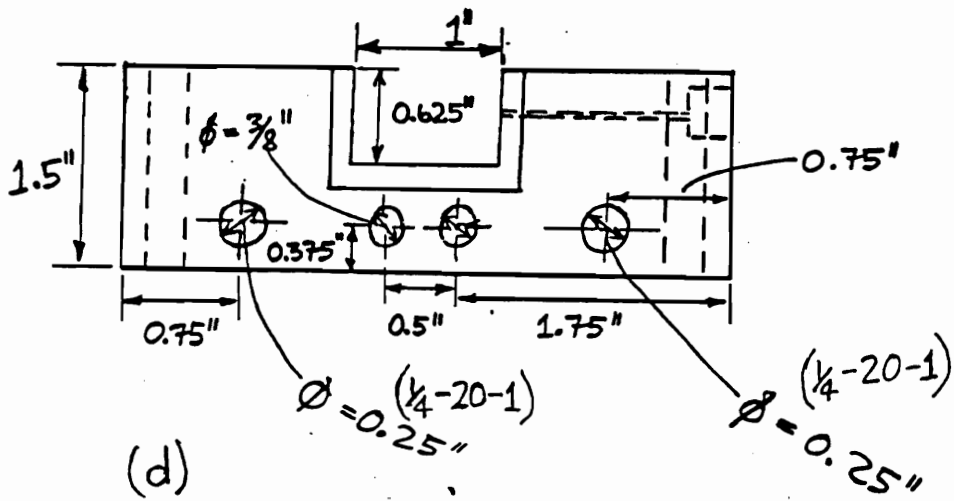
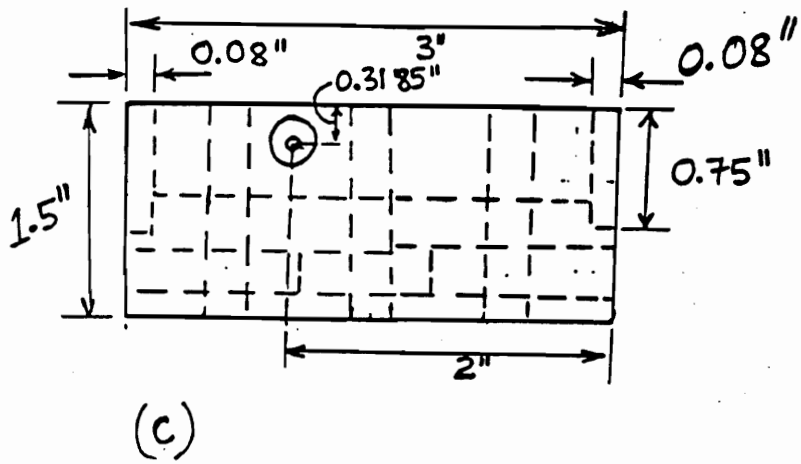


Figure B.4: Side view (c), and Front view (d), of the bottom half of the middle section

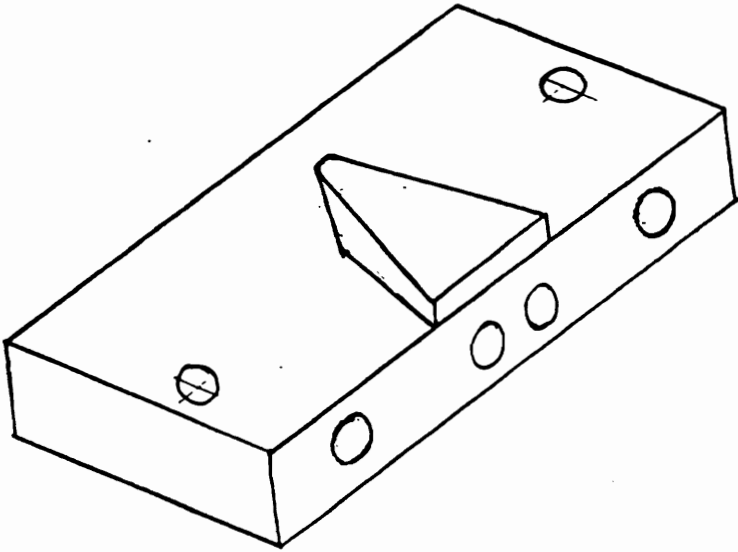


Figure B.5 (a): Isometric view of the top half of the inlet section

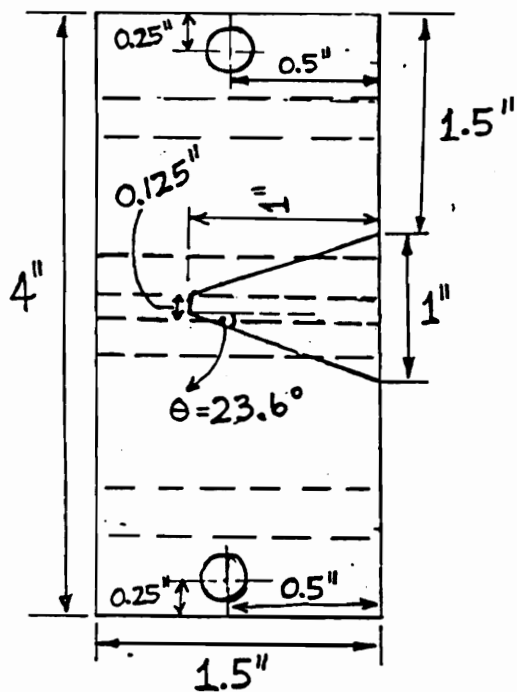
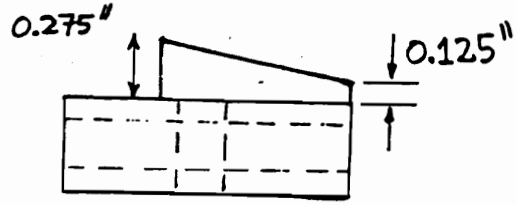
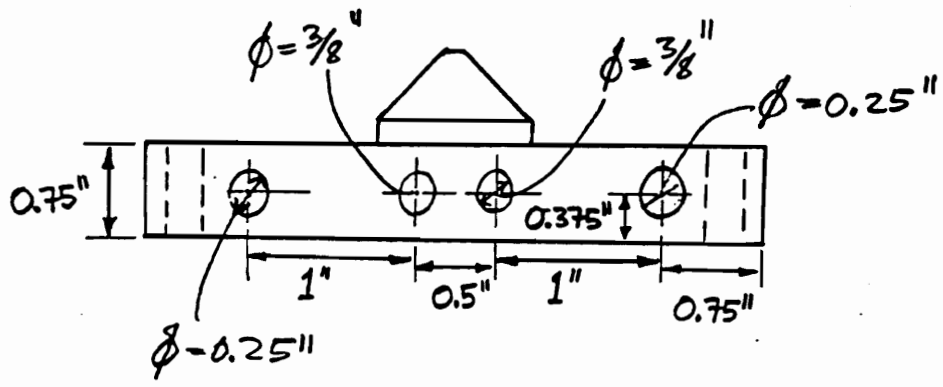


Figure B.5 (b): Top view of the top half of the inlet section



(c)



(d)

Figure B.5: Side view (c), and Front view (d), of the top half of the inlet section

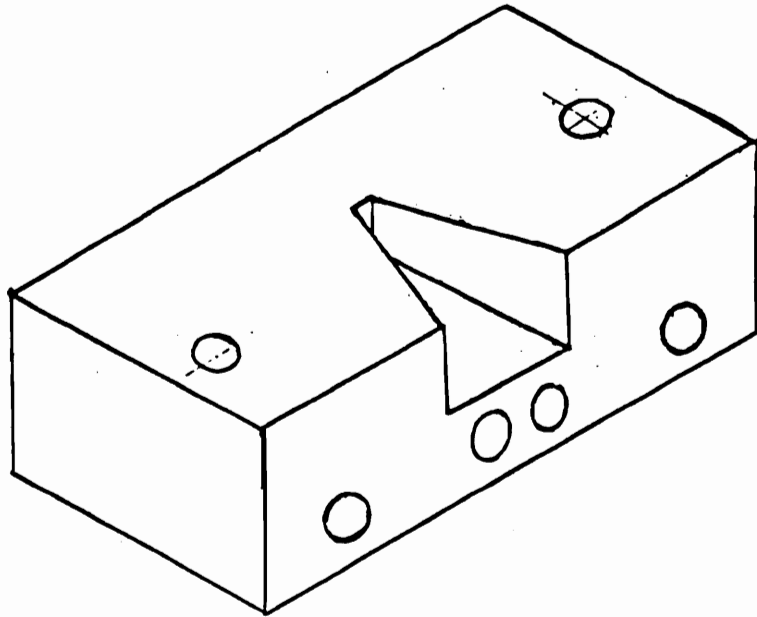


Figure B.6 (a): Isometric view of the bottom half of the inlet section

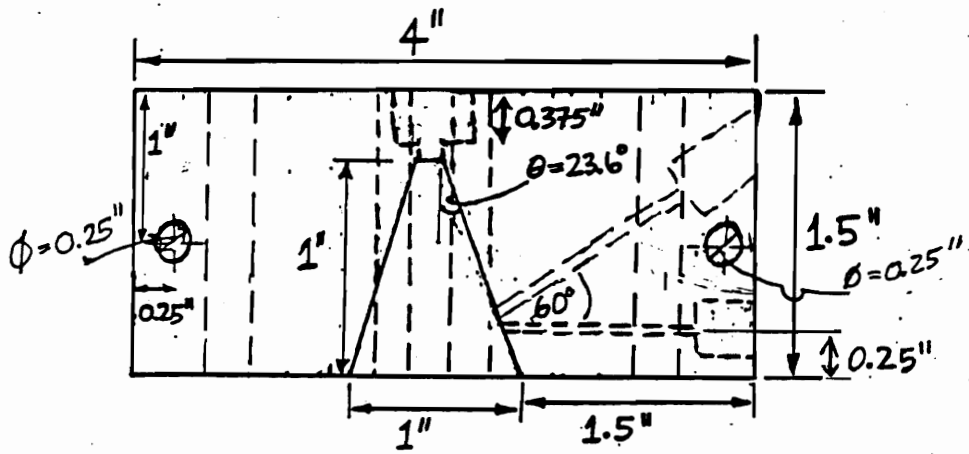
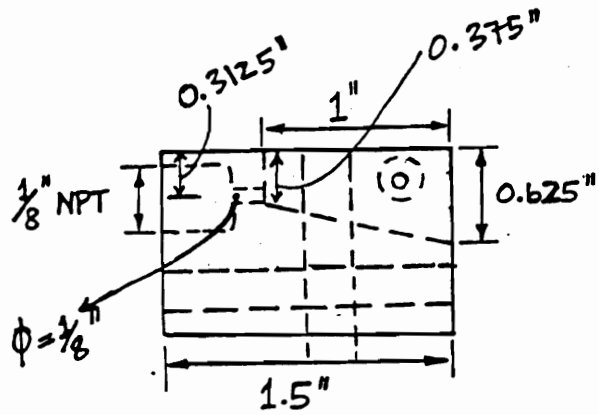
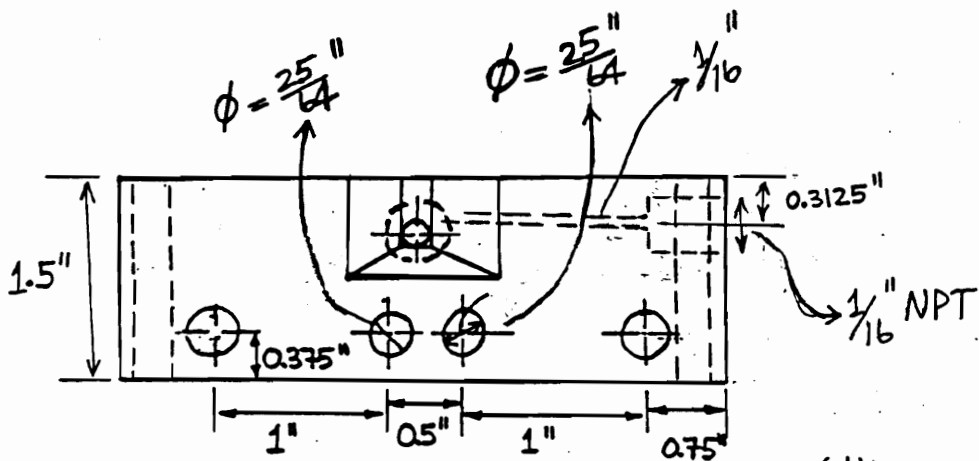


Figure B.6 (b): Top view of the bottom half of the inlet section



(c)



(d)

Figure B.6: Side view (c), and Front view (d), of the bottom half of the inlet section

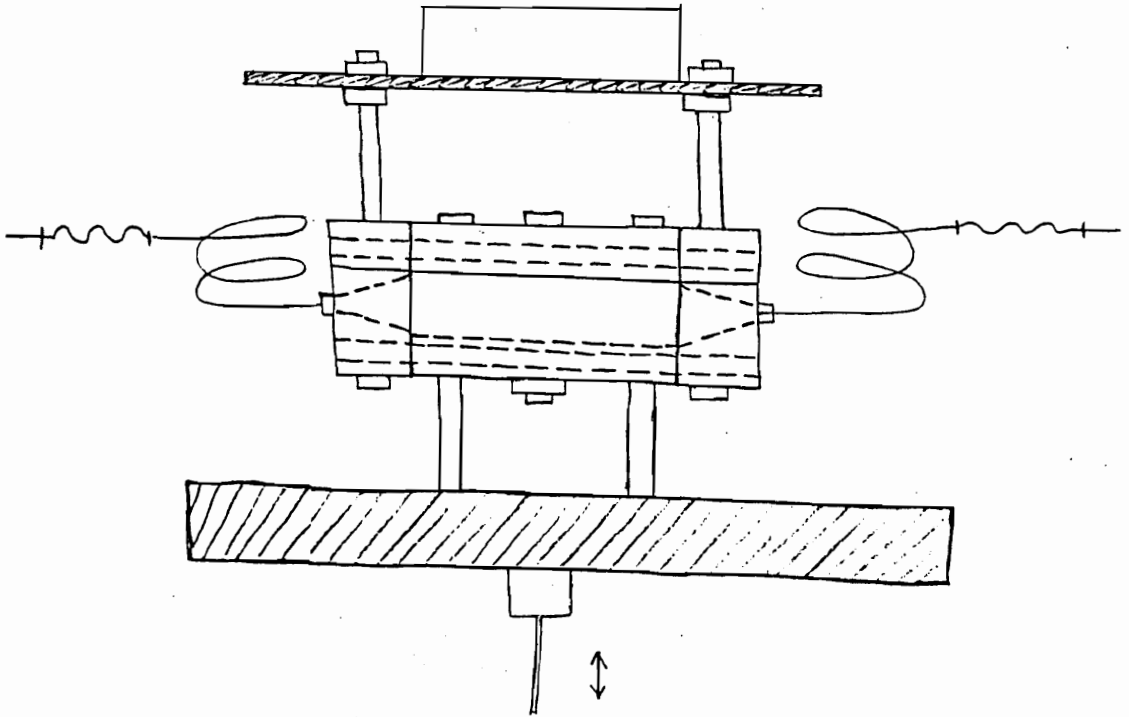


Figure B.7: Complete assembled microreactor.

B.2: Horizontal Duct Length of 22.86 cm

Figure B.8 shows the basic design of the vibrated bed microreactor. The microreactor is made up of three main sections, namely the inlet section, middle section and outlet section. Each of these sections has two parts, namely the top and the bottom.

Figure B.9 shows all of the six individual pieces making up the microreactor. The two middle pieces make up the reaction zone at a horizontal duct length of 22.86 cm. The inlet section and outlet section are similar. Design dimensions of the middle section (both top and bottom parts) and the inlet section (both top and bottom parts) are presented in the following figures.

B.2.1 Middle Section

Several views of the top half of the middle section (viz. mid-top section) are shown in Figure B.10 namely (a) Isometric view, (b) Top view, (c) Side view and (d) Front view.

Several views of the bottom half of the middle section (viz. mid-bottom section) are shown in Figure B.11 namely (a) Isometric view, (b) Top view, (c) Side view and (d) Front view.

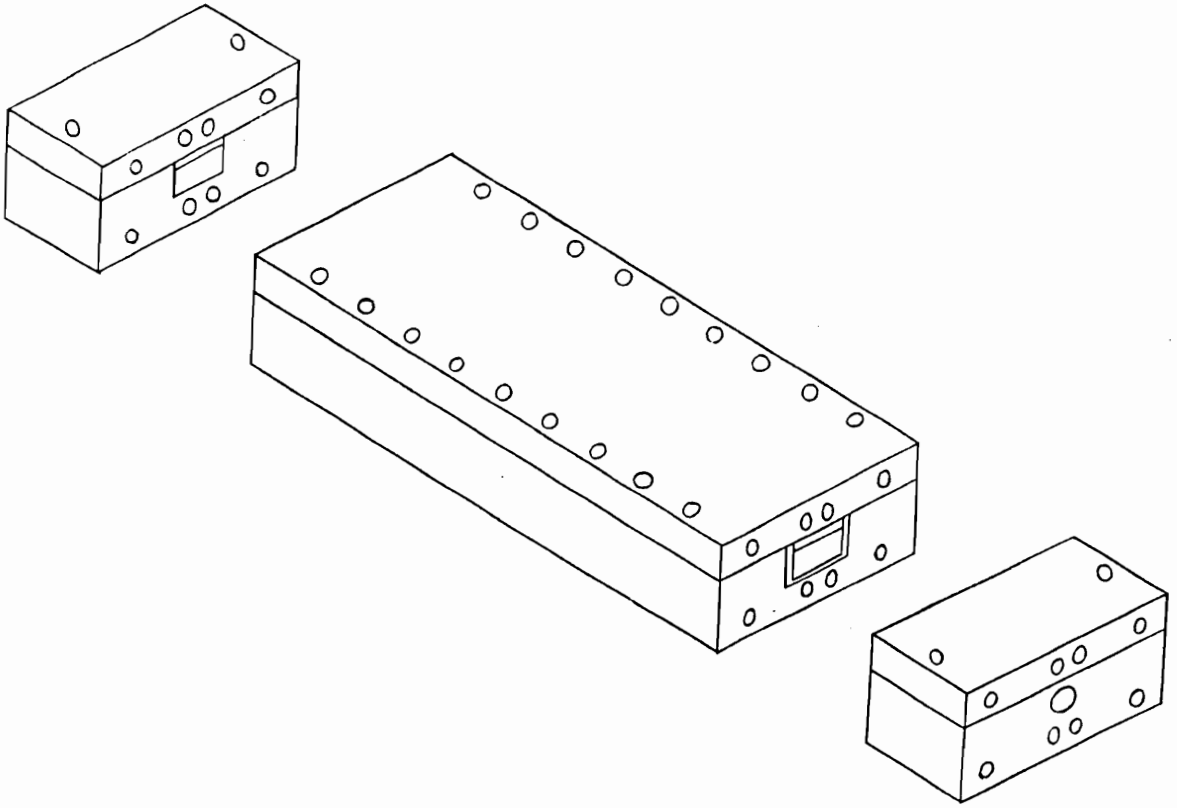


Figure B.8: Isometric drawing of the microreactor at 22.86-cm horizontal duct length. The figure shows three main sections of the microreactor, Inlet section, Middle section and Outlet section.

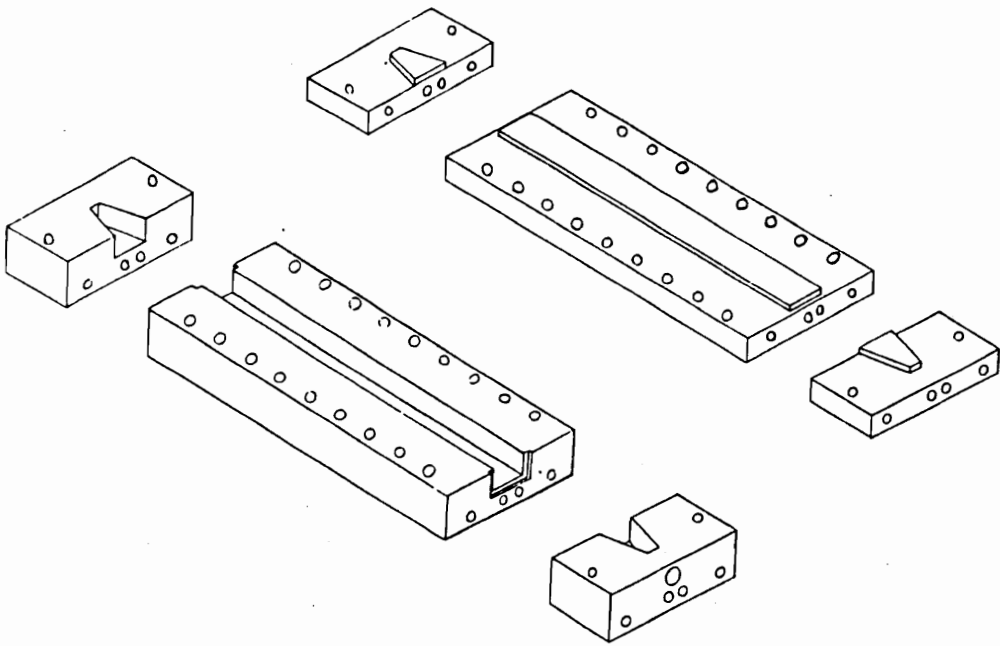


Figure B.9: Individual pieces making up the microreactor. Center pieces are for horizontal duct at a length of 22.86-cm. Inlet section and Outlet section are similar.

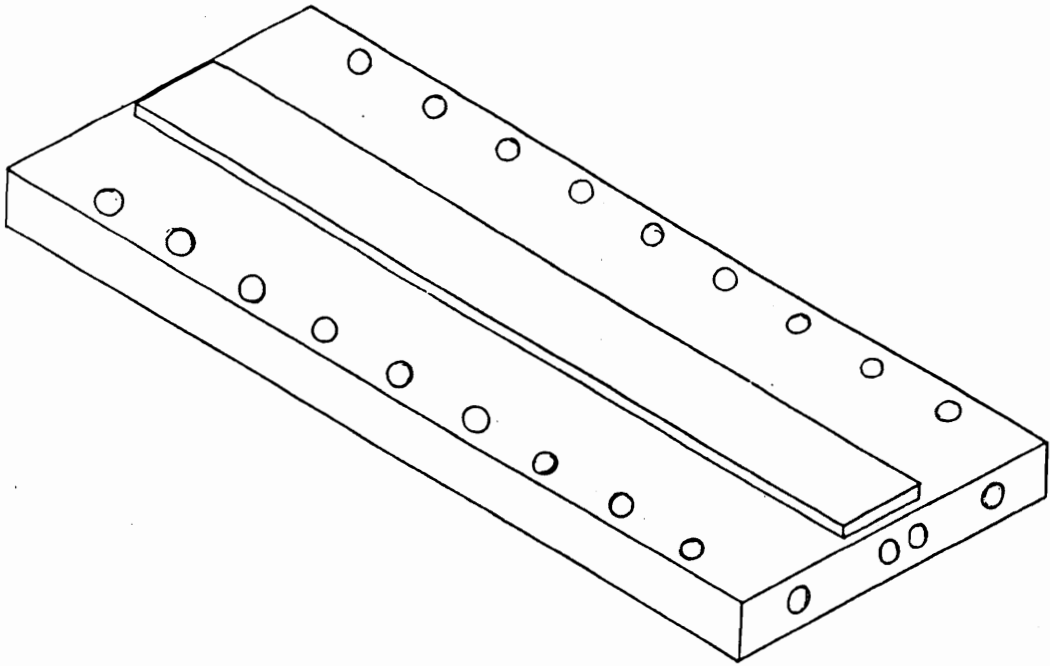


Figure B.10 (a): Isometric view of the top half of the middle section

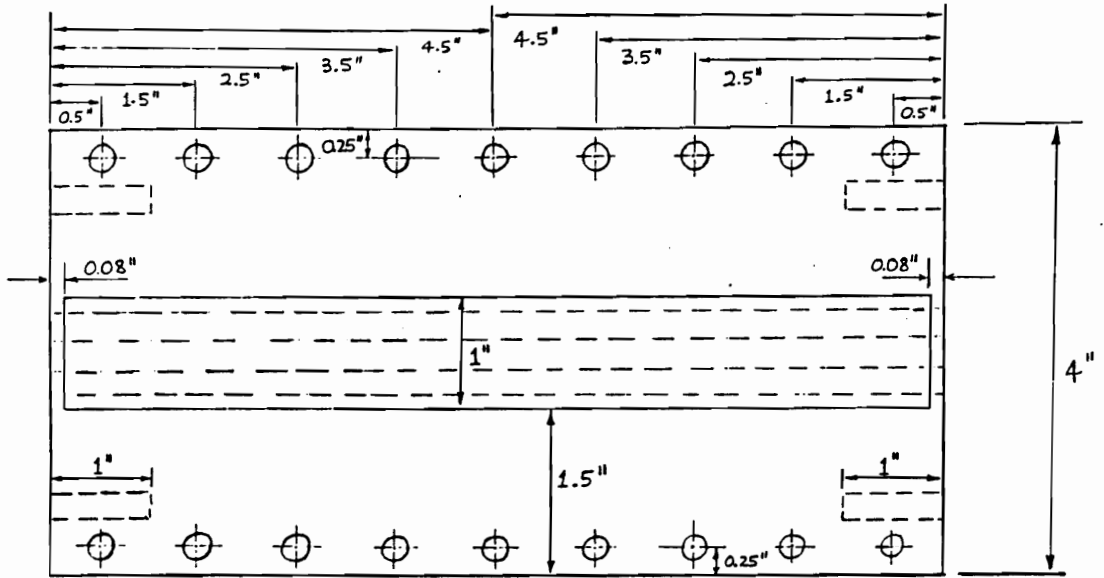


Figure B.10 (b): Top view of the top half of the middle section

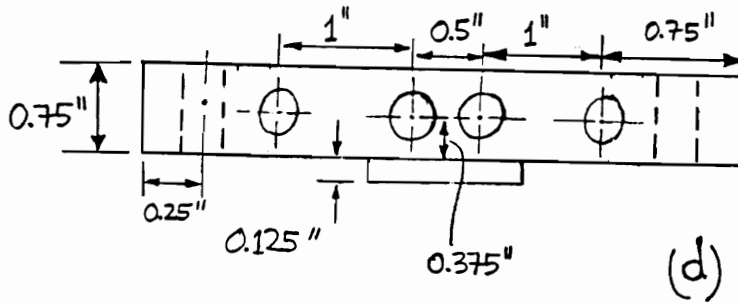
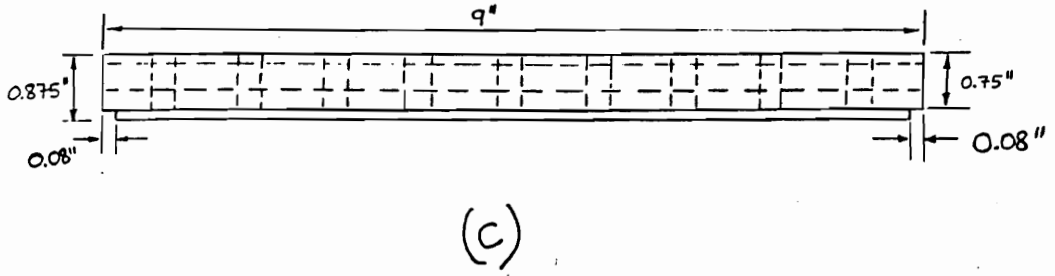


Figure B.10: Side view (c), and Front view (d), of the top half of the middle section

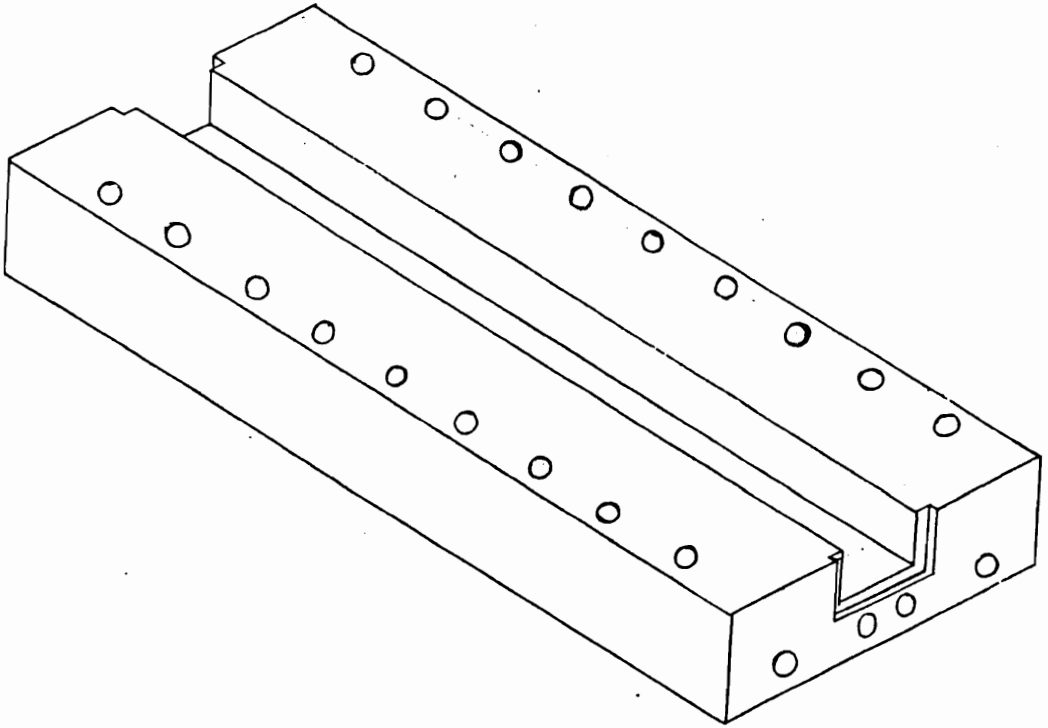


Figure B.11 (a): Isometric view of the bottom half of the middle section

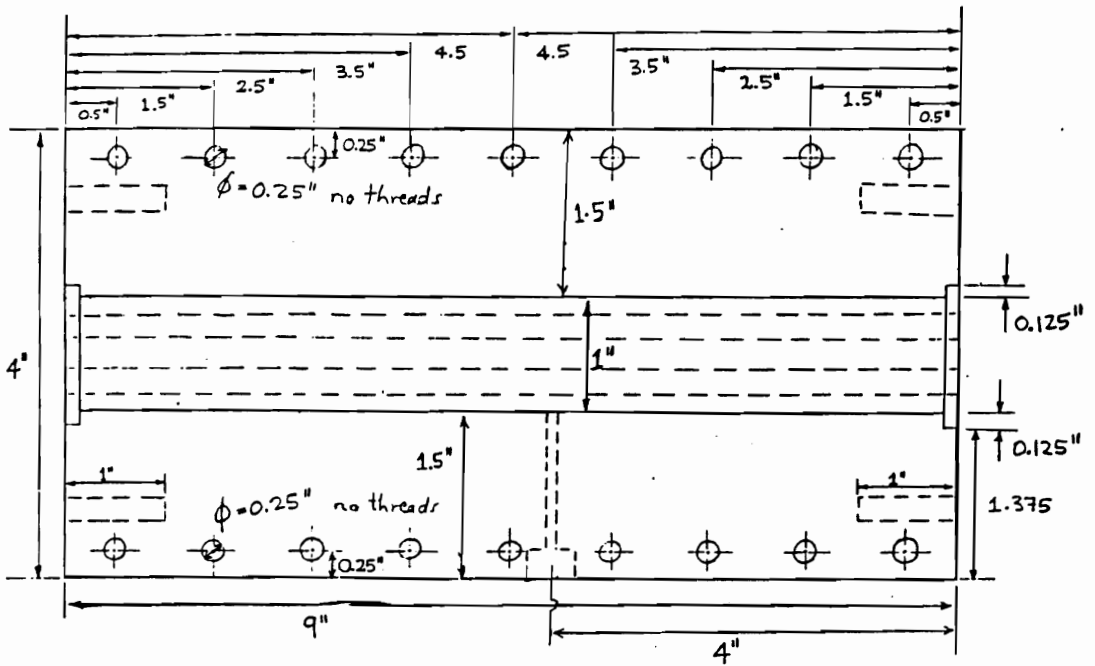


Figure B.11 (b): Top view of the bottom half of the middle section

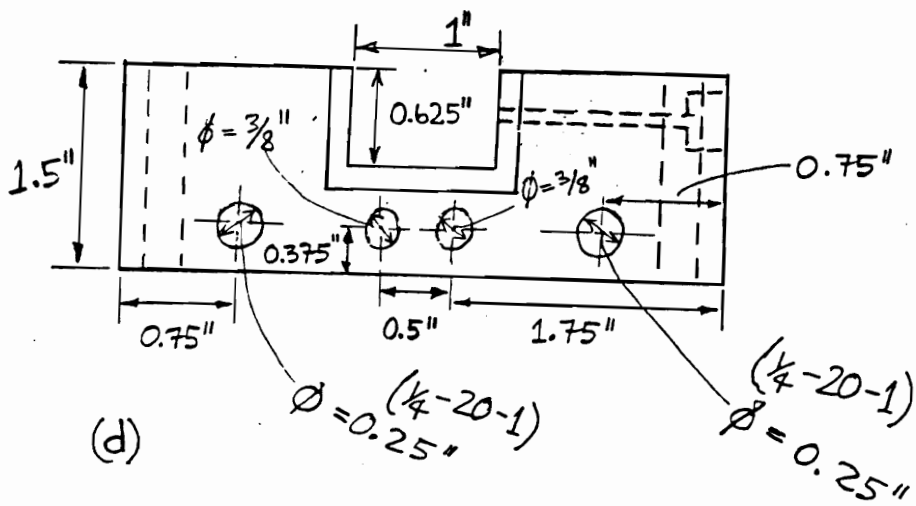
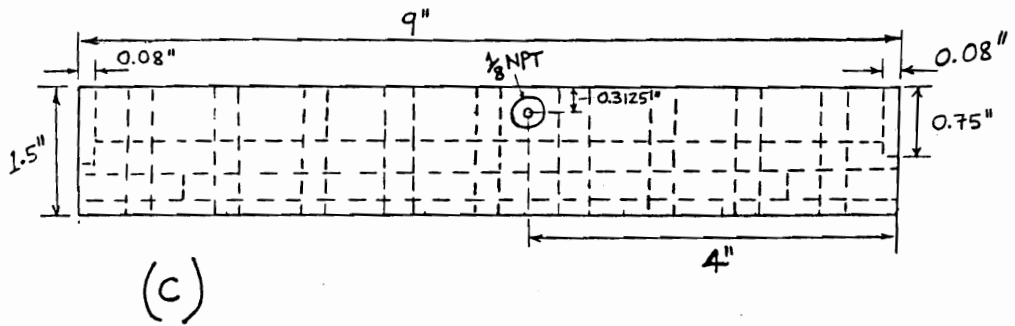


Figure B.11: Side view (c), and Front view (d), of the bottom half of the middle section

B.2.2 Inlet Section

Wedges were put in after the design to make the inlet section and the outlet section have the conical shape, which we felt necessary to eliminate dead zone and ensure an even plug-flow into the horizontal duct length.

Several views of the top half of the inlet section (viz. inlet-top section) are shown in Figure B.12 namely (a) Isometric view, (b) Top view, (c) Side view and (d) Front view.

Several views of the bottom half of the inlet section (viz. inlet-bottom section) are shown in Figure B.13 namely (a) Isometric view, (b) Top view, (c) Side view and (d) Front view.

Figure B.14 shows an assembled microreactor.

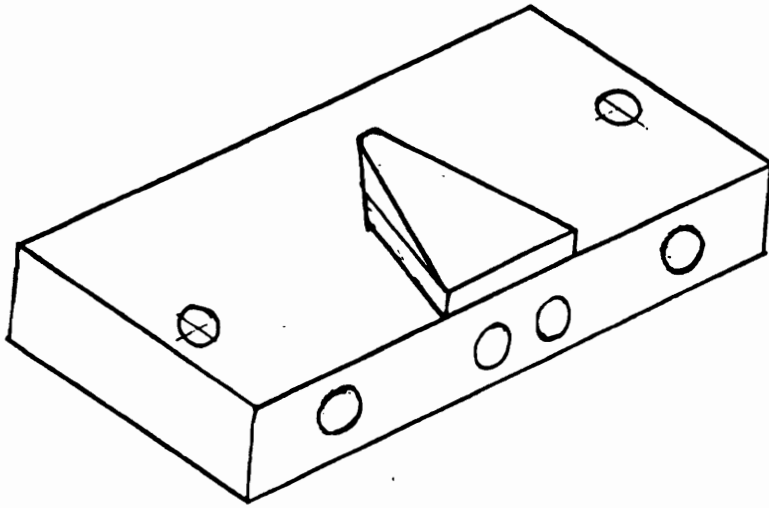


Figure B.12 (a): Isometric view of the top half of the inlet section

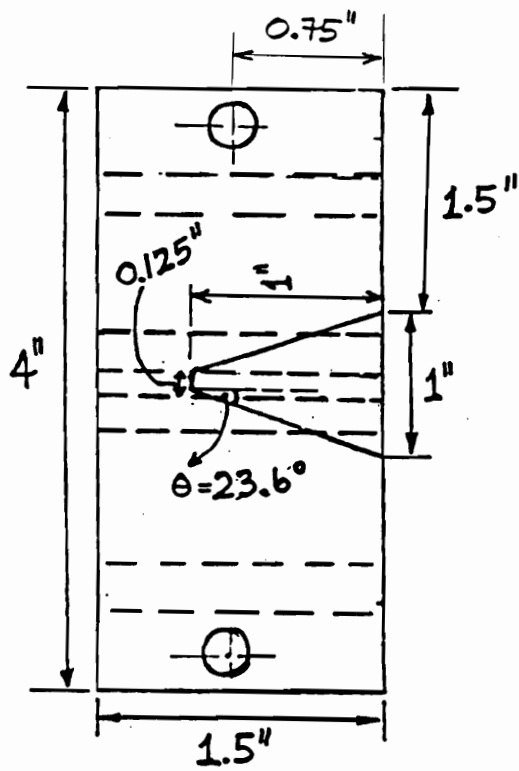
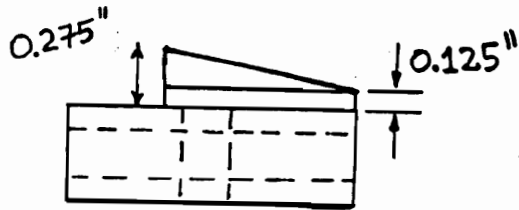
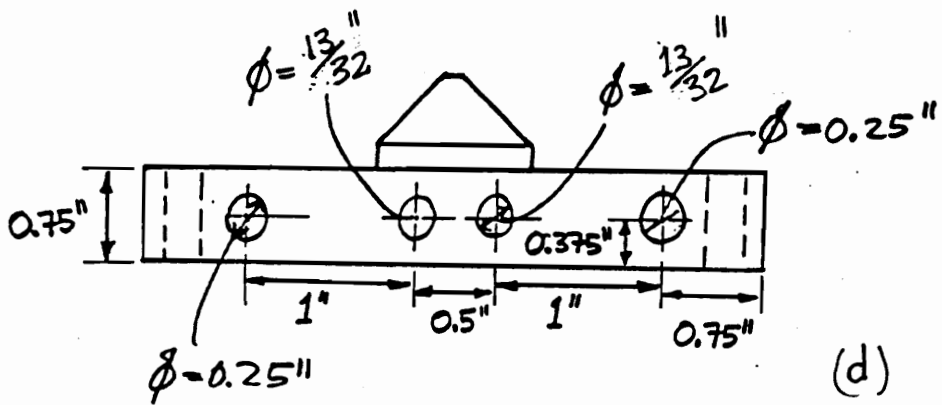


Figure B.12 (b): Top view of the top half of the inlet section



(c)



(d)

Figure B.12: Side view (c), and Front view (d), of the top half of the inlet section

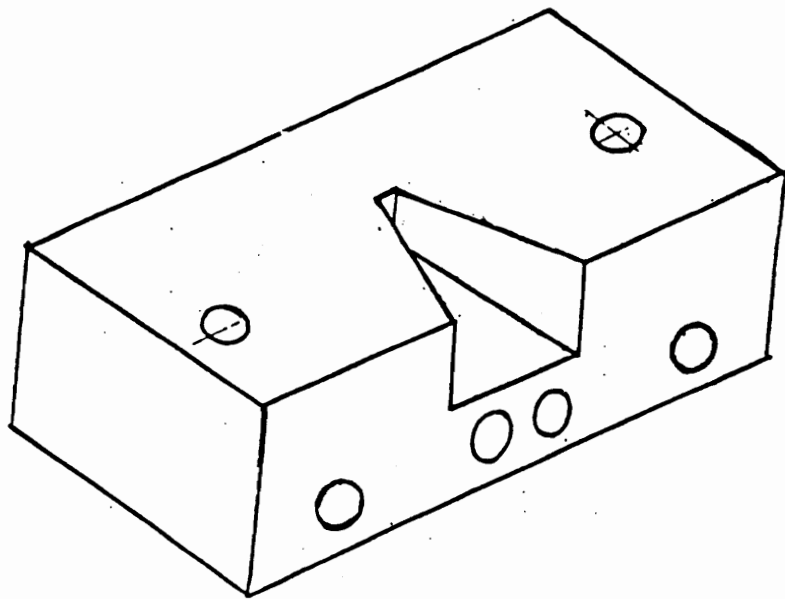


Figure B.13 (a): Isometric view of the bottom half of the inlet section

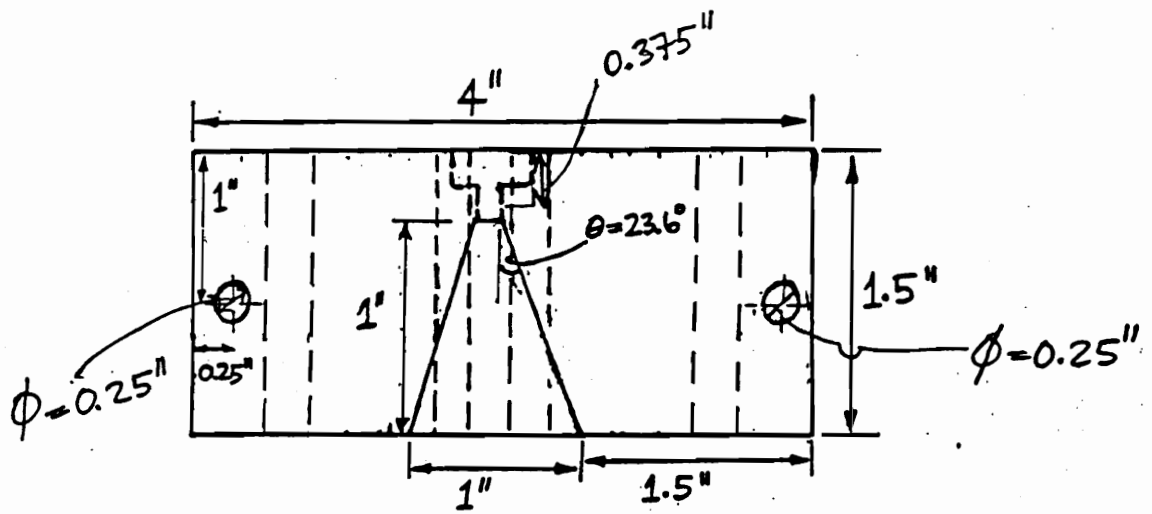
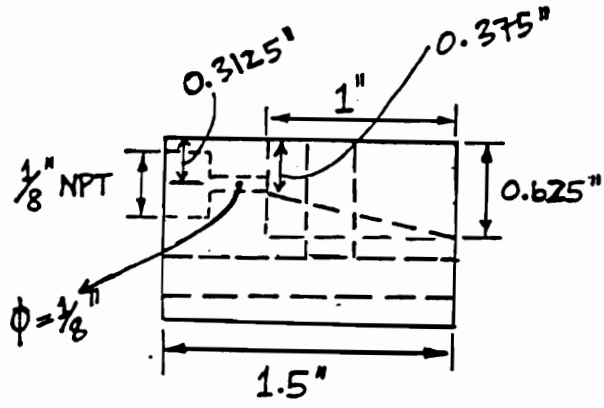
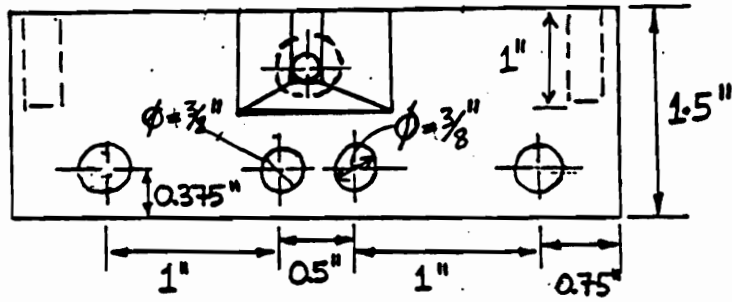


Figure B.13 (b): Top view of the bottom half of the inlet section



(c)



(d)

Figure B.13: Side view (c), and Front view (d), of the bottom half of the inlet section

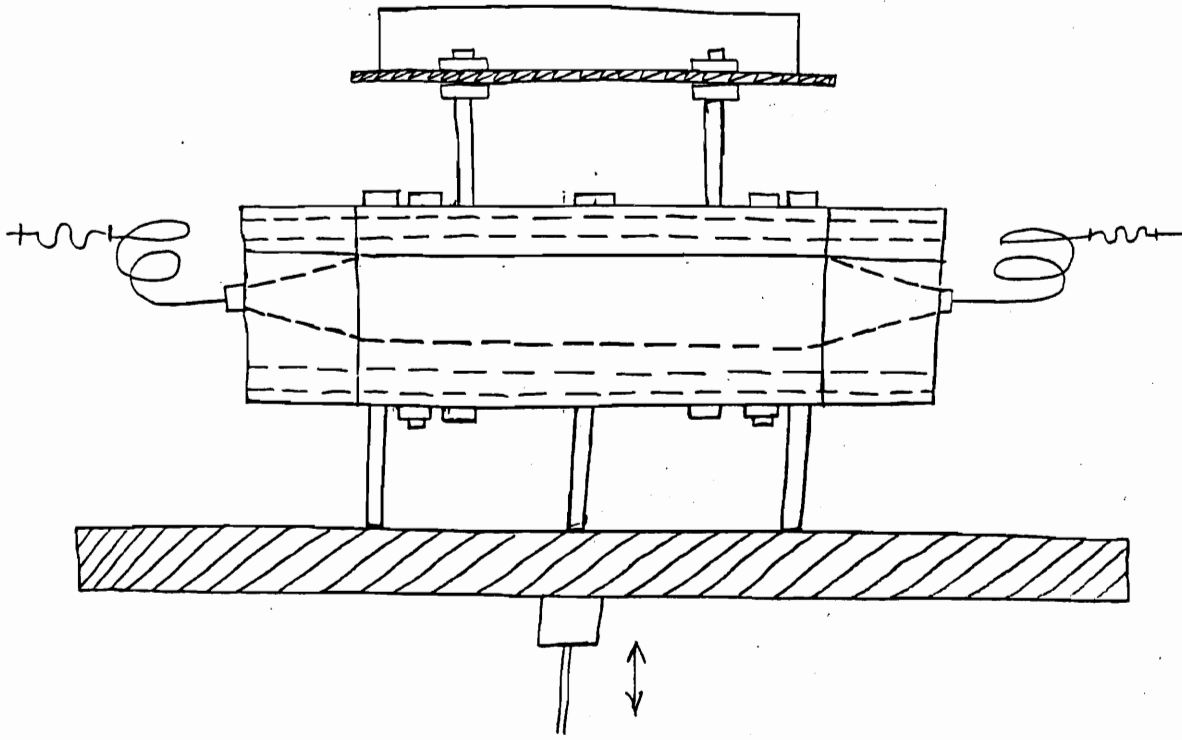


Figure B.14: A complete assembled microreactor.

APPENDIX C : ANALYSIS OF REACTION INDEX

Hydrocarbon product from MTO reaction is Olefins, Paraffins Cycloparaffins and Aromatics. The primary goal in MTO reaction is to maximize Yield of Light Olefins.

Reaction Index (RI) is defined by the propane/propene ratio and is a criterion of catalyst activity. Avidan writes, “ since the measurement of on-line catalyst activity is difficult, we found it convenient to follow an on-line reaction index (RI), which is a selectivity ratio. The propane/propene RI can be easily monitored by an on-line Gas Chromatograph.”.

The Appendix presents Reaction Index and examines how it varies with Sample Time as well as with Peclet Number.

C.1 SAMPLE TIME

Figure C.1 shows Reaction Index observed from runs done in VBMR-3 (horizontal duct length = 7.62 cm) plotted against Sample Time. Reaction Index for the first run started off at 0.0 and increased to 0.115. Reaction Index for the second run started off at 0.101, went up to 0.160 and then dropped down to 0.028. Reaction Index observed in the third run started off at 0.425 and gradually dropped to 0.123.

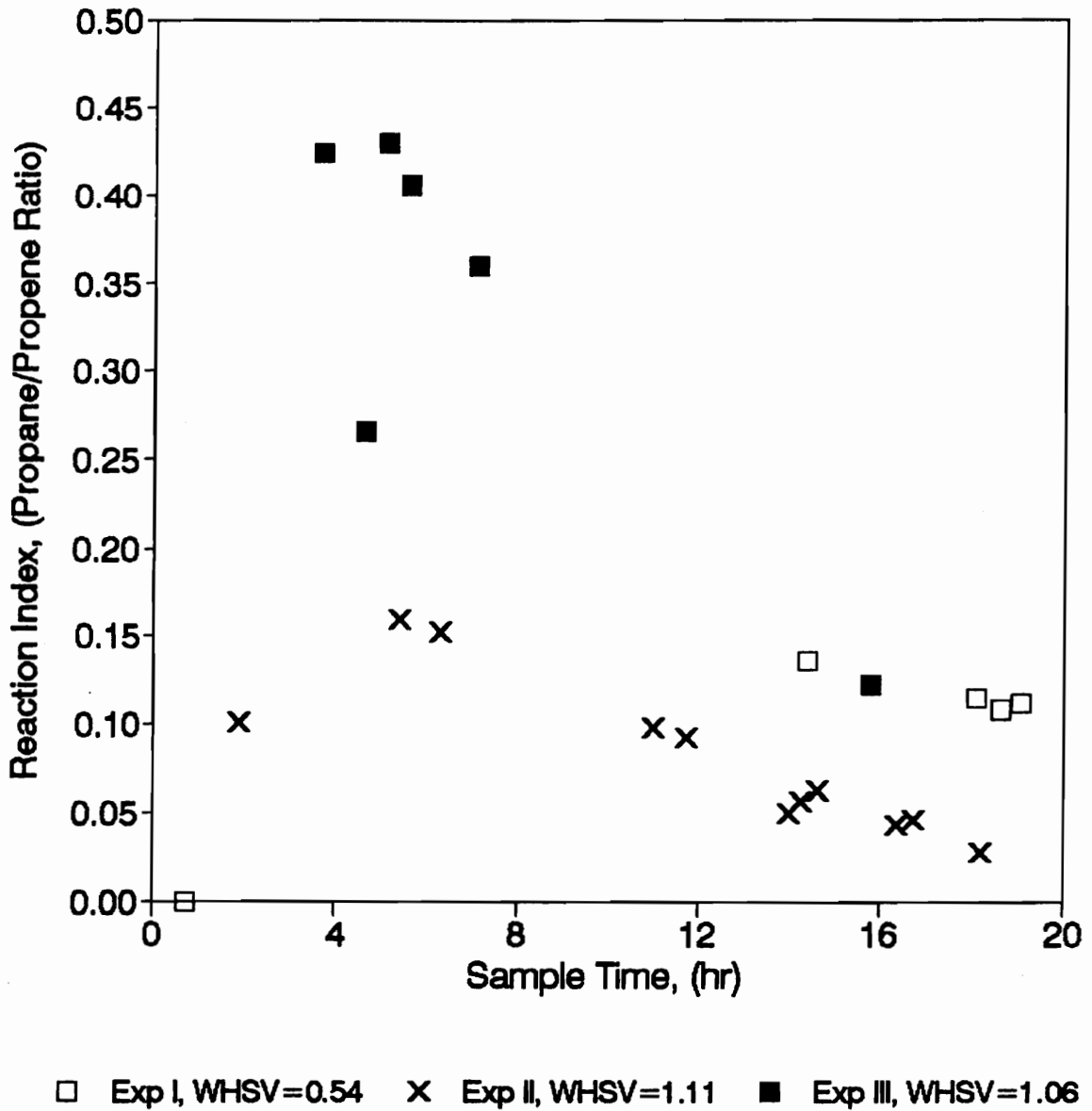


Figure C.1: Reaction Index observed from runs done in VBMR-3 (horizontal duct length = 7.62 cm) plotted against Sample Time. Experimental runs conducted at WHSV of 0.54, 1.11 and 1.06.

Figure C.2 shows Reaction Index observed from runs done in VBMR-6 (horizontal duct length = 15.24 cm) plotted against Sample Time. Reaction Index for the first run started off at 0.25, gradually dropped and appeared to settle around 0.176. Reaction Index for the second run started off at a value of 0.35 and dropped down to 0.25.

Figure C.3 indicates Reaction Index observed from runs done in VBMR-9 (horizontal duct length = 22.86 cm) plotted against Sample Time. Reaction Index for the first run started off at 0.45, gradually dropped and appeared to settle around 0.216. Reaction Index for the second run started off at a value of 0.00 and increased up to a value of 0.107.

In summary, plots of Reaction Index versus Sample Time showed quite a scatter in the data. In some of the runs (e.g. empty squares in Figure C.3; empty squares in Figure C.1), Reaction Index appeared to settle at a particular value but this cannot be asserted with maximum confidence in the light of insufficient data.

Reported Data from Fluid Bed

No data was available on the history of Reaction Index with respect to Sample Time for work done in the 4 BPD Pilot Plant and Bench Scale Unit.

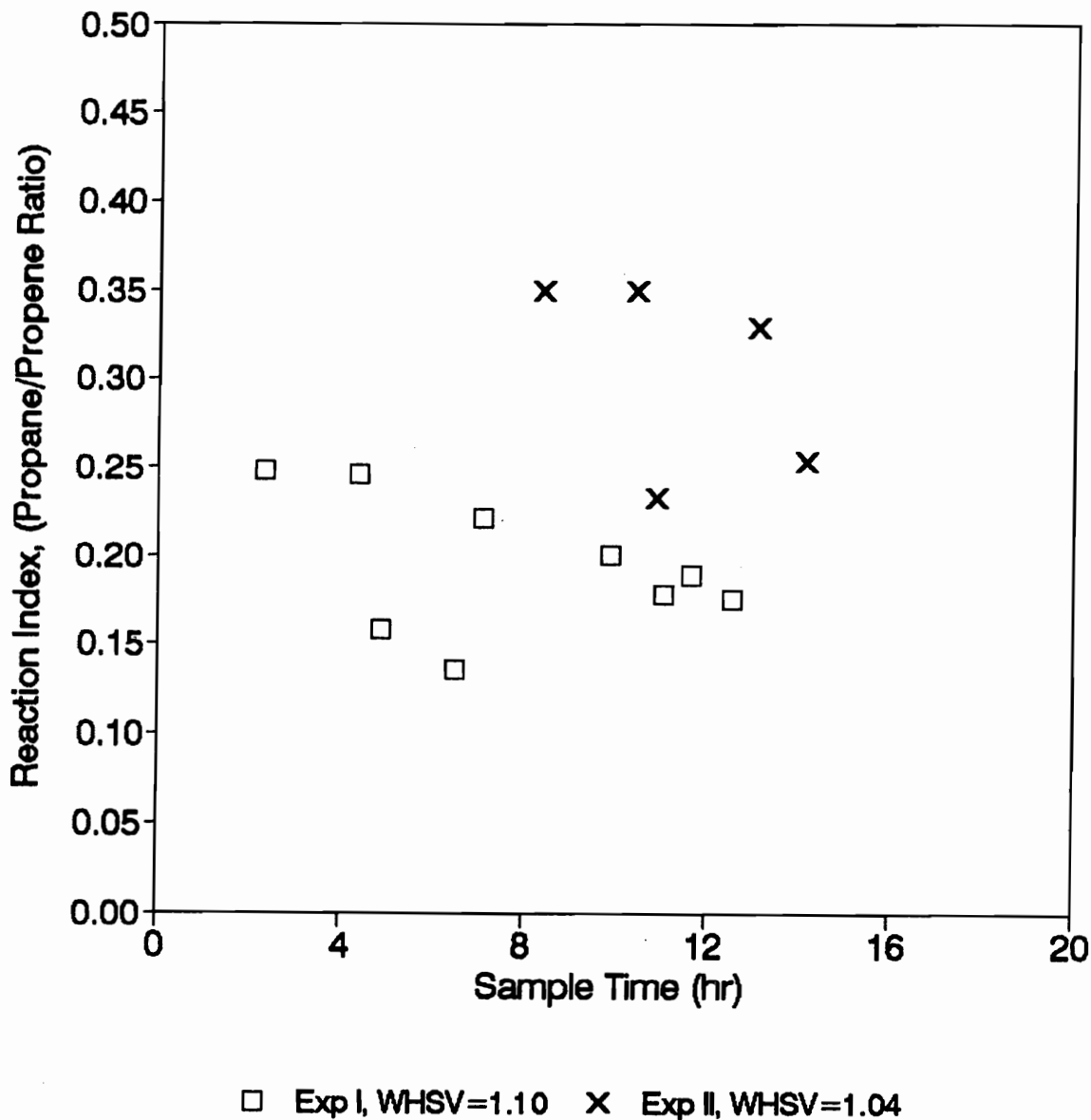
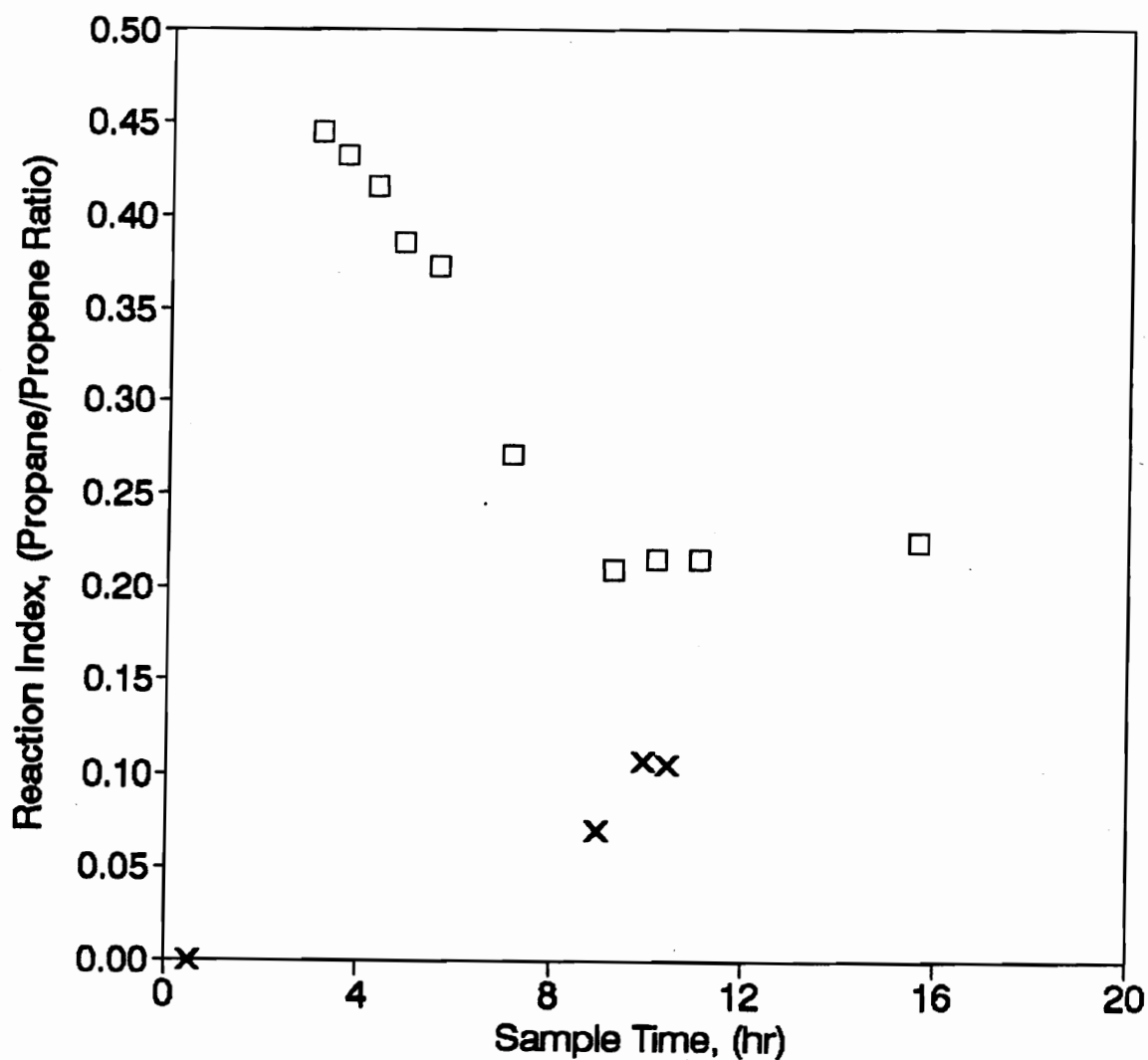


Figure C.2: Reaction Index observed from runs done in VBMR-6 (horizontal duct length = 15.24 cm) plotted against Sample Time. Experimental runs conducted at WHSV of 1.10 and 1.04.



□ Exp I, WHSV=1.15 × Exp II, WHSV=1.10

Figure C.3: Reaction Index observed from runs done in VBMR-9 (horizontal duct length = 22.86 cm) plotted against Sample Time. Experimental runs conducted at WHSV of 1.15 and 1.10.

Figure C.4 indicates Reaction Index observed from two experimental runs done by MRDC in 100 BPD Demonstration Plant plotted against Sample Time (Keim et al, 1987). Both runs were conducted at WHSV of 1.15.

Reaction Index for the first run started off at 0.75 and gradually dropped and appear to settle around 0.20. Reaction Index for the second run started off at 0.67 and dropped down to 0.18. It is worth noting that MRDC ran the plant for 42 days (1008 hours) continuously before this seemingly well defined trend could be established.

Comparing Vibrated Bed Microreactor Data with Fluid Bed Data

In comparing the Reaction Index data obtained from Vibrated Bed Microreactors with that reported by MRDC, it needs to be pointed out that: (i) Reaction Index in the 100 BPD Demonstration Plant did not drop below 0.20 until after 210 hours (i.e. 8.75 days) of continuous operation, whereas Reaction Index in the microreactors in most cases dropped to or below 0.20 within 20 hours of operation.

(ii) MRDC did not observe Reaction Index below 0.10 during the entire 1008 hours (i.e. 42 days) of continuous operation, in the 100 BPD Demonstration Plant, whilst some of the runs done in the microreactors (VBMR-3 and VBMR-9) gave Reaction Index below 0.10 and down to zero.

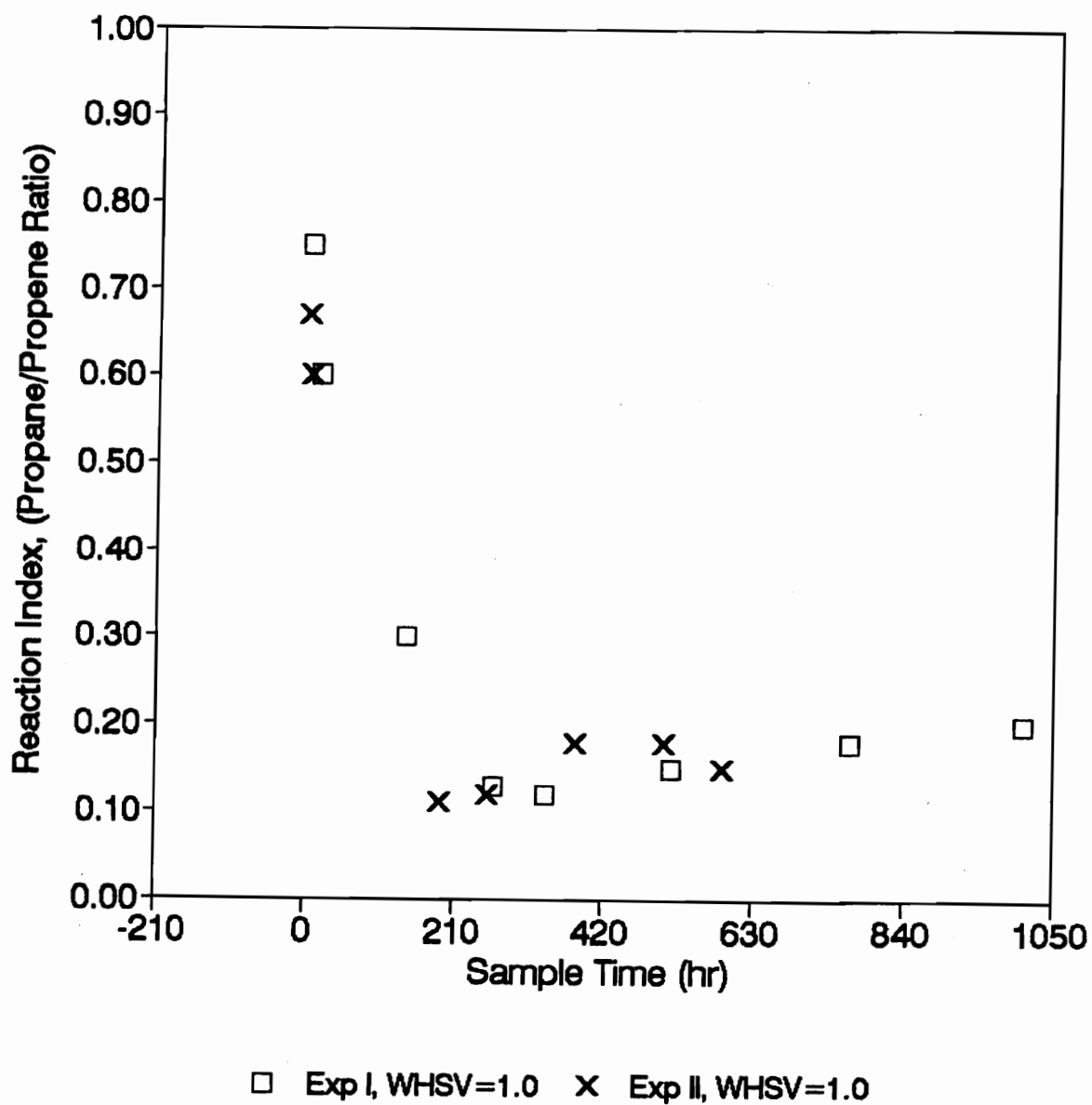


Figure C.4: Reaction Index observed by MRDC in 100 BPD Demonstration Plant plotted against Sample Time (Keim et al, 1987). Both runs were conducted at WHSV of 1.15.

(iii) the first run conducted in VBMR-9 (WHSV = 1.15) appears to show, within 16 hours of its operation, a trend very similar to that seen by MRDC in the 100 BPD Demonstration Plant (WHSV = 1.15). There is not enough data to conclude if the fact that WHSV was the same in both cases has something to do with the similarity.

C.2 PECKET NUMBER

Three microreactors were designed with horizontal duct lengths of 7.62 cm (VBMR-3), 15.24 cm (VBMR-6) and 22.86 cm (VBMR-9).

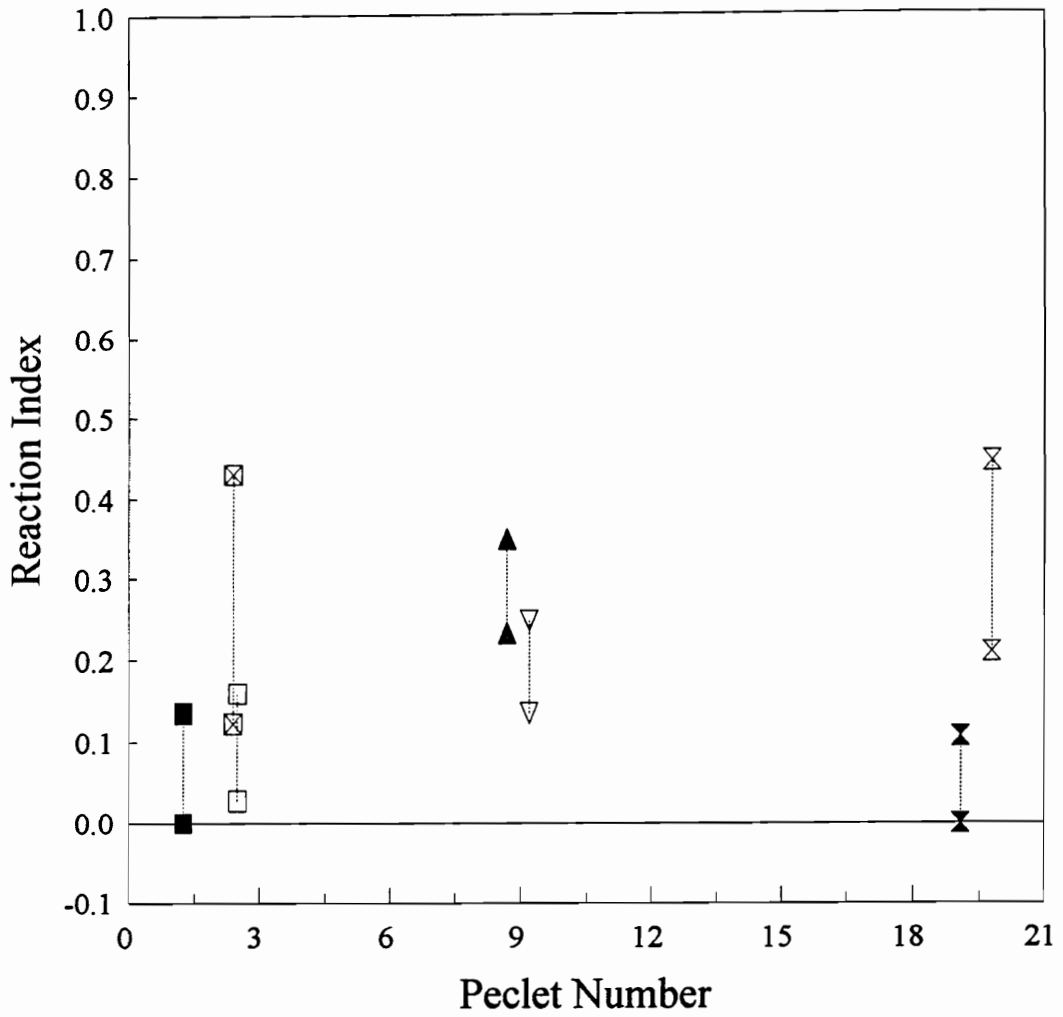
Figure C.5 indicates a plot of the range of Reaction Index observed in each microreactor (maximum and minimum values) against Peclet Number.

The range of Reaction Index obtained from VBMR-3 is:

- (i) between 0.0 and 0.14 at Peclet Number of 1.27
- (ii) between 0.12 and 0.43 at Peclet Number of 2.4
- (iii) between 0.03 and 0.16 at Peclet Number of 2.5

The range of Reaction Index obtained from VBMR-6 is:

- (i) between 0.23 and 0.35 at Peclet Number of 8.7
- (ii) between 0.14 and 0.25 at Peclet Number of 9.2



■ (7.6 cm), Exp I ⊠ (7.6 cm), Exp III □ (7.6 cm), Exp II ▲ (15.2 cm), Exp II
 ▽ (15.2 cm), Exp I ✕ (22.9 cm), Exp II ⊗ (22.9 cm), Exp I

Figure C.5: Plot of the range of Reaction Index (maximum and minimum values) observed in each microreactor against Peclet Number.

The range of Reaction Index obtained from VBMR-9 is:

- (i) between 0.0 and 0.11 at Peclet Number of 19.1
- (ii) between 0.21 and 0.45 at Peclet Number of 19.8

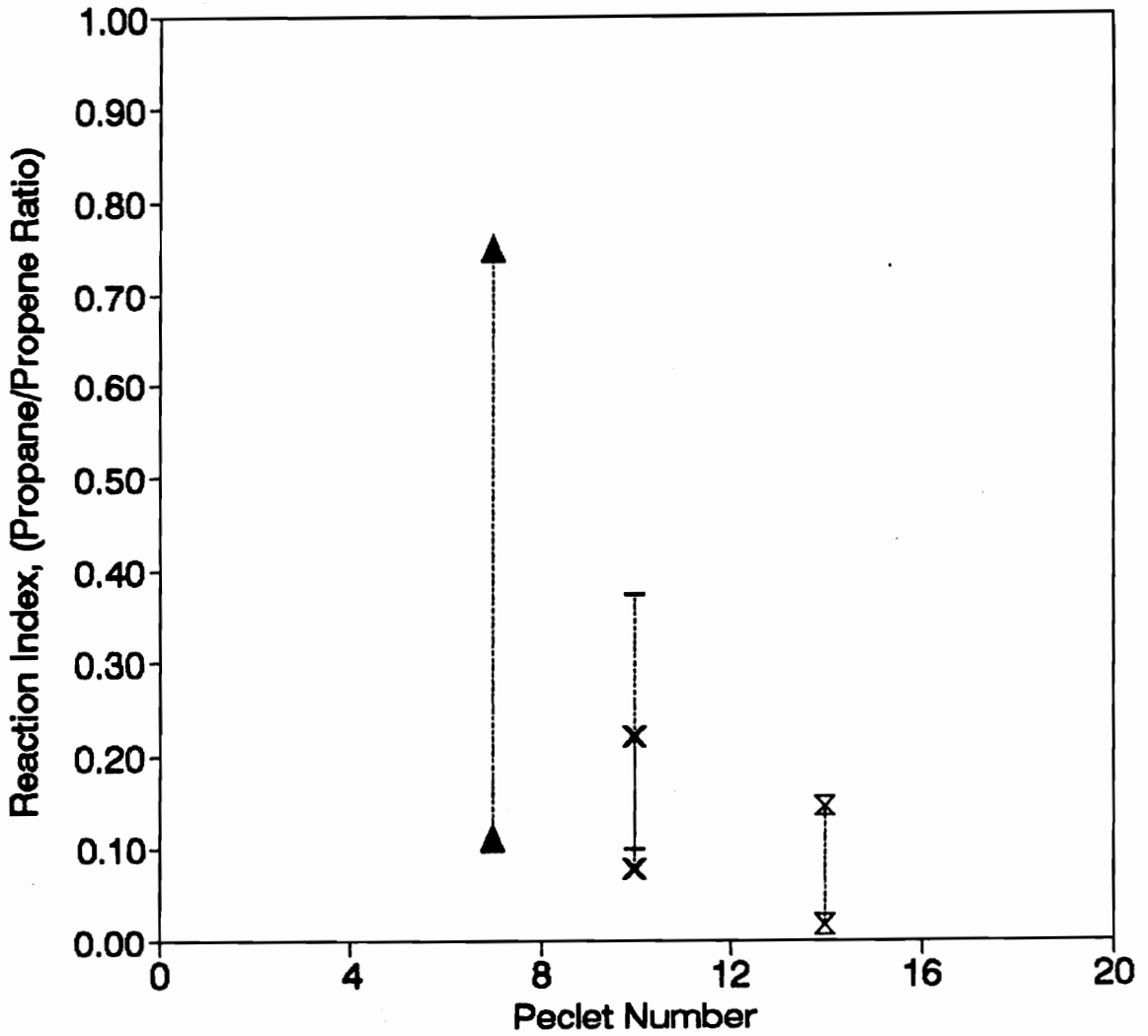
The range of Reaction Index does not reveal any significant trend with regard to Peclet Number.

Reported Data from Fluid Bed

Figure C.6 indicates a plot of the range of Reaction Index, reported by MRDC, against Peclet Number. The range of Reaction Index at;

- (i) Peclet Number (100 BPD Demonstration Plant) is between 0.18 and 0.45,
- (ii) Peclet Number (4 BPD Pilot Plant) is between 0.08 and 0.38 and
- (iii) Peclet Number (Bench Scale Unit) is between 0.02 and 0.15.

MTO reaction was reportedly operated at two different conditions at Peclet Number of 10 ([A: 482 C; 103 kPa; in 4 BPD plant; open square] and [B: 500 C; 250 kPa; in 100 BPD plant with baffles; cross]). Reaction Index range appears to vary widely with operation at higher temperature and higher pressure. It appears to vary narrowly at 482 C and 103 kPa at the same Peclet Number of 10.



--x-- Micro (482 C) --x-- Pilot (482 C) --- Pilot (500 C) --▲-- Demo (500 C)

Figure C.6: Plot of the range of Reaction Index, reported by MRDC, against Peclet Number.

Reaction Index range observed by MRDC appear to drop with an increase in the Peclet Number. It drops past 0.10 at Peclet Number of 10 and continues to drop to 0.07 at Peclet Number of 14.

Comparing Vibrated Bed Microreactor Data with Fluid Bed Data

In comparing the range of Reaction Index with Peclet Number for the data from microreactor and from fluid bed it has to be noted that:

- (i) it is highest at a Peclet Number of 7 (100 BPD Demonstration Plant)
- (ii) it drops significantly with Peclet Number for fluid bed data, and does not appear to vary much for microreactor data.

C.3 SUMMARY OF OBSERVATION ON RESULTS

Reaction Index data obtained from microreactors when plotted against Sample Time appeared scattered and did not appear to settle out at any particular value, as was the case with Fluid Bed.

Results obtained by MRDC imply that Reaction Index takes much longer, than is possible with the Vibrated Bed Microreactor, to steady out and settle at a particular value of say 0.2 as is the case in the 100 BPD Demonstration Plant operated by MRDC.

Lower values of Reaction Index were attained much quicker in the Vibrated Bed Microreactors than in Fluid Beds. This may suggest that the catalyst in the Vibrated Bed Microreactor reaches steady state activity more quickly than is the case with the catalyst in the Fluid Bed.

The range of Reaction Index data obtained from Vibrated Bed Microreactor did not appear to vary with Peclet Number.

Reaction Index does not appear to be as useful for characterizing vibrated bed microreactor data as MRDC found this parameter to be in analysis of fluid-bed data.

The range of Reaction Index obtained from Fluid Bed, when plotted against Peclet Number:

- (i) drops with an increase in Peclet Number.
- (ii) increases with an increase in temperature and pressure for the same Peclet Number.

VITA

Samuel Nhlanganiso Tshabalala, son of Amos Cornelius and Roselina Nomashinini was born on March 25, 1961 in Bethlehem, South Africa.

Sam obtained a BSc in Chemical Engineering from the University of the Witwatersrand (Wits University), Johannesburg in December 1985.

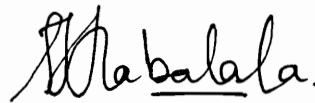
He spent time in industry, with Anglo American Research Laboratories, Johannesburg and then with SAPREF, Durban.

He came back to pursue graduate studies in Chemical Engineering at Wits University in November 1987, and left for the USA in September 1989, on a fellowship to pursue doctoral studies in Chemical Engineering at University of Pennsylvania, Philadelphia.

He transferred to Virginia Polytechnic Institute & State University, Blacksburg, in June 1990, to work with Prof A.M. Squires's research group.

While working toward his doctorate, Sam completed a thesis for the work done at Wits University, and graduated with an MSc in Chemical Engineering in December 1991.

Sam obtained a Ph.D in Chemical Engineering from Virginia Polytechnic Institute & State University in August, 1995.



Samuel Nhlanganiso Tshabalala